Robust Decision and Data Science Application for Reservoir Management.

Probabilistic Forecasting, History Matching, Sequential Decision Making and Value-of - Information

by

Amine Tadjer

Thesis submitted in fulfilment of
the requirements for the degree of
PHILOSOPHIAE DOCTOR
(PhD)

Department of Energy Resources
Faculty of Science and Technology
2021

University of Stavanger
NO-4036 Stavanger
NORWAY
www.uis.no

ISBN: 978-82-8439-144-1
ISSN: 1890-1387
PhD: Thesis UiS No. 680

Preface

This thesis has been written to partially fulfill the graduation requirements of the Philosophiae Doctor (PhD) degree at the Department of Energy Resources. Faculty of Science and Technology, University of Stavanger, Norway. I was engaged in writing this thesis from March to June 2021.

This research was conducted under the main supervisor, Prof. Reidar B. Bratvold at the University of Stavanger and the co-supervisor, Dr. Hanea Remus, Lead Scientist at Equinor. It was funded by the DIGIRES from October 2018 to October 2021.The work was conducted mainly at the University of Stavanger.

This work intends to illustrate and discuss the implementation of data-driven decision techniques to manage geological and petrophysical uncertainties for supporting decision making process in the context of reservoir management.

I believe that this work will be of great interest to both managers and engineers in oil and gas companies and to researchers at academic and research institutes, who are engaged in improving the quality of oil and gas operation related decisions.

Amine Tadjer
Stavanger, May 2021.

Abstract

Reservoir Management (RM) is defined as the utilization of available technology, financial assets, and human resources to maximize the economic recovery of a reservoir. This type of management involves a series of operations and decisions, from the initial stage of the discovery of a reservoir to the final stage of field abandonment. Thus, RM is a decision-oriented activity, for which Decision Analysis (DA) will add value. Indeed, decisions are the only means we have to create value. DA is an approach intended to provide clarity of action on the decisions which we focus our attention. Due to the inherent uncertainty in the outcomes from our decisions, good decisions can have bad or good outcomes. A good decision is logically consistent with alternatives, information, and preferences available at the time the decision is made. The most challenging phenomenon we face in decision making is uncertainty. Uncertainty is inseparable from all significant decisions. Hence, clear thinking about uncertainty is a requirement for making good decisions. Although the oil and gas industry has long been aware of the importance of uncertainty understanding and management, data-driven decision approaches that include consistent uncertainty quantifications are not commonly or comprehensively used.

This dissertation address three of the main challenges commonly encountered in reservoir management: production forecasting, uncertainty quantification for history matching problems and sequential decision making. We propose solutions to each problem that employ different algorithms of data-driven decision techniques and model-based forecast that allow a coherent integration of uncertainty and decisions.

The first challenge is addressed through illustrating and discussing the implementation of probabilistic Machine Learning (ML) techniques in decline curve analysis. Unlike decline curve models, the ML approach can be regarded as "model-free" (non-parametric) because the pre-determination of decline curve models is not required. However, the main problem of pure ML techniques is lack of stability in long-term forecasts. To solve this, we have combined the decline curve model, a recognized technology in the reservoir engineering community, that provides stable long-term forecasts in an unconventional reservoir, with neural networks to automatically adjust decline curve model's parameters. We illustrated the incorporation of Neural Ordinary Differential Equations (ODEs) with Bayesian Inference, The No-U-Turn MCMC sampler (NUTS) (Hoffman et al., 2014), which allows the prediction uncertainty of Decline Curve Analysis (DCA) to be quantified. Physics-based neural networks, which are a relatively new technique that makes it possible for physics constraints to be integrated into neural network architecture, are the foundation of this approach.

The second challenge is addressed through illustrating and discussing the implementation of two techniques in uncertainty quantification and reservoir model calibration with much-reduced simulation computation time; one relies on ML Dimensionality Reduction (DR) techniques and the other one on Bayesian Evidential Learning (BEL) framework. The ML-DR approach is based on a sequential combination of nonlinear dimensionality reduction techniques: t-Distributed Stochastic Neighbor Embedding (t-SNE), the Gaussian Process Latent Variable Model (GPLVM), and clustering K-means, along with the data assimilation method Ensemble Smoother with Multiple Data Assimilation (ES-MDA). Cluster analysis with t-SNE and GPLVM is used to reduce the number of unknown parameters and select a set of optimal reservoir models that have similar production performance to the observed data from the field. We then apply ES-MDA for data assimilation. BEL is a general data scientific

framework used to quantify uncertainty within the decision-making context. BEL relies mainly on data, model, prediction, and decision applying Bayesian inference methodologies. BEL is usually divided into six main stages: (1) Formulation and definition of the decision problem; (2) prior model definition and specification; (3) Monte Carlo simulation and falsification of the prior uncertainty models; (4) Global sensitivity; (5) Uncertainty reduction using data; (6) Posterior falsification and decision making. In step 5, one may opt for classical inversion or direct forecasting (DF). DF utilizes a combination of statistical learning techniques and the Monte-Carlo sampling method to ensure direct relationships between the data and the prediction variables. It should be noted that this method requires no completed explicit model inversions (update the model parameters). This results in it being less computationally expensive when compared to the standard inversion methods.

The third challenge is addressed the problem of making optimal decisions while considering the evolution of uncertainty (learning over time). To efficiently account for the impact of future information on optimal decisions, we have used an Approximate Dynamic Programming (ADP) approach, often described as simulation-regression method to address a significant number of decision-making problems related to RM. RM is regarded as sequential problem, as most petroleum engineers and geoscientists are used to consider the gathered information, support their future decision making, and maximize the value created by the reservoirs. However, the models for reservoir management decisions may be computationally prohibitive and intractable if the state-space which involves the number of decisions, the number of alternatives for each decision and the number of uncertainties are included. To solve this issue and provide better good RM decisions, DA is recommended due to its several advantages. Howard (1980) stated that "DA is a systematic procedure for transforming opaque decision problems into transparent decision problems through a series of transparent procedures." In the context of reservoir management, DA is used as a consistent mean for evaluating different approaches and alternatives to determine the optimal scenario to maximize the profitability of investment of any project e.g., Net Present Value (NPV). In addition, to utilize fewer computational resources, ADP, is a viable technique that can handle complex, large-scale problems and discover a near-optimal solution for intractable sequential decision making. Furthermore, we present and test the performance of several machine learning techniques to quantify geological uncertainty with the reservoir development plan and making sequential decision in the context of the Enhanced Oil Recovery (EOR) process and CO_2 storage monitoring.

This work presents several examples to demonstrate the value of applying ML and DA techniques in RM. The main contribution of the dissertation is the investigation of how ML methods can contribute to probabilistic forecasts, uncertainty quantification and sequential decision making in RM. To achieve this goal, we:

1. Show how to integrate and apply Bayesian ML for unconventional oil production forecasting to inform and support RM decision-making;
2. Illustrate and discuss how to use ML dimensionality reduction techniques to support history matching and reservoir model calibration with significant reduction in computing time;
3. Illustrate and discuss how to use the BEL framework to quantify uncertainty in the context of CO_2 storage monitoring;
4. Show how to apply simulation-regression method for EOR processes and CO_2 storage operations to maximize the value and reliability of the reservoir development plan.

We believe that this work is relevant and material in demonstrating the benefits and value creation potential of implementing DA and ML methods to support RM decisions. Although the current implementations may be somewhat simplified, they can serve as a guidance for future research attacking the challenges involved in implementations in real-world settings.

Acknowledgments

This thesis would not have been possible without the help and support from many people to whom I would like to express my sincere gratitude.
First and foremost, I would like to express my deepest gratitude to my supervisor Professor Reidar B. Bratvold for his continuous support, guidance, and motivation throughout my research journey. His highly organized way of formulating research ideas has been a source of inspiration for me. His insights, supervision and guidance have nourished my maturity both intellectually and personally. Working under his supervision is such an honor.

My sincerest thanks also go to Dr. Remus Hanea and Dr. Aojie Hong for their support, discussion, and considerable encouragement. They expanded my view on uncertainty quantification in reservoir management and helped me to mature my understanding of history matching and sequential decision-making framework.

I gratefully acknowledge the financial support of financial support from the Research Council of Norway through the Petromaks-2 project DIGIRES (RCN no. 280473) and the industrial partners AkerBP, Wintershall DEA, ENI, Petrobras, Equinor, Lundin, and Neptune Energy.

I am thankful to those in DIGRES and Data and Decision Analysis group for all the thought-provoking discussions. The collaborations have been very constructive and fruitful for shaping my research ideas. It is also my pleasure to wholeheartedly pay a tribute to Daniel Busby. I am forever indebted for his support and advice and for entrusting me with valuable data analytics internship opportunities within TOTAL, from which I learned immensely.

My life in Norway has been blessed with friends who have always been supportive and inspiring. I am deeply appreciative to have met them.

Last but not least, I would like to thank my family, whom I owe my deepest gratitude to. They have provided me with their unequivocal love and support such that my mere expressions of thanks would not sufficiently express my appreciation. This thesis is dedicated to the memory of my grandfather, Said Tadjer, who was my first teacher and who had always inspired me to pursue higher studies.

Finally, I would like to thank everybody essential to the successful realization of this dissertation. I also would like to apologize that I could not personally mention all the names.

Amine Tadjer

List of Papers

Paper I: Machine Learning based Decline Curve Analysis for Short-Term Oil Production Forecast.
Amine Tadjer, Aojie Hong and Reidar B. Bratvold.
Published in Energy Exploration & Exploitation.
https://doi.org/10.1177/01445987211011784

Paper II: Bayesian Deep DCA: A New Approach for Well Oil Production Modeling and Forecasting.
Amine Tadjer, Reidar B. Bratvold and Aojie Hong.
Published in SPE Reservoir Evaluation & Engineering 2022.
https://doi.org/10.2118/209616-PA

Paper III: Managing Uncertainty in Geological CO_2 Storage using Bayesian Evidential Learning.
Amine Tadjer and Reidar B. Bratvold.
Published in Energies 2021, 14, 1557. https://doi.org/10.3390/en14061557

Paper IV: Efficient Dimensionality Reduction Methods in Reservoir History Matching.
Amine Tadjer, Reidar B. Bratvold and Remus Hanea.
Published in Energies 2021,14(11), 3137. https://doi.org/10.3390/en14113137

Paper V: Application of Machine Learning to Assess the Value of Information in Polymer Flooding.
Amine Tadjer, Aojie Hong, Reidar B. Bratvold and Remus Hanea.
Published in Petroleum Research. https://doi.org/10.1016/j.ptlrs.2021.05.006.

Paper VI: A Sequential Decision and Data Analytics Framework for Maximizing Value and Reliability of CO_2 Storage Monitoring.
Amine Tadjer, Aojie Hong and Reidar B. Bratvold.
Published in Journal of Journal of Natural Gas Science and Engineering.
https://doi.org/10.1016/j.jngse.2021.104298

Contents

List of Figures

Abbreviation

2D/3D	Two dimensional/ Three Dimensional
ADP	Approximate Dynamic Programming
ANN	Artificial Neural Network
AR	Auto Regressive
BEL	Bayesian Evidential Learning
CLRM	Closed Loop Reservoir Management.
CRPS	Continuous Ranked Probability Score
DA	Decision Analysis
DCA	Decline Curve Analysis
DF	Direct Forecasting
DGSA	Distance-Based Generalized Sensitivity Analysis
DM	Decision Maker
DP	Dynamic Programming
DR	Dimensionality reduction
DWI	Decision With Information
DWII	Decision With Imperfect Information
DWOI	Decision Without Information
DWPI	Decision With Perfect Information
ENPV	Expected NPV
EOR	Enhanced Oil Recovery
ES-MDA	Ensemble Smoother with Multiple Data Assimilation
EUR	Estimated Ultimate Recovery
EV	Expected Value
EVWI	Expected Value With Information
EVWII	Expected Value With Imperfect Information
EVWOI	Expected Value Without Information
EVWPI	Expected Value With Perfect Information
FOPR	Field Oil Production rate
GPLVM	Gaussian Process Latent Variable Model
GRU	Gated Recurrent Unit
HMC	Hamiltonian Monte Carlo
LSM	Least-squares Monte Carlo
LSTM	Long Short-Term Memory
MC	Monte Carlo
MCMC	Markon-Chain Monte Carlo
MCS	Monte Carlo simulation
MAPE	Mean Absolute Percentage Error
ML	Machine Learning
NFD	Normalized Frequency distribution
NPV	Net Present Value
NUTS	No-U-Turn Sampler

O&G	Oil and Gas
ODE	Ordinary Differential Equation
Pan CRM	Pan's Combined Capacitance Resistance Model
PCA	Principal component analysis
PDF	Probability Density Function
PINN	Physics Informed Neural Network
PO	Production Optimization
R^2	Coefficient of Determination
RM	Reservoir Management.
RMSLE	Root Mean Squared Logarithmic Error
RNN	Recurrent Neural Network
SDP	Stochastic Dynamic Programming
SEDM	Stretched Exponential decline model
SHAP	Shapley Additive Explanations
SMD	Sequential Model Decomposition
SR	Simulation-Regression
SRDM	Sequential Reservoir-Decision-Making
TPOT	Tree-Based Pipeline Optimization Tool
t-SNE	t-distributed stochastic neighbor embedding
UQ	Uncertainty Quantification
UR	Uncertainty Reduction
USD	US Dollar
VOI	Value of information
VOPI	Value of perfect information

1 Introduction

1.1 Motivation

Reservoir management (RM) consists of decision-oriented processes in which decision makers apply their current knowledge to find optimal production strategies that maximize the value of hydrocarbon production from a reservoir. Among the many decisions that are commonly encountered in RM, three example problems are selected and solved in this dissertation: oil production forecasting, uncertainty quantification for history matching problems, and sequential decision making. The solutions to these problems will exemplify ways in which decisions and uncertainties are systematically integrated to logically and intuitively approach optimal decisions.

Production Forecasting: Accurate prediction of future reservoir performance and well production rates is important for decision support in a reservir development plan. In the absence of geological or petrophysical (physics-based) information, time-series analysis can be used to predict future performance from past data. Traditional decline curve analyses (DCAs), both deterministic and probabilistic, use physics (or empirical)-based models fitted to historical production data for production forecasting. Different decline curve models have been suggested and applied to unconventional wells, including the Arps model, stretched exponential model, Duong model, and PanCRM. However, although it may be relatively easy to set a given model's parameters through production data fitting, it is difficult to decide which model to use, as multiple models may fit the historical production equally well yet result in different forecasts. Randomly selecting a decline curve model for probabilistic DCA can underestimate the uncertainty in a production forecast (Hong et al., 2019). Thus, several studies have utilized different machine learning (ML) algorithms to conduct robust oil production forecasting for both conventional and unconventional reservoirs. ML is regarded as "model-free" and does not require pre-determination of decline curve models. In addition, ML can forecast oil production based on a given history of oil rates.

Uncertainty Quantification: Better knowledge of uncertainty reduces risk and leads to better decisions (e.g., Bratvold and Begg, 2010). Begg et al. (2014) presented a useful definition of uncertainty: Not knowing if a statement (or event) is true or false". The standard methods for quantifying uncertainty rely on a consideration of many plausible geological realizations (ensemble models) and quantification of the statistical measures for the ensemble parameters. Several oil companies are testing methods for uncertainty prediction and model conditioning (model-based approaches). Ensemble methods provide consistent probability estimates that can serve as input for probabilistic decision making. However, generating a set of posteriors properly conditioned to all historical data that preserves geological realism is a very challenging process. The limitations have been well-detailed in (Oliver et al., 2011); one issue is that due to the limited size of the ensemble, spurious correlations may be generated leading to loss of geological realism and underestimation of uncertainties (ensemble collapse).

Sequential Decision Making The oil and gas sector has long been aware of the significance of uncertainty quantification (Bratvold and Bickel 2009). However, decision analysis (DA), which utilizes consistent probabilistic methods to handle uncertainties for better decision making, is not commonplace in the industry because of technical and non-technical challenges. Thus, common assessment and decision models consider only a strategy made

upfront without considering the opportunities for later adjustment or changes within the strategy (Smith 1999). This approach is called a naïve or a single decision approach. However, the naïve approach has significant drawbacks, often undervaluing investment opportunities leading to myopic decisions. In addition, a significant number of decision-making problems related to RM are regarded as sequential problems, as most petroleum engineers and geoscientists consider the information gathered, support their future decision making, and maximize the value created by the reservoirs. However, the models for RM decisions may be computationally prohibitive and intractable if several sequential decisions and uncertainties are involved.

This thesis aims to address these challenges, and the research objectives of this thesis are summarized as follows.

1. How can we improve short- and long-term oil production forecasts and support decision-making processes in the field development plan?
2. How can we circumvent the different challenges associated with model-based approaches without a loss of fidelity in the results?
3. How can the curse of dimensionality arising in sequential RM decision making be overcome?

1.2 Research Goals

Value can only be created through high-quality decision making, which in turn relies on high-quality uncertainty assessment. Our objective is to demonstrate the usefulness of novel and different data-driven decision methods in creating value by supporting decision making in complex and uncertain environments for reservoir management. To pursue this objective, we develop a framework that investigates the following problems:

1. The implementation of probabilistic ML and physics-guided ML predictive models for robust production forecasting, with a focus on integrating and accounting for model uncertainty in probabilistic decline curve analysis for unconventional oil production forecasting (Paper I and II).

2. The implementation of dimensionality reduction techniques and Bayesian evidential learning with a focus on how to speed up the process of reservoir calibration and uncertainty quantification in the history matching process while preserving the geological realism (Paper III and VI).

3. The implementation of the simulation-regression method and value of information concept to provide fast analysis and decision information in the context of polymer flooding and CO_2 storage monitoring (Paper V and IV).

2 Scientific Background

This chapter gives an overview of scientific background relevant for this thesis.

2.1 Introduction to Machine Learning

Machine learning has recently played a vital multidisciplinary role in various fields of science like pharmacology (Kadurin et al., 2017), medicine (Shen et al., 2017), chemistry (Schutt et al., 2017), and biology (Ching et al., 2018). In particular, one method that has been widely applied is the deep neural network. Machine learning (ML) is defined as an aspect of applied statistics that focuses on developing computational models based on pattern recognition and inference rather than explicit sets of rules. It is commonly considered as a subfield of artificial intelligence (AI), where Turing (1950) is seen as the first to introduce the concept of AI. The term "Machine Learning" was coined by Samuel (1959) whereas Mitchell et al. (1997) provided a widely-accepted definition:

> "*A computer program is said to learn from experience E with respect to some class of tasks T and performance measure P if its performance at tasks in T, as measured by P, improves with experience E.*"
>
> Mitchell et al. (1997)

This implies that a ML model is defined by a combination of tasks. A task such as, classification, regression, or clustering is improved by conditioning of the model on a training data set. The model's performance is calculated in terms of a loss, also known as metric, which numerically estimates how a machine learning model performs on the given data. This would be measured, in regression, as the data's misfit from the expected values. The ML model usually improves when it is exposed to more data sets. A good model can eventually be applied to new data, which was not included in the training set.

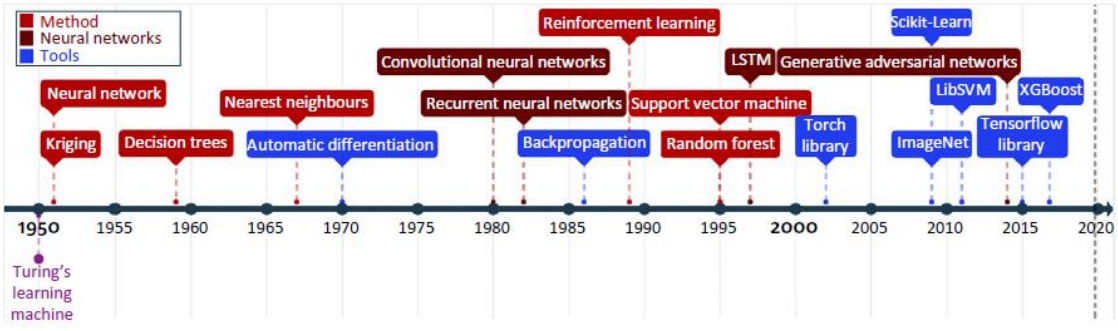

Figure 2.1— Machine learning timeline, adopted from Dramsch (2019).

As seen in **Figure 2.1**, a lot has changed between 1950 and 2020. Following the development of different specialized hardware, ML and AI became an area of great interest in the 1980s.

While neural networks were introduced in 1950. Given the enormous availability of computational resources these days, major companies (Google, Facebook, Microsoft, and Amazon) have made high-quality ML software easily accessible (Tensorflow, Pytorch, CNTKb, Mxnet). In addition, to independent developments xgboost (Chen & Guestrin, 2016) and scikit-learn (Pedregosa et al., 2011).

ML algorithms can be classified into 4 major categories, as displayed in **Figure 2.2**. In supervised learning tasks, such as prediction and classification, the goal is to learn a general model based on known (labeled) examples of the target pattern. Unsupervised learning differs from supervised learning, mostly it does not require manually labeled data. Instead, it learns structure in the data, such as sparse or low-dimensional feature representations. Other classes of ML tasks include semi-supervised learning, in which both labeled and unlabeled data are available to the learning algorithm, and reinforcement learning, in which uses trial and error to constantly train itself.

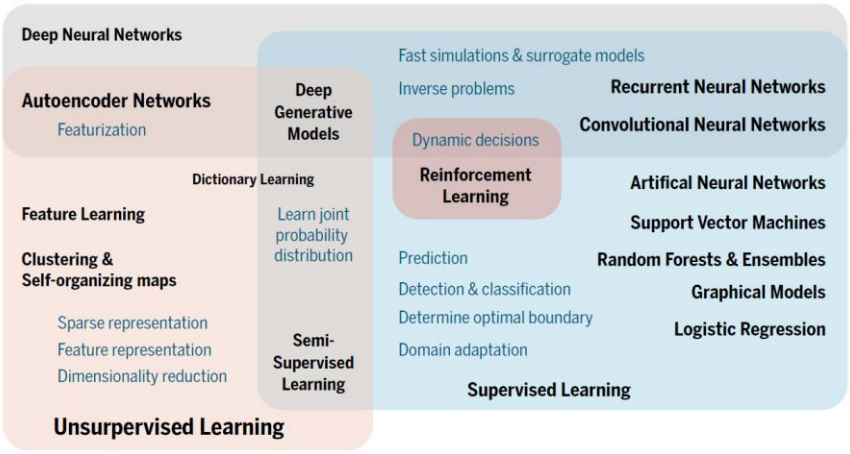

Figure 2.2 — Different Categories of Machine Learning Techniques.

2.2 Hydrocarbon Production forecasting.

Hydrocarbon production forecasting includes the estimation of the ultimate recoveries and the lifetimes of wells, which are material factors for decision-making in the oil and gas industry because they can significantly impact economic evaluation and field development planning. Although mathematically richer forecasting models (e.g., grid-based reservoir simulation models) have been developed over the past few decades, decline curve analysis (DCA) is still widely used because of its speed and simplicity; mathematical formulations of DCA models are simple with only a few parameters, and only production data are required to calibrate these parameters. The Arps model (Arps 1945) has been used for DCA for more than 60 years and has been proven to perform well for conventional reservoirs. However, because of the complexity of flow behavior in unconventional reservoirs, where several flow regimes are involved (Adekoya, 2009; Nelson, 2009; Joshi, 2012), the Arps model may not be ideal, and many other alternative DCA models have been proposed (e.g., the stretched exponential decline model (SEDM) (Valko and Lee, 2010), Duong model (Duong 2011), and combined capacitance-resistance model proposed by Pan (Pan 2016)). However, there are still

conceptual challenges associated with applying DCA methods (Arps, Duong, SEDM, PanCRM, etc.), as the results obtained lead to a deterministic forecast, and it is obvious that a single model should not be trusted 100%. In addition, the reserve estimation for Securities and Exchange Commission (SEC) is declared based on the P90 probability (Busby 2020), and there is no standard rule on how to perform proper uncertainty quantification.
Lately, several researchers have discussed the application of machine learning (ML) for oil production forecasting (Shelley et al. 2012; Lafollette et al. 2012; Newgord et al. 2015; Schuetter et al. 2015; Lolon et al. 2016; Mohaghegh et al. 2017; Tian et al. 2017; Lee et al. 2019; Han et al. 2020; Liao et al. 2020; Mehana et al. 2021). Nevertheless, although several ML and deep learning models have been proposed to better address multiple seasonal patterns in oil production data (Luo et al. 2019; Liao et al. 2020), the main problem of ML techniques concerns their lack of stability in long-term forecasts and occurrences of nonphysical results; as a result, reservoir engineers often do not trust the technology (Busby 2020).

2.3 Uncertainty Quantification in Reservoir Management

The standard methods for quantifying uncertainty consider an ensemble of models and statistical measures of the uncertain parameters. Performing high-resolution simulations on all members of a large ensemble can quickly become computationally intractable. This problem can be solved either by reducing the ensemble size or by speeding up the simulation for each geomodel realization. For this purpose, assisted history matching (AHM) built on ensemble-based analyses such as the ensemble smoother (ES) and ensemble Kalman filter (EnKF) are useful in estimating models that preserve geological realism and have predictive capabilities. However, these methods tend to be computationally demanding, as they require a large ensemble size for stable convergence. The limitations have been well detailed in Olivier et al. (2011), one of which is that using a limited ensemble size results in sampling errors and spurious correlations. Such spurious correlations might lead to unphysical updates of the model's uncertain parameters and contribute to the underestimation of the ensemble variance. Lately, several researchers have discussed the application of machine learning dimensionality reduction techniques for data assimilation. For instance, Vo and Durlofsky (2014) used principal component analysis (PCA) to reparametrize high dimension data into low dimensional space, then regenerated new realizations based on principal parameters from PCA for data assimilation, while others have used singular value decomposition (Rezaie et al., 2012) and Kernel PCA (KPCA) (Sarma et al., 2008). Muzammil. H et al. (2019) applied PCA to account for the model-error component during model calibration. Kang et al. (2017) and Kang et al. (2019) also introduced PCA to select suitable models for EnKF. Tolstukhin et al. 2019 demonstrated how data analytics can improve efficiency of ensemble history matching by analyzing the statistics that link the static model ensemble and the dynamic model ensemble update. Dimensionality reduction techniques such as PCA and SVD, however, are linear approaches that may not accurately represent the relationship between high dimensional parameters and latent variables in reduced space, which likely lead to poor performance of model assimilation and prediction. Recently, several approaches have demonstrated that it is possible to provide the outcomes of subsurface models without model updating and solving the inverse problem. In this context, (Scheidt et al., 2015) and (Satija et al., 2015) introduced a new framework for making decisions under uncertainty called Bayesian evidential learning (BEL). BEL is a general data scientific framework used to design uncertainty quantification within the decision-making context. Based on the description provided in (Scheidt et al.,

2018), it can be said that BEL relies mainly on data, models, predictions, and decisions under the scientific methodologies and philosophy of Bayesianism. The data are used as evidence to infer model or/and prediction hypotheses via "learning" from the prior distributions, whereas decision-making is ultimately informed by the model and prediction hypotheses. BEL is usually divided into six main stages (Yin et. al., 2020): (1) Formulation and definition of the decision problem; (2) prior model definition and specification; (3) Monte Carlo simulation and falsification of the prior uncertainty models; (4) Global sensitivity; (5) Uncertainty reduction using data;(6) Posterior falsification and decision making. In step 5, one may opt for classical inversion or direct forecasting (DF). The main steps involved in DF are as follows (Satija and Caers, 2017):

1. Monte Carlo: N samples are generated from the prior for both the global and spatial model variables.
2. Forward functions: data and prediction variables are evaluated using the reservoir simulators model.
3. Orthogonality: PCA is conducted on data and prediction variables.
4. Linearization: canonical correlation analysis (CCA) is conducted to maximize linear correlation between data and the prediction variables
5. Bayes-linear-Gaussian: conditional mean and covariance of transformed prediction variables are calculated.
6. Sampling: samples are drawn from the posterior distribution of transformed prediction variables
7. Reconstruction: inversion is performed for all bijective operations.

2.4 Sequential Decision Making

In reservoir management, two different approaches are used to include the impact of information: closed-loop reservoir management (CLRM) and sequential reservoir decision making (SRDM). These approaches serve as a priori analyses, and each technique is implemented before the collection of additional information. Thus, whenever additional data are gathered, both CLRM and SRDM can be readily applied to make use of these data. However, for a complicated decision-making problem with many uncertain outcomes, alternatives, and decision points, these approaches suffer from the "curse of dimensionality." To resolve these issues and provide solutions that are less computationally demanding, we instead make use of a viable alternative called approximate dynamic programming (ADP), which is often described as a simulation-regression method, a powerful solution technique that can handle complex, large-scale problems and determine a near-optimal solution for intractable sequential decision making.

2.4.1 Closed Loop Reservoir Management (CLRM)

A common practice within the industry to develop and manage an oil field is to apply the closed-loop reservoir management (CLRM) workflow, as displayed in Fig 2.3. This method introduced the mechanism of model-based optimization in tandem with the assimilation of data to maximize value creation from a reservoir over the lifetime of production (Jansen et al., 2009).

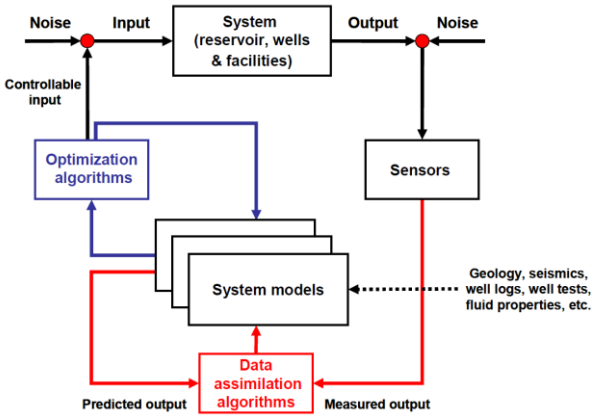

Figure 2.3 — Key elements of CLRM, adopted from Jansen et al. (2009).

Figure 2.3 illustrates the mechanism of CLRM, which comprises two fundamental steps. The first step consists of history matching (inverse problem) in which data is assimilated, and the second step involves robust optimization, where control parameters are adjusted based on the history-matched model (updated model) to optimize production. In addition, this approach gets its name "closed-loop" because it tends to follow a loop strategy: each time new data is collected, the reservoir or production model is updated, and reservoir performance optimization is carried out. Repeating the process keeps the reservoir model up to date.

(Hong et al., 2018) discussed the general framework of the CLRM approach and argued that CLRM belongs to the myopic or naïve decision policy class as future uncertainties and decisions are not integrated in the process; only uncertainties and decisions associated with currently available data are considered.

The myopic formulation is clearly represented by using a schematic decision tree, as illustrated in Figure 2.4, where D_k refers to decisions made at t_k and U_k denotes the uncertainties associated with the ongoing available data until t_k. U_k is usually represented by a production model with many geological realizations. The production strategy $D_k, D_{k+1}, \dots, D_{end}$ is determined by considering only the immediately relevant U_k.

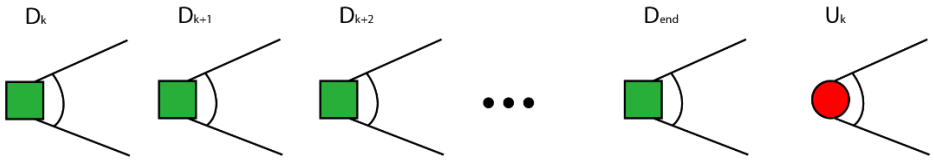

Figure 2.4 — Decision-tree representation of CLRM.

Although the CLRM approach considerably simplifies the structure of reservoir management decisions with reduced computational time, it does not reflect the full structure of a reservoir management decision problem, as it only considers the effect of the information obtained before a decision is made and not later information, and thus may lead to a suboptimal production strategy.

2.4.2 Sequential Reservoir-Decision-Making (SRDM).

Unlike CLRM, SRDM represents the full learning and decision structure of reservoir management. It is a look-ahead policy because it solves a sequential decision-making problem based on both previous and future information. To illustrate the framework of

SRDM, the decision trees are displayed in **Figure 2.5**. As can be observed, it explicitly considers all possible information or data to yield an optimal policy.

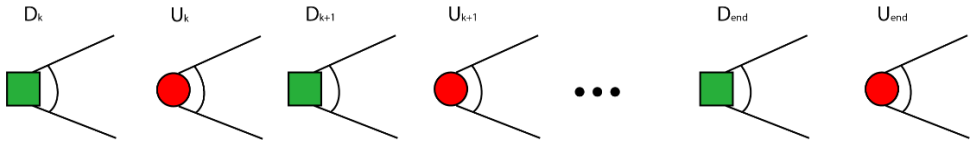

Figure 2.5 — Illustration of Decision tree of SRDM.

SRDM explicitly considers both the uncertainties associated with currently available data and information (U_k) and those with future data and information ($U_{k+1}, \dots, U_{end}$). Therefore, the current decision (D_k) depends on both the uncertainties that a decision maker has made at time t_k and the uncertainties that the decision maker will make at times $t_{k+1}, \dots, t_{end}$. In addition, the responses corresponding to the decision nodes at different points of time are also integrated ($D_{k+1}, \dots, D_{end}$). The optimal decision policy corresponding to SRDM can also be solved by rolling back the decision tree. However, SRDM can be computationally intensive or prohibitive.

2.4.3 Stochastics Dynamic Programming.

Dynamic programming (DP) is an optimization algorithm that is used to support multistage, interrelated decisions. DP approaches commonly break decisions into smaller problems, which are called decision stages. These subproblems are then solved and stored to avoid recalculating the solutions when exact subproblems occur. Multiple possible outcomes, called states, exist at each decision stage.

In stochastic dynamic programming (SDP) problems, the state at the next decision stage cannot be completely determined by the state and decision policy at the current stage, and a probability distribution is used instead. The optimal solution for an overall problem can be determined by recursively solving the subproblems. The basic structure of the SDP problem is illustrated in **Figure 2.6.**

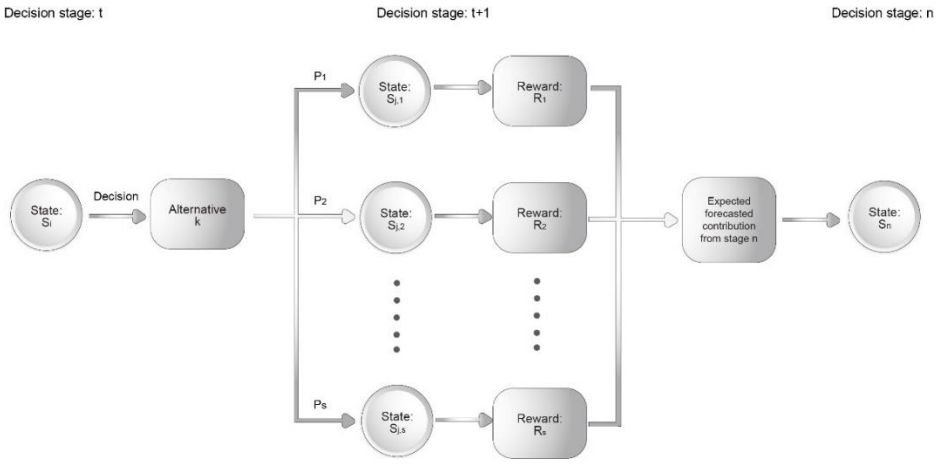

Figure 2.6 — Basic structure of SDP problem.

.

2.4.4 Simulation-Regression

Simulation-regression (SR) methods are often described as approximate dynamic programming or least square Monte Carlo (LSM) (Longstaff, 2001) algorithms that approximate the conditional future value of an alternative by regression. They do not suffer from the "curse of dimensionality" induced by uncertainties. The computational time for the SR increases linearly with the computational time of the chosen production model and the number of decision points, and exponentially with the number of alternatives. Therefore, SR is effective for solving an SRDM problem with a computationally attractive production model and a limited number of alternatives. The SR method involves a Monte Carlo simulation (MCS) for forward modeling and regression for (approximately) calculating the conditional expected value given data and information at any point in time.

MCS. Many possible realizations of state variables (x^b) such as porosity and permeability, are generated based on the Monte Carlo simulation model. Forward modeling is performed to generate the corresponding samples ($y^b = f(x^b)$), and net present value (NPV) $NPV_a^b = NPV(\mathrm{x}^\mathrm{b}, a)$ for each decision alternative a.

Backward Regression. Starting recursively from the last decision point in time, in order to estimate the expected NPV (ENPV) with alternative a conditional on the modeled sampling data, $ENPV\ (x;\ a)|y$, we regress $NPV(\mathrm{x}^\mathrm{b}, a)$ on the modeled sampled data. This procedure is repeated for each alternative. The optimal decision is then determined by choosing the alternative that achieves the highest value of the conditional ENPV, given the known information.

Various methods (linear or non-linear) can be used for regression to calculate the conditional ENPV. The choice of regression method depends mainly on the dimensionality and type of data.

2.4.5 Value of Information Analysis (VOI)

VOI in any information-gathering activity depends on two fundamental uncertainties: (1) the uncertainties we hope to learn about but cannot directly observe; these constitute "events of interest," and (2) the test results referred to as observable distinctions (Bratvold et al., 2009). In reservoir management, the data gathered until time t when a decision is made is the observable distinction, and predictions after time t comprise the events of interest. We denote the observable distinction as x. Since x has a very large number of dimensions, it is difficult to represent the distribution of x in an analytical form, and we usually approximate it with the help of Monte Carlo sampling.

In terms of a risk-neutral decision-maker, VOI is defined as follows:

$$\mathbf{VOI} = \left[\begin{matrix}\textbf{Expected value with}\\ \textbf{additional information}\end{matrix}\right] - \left[\begin{matrix}\textbf{Expected value without}\\ \textbf{additional information}\end{matrix}\right]$$

In mathematical form,

$$\boldsymbol{VOI} = \boldsymbol{max}\{\mathbf{0}, \Delta\}$$
$$\Delta = \mathbf{E\,VWI} - \mathbf{EVWO}$$

where EVWI is the expected value with additional information, and EVWO is the expected value without additional information. The lower limit of VOI is always 0, since if Δ is negative when EVWOI > EVWI, the decision-maker can always choose not to gather information.

In a decision-making context, the decision without information (DWOI) is an alternative that optimizes the expected value (EV) over the prior value, and EVWOI is the optimal EV over the prior.

$$\mathbf{EVWOI} = \boldsymbol{max}_{\boldsymbol{a}\in\boldsymbol{A}}\left[\int_{\boldsymbol{x}} \boldsymbol{v}(\boldsymbol{x},\boldsymbol{a})\boldsymbol{p}(\boldsymbol{x})\boldsymbol{dx}\right] \approx \boldsymbol{max}_{\boldsymbol{a}\in\boldsymbol{A}}\left[\frac{\mathbf{1}}{\boldsymbol{b}}\sum_{\boldsymbol{b}=\mathbf{1}}^{\boldsymbol{B}} \boldsymbol{v}\left(\boldsymbol{x}^{\boldsymbol{b}},\boldsymbol{a}\right)\right] \ldots\ldots\ldots\ldots (\mathbf{2.1})$$

Here a is the decision alternative from the a set of A, x represents the distinctions of interests, $v(x, b)$ is the value function that assigns a value to each alternative outcome pair for a given x and realization b, and $p(x)$ is the prior probability distribution of x. Similarly, if we have perfect information regarding the value of x that the distinction of interests would take, we will choose the optimal action for that value of x. The decision with imperfect information (DWII) is an alternative that optimizes the expected value over the posterior value:

$$\boldsymbol{EVWI} = \int \boldsymbol{max}_{\boldsymbol{a}\in\boldsymbol{A}}\left[\boldsymbol{E}[\boldsymbol{v}(\boldsymbol{x},\boldsymbol{a})|\boldsymbol{y}]\boldsymbol{p}(\boldsymbol{y})\boldsymbol{dy}\right] \approx \frac{\mathbf{1}}{\boldsymbol{b}}\sum_{\boldsymbol{b}=\mathbf{1}}^{\boldsymbol{B}} \boldsymbol{max}_{\boldsymbol{a}\in\boldsymbol{A}}\boldsymbol{E}[\boldsymbol{v}\left(\boldsymbol{x}^{\boldsymbol{b}},\boldsymbol{a}\right)|\boldsymbol{y}^{\boldsymbol{b}}] \ldots . (\mathbf{2.2})$$

Where $p(y)$ is the marginal probability distribution over y.

Additionally, the decision with perfect information (DWPI) can also be determined in this decision-making context. For instance, in reservoir engineering, perfect information reveals the true reservoir properties and impacts of the recovery mechanism. Taking the EOR initiation problem as an example, the EV with perfect information (EVWPI) is the maximum NPV for every path based on prior realizations or distributions. Averaging these NPVs over the paths would result in EVWPI. In this way, every path would involve an optimal decision with perfect information. The difference between EVWPI and EVWOI is the value of perfect information (VOPI).

3 Summary and implication of papers.

This chapter presents a summary of the six papers of this thesis that have been published in a peer-reviewed journal paper.

3.1 Paper I: Machine Learning Based Decline Curve Analysis for Short-Term Oil Production Forecast

This study introduces a data-driven approach for performing short-term predictions of unconventional oil production. Two state-of-the-art models, DeepAR and Prophet time series analysis, were tested on petroleum production data, as these two models outperform other forecasting methods for many problems (David et al., 2019, Sean and Benjamin, 2007). Deep AR is a generative autoregressive model. It consists of a recurrent neural network (RNN) using long short-term memory (LSTM) or gated recurrent unit (GRU) (Kyunghyun et al., 2014) cells, which takes the previous time points and covariates as input. Unlike other forecasting methods, DeepAR jointly learns from every time series. Prophet forecasting is a Bayesian nonlinear univariate generative model for time-series forecasting, which was developed by the Facebook Research team (Sean and Benjamin 2007) for the purpose of creating high-quality multistep-ahead forecasting. This model addresses the following difficulties common to many types of time series forecasting and modeling: seasonal effects caused by human behavior: weekly, monthly, and yearly cycles, dips and peaks on public holidays, changes in trends due to new products and market events, and outliers. Compared with the traditional approach using decline curve models, the machine learning approach can be regarded as “model-free” (non-parametric) because the pre-determination of decline curve models is not required. This work aims to develop and apply neural networks and time series techniques to oil well data without having substantial knowledge regarding the extraction process or physical relationship between the geological and dynamic parameters. The proposed method was applied to a selected Midland field well from the USA. We selected 22 Midland wells with relatively smooth data, which indicated fewer significant operational changes. The selected Midland wells, which were located in a naturally fractured reservoirs, were completed and measured monthly. However, there are some missing measurements (i.e., no recorded values) for a few months for each selected well. We ignored these missing values. Some measurements have recorded zero values, and we suspect that they indicate a temporary shut-down for operations (e.g., a workover). The zero values may interfere with the training process, so we removed them from the data, and then the datasets were rescaled with standardization. Standardization is included in deep learning to improve the convergence of neural networks.

Figure 3.1 demonstrates the forecast results for some selected wells using DeepAR; the means of forecasts (dashed steel blue curve) are compared to blind-test data (dashed red curve) and the Pan CRM model (black line curve). In general, the production forecast seems to be reasonable, as the DeepAR model can forecast both the upward and downward trends well and outperform the Pan CRM model, and it is observed that the prediction intervals mostly contain the correct values, except for well-ID11, which may be explained by the inability to predict when production changes occur. We quantify the accuracy of the probabilistic forecast using the mean continuous ranked probability score (CRPS), which is a

quadratic measure of the difference between the forecast cumulative distribution function (CDF) and the empirical CDF of the observation (Hersbach, 2000). Higher values of mean CRPS indicate less accurate results. The mathematical formulation of the mean CRPS is presented in **Paper I**.

Figure 3.2 shows forecasts from the trained Prophet models. The means of forecasts (the dashed Steel blue curve) follow the blind-test data (dashed red curve in **Figure 3.2**) generally well. The P5-P95 prediction intervals (grey band in **Figure 3.2**) covers most of the blind-test data. However, for Well-ID8, the forecast significantly deviates from blind-test data and fails to capture both trends and the peaks and troughs reasonably; more specifically, the forecast underestimates the oil production rates.

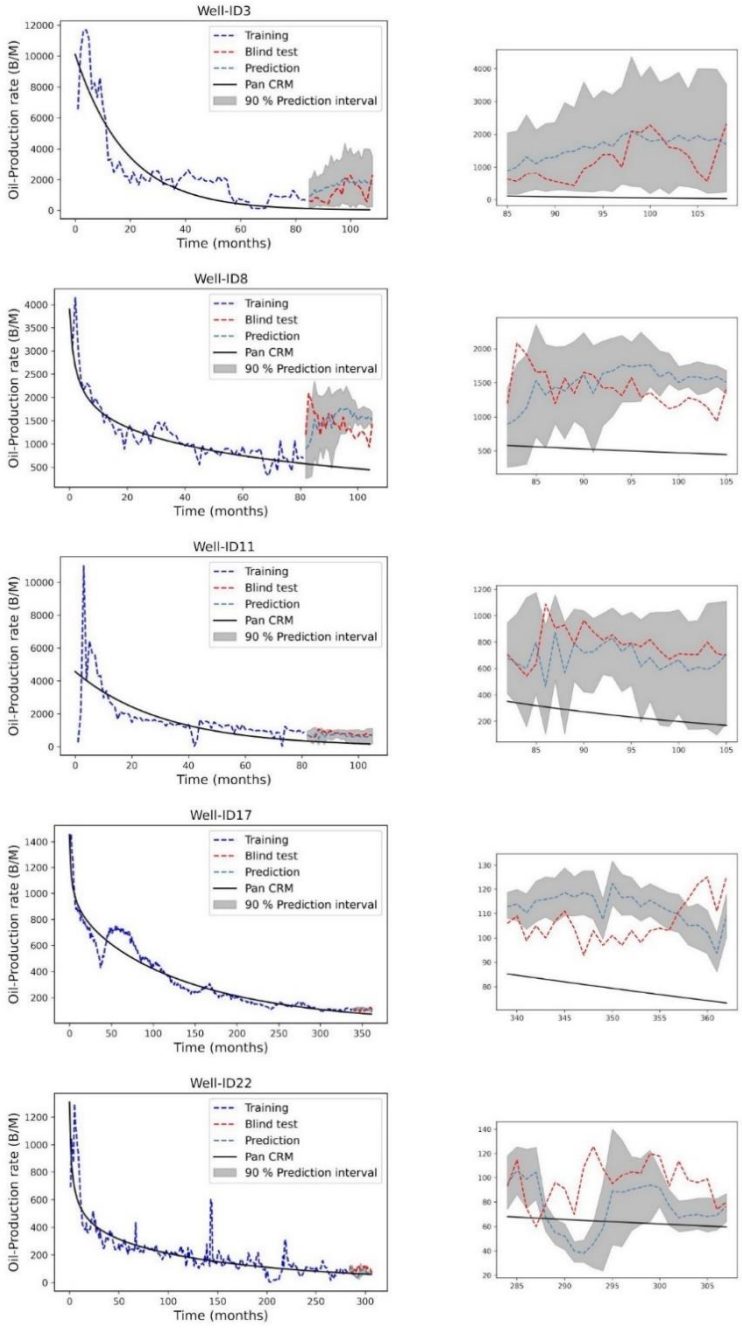

Figure 3.1— Oil production time series forecast- DeepAR. Left: Overview of forecast. Right: zoomed forecast.

Compared to Prophet, the DeepAR models represent distinct trends in the mean CRPS score, as listed in **Table 3.1**. This is possibly due to the DeepAR layer's capacity to "memorize" long-term patterns. In contrast, Prophet's predictions rely primarily on the pattern of most previous historical data. In addition, the lowest CRPS errors occurred for DeepAR. Simultaneously, the difference in values is minimal, even though this statement is only valid for the 5-th and 95-th percentiles. This is demonstrated by the better coverage earned by the longer periods that compensate for the 50-th percentile's low accuracy.

Well ID	**3**	**5**	**8**	**9**	**11**	**14**	**15**	**16**	**17**	**18**	**20**
Mean CRPS	69	29.15	74	93.5	80.9	15.25	7.89	19.17	9.91	12.01	15.18
Well ID	**21**	**22**	**72**	**142**	**156**	**157**	**171**	**181**	**206**	**249**	**524**
Mean CRPS	23.18	22.14	8.35	27.29	3.47	10.50	21.67	21.37	19.69	27.80	29.91

Table 3.1 -Mean CRPS of probabilistic forecast from DeepAR model.

Well ID	**3**	**5**	**8**	**9**	**11**	**14**	**15**	**16**	**17**	**18**	**20**
Mean CRPS	63.40	29.15	174	153.5	180.9	22.83	14.45	32.06	9.41	16.45	25.73
Well ID	**21**	**22**	**72**	**142**	**156**	**157**	**171**	**181**	**206**	**249**	**524**
Mean CRPS	38.21	33.06	14.55	34.27	13.42	14.20	24.65	27.24	18.39	28.63	36.21

Table 3.2 – Mean CRPS of probabilistic forecast from Prophet model for each well.

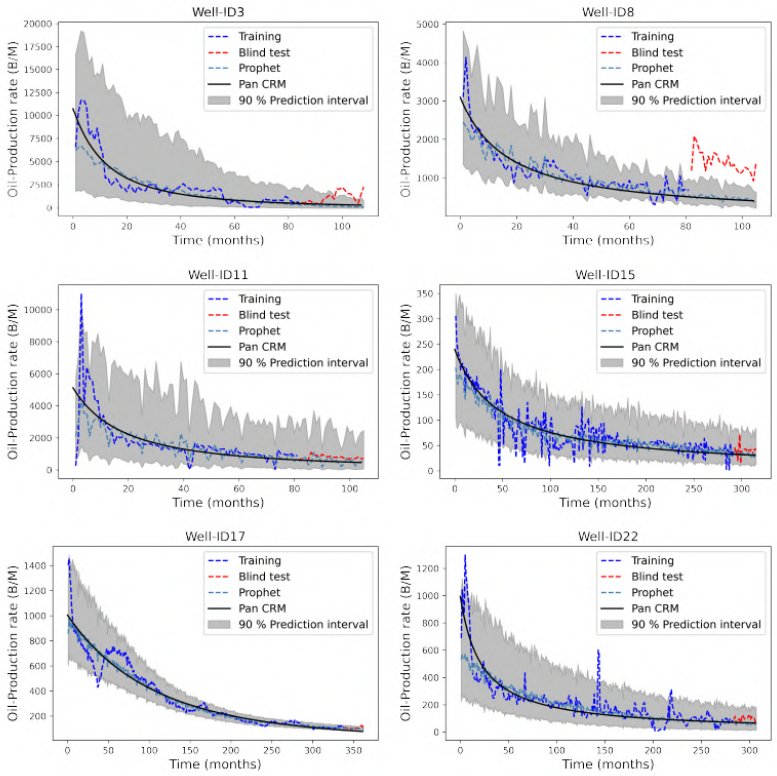

Figure 3.2 — Oil production time series forecast- Prophet.

Limitation. In the previous example, we presented DeepAR and Prophet's results for a forecast horizon of 24 months (2 years). We evaluated the performance of the two methods for a forecast horizon of 48 months, as displayed in both **Figure 3.3** and **3.4**, and it can be clearly seen that the two methods exhibited quite similar performance when the length of wells was more than 300. For the most part, they captured the trends of oil production rate in blind tests, and the predictions yielded by each of the models appear to be quite similar. The models were good at predicting trends and flat lines, but sometimes undershot/overshot the peaks and troughs, as seen, for example, for Well-ID8. However, both Prophet and DeepAR did not match production data, including uncertainty quantification, with a small historical data length. Based on the previous results, we can highlight that the two methods enrich the family of time series analysis models by extracting the weighted differencing/trend feature and contribute to better performance in short-term oil production forecasts; they can thus be an alternative for oil production forecasting in practical applications.

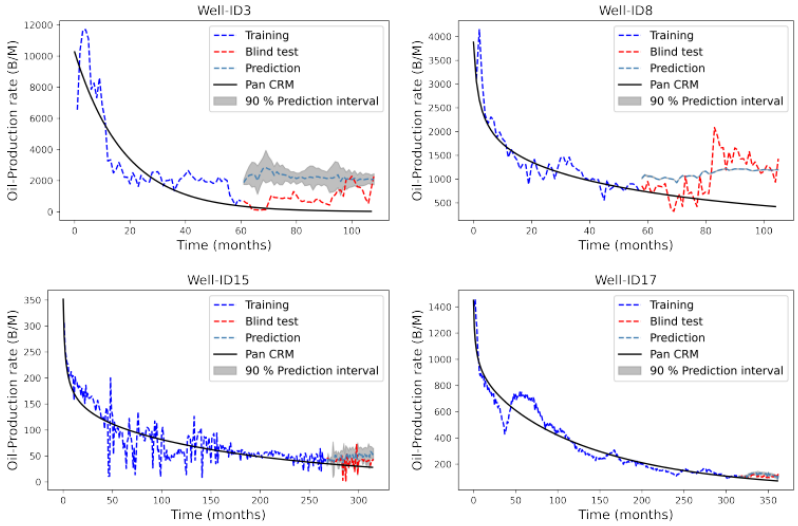

Figure 3.3 — Oil production time series forecast- DeepAR - 48 months horizon forecast.

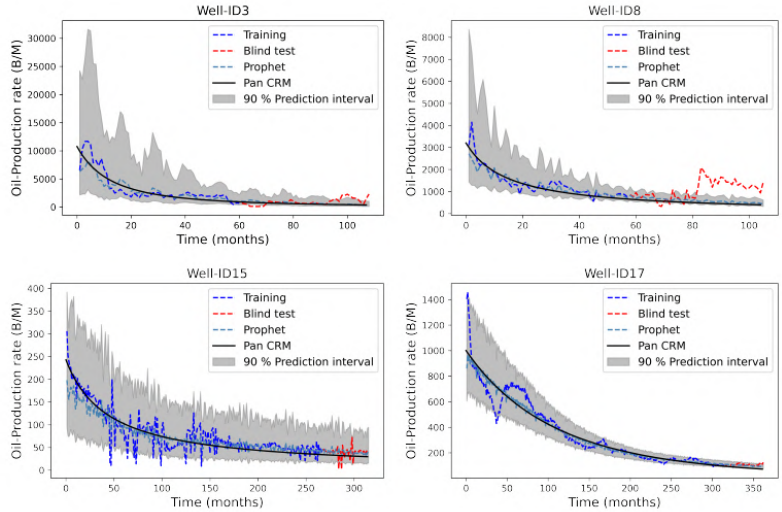

Figure 3.4 — Oil production time series forecast- Prophet - 48 months horizon forecast.

3.2 Paper II: Bayesian Deep DCA: A New Approach for Well Oil Production Modeling and Forecasting

This paper presents a simple and intuitive method for improving the long-term forecasting of unconventional oil production. A novel framework is proposed to automatize the decline curve analysis (DCA) calculation robustly and to predict oil production using the state-of-the-art Bayesian neural ordinary differential equation (BN-ODE), which is a powerful method that can be used to model physical simulations, even when the ODEs that govern the system are not explicitly defined. The novelties of the proposed approach are: (1) it combines an automatic ML method for supervised learning and a BN-ODE framework for time-series modeling, (2) it uses the decline curve analysis (DCA) model (Duong, SEMD and PanCRM)

to inform the BN-ODE framework of "physics" and regulate the BN-ODE forecasts, and (3) several completion parameters (such as locations, lengths, and slick water volume) of individual wells are analyzed and included as inputs for model building, in addition to measured oil production rate data. Specifically, the automatic ML method is first used to model the relationship between the well completion parameters and the DCA parameters, and the BN-ODE framework was then used to model the relationship between the DCA parameters and the time-series oil production rates.

This study used data from oil wells in the Bakken shale formation. The Bakken shale-play basins are located in western North Dakota and eastern Montana, including parts of Manitoba and Saskatchewan in the Williston Basin (Pollastroet al., 2012). Approximately 396 horizontal wells were selected for this study. The response and predictor variables are listed in Table 3.3. In addition to estimating the SEDM parameters (τ and n), Duong parameters ($m\ and\ \alpha$), and PanCRM parameters ($\Delta P, \beta, J\ and\ CP$) for existing wells, we used the Auto ML algorithm, the tree-based pipeline optimization tool (TPOT) [1](Olson and Moor, 2016), to develop a model capable of estimating the EUR and DCA parameters with given values of predictor variables (i.e., completion inputs), based on data from existing training wells (298 wells). Here, the forecast for the testing wells (98 wells) was performed using Auto-ML. The impact on the EUR and DCA parameters were investigated based on the given inputs.

Decline Model	Machine Learning Algorithms	Predictor Variables	Response Variables
SEDM **Duong Model** **PanCRM Model**	AutoML.	Initial flow rate(qi), initial water rate (wi), total proppant amount, Latitude and Longitude, Bottom Hole Latitude and Bottom Hole Longitude, Lateral length, Slick water volume, gal Gas oil ratio.	$\tau, n,$ $m, \alpha,$ $\Delta P, \beta, J, CP,$ EUR

Table 3.3 – Predictors, responses, and Machine learning algorithm

To verify the trained ML model, we compared the ML model predicted values (n, τ, and EUR) with the historical data fitted values for both the training and testing datasets. The comparison is visualized in **Figure 3.5** and **Figure 3.6**. To quantify the accuracy of the ML model, we calculated the root mean squared log error (RMSLE) and R^2 score. The RMSLE and R^2 scores of the tested model were (0.22, 63%) and (0.07, 87%) for m, and α, respectively. For τ, and n, the RMSLE and R^2 scores of the tested model are (0.17, 71%) and (0.07, 74%), respectively. For $\Delta P, \beta, J\ and\ CP$, the RMSLE and R^2 scores were (0.31, 78%), (0.78, 52%), (0.37, 62%) and (0.21, 65%) respectively. For EUR, the Auto-ML method provides the highest prediction accuracy in terms of the R^2 score and RMSLE, which

[1] The tree-based pipeline optimization tool (TPOT) optimizes various machine-learning pipeline techniques using stochastic search algorithms, such as genetic programming.

indicates that this method is an effective and useful tool for estimating the EUR in shale reservoirs. The Auto-ML method also provides good prediction accuracy for the DCA parameters.

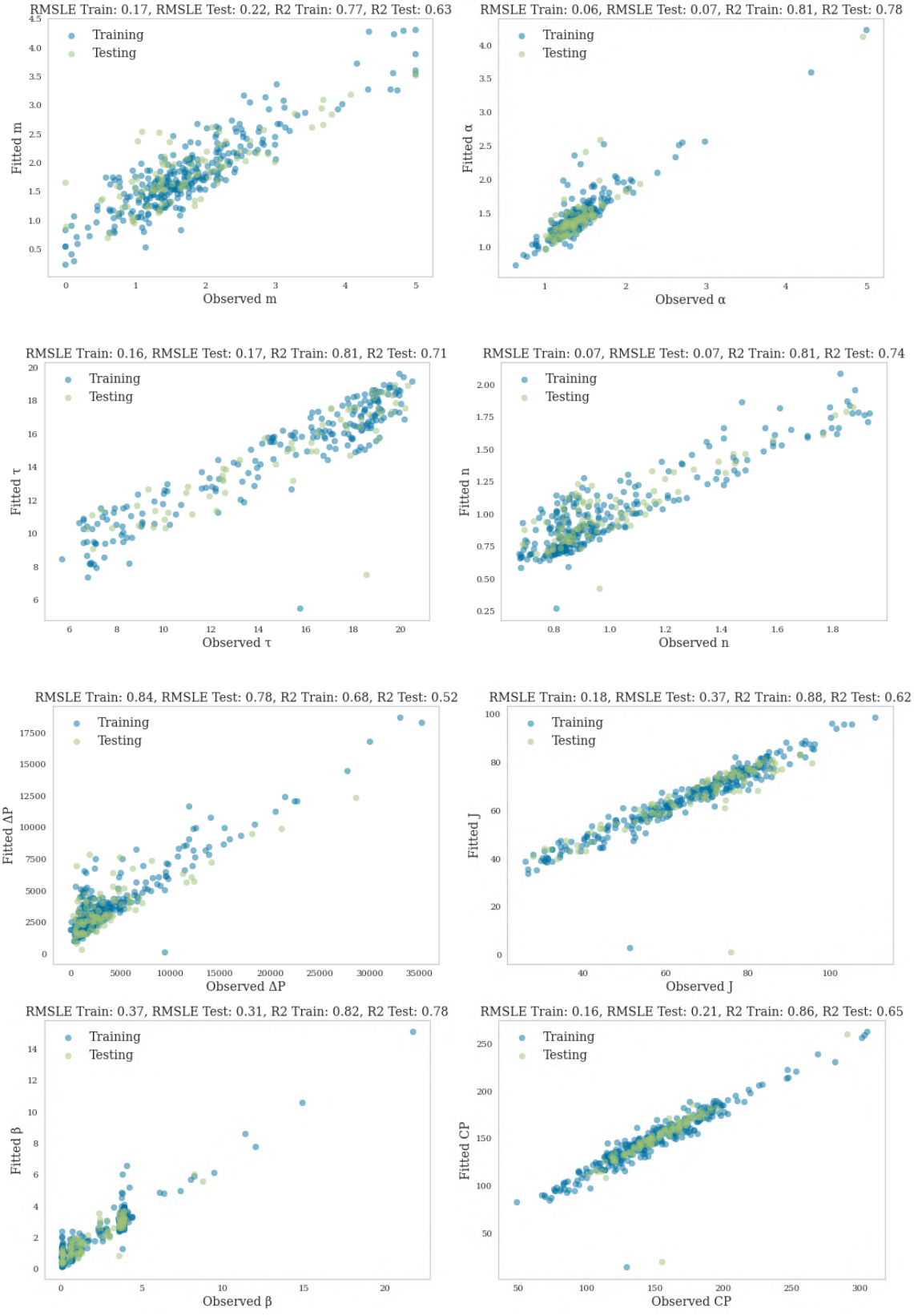

Figure 3.5 — Comparison of the ML model predicted values and the historical data fitted values for DCA parameters.

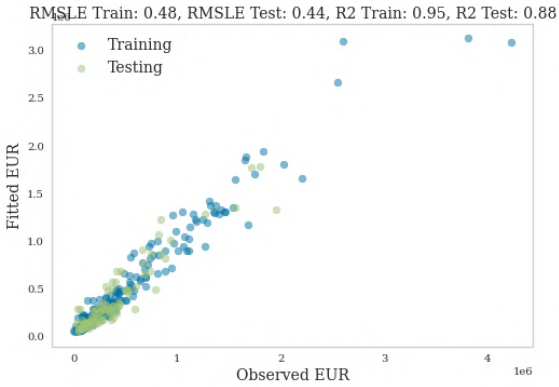

Figure 3.6 — Comparison of the ML model predicted values and the historical data fitted values for EUR.

Based on the predicted DCA parameters for SEDM (n and τ), Duong (m, α), and PanCRM ($\Delta P, \beta, J, CP$) for each well, a probabilistic forecast of the well's oil production rates can be generated using the BN-ODE framework. We collected 500 posterior samples and used the tanh activation function as the neural ODE architecture, with one layer containing 40 neurons as it provides the optimal loss performance, with a considerably better timing performance. **Figure 3.7**, **Figure 3.8** and **Figure 3.9** illustrate the probabilistic forecasts vs. the actual production rates of some wells for testing (i.e., the data of these wells are not included in the data for training the ML model). There are 298 wells for training and 98 wells for testing, but here, we show only six wells for illustration purposes. In each plot, the dark curve is the measured data of the oil production rate (which we aim to forecast) from a well for testing, the red dashed line is the fit of the DCA model (to the oil production rate data), and the blue curve is the best-fit forecast sample (to the DCA model). The gray region indicates 90% of the prediction interval (PI) of the Monte Carlo samples of the probabilistic forecast resulting from the BN-ODE framework. The trend of the probabilistic forecast (represented by the gray bands) follows the trend of the fitted DCA model (the red dashed line), which indicates that introducing the DCA parameters successfully "informs" the BN-ODE framework of the DCA modeled decline behavior and "regulates" the BN-ODE framework's forecasts. For most of the wells for testing, the uncertainty intervals (i.e., the grey regions) cover the oil production rate data. Probabilistic forecasts are poor at the beginning of production because of larger fluctuations in early period data. This occurs as a result of more frequent changes in operating conditions due to well tests and other operational tests. The testing shows that the BN-ODE framework can provide a good probabilistic forecast for a well, capturing the trend of oil production rate decline and assessing the uncertainty in the forecast, in contrast to a deterministic forecast from the traditional DCA. However, because of the regulation by the SEDM, Duong, and PanCRM, a BN-ODE forecast is smooth and cannot capture sharp changes in oil production rates associated with significant changes in operating conditions.

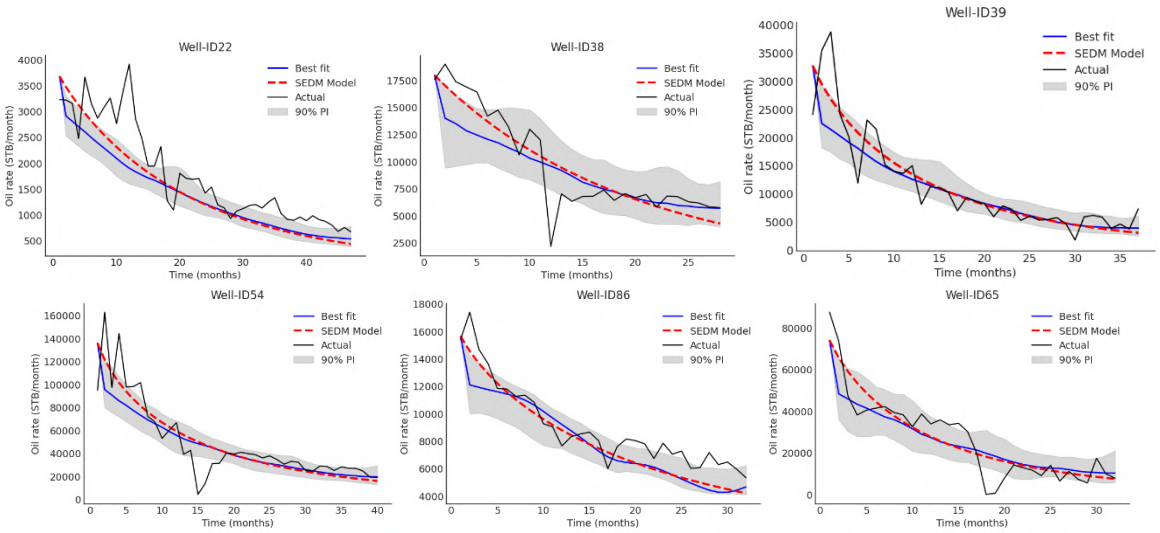

Figure 3.7 — Comparison of the BN-ODE estimation compared to SEDM model and actual oil production.

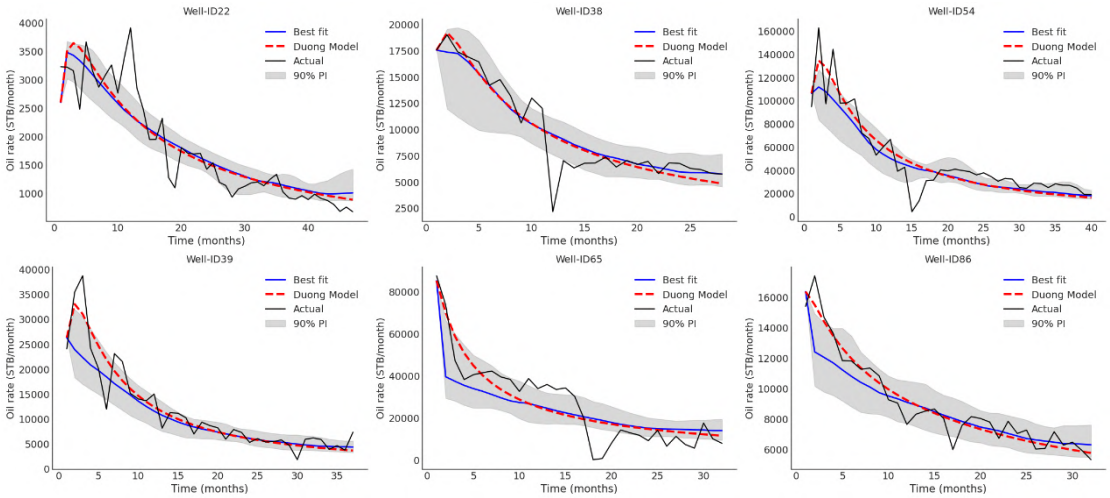

Figure 3.8 — Comparison of the BN-ODE estimation compared to Duong model and actual oil production.

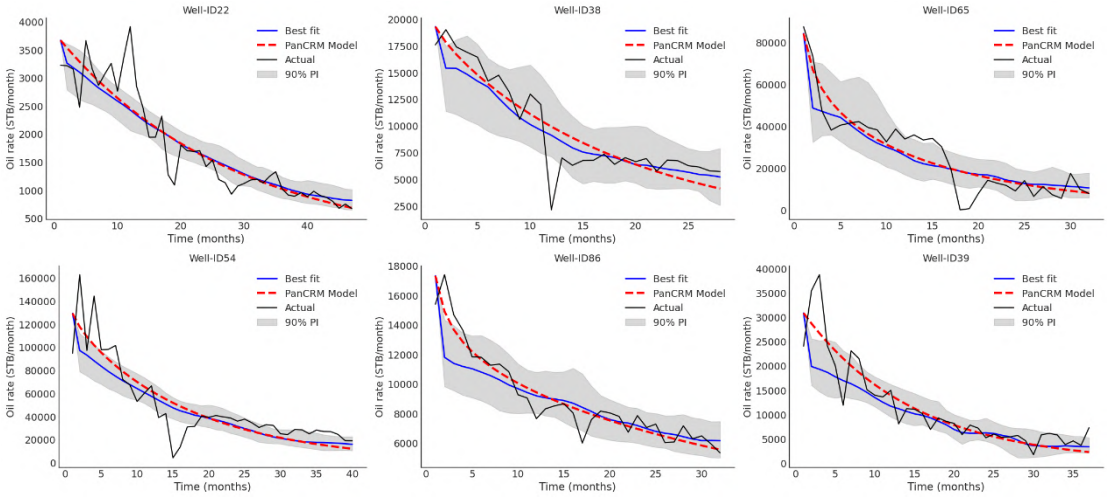

Figure 3.9 — Comparison of the BN-ODE estimation compared to PanCRM model and actual oil production.

For a quantitative comparison, we applied the mean absolute percentage error (MAPE) (de Myttenaere et al., 2016) metric to further evaluate the methods used for all testing well data from the modeled DCA model over the prediction data (best fit obtained from BN-ODE), as displayed in **Figure 3.10**. Applying PanCRM-guided BN-ODE provides interesting results, with a MAPE range of around 4–30%, compared to SEDM; the results seem to be comparable to those of Duong.

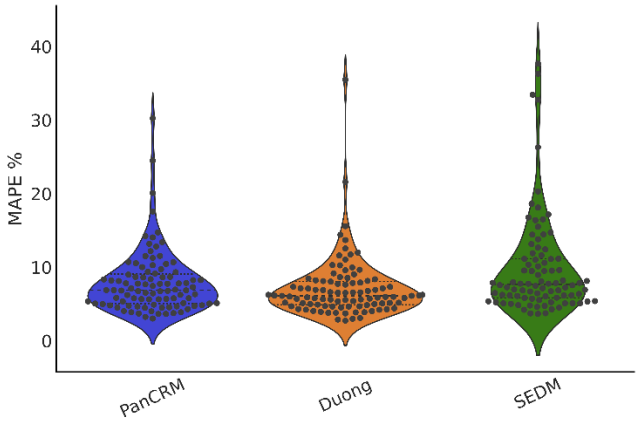

Figure 3.10 — Violin plot of the MAPE of the DCAs model and prediction data (best fit).

Limitation. It is important to emphasize that the prediction accuracy and learning performance of our framework rely mainly on the presence of specific well stimulation, location and completion data. The quality of the data has a big impact and influence, and the presence of data anomalies would consequently affect the veracity of the results. Ideally and in practice, geologic parameters should be included. Thus, it will be useful to include other more-detailed data sets, including pressure, permeability, porosity, fracturing proppant, fluid types, and total organic carbon content, to improve the prediction accuracy of the ML model. In addition, more practical cases should be considered and tested for wells with long shut-in times and different flow regimes. Efforts can be made to further improve the performance of forecasting over long time horizons and quantify the uncertainty, using other sampling

methods such as stochastic Langevin gradient descent (Welling & Teh 2011b) and variational inference (Hoffman et al. 2013), which could serve as an estimator of the posterior.

3.3 Paper III: Managing Uncertainty in Geological CO_2 Storage Using Bayesian Evidential Learning

Carbon capture and storage (CCS) represents a unique potential strategy that can minimize CO_2 emissions in the atmosphere, and it creates a pathway toward a neutral carbon balance. So far, geological reservoirs, such as depleted oil, gas fields, or deep saline aquifers, are considered appropriate for the storage of CO_2 emissions at a depth of several thousand meters (Harp et al., 2017; Jin et al., 2017; Nilsen et al., 2015a). To contribute to the decision-making process and ensure that CCS is successful and safe, an adequate monitoring program must be implemented to prevent storage reservoir leakage and contamination of drinking water in groundwater aquifers. However, geological CO_2 sequestration (GCS) sites are usually associated with substantial uncertainty in terms of geological properties, such as permeability and porosity fields, making it difficult to predict the behavior of the injected gases, CO_2 plume migration, and CO_2/brine leakage rates through wellbores. Data assimilation in reservoir models (history matching) can help mitigate uncertainty and improve predictive capacity. This study presents a unique scientific contribution to CO_2 storage monitoring. In this example, we apply a direct forecasting (DF) framework to potentially reduce the uncertainty associated with forecasting potential leakages during the implementation of CO_2 storage processes. The paper also introduces a new DF implementation using an ensemble smoother and shows that the new implementation can make the computation more robust than the standard method. Here, we use a case study problem based on the Utsira sand reservoir, which is a saline aquifer located on the Norwegian continental shelf (NCS), as displayed in **Figure 3.11**.

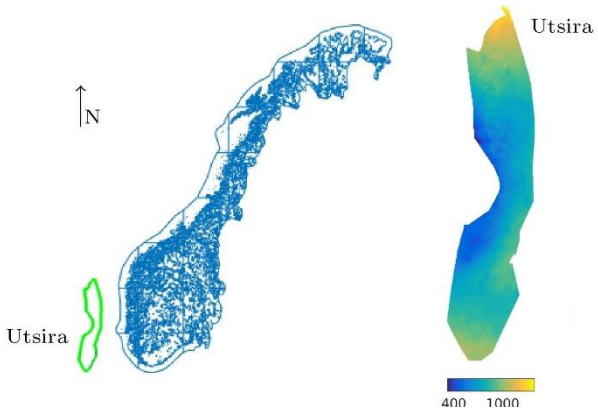

Figure 3.11 — Utsira formation. Location along the Norwegian Continental Shelf (left). Maps of geomodel depths in meters (below the seabed) (right), adopted from (Allen et al. (2018).

We assumed that the Utsira reservoir had one injection well at a depth of 1012 m. Then, an injection rate of 10 Mt per year was considered for a period of 40 years, followed by a 3000-year migration (post-injection) period. All flow simulations were performed using the open-

source software MRST-CO_2 lab developed by SINTEF. CO_2 lab computational tools in MRST were specifically designed for studying the long-term and large-scale storage of CO_2. A set of N=200 prior reservoir models was generated using a normal Gaussian distribution. There are uncertainties in terms of porosity, permeability, caprock elevation, temperature, and pressure. In all cases, a "reference" model was considered.

The CO_2 saturation data were collected in the near-wellbore region during the 40-year injection period and referred to by vector d. We aimed to assess the quantity of CO_2 mass stored and the corresponding CO_2 leakage at the end of the tracking period (3000 years). The forecast (quantity of CO_2 mass injected and CO_2 leakage) is represented by h. The prior distribution of CO_2 saturation for the injection well as well as the forecasts (quantity of CO_2 mass injected, stored, and CO_2 leakage) are shown in **Figure 3.12** and **Figure 3.13**. From both figures, we notice that the uncertainties are large, which implies a significant risk for decision making in field development.

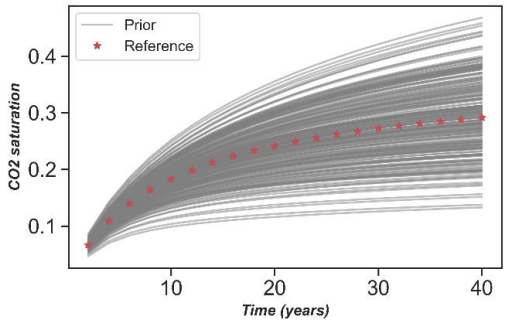

Figure 3.12 — Prior measurement data variables.

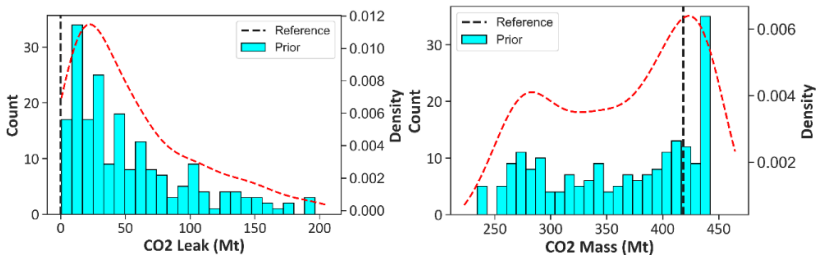

Figure 3.13 — Prior distribution of prediction data variables – 3000 years.

Dimension reduction and linearization. To establish a relationship between the data and forecast variables, it is necessary to ensure low dimensionality in both variables. For this purpose, we performed PCA on the data variables d and h by selecting the principal components (PCs) that preserve 90 % variance. Accordingly, three dimensions were retained for both the data and forecast variables (CO_2 mass and CO_2 leak). Thereafter, CCA is conducted on the reduced data and prediction sets to maximize the linearity between the reduced data and forecast. As shown in Figure **3.14** and **3.15**, the relationship between the components in the functional domain is not linear, and the application of CCA subsequently increases the correlation between the components in the latent space, except in the third dimension, as displayed in **Figure 3.15**, for which a unique linear relationship is not established.

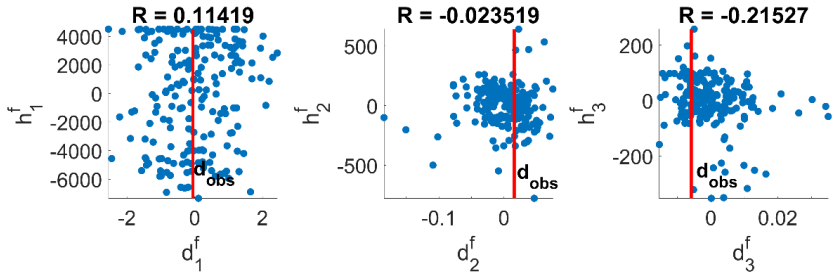

(a) PCA Correlation Analysis.

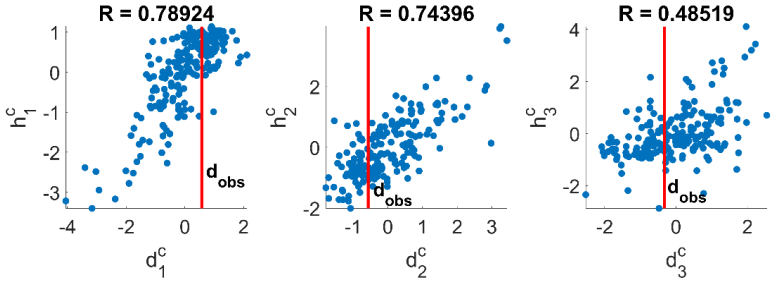

(b) PCA Correlation Analysis in Canonical Space.

Figure 3.14 — Functional components correlation analysis. Red lines correspond to the observed (CO2 mass injected).

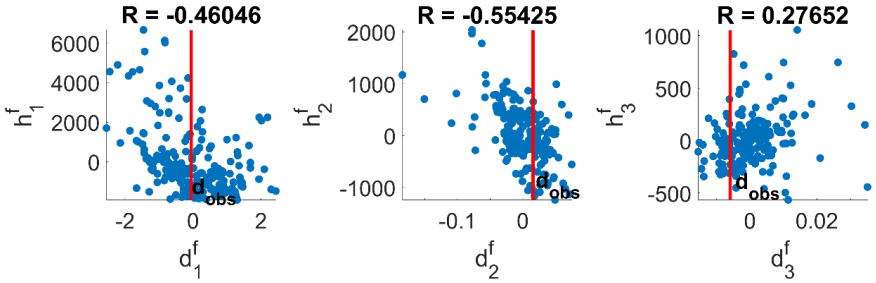

(a) PCA Correlation Analysis.

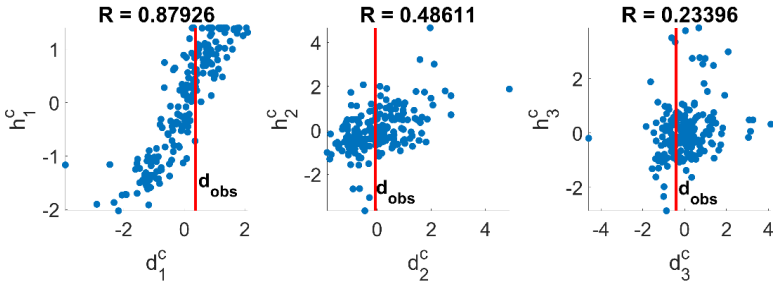

(b) PCA Correlation Analysis in Canonical Space.

Figure 3.15 — Functional components correlation analysis. Red lines correspond to the observed (CO2 leak).

Reconstruct the posterior model After the linear correlation with low dimensions has been established, we estimate the posterior distribution of the forecast components. First, we use the linear Gaussian regression equation described in one of the previous sections, for which h^c must first be transformed using a normal score to obtain h^c_{gauss}. The Gaussian regression produces a multivariate normal posterior $f\,(h^c_{gauss}\,|d_{obs})$ that can be easily sampled to

produce forecast components that are conditioned to d_{obs}^{c}. Second, we apply the modified ES-MDA explained previously to generate the posterior distribution of the forecast variables h^{c}. These observations are perturbed by adding random Gaussian noise with zero mean and standard deviation corresponding to 10% of the data predicted by the reference model.

Once the posterior distribution of the prediction in the reduced dimension space is established, it can be easily sampled and transformed back into the original space, where the posterior distribution of the prediction is displayed in **Figure 3.16** and **3.17**. As a result, we notice that the DF with Gaussian regression techniques predicts a larger uncertainty range for both CO_2 mass and leakage after 3000 years compared to DF with ES-MDA, for which the results are reasonable, and the data match is excellent; the uncertainty bands are reduced for both CO_2 mass and leakage at the end of 3000 years. The results indicate that the proposed DF-ESMDA is more robust than the original DF. Both methods are fast in terms of computation, but they require running reservoir simulations of the prior ensemble, which clearly consumes considerable computational time.

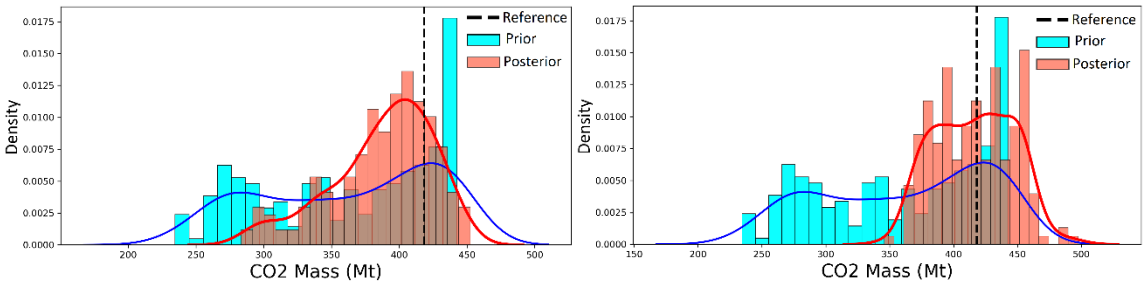

(a) DF. **(b) DF-ESMDA.**

Figure 3.16 — Reconstruct posterior CO_2 mass injected

.

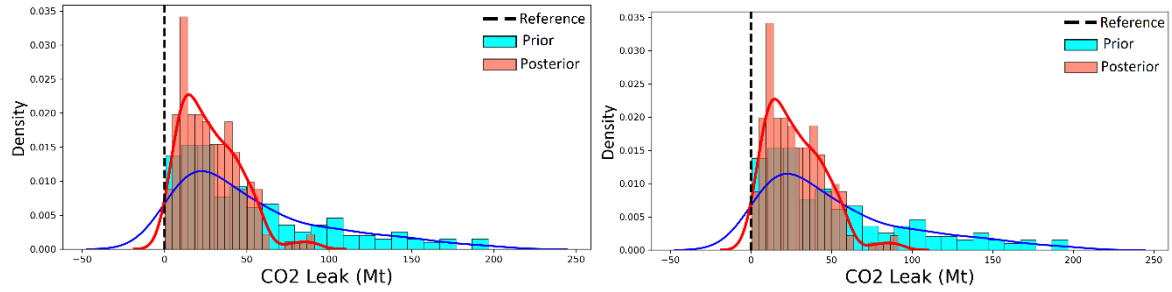

(a) DF. **(b) DF-ESMDA.**

Figure 3.17 — Reconstruct posterior CO2 leak.

***Limitation*.** We presented a novel method for history matching, where one relies on direct forecasting methodology (establishing a statistical relationship between dynamic data). However, some criteria must be addressed to ensure the high-quality formulation of this methods, as the key successful its application is based on the initiation of the prior model, which should retain geological realism; an unrealistically large uncertainty range may impact the data-prediction relationship and minimize accuracy. In addition, the dimensionality of the variables is reduced by linear PCA. Linear PCA is simple and fast, but not optimal for non-Gaussian variables. For non-Gaussian variables, model variables can be reparametrized to

follow a multivariate normal distribution or nonlinear PCA, and other machine learning dimensionality techniques can be used. In addition, the proposed method can be integrated with other inversion methods to increase the matching quality with fewer iterations.

3.4 Paper IV: Efficient Dimensionality Reduction Methods in Reservoir History Matching

This paper presents an approach for uncertainty quantification and reservoir model calibration with a significantly reduced computation time. This approach is based on a sequential combination of nonlinear dimensionality reduction techniques: t-distributed stochastic neighbor embedding (t-SNE), the Gaussian process latent variable model (GPLVM), and clustering K-means, and the data assimilation method ensemble smoother with multiple data assimilation (ES-MDA). Cluster analysis with t-SNE and GPLVM is used to reduce the number of unknown parameters and select a set of optimal reservoir models that have similar production performance to the reference model. The ES-MDA was then applied for data assimilation. The procedure used in this study involved several stages. The first stage included generating ensemble reservoir models, in which the dataset used in our study was provided by TNO. Next, we checked whether the observed prior data could predict the posterior distribution corresponding to the prior range. Otherwise, the prior model was considered incorrect. In the third stage, we reduced the ensemble dimension and constructed a 2D space using t-SNE and GPLVM. The fourth stage used clustering K-means to extract a set of reservoir models with the least production error compared to the reference model. After extracting and selecting the reservoir models, we began the HM process using ES-MDA, and compared the performance of the history-matching analysis of the proposed workflow with the standard ES-MDA without using dimensionality reduction techniques. The main steps of this approach are shown in **Figure 3.18**. In this example, we have focused only on steps 2,3 and 4. The other steps are illustrated and discussed in **section III.**

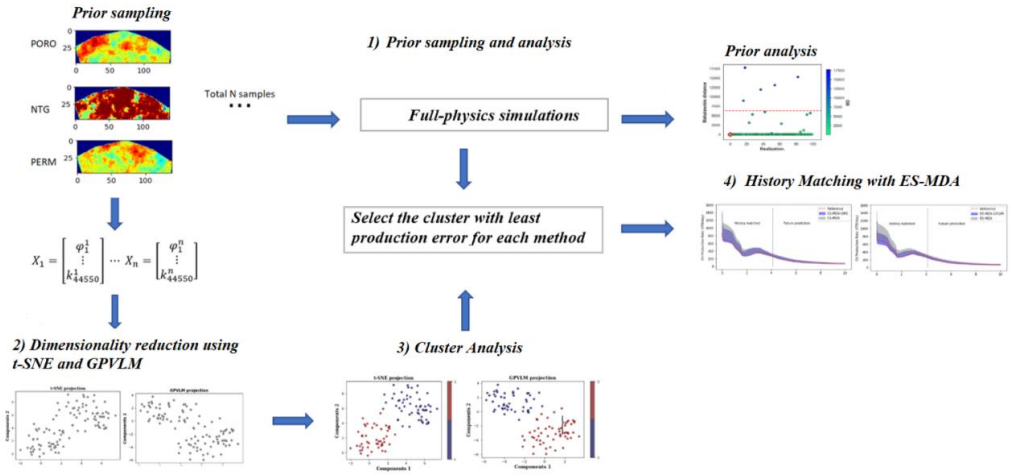

Figure 3.18 — Flow chart for the history matching with dimensionality reduction framework.

We tested the performance of the proposed methodology in a Brugge-field case study (Peters et al. 2010). The Brugge field is a complex oilfield constructed using the TNO. The model

consisted of nine layers, and each layer had 139×48 grid blocks. The total number of grid blocks was 60,048, with 44,550 active cells. There were 20 producers and 10 injectors in the reservoir model. We used 104 initial ensembles provided by TNO and assumed 104 as a reference model. In the AHM analysis, oil production rates (OPR), water cuts (WCT), and bottom hole pressure (BHP) were considered, and the model variable to be updated included permeability (PERMX, PERMY, PERMZ), porosity, and NTG at all active cells. **Figure 3.19** shows the log permeability in the first layer for six random realizations.

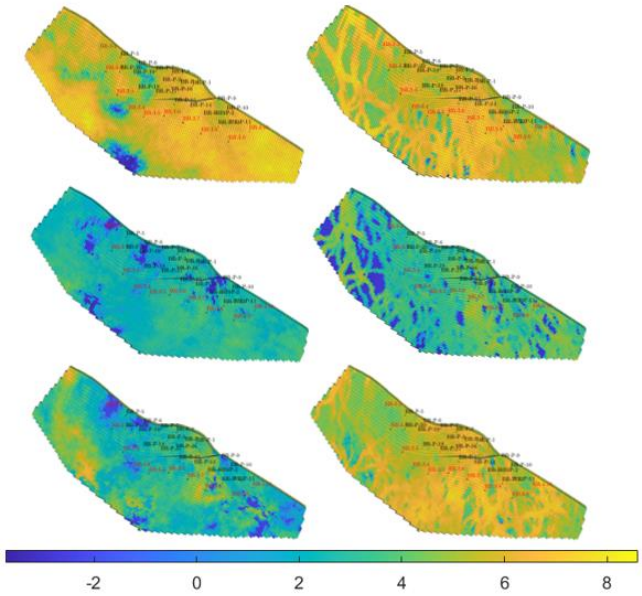

Figure 3.19 — Example Log of permeability (K) distribution for six of 103 different geological realizations of the Brugge field.

.

Data assimilation was conducted using ES-MDA with localization for N = 5, in addition to ES-MDA-tSNE and ES-MDA-GPLVM. We performed the HM on assimilation observation data for the first four years and the rest (six years) for forecasting.

We applied t-SNE and GPLVM to reservoir models and reduced the dimension into 2D space and conducted a sensitivity analysis of cluster numbers using the silhouette method for both GPLVM and t-SNE 2D space. As displayed **in Figure 3.20**, the dashed line indicates the mean of the silhouette values, and we compare the values for the range from two to seven clusters. As the silhouette plot with two clusters is associated with the largest value, we grouped the models into two clusters.

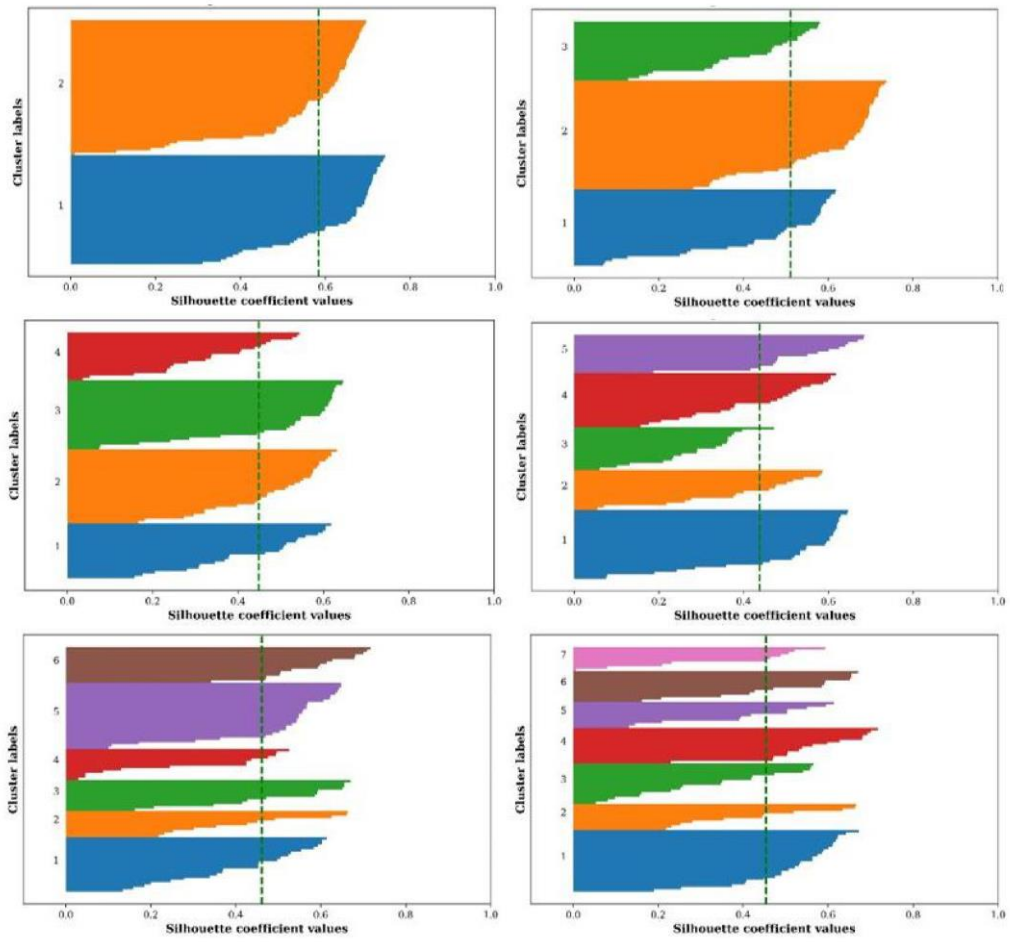

Figure 3.20 — Silhouette plots with different cluster numbers (t-SNE 2D space).

Figure 3.21 shows a scatter plot of the 103 models on the 2D plane, with the dots indicating individual models. When selecting the cluster with the least production error and comparing the forecast accuracy of different forecasting methods using several datasets, there are many performance measures from which to select. In this study, we evaluated our forecasting results using a probabilistic metric called the mean continuous ranked probability score (CRPS). We compared the field oil production errors between each cluster and reference model and selected the cluster with the least production error for the data assimilation process, as displayed in **Table 3.4**. Only 46 models were selected using t-SNE and 44 models using GPLVM.

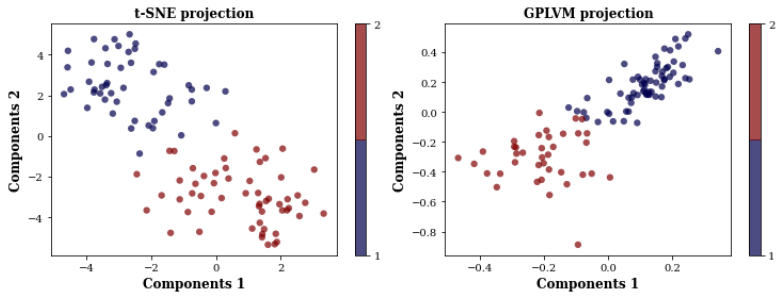

Figure 3.21 — Model selection using t-SNE and GPLVM.

Methods	t-SNE		GPLVM	
	CRPS	**Realization**	**CRPS**	**Realization**
Cluster 1	96.77	46	89.78	44
Cluster 2	130.67	57	128.66	59

Table 3.4- Measurement error between reference model and each cluster

The total simulation times for each method are stated in **Table 3.5**. We can see that ES-MDA uses approximately 220 min for the entire process, while ES-MDA-tSNE and ES-MDA-GPLVM use around 120 min and 101.5 min, respectively. By employing reduction techniques, more than 45% of the total simulation time was saved.

Method	CPU time (minutes)	Time reduction
ES-MDA	220	0
ES-MDA-tSNE	120	45.54%
ES-MDA-GPLVM	101.5	53.86%

Table 3.5- CPU time for the entire process.

Figure 3.22 and **Figure 3.23** depict the HM profiles for both oil and water cuts of the two methods (ES-MDA-tSNE and ES-MDA-GPLVM) for producers BR-P5, BR-P6, and BR-P19, with respect to the standard ES-MDA and reference model. The vertical dashed line indicates the last assimilation process. The predictions from the two methods appear to be consistent with the production forecast unlike the standard ESMDA, although only 45.54% and 53.86% of the simulation time is required for ES-MDA-tSNE and ES-MDA-GPLVM, respectively. However, the ESMDA-tSNE predicts the WOPR data for BR-P6 better than the ES-MDA-GPLVM, which is likely related to the fact that WWCT data BR-P6 are better with the ESMDA-tSNE. The matching and forecast ranges with ES-MDA-GPLVM deviate from the reference, especially for BR-P6.

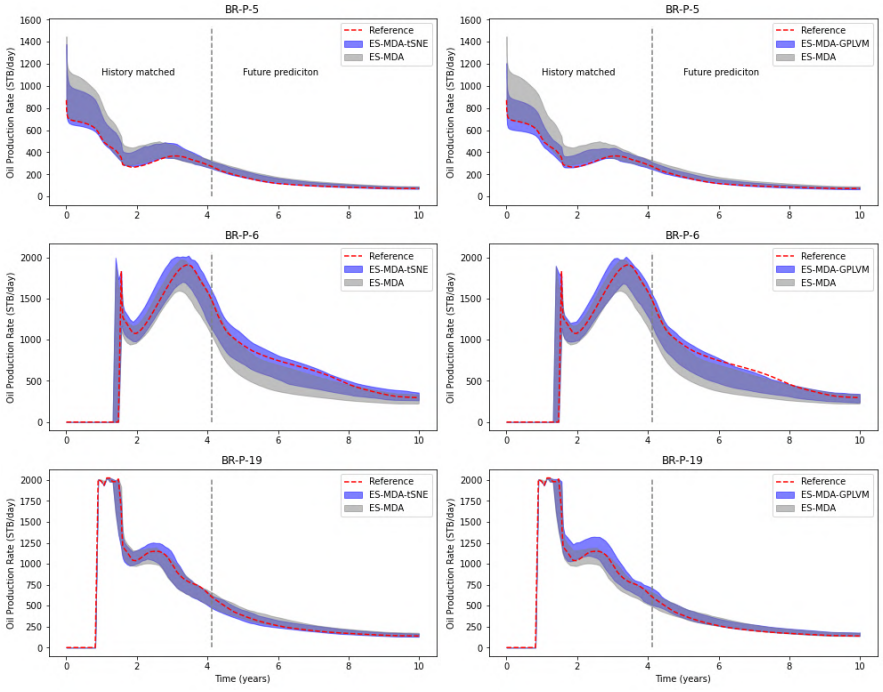

Figure 3.22 — Oil production rate (STB/day) for three wells with ESMDA, ES-MDA-tSNE and ES-MDA-GPLVM. The vertical dashed line indicates the end of the history

and beginning of the forecast period. The red line indicates the observed data points and the prediction from the reference model. The grey region corresponds to the predictions within the percentiles P10–P90 obtained with the ES-MDA. The light blue region corresponds to the predictions within the percentiles P10–P90 obtained with ES-MDA-tSNE or ES-MDA-GPLVM.

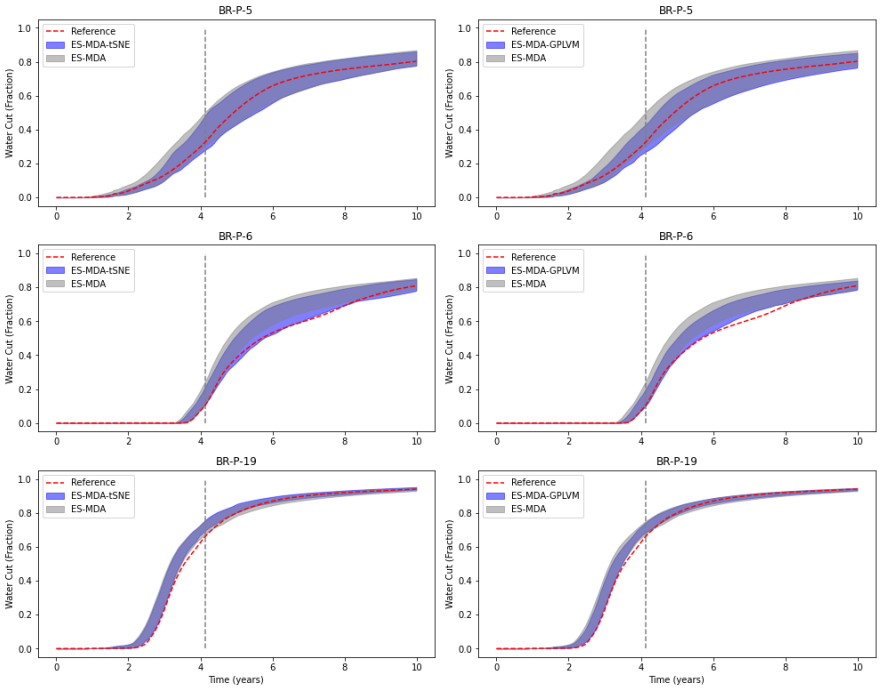

Figure 3.23 — Water cuts for three wells with ESMDA, ES-MDA-tSNE and ES-MDA-GPLVM. The vertical dashed line indicates the end of the history and beginning of the forecast period. The red line indicates the observed data points and the prediction from the reference model. The grey region corresponds to the predictions within the percentiles P10–P90 obtained with the ES-MDA. The light blue region corresponds to the predictions within the percentiles P10–P90 obtained with ES-MDA-tSNE or ES-MDA-GPLVM.

For a quantitative comparison, we applied the mean CRPS metric to further evaluate the methods used for all simulated well data from the history-matched ensembles over the historical and prediction periods, as displayed in **Figure 3.24**. The ES-MDA-tSNE and ES-MDA-GPLVM provided interesting results, with the lowest CRPS average compared to the prior, and although we used few ensemble models and saved around 45-53% of the simulation time, the results appear to be comparable to the standard ES-MDA.

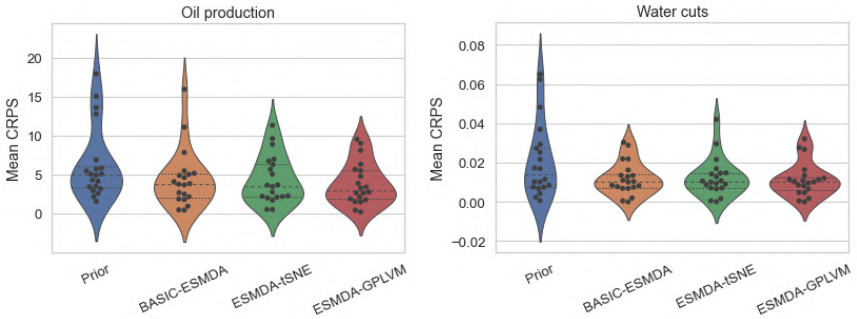

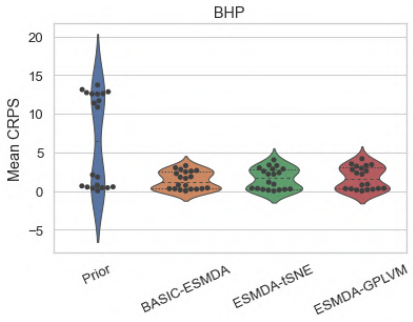

Figure 3.24 — Violin plot of Mean CRPS of historical and prediction data (WOPR, Water cut and BHP).

***Limitation*.** In this work, we presented a method for history matching based on the ML dimensionality reduction technique along with ES-MDA. However, some criteria must be addressed to ensure the high-quality formulation of this method, as the key successful application of these two methods is based on the initiation of the prior model, which should retain geological realism; an unrealistically large uncertainty range may impact the data-prediction relationship and minimize accuracy. Here, we only used K-means clustering. However, K-means is associated with inconsistency due to varying results for different runs of an algorithm; moreover, it may produce clusters with uniform sizes even when the input data have different sizes, in addition to being very sensitive to scale and dimensionality of data. Therefore, other clustering techniques must be tested. In our example, the ES-MDA can be applied to estimate the posterior uncertainty. However, sampling efficiency can also be enhanced by integrating other inverse modelling techniques, such as the iterative ensemble smoother regularized Levenberg–Marquardt (IES-RLM) and the subspace ensemble random maximum likelihood (SEnRML).

3.5 Paper V: Application of Machine Learning to Assess the Value of Information in Polymer Flooding

This paper presents a framework in which we perform a VOI analysis in the context of initiating polymer flooding in a reservoir development plan. We want to determine the optimal time to switch from water flooding to polymer injection based on the information from production profiles and oil prices, and the switch happens only once. The analysis is done on a constructed case study involving a heterogeneous reservoir model, Further, we use various machine learning regression approaches (detailed in Paper V) to directly estimate the conditional expected value given the data without approximating the posterior probabilities of reservoir properties. The simulation-regression approach utilized here accounts for the effect of the information of both production profiles and oil prices obtained before a decision is made and the effect of the information that might be obtained to support future decisions. We consider a modified version of the standard Egg reservoir model, which is a 3D channel model (Jansen et al. 2009) that contains eight injection wells and four production wells. The model consists of 100 realizations of channelized reservoirs with 60×60×7 grid cells, of which only 18,553 cells are active, thus resulting in an Egg shape, as illustrated in **Figure 3.25.**

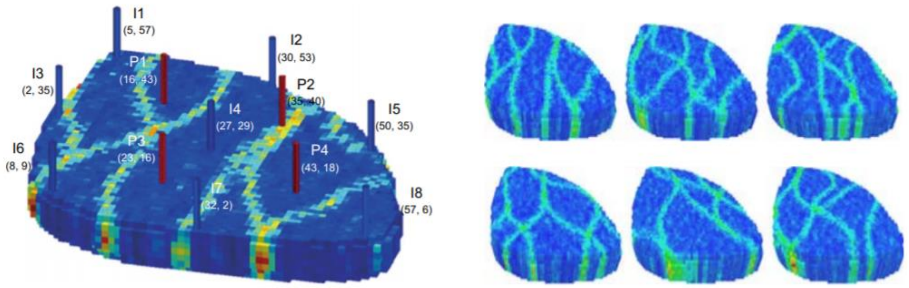

Figure 3.25 — (Left) Reservoir model displaying the position of the injectors (blue) and producers (red). (Right) Six randomly chosen realizations (From Jansen et al., 2009).

The oil and water production levels of 100 ensembles were modeled using the Eclipse reservoir simulation model and inform the switching decision. The measurement errors were considered to be normally distributed with a mean of zero and standard deviation of 10% of the modeled rates and added to the modeled rates.

Figure 3.26 shows the oil and water production for all realizations for both decision alternatives (i.e., injecting the polymer during the ninth year or maintaining the water-flooding recovery process for the whole life of the production cycle).

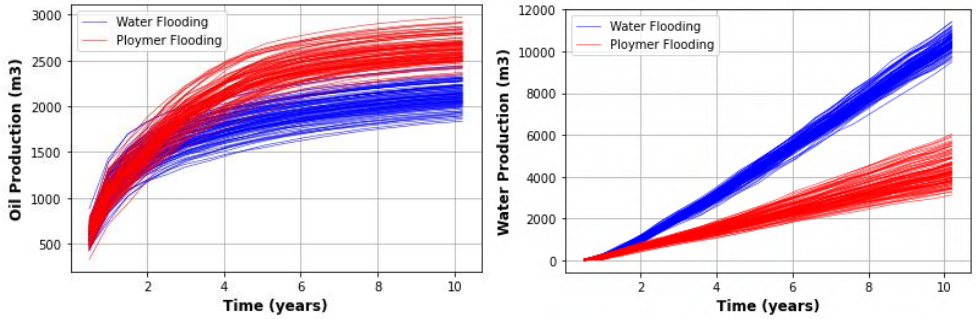

Figure 3.26 — The oil production and the water production profile for the realization of the alternative "inject polymer flooding at the end of the first year" and for the alternative "inject water flooding".

The value function is defined as the NPV for each decision alternative corresponding to each realization. NPV is a function of revenue from oil production and the costs of water production, water injection, and polymer injection. NPV was calculated using the following equation:

$$v(x^b, a) = NPV(x^b, a) = \sum_{k=1}^{n_T} \frac{[q_0^k(x^b,a)P_0 - q_{wp}^k(x^b,a)P_{wp} - q_{wi}^k(x^b,a)P_{wi} - q_{ci}^k(x^b,a)P_{ci}]\Delta t}{(1+r)^{t_k/\tau}}$$

where k is the index of the time step, n_T is the total number of time steps, x^b is the realization of the reservoir, q_0^k is the field oil production rate at time k, q_{wp}^k is the field water production rate at time k, q_{wi}^k is the field water injection at time $k, and\ q_{ci}^k$ is the total polymer injection rate at time t_k, with P_0,P_{wp}, P_{wi}, and P_{ci} .

The values of the used economic parameters are also listed in **Table 3.6**.

Parameter	Value	Unit
P_0	220	$\$/m^3$
P_{wp}	47.5	$\$/m^3$
P_{wi}	12.5	$\$/m^3$
P_{ci}	12	\$/kg
r	8%	-
τ	365	Days
Δt	30	Days

Table 3.6 – Values of economic parameters.

We consider a maximum life cycle of 10 years. We analyze the optimal time to switch from water flooding to polymer injection for each year of production using simulation-regression approach, with the switch occurring only once. This indicates that there would be nine possible switch times. We consider two cases, where for the first case, the oil price is set to a fixed value, and in the second case, the oil price is treated as an uncertain parameter and considered in the regression analysis to determine the optimal switch time.

The Ornstein–Uhlenbeck (OU) stochastic process (also known as a mean-reverting model) is used to model and quantify the uncertainty in oil prices. The least-squares polynomial regression method is used to calibrate the input parameters for modeling the oil price, resulting in a mean reversion. Ornstein–Uhlenbeck and the calibration procedure are detailed in **Papers V and VI.** For illustration, we used the annual oil price data from the NYMEX futures prices of 1985–2019 (considering only historical yearly spot prices), as shown in **Figure 3.27a.** The data are available on the U.S. Energy Information Administration website (2019). **Figure 3.27b** presents a probabilistic model of oil price.

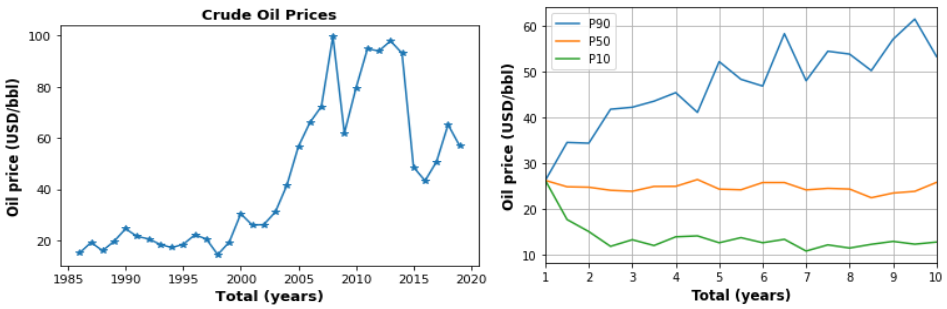

(a) **Historical data of annual oil price** **(b) Oil prices modelled using the mean- reverting process**

Figure 3.27 — Oil price modelling.

For both approaches (with and without uncertainty in oil price), the decision without information (DWOI) involves injecting the polymer by the end of nine years. The expected values and VOI estimates are presented in **Table 3.7**. The EVWOI, EWPI, and EVII for Case 2 were higher than those in Case 1; however, the VOI was lower. This means that the oil price has a significant impact on the decision. The VOI analysis informs us that we should not proceed with any information-gathering activity if the cost of the activity is more than \$1.52 million.

Approach	**EVWOI**	**EVWPI**	**EVWII**	**VOPI**	**VOI**
Case 1	$133.91 million	$136.7 million	$135.92 million	$2.79 million	$2.01 million
Case 2	$134.53 million	$137.98 million	$136.04 million	$3.46 million	$1.52 million

Table 3.7- Expected values and VOI estimates.

The normalized frequency distributions (NFDs) of the waterflooding injection lifetime are illustrated in **Figure 3.28.** For Case 1, 51 % of the realizations initiated the EOR phase at 9 years, with 33 % of the realizations indicating switching at 8 years, and 16 % at 7 years of water-flooding recovery. For Case 2, the frequency distribution recommends switching from water flooding to polymer injection in years 8 and 9 (i.e., there is a 53 % chance that the polymer recovery mechanism should be started in the year 9). There is only a 32 % chance that it will be optimal to switch at 8 years and 5 % after both 6 and 7 years of water-flooding recovery. The specific switch time depends mainly on the measured production uncertainty of geological realizations and oil prices.

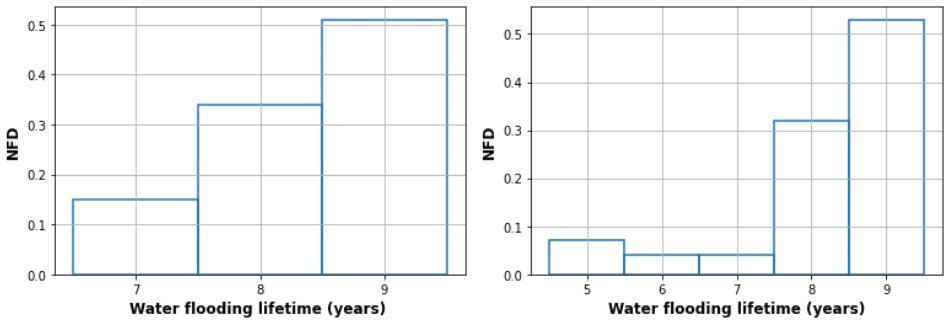

(a) – Fixed oil price **(b) – Uncertainty in oil price**

Figure 3.28 — NFDs of the polymer injection corresponding to the decision-making with ML

.

3.6 Paper VI: A Sequential Decision and Data Analytics Framework for Maximizing Value and Reliability of CO_2 Storage Monitoring.

This paper presents a consistent decision based VOI analysis to assess the value of seismic monitoring of CO_2 storage, in which CO_2 is injected into a reservoir and seismic surveys are conducted to decide between continuing or stopping the injection, based on information from the survey results. The actual VOI calculation in our case is computed using the simulation-regression methodology. The simulation-regression methodology used here illustrates both the impact of the seismic survey data obtained before a decision is taken and the effect of the data information that can be obtained to support future decisions. The analysis is performed on a constructed case study involving the Utsira storage site. Furthermore, we use a machine learning regression approach to estimate the VOI and determine the optimal time to stop the CO_2 injections into the reservoir.

With regard to the problem setting of this example, we assume that the Utsira reservoir has one injection well at 1012 m depth, then a total period of 60 years of injection time is proposed, followed by a 3000-year migration (post-injection) period. All flow simulations were performed by using the open-source software MRST-CO2lab developed by SINTEF. We consider two options: continuing or stopping the injection. We then analyze the optimal time to stop the injection based on seismic surveys. This analysis provides useful insights into the reservoir development plan and learning over time affects decisions. A total of N= 100 prior geological realizations were generated using a normal Gaussian distribution to sample permeability, porosity, temperature, pressure, and caprock elevation

In addition, we let $t \in \{14,26,32,40,50,55\}$ denote the time in years at which the decision of whether to stop the CO_2 injection operation entirely has to be made. We assume that the injection cannot be resumed once it has stopped. This indicates that the number of decision alternatives in this case is 1200 (*alternatives* $\times$ *time points* $\times$ *realizations*) (see **Table 3.8**).

Injection period	60 years
Alternative	**Continue** or **stop** the injection at times {14,26,32,40,50,55}
Uncertainty / States	Permeability, porosity, temperature, pressure and caprock elevator. (100 realizations)
Value derived from the decision situation	Net present value
Information data	AVO attributes

Table 3.8 - Decision Problem Setting

To compute the VOI using simulation regression, the net present value (NPV) for each decision alternative corresponding to each realization has to be evaluated. As our objective is to maximize the NPV and minimize the CO2 leakage, the simplest objective function would simply measure the amount of CO_2 injected M_{inj} and penalize the amount of CO_2 M_{leak} that has left the aquifer through the open boundaries or by leakage through the caprock, associated with project costs and penalty fines if leakage occurs. The net present value function will then conceptually be of the form of the amount of money saved by storing CO_2 minus both the project costs and the penalty fine. For illustration purposes, \$34 /t CO_2 would be used as the market price in the form of carbon credits to avoid CO_2 emissions, and \$1.2/t CO_2 would be utilized as a leakage-related penalty. The cost of the CO_2 captured is in the range of \$11/t CO_2 –\$32/t CO_2 (Puerta-Ortega et al., 2013), and this value was fixed at approximately \$25/t CO_2 for our study (Sintef, 2019). \$3.5/t CO_2 was set to cover the costs of construction, operation, and maintenance (Bock et al., 2003). The cost estimate for storage in the onshore USA saline formation is \$2.8/t CO_2 (IPCC, 2005), and the monitoring cost is in the range of \$0.2/t CO_2. The net cost would then be \$25/t CO_2+ \$3.5/t CO_2+\$2.8/t CO2 +\$0.2/t CO_2 = \$31.5/t CO_2; hence, the NPV can be expressed as follows:

$$\boldsymbol{NPV = Revenu - Cost - Penality}$$

Where,

$$Revenu = \$34\ /t\ CO2 \times (M_{inj} - M_{leak})$$
$$Cost = \$31.5\ /t\ CO2 \times M_{inj}$$
$$Penality = \$1.2\ /t\ CO2 \times M_{leak}$$

To compute the VOI, we assumed three scenarios: (1) a fixed value of carbon price, (2) sensitivity analysis of amplitude versus offset (AVO) attributes, R0 (intercept), and G (curvature) are normally distributed using the likelihood model described in (Eidsvik et al., 2015). More details regarding Scenario (2) are cited in Paper **VI.** In scenario (3), the carbon price is treated as an uncertain parameter for each realization and alternative. We used the OU process to model the carbon price, as illustrated in **Figure 3.29.**

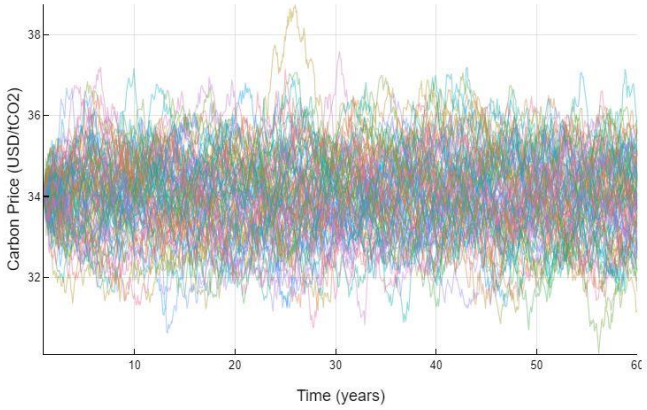

Figure 3.29 — Carbon prices modelled using the OU mean-reverting process.

The resulting VOIs for the three scenarios are listed in **Table 4.4**. The values of scenarios (1) and (2) are close. However, scenario (3) resulted in a high VOI value. This indicates that including the effect of future learning and decision making on carbon prices could improve the expected value. In addition, this analysis indicates that seismic data should not be gathered if the cost is greater than $432.5 million.

Scenario	**(1)**	**(2)**	**(3)**
VOI [Million USD]	242.85	231.48	432.50

Table 3.9 – VOI estimates for the example with CO_2 storage monitoring.

For all three scenarios, the DWOI involves stopping CO_2 injection by the end of 26 years. The normal frequency distributions (NFDs) of the total lifetime corresponding to decisions with machine learning are illustrated in **Figure 3.30**. Based on these results, CO_2 injection should be stopped after 14–40 years. The specific stopping time depends mainly on the uncertainty of the geological parameters (permeability, porosity, caprock elevation, pressure, and temperature), in addition to three different scenarios: fixed carbon price, perturbed measured seismic data, and uncertainty in carbon price.

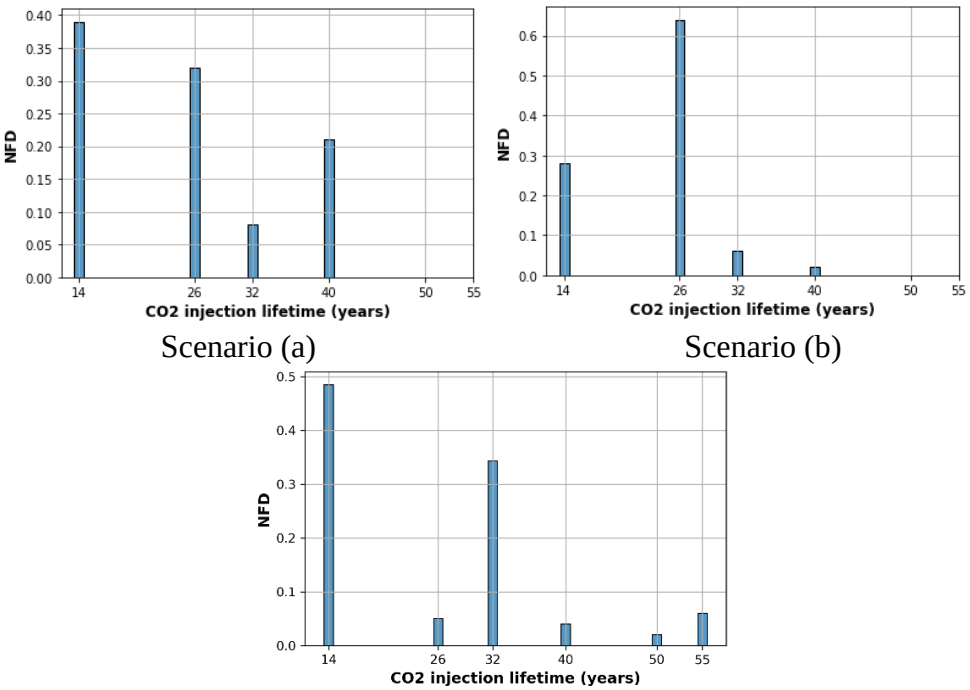

Scenario (a) Scenario (b)

Scenario (c)

Figure 3.30 — NFDs of the CO2 Optimal Stop Injection Time corresponding to the Decision-making with ML.

Limitation. We demonstrate the usefulness of utilizing the concepts of decision analysis and value information to support value creation in the field development plan with limited computational resources. However, the impact of changing economics (cost of the CO_2 captured, water injection and production, etc.), and the sensitivity of the decision model and objective values to variations in reservoir parameters have not been analyzed in this study. In addition, one of the limitations of the value of information analysis is that estimation quality depends on the model and specification of parameter uncertainty. It might be beneficial to increase the number of realizations or reduce the number of alternatives in innovative ways.

4. Concluding remarks.

In this dissertation, we explore, illustrate, and discuss implementation examples of decision and data science in managing uncertainty in three areas in reservoir management, production forecast, uncertainty quantification and reservoir calibration (history matching), and sequential decision making.

Production Forecast. First, we propose a method that applies machine learning that can replace or accelerate manual decline curve analysis for short-term oil and gas well forecasting. Probabilistic prophet time series analysis and more accurate deep learning models, DeepAR, were considered to solve this problem. These two have been selected as they outperform state-of-the-art forecasting methods in many areas. For time series forecasting, the prophet is a Bayesian nonlinear generative model proposed by Facebook. Prophet is also a structural time series analysis method that specifically models the impact of patterns, seasonality, and events. In contrast, DeepAR is an auto-regressive model based on cells with gated recurrent units or long short-term memory recurrent neural networks. It learns the parameters for each forecast horizon from a given probability allocation. Then, by sampling several times, one can sample from probability distributions to forecast each horizon or compute confidence intervals. The results concluded that the deep learning approach and prophet analysis yielded satisfactory results in short-term forecasts, but they may fail to identify long-term trends in production unless the predictions are constantly adjusted. However, both approaches rely on the volume and granularity of data to develop the capability for predicting production over a long-time horizon. To solve this problem, we presented a new workflow to quantify uncertainty associated with DCAs modelling. The results show that the incorporation of decline curve model parameters in the Bayesian Neural ODE model can effectively regulate the forecasts and that the resulting probabilistic forecasts can reasonably cover the measured oil production rates. In this work, we integrated some locations properties and well-completion parameters in the Bakken Field, and then applied a data-driven technique to provide relevant information about well production performance. Machine learning is used to link the location and completion variables to decline model parameters. Subsequently, the Bayesian Neural ODE framework, No-U-Turn MCMC sampler (NUTS), is integrated with these decline analysis curve estimated parameters to rapidly forecast probabilistic decline curves without using expensive reservoir simulators. This methodology has been found to predict the rate decline. By leveraging data collected from existing wells, the ultimate recovery of a new well can also be predicted using this method. This work provides a practical application of combining Bayesian neural ODE with machine learning, which has the capacity to replace manual DCA in the long-term prediction of oil and gas wells. This approach might be particularly suitable for green fields with an extremely large number of wells.

Uncertainty quantification and reservoir calibration. To quantify geological uncertainty in history matching, we presented a history matching framework with dimensionality reduction while preserving realistic geology and matching the production data, which was achieved by explicitly integrating t-distributed stochastic neighbor embedding (t-SNE) or the Gaussian process latent variable model (GPLVM), and clustering K-means with ensemble smoother with multiple data assimilation (ES-MDA) to reduce the simulation time and quantify the uncertainty in reservoir models. The proposed procedure yielded reliable results by selecting a

set of good prior ensemble reservoir models, with production performance similar to that of the reference model, before applying the data assimilation process. Accordingly, we compared the new implementation with the standard ES-MDA in a field reservoir problem with a long production history and a large number of wells. Based on the obtained results for these test problems, the proposed ES-MDA with dimensionality reduction is concluded to be computationally faster than the original one, and it is very simple to implement and integrate with different types of data and models. In addition, several approaches have demonstrated that it is possible to provide the outcomes of subsurface models without the need for model updating and solving the inverse problem. In this context, we applied direct forecasting (DF) to quantify uncertainty in CO_2 storage and migration in deep saline aquifers. We present a new DF implementation coupled with an ES-MDA. The proposed DF-ES-MDA was compared with the original DF. Both of the original methods mitigate the uncertainty reduction to a linear problem by reducing the high dimensionality of the original data using principal component analysis and canonical correlation analysis, and we established a statistical relationship between the data and forecast for direct forecasting. This estimated relationship combined with Bayesian Gaussian regression is thus used to generate a statistical forecast of the quantities of interest—in our study, CO_2 injected mass and leakage. The new implementation preserves the main advantage of the original DF—its ability to provide an ensemble of CO_2 injected mass and leakage forecasts without iterative data inversion or history matching problems that can be computationally expensive and difficult. The two methods are advantageous, even though the time required to execute the reservoir simulations for the prior models tends to be time-consuming. We compared the DF-ES-MDA with the original DF of a real field case and concluded that the accuracy of the DF-ES-MDA was consistently enhanced, and a higher degree of uncertainty reduction could be achieved.

Sequential decision making. Closed-loop reservoir management (CLRM) is a state-of-the-art approach for managing geological uncertainty in reservoir management. It closes the loop of history matching and production optimization by continuously updating a production model and performing life-cycle optimization whenever new data become available. However, it is based on a myopic decision policy, in that it does not account for future uncertainty revelations and their impacts on future decisions. Thus, the CLRM solution was suboptimal. Because reservoir management is a sequential decision-making problem, it should consider whether geological uncertainty is informed by current data or future information. These sequential decision problems are often solved and modeled as approximate dynamic programming, often described as simulation-regression, which is a powerful solution technique that can handle complex large-scale problems and discover a near-optimal solution for intractable sequential decision making. We demonstrated and described the usefulness of utilizing the concepts of simulation-regression and value information to support the recovery phase in the field of oil development with limited computational resources. We applied linear and nonlinear machine learning regressions to compute the VOI, which yielded comparable results and globally optimal solutions. In relation to the context, we presented a value of information framework that can be used to compute the value of information in a CO_2 storage development plan. Specifically, we applied the framework to evaluate the VOI of time-lapse seismic data in the detection of potential CO_2 leakage. A case has been developed where, based on information from seismic surveys and carbon credit prices, a decision-maker must decide on the best time to continue or stop the CO_2 injection. The reliability of a seismic survey and carbon prices are likely to increase with time and the amount of CO_2 injected into the reservoir.

In conclusion, the VOI framework can generally be applied to any type of spatial data and in the context of decisions other than reservoir development. The framework can be evaluated as an interplay between three key factors: the decision-making situation consisting of alternatives and prospect values, the uncertain variables of interest that affect the prospect values, and the data that informs about these variables of interest. Moreover, the machine learning regression method can be used to approximate the value functions that appear in dynamic programming and can be considered a robust approach, as it includes and quantifies uncertainties in dynamic and state variables, including uncertainty in economic parameters, which are important to make good and insightful decisions

5. Further Works

This thesis has demonstrated the usefulness of novel and different methods for creating value by supporting decision making in complex and uncertain environments for reservoir management. There are many opportunities to extend our work and address some limitations. Some relevant areas for further research include the following:

1- The long-term oil forecasting performance of the model can be further improved through numerous steps involving the use of other sampling techniques, such as variational inference and stochastic Langevin gradient descent, which could also help to quantify the uncertainty and estimate the posterior. This may be applied to spatiotemporal tasks or the use of an encoder-decoder from sequence to sequence, where the contextual data (static and dynamic) are integrated into the model architecture. Additionally, it integrates physical constraints during the training of a deep neural network. An advantage of such an approach is that physics can be introduced into ml approaches and could replace or speed up manual decline curve analysis to perform long-term forecasting of oil and gas wells.

2- The performance of history matching with dimensionality reduction techniques is highly dependent on the ability and quality of the prior ensemble to provide unbiased estimates of prior uncertainty. In practice, we should revise the prior ensemble before using it for data assimilation; ideally, the prior ensemble should provide an unbiased estimate of the prior uncertainty. We recommend that further studies apply history matching with dimensionality reduction techniques to more complex geological models such as bimodal channelized systems; it will also be interesting to introduce into the framework more non-linear dimensionality reduction techniques, such as the deep autoencoder, stacked autoencoder, and generative adversarial network. Additionally, combining the data-space inversion method with an ensemble smoother may also more accurately predict oil production with computationally faster simulations.

3- In the Direct forecasting framework for CO_2 storage, the dimension-reduction method should be selected based on the nature of the variable itself. Accordingly, we observed that principal component analysis was practical in our study for a smoothly diversified time-series dataset (CO_2 saturation around the near wellbore region), and PCA was chosen because it is simple and bijective. Notably, multiple dimension reduction techniques, such as auto-encoder and Gaussian process latent variable models, can be included in the BEL framework. Additionally, the choice of regression technique is guided by the type, dimension, and relationship of the measurements, data, and forecast variables (linear or nonlinear). Owing to the high-dimensionality problems, parametric regression is usually chosen instead of nonparametric techniques, except that a large number of prior samples are available. This work can be improved and extended in several ways. It is important to note that for this study, we have only considered quantities such as CO_2 saturation through wellbores and their respective CO_2 mass and leakage. This approach can be applied to examine the effectiveness of monitoring and monitoring duration to lower uncertainty in risk metrics, such as top-layer CO_2 saturation, plume mobility, and seismic time-lapse data.

Accordingly, it will also be useful to apply direct forecasting procedures to more complex geological models, such as bimodal channelized systems, which can be challenging for traditional (model-based) history matching methods, kernel density estimation, and extensions of canonical correlation analysis can be included in the Bayesian evidential learning framework to tackle more complex nonlinear inverse problems. Finally, using data space inversion (DSI), as described by (Sun and Durlofsky, 2021) CO_2 leakage detection under uncertainty should also be considered.

4- The value of the information framework can generally be applied to any type of spatial data, and in the context of decisions other than reservoir development. The associated computational efficiency allows the value of information computation in complex decision situations. However, the value of information is still quite uncertain, and to consistently provide good estimates of the value of information in complex sequential decision cases, it might be beneficial to increase the number of realizations or reduce the number of alternatives in innovative ways. Therefore, a new procedure and methodology based on clustering techniques, in combination with proxy models, must be developed to reduce computational costs and efficiently solve real-world sequential decision-making problems.

6. References

Adekoya, F. 2009. Production decline analysis of horizontal well in gas shale reservoirs. Master thesis, West Virginia University, Morgantown, WV, USA.

Allen, R.; Nilsen, H.; Lie, K.A.; O, M.; Andersen, O. 2018. Using simplified methods to explore the impact of parameter uncertainty on CO_2 storage estimates with application to the Norwegian Continental Shelf. Int. J. Greenh. Gas Control, 75, 198–213.

Arps, JJ. 1945. Analysis of decline curves. Trans.

Athens, N.D.; Caers, J. 2019. A Monte Carlo-based framework for assessing the value of information and development risk in geothermal exploration. Appl. Energy, 256, 113932.

Betancourt, M., 2018. A conceptual introduction to hamiltonian monte carlo. arXiv:1701.02434.

Bickel, J.E. and Bratvold, R.B. 2007. Decision Making in the Oil and Gas Industry: From Blissful Ignorance to Uncertainty-Induced Confusion. Paper SPE 109610 presented at the SPE Annual Technical Conference and Exhibition, Anaheim, California, 11–14.

Bock B., Rhudy R., Herzog H., Klett M., Davison J., Ugarte D.G.D.L.T., Simbeck D. 2003. Economic evaluation of CO2 storage and sink enhancement options, 10.2172/826435.

Bratvold, R.B., Begg, S., 2010. In: Making Good Decisions, first ed. Society of PetroleumEngineers, Texas, USA.

Bratvold, R.B., Bickel, J.E., Lohne, H.P., 2009. Value of information in the oil and gas industry: past, present, and future. SPE Reservoir Eval. Eng. 12 (4), 630–638. SPE- 110378-PA. https://doi.org/10.2118/110378-PA.

Bratvold, R.B., Thomas, P., 2014. Robust discretization of continuous probability distributions for value-of-information analysis. In: Presented at the International Petroleum Technology Conference, Kuala Lumpur, Malaysia, 10–12 December. IPTC- 17975-MS. https://doi.org/10.2523/IPTC-17975-MS.

Dandekar, R., Dixit, V., Tarek, M., Garcia-Valadez, A. & Rackauckas, C. 2020. Bayesian neural ordinary differential equations.

David, S., Valentin, F., Jan, G. 2019. Deepar: Probabilistic forecasting with autoregressive recurrent networks.

de Myttenaere, A., Golden, B., Le Grand, B. & Rossi, F. 2016. Mean absolute percentage error for regression models, Neurocomputing 192, 38–48. Advances in artificial neural networks, machine learning and computational intelligence.

Duane, S., Kennedy, A., Pendleton, B.J., Roweth, D. 1987. Hybrid monte carlo. Physics Letters B 195, 216-222.

Duong, A. N. 2011. Rate-decline analysis for fracture-dominated shale reservoir. SPE Reservoir Evaluation & Engineering 14(3): 377–387.

Eidsvik J., Mukerji T., Bhattacharjya D. 2015. Value of Information in the Earth Sciences Cambridge Univeristy Press, Cambridge.

Emerick, A.; Reynolds, A. 2013. Ensemble smoother with multiple data assimilation. Comput. Geosci, 55, 3–15.

Longstaff, F., Schwartz, E. 2011. Valuing american options by simulation: a simple least-squares approach Rev. Financ. Stud., 14 (1), pp. 113-147, 10.1093/rfs/14.1.113

Gaspari, G.; Cohn, S. 1999. Construction of correlation functions in two and three dimensions. Q. J. R. Meteorol. Soc.

Geron, A. 2017. Hands-On Machine Learning with Scikit-Learn and TensorFlow: Concepts, Tools, and Techniques to Build Intelligent Systems. USA: OSA: Intelligent Sy.

Greff, K, Srivastava, RK, Koutnik, J, et al. 2017. Lstm: A search space odyssey. IEEE Transactions on Neural Networks and Learning Systems 28(10): 2222–2232.

Harp, D.R.; Stauffer, P.H.; O'Malley, D.; Jiao, Z.; Egenolf, E.P.; Miller, T.A.; Martinez, D.; Hunter, K.A.; Middleton, R.; Bielicki, J. 2017. Development of robust pressure management strategies for geologic CO_2 sequestration. Int. J. Greenh. Gas Control, 64, 43–59.

Hermans, T., Lesparre, N., De Schepper, G., Robert, T. 2019. Bayesian evidential learning: A field validation using push-pull tests. Hydrogeol. J. 27, 1661–1672.

Hersbach, H. 2000. Decomposition of the Continuous Ranked Probability Score for Ensemble Prediction Systems. Weather. Foracsting, 15, 559–570.

Hochreiter, S, Schmidhuber, J. 1997. Long short-term memory. Neural Computation 9(8): 1735–1780.

Hoffman, M.D., Gelman, A. 2014. The no-u-turn sampler: Adaptively setting path lengths in hamiltonian monte carlo. J. Mach. Learn. Res. 15, 1593-1623.

Hong, A., Bratvold, R. B., Lake, L. W. & Maraggi, L. M. R. 2019. Integrating model uncertainty in probabilistic decline-curve analysis for unconventional-oil-production forecasting', SPE Res Eval & Eng 22, 861–876

Howard, R.A., 1980. An Assessment of Decision Analysis. Operations Research, 28(1): 4–27.

Isaaks, E. H., & Srivastava, R. M. 1989. An introduction to applied geostatistics. Oxford. University Press, New York.

Jain, A.K. Data clustering: 50 years beyond K-means. Pattern Recognit. Lett. 2010, 31, 651–666.

Jansen, J.-D., Brouwer, R., Douma, S.G. 2009. Closed Loop Reservoir Management. Presented at the SPE Reservoir Simulation Symposium, The Woodlands, Texas, 2-4 February. SPE-119098-MS. https://doi.org/10.2118/119098-MS.

Jin, L.; Hawthorne, S.; Sorensen, J.; Pekot, L.; Kurz, B.; Smith, S.; Heebink, L.; Hergegen, V.; Bosshart, N.; Torres, J.; et al. 2017. Advancing CO_2 enhanced oil recovery and storage in unconventional oil play—Experimental studies on Bakken shales. Appl. Energy, 208, 171–183.

Jolliffe Ian T. and Cadima Jorge. 2016. Principal component analysis: a review and recent developments Phil. Trans. R. Soc. A.3742015020220150202

Joshi, K. J. 2012. Comparison of various deterministic forecasting techniques in shale gas reservoirs with emphasis on the duong method. PhD thesis, Texas A&M University, College Station, TX, USA.

Kyunghyun, C, Bart van, M, Caglar, G, et al. 2014. Learning phrase representations using RNN encoder-decoder for statistical machine translation,

Lawrence, N.D. 2005. Probabilistic non-linear principal component analysis with Gaussian process latent variable models. J. Mach. Learn. Res. 6, 1783–1816.

Nelson, P.H. 2009. Pore-throat sizes in sandstones, tight sandstones, and shales. AAPG Bulletin 93(3): 329–340.

Ng, AY, Jordan, MI. 2002. On discriminative vs. generative classifiers: A comparison of logistic regression and naive bayes. Advances in Neural Information Processing Systems 14: 841–848.

Nilsen, H.M.; Lie, K.A.; Andersen, O. 2015. Analysis of CO_2 trapping capacities and long-term migration for geological formations in the Norwegian North Sea using MRST-co2lab. Comput. Geosci. 79, 15–26.

Oliver, D.S., Chen, Y. 2011. Recent progress on reservoir history matching: a review. Comput Geosci 15, 185–221. https://doi.org/10.1007/s10596-010-9194-2.

Olson, R. S., Bartley, N., Urbanowicz, R. J. & Moore, J. H. 2016. Evaluation of a tree-based pipeline optimization tool for automating data science, in 'Proceedings of the Genetic and Evolutionary Computation Conference 2016', GECCO '16, Association for Computing Machinery, New York, NY, USA, p. 485–492

Pan, Z. 2016. Revised productivity index equation to improve transient history match for the capacitance resistance model. Master thesis, University of Texas at Austin, Austin, USA.

Peters, E.; Arsts, R.; Brouwer, G.; Geel, C.R.; Cullick, S.; Lorentzen, R.J.; Chen, Y.; Dunlop, N.B.; Vossepoel, C.; Xu, R.; et al. 2010. Brugge Brenchmard study for flooding Optimiztion and History Matching. SPE Reserv. Eval. Eng.13, 391–405.

Pollastro, R. M., Roberts, L. N. R. & Cook, T. A. 2012. Geologic Model for the Assessment of Technically Recoverable Oil in the Devonian–Mississippian Bakken Formation, Williston Basin, in 'Shale Reservoirs—Giant Resources for the 21st Century', American Association of Petroleum Geologists.

Puerta-Ortega C., Bickel J.E., Hovorka S. 2013. Assessing the value of permeability data in a carbon capture and storage project Int. J. Greenhouse Gas Control, 17, pp. 523-533, 10.1016/j.ijggc.2013.06.003.

Satija, A.; Caers, J. 2015. Direct forecasting of subsurface flow response from non-linear dynamic data by linear least-squares in canonical functional principal component space. Adv. Water Resour.

Satija, A.; Scheidt, C.; Li, L.; Caers, J. 2017. Direct forecasting of reservoir performance using production data without history matching. Comput. Geosci. 21, 315–333

Scheidt, C.; Li, L.; Caers, J. 2018. Quantifying Uncertainty in Subsurface Systems, 1st ed.; John Wiley & Sons: Hoboken, NJ, USA.

Scheidt, C.; Renard, P.; Caers, J. 2015. Prediction-focused subsurface modeling: Investigating the need for accuracy in flow-based inverse modeling. Math. Geosci.

Thompson, B. 1984. Canonical Correlation Analysis: Uses and interpretation series: Quantitative applications in the social sciences. 47: 1-71.

Tarantola, A. 2005. Inverse Problem Theory and Methods for Model Parameter Estimation, 1st ed.; SIAM: New Orleans, LA, USA.

Sean J. Taylor & Benjamin Letham. 2018. Forecasting at Scale, The American Statistician, 72:1, 37-45, DOI: 10.1080/00031305.2017.1380080

Valkó, P. P, Lee, W. J. 2010. A better way to forecast production from unconventional gas wells. In: SPE annual technical conference and exhibition.

Van der Maaten, L.; Hinton, G. 2008. Visualizing Data Using t-SNE. J. Mach. Learn. Res. 9, 2579–2605.

Watanabe, S., Datta-Gupta, A. 2011. Use of phase streamlines of covariance localization in Ensemble Kalman Filter for three-phase history matching. In Proceedings of the SPE Western North American Region Meeting, Anchorage, AK, USA.

Wattenbarger, RA, El-Banbi, AH, Villegas, ME, et al. 1998. Production analysis of linear flow into fractured tight gas wells. In: SPE Rocky Mountain Regional/low-permeability reservoirs symposium, Denver, USA, 5–8 April.

Welling, M. & Teh, Y. W. 2011. Bayesian learning via stochastic gradient langevin dynamics, ICML 11, Omnipress, Madison, WI, USA, p. 681–688

Yin, Z.; Strebelle, S.; Caers, J. 2021. Automated Monte Carlo-based Quantification and Updating of Geological Uncertainty with Borehole Data (AutoBEL v1.0). Geosci. Model. Dev. 2019, 13, 651–672.

Zuo, L., Yu, W., Wu, K., 2016. A fractional decline curve analysis model for shale gas reservoirs. International Journal of Coal Geology 163, 140-148.

Paper I

Machine Learning based Decline Curve Analysis for Short-Term Oil Production Forecast.

Amine Tadjer, Aojie Hong and Reidar B. Bratvold.

Research Article

ENERGY EXPLORATION & EXPLOITATION

Energy Exploration & Exploitation
0(0) 1–23

DOI: 10.1177/01445987211011784
journals.sagepub.com/home/eea
SAGE

Machine learning based decline curve analysis for short-term oil production forecast

Amine Tadjer, Aojie Hong and Reidar B Bratvold

Abstract

Traditional decline curve analyses (DCAs), both deterministic and probabilistic, use specific models to fit production data for production forecasting. Various decline curve models have been applied for unconventional wells, including the Arps model, stretched exponential model, Duong model, and combined capacitance-resistance model. However, it is not straightforward to determine which model should be used, as multiple models may fit a dataset equally well but provide different forecasts, and hastily selecting a model for probabilistic DCA can underestimate the uncertainty in a production forecast. Data science, machine learning, and artificial intelligence are revolutionizing the oil and gas industry by utilizing computing power more effectively and efficiently. We propose a data-driven approach in this paper to performing short term predictions for unconventional oil production. Two states of the art level models have tested: DeepAR and used Prophet time series analysis on petroleum production data. Compared with the traditional approach using decline curve models, the machine learning approach can be regarded as" model-free" (non-parametric) because the pre-determination of decline curve models is not required. The main goal of this work is to develop and apply neural networks and time series techniques to oil well data without having substantial knowledge regarding the extraction process or physical relationship between the geological and dynamic parameters. For evaluation and verification purpose, The proposed method is applied to a selected well of Midland fields from the USA. By comparing our results, we can infer that both DeepAR and Prophet analysis are useful for gaining a better understanding of the behavior of oil wells, and can mitigate over/underestimates resulting from using a single decline curve model for forecasting. In addition, the proposed approach performs well in spreading model uncertainty to uncertainty in production forecasting; that is, we end up with a forecast which outperforms the standard DCA methods.

Department of Energy Resources, University of Stavanger, Stavanger, Norway

Corresponding author:
Amine Tadjer, University of Stavanger, Kjell Arholms gate 41, Stavanger 4036, Norway.
Email: amine.tadjer@uis.no

Keywords
Deep learning, probabilistic modeling, production forecasting, time series analysis

Introduction

Hydrocarbon production forecasting includes estimation of the ultimate recoveries and the lifetimes of wells, which are material factors for decision-making in the oil and gas industry because they can impact significantly economic evaluation and field development planning. Although mathematically richer forecasting models (e.g., grid-based reservoir simulation models) have been developed over the past decades, decline curve analysis (DCA) is still widely used because of its simplicity: The mathematical formulations of DCA models are simple with only a few parameters, and only production data are required to calibrate the parameters. The Arps model (Arps, 1945) has been used for DCA for more than 60 years and has been proved to perform well for conventional reservoirs. However, because of the complexity of flow behaviors in unconventional reservoirs as several flow regimes are involved (Adekoya, 2009; Joshi, 2012; Nelson, 2009) the Arps model may not be ideal, and many other models have been proposed (e.g., the Stretched Exponential decline model (Valkó and Lee, 2010), the Duong model (Duong, 2011) and the combined capacitance-resistance model proposed by Pan (Pan, 2016). The Pan model is subsequently referred as Pan CRM in this paper. Some researchers (e.g. Gonzalez et al., 2012) have attempted to identify a single "best" model among several DCA models. However, Hong et al. (2019) have argued that selecting a single "best" model eliminates other potentially good models and exhibits overconfidence (i.e., trust the single model 100%), which can cause significant over/underestimates. Thus, their proposed approach incorporates multiple models by using Monte Carlo simulation to assess the probability of each model and consequently provides a probabilistic forecast of production. Some limitations of Hong et al.'s approach are: (1) a collection of DCA models still needs to be predefined, and (2) the assessed probability of each model is only a measure of the model's relative goodness to other models. If, for example, all the candidate models overestimate production, using Hong et al.'s approach will still result in an overestimated forecast. Thus, an approach that does not require the predefinition of DCA models is deemed preferable; i.e., using a nonparametric model. Machine learning (ML) is still a relatively new technique in the oil and gas industry. Several researchers have discussed the applications of ML for DCA. For instance, (Gupta et al., 2014) used neural networks (NNs)—a ML technique—for DCA. They first trained the NNs using historical data to capture the decline in production in shale formations, and the trained model was then used for prediction. This study also used the autoregressive integrated moving average (ARIMA) (George et al., 2015), a time series analysis to analyze the historical data and identify the trends and relationships of historical and predicted data. Although they applied these two methods for a sample size of around 30 wells, but they did not quantify uncertainties in the forecasted results. (Ma and Liu, 2018) predicted the oil production using the novel multivariate nonlinear model based on traditional Arps decline model and a kernel method. (Aditya et al., 2017) developed a novel predictive modeling methodology that linked well completion and location features to DCA model parameters. The objective of the methodology was to generate predicted decline curves at potential new well locations. (Han et al., 2020) used Random Forest (RF) to develop a

predictive model that can be used to predict productivity during the early phase of production (within 6 months). The required datasets were obtained from 150 wells, targeting shale gas, stationed at Eagle Ford shale formations. Reservoir properties, well stimulation and completion were considered as key input parameters whilst the cumulative production of gas during a span of 3 years was identified as the target variable. Although (Aditya et al., 2017; Han et al., 2020) results were promising, the applicability of their methodology depends heavily on the presence of specific geological, well stimulation and completion data, and the quality and accuracy of the data have a big impact and influence, any anomaly in data consequently make their results less promising. In the context of deep learning, (Luo et al., 2019) built non-linear models using RF and Deep Neural Network (DNN) algorithms to forecast the cumulative production of oil during a span of 6 months. The whole dataset was obtained from around 3600 wells positioned at Eagle Ford formations. Key parameters associated with geological parameters such as structural depth, thickness of the formation, total organic carbon (TOC), number of calcite layers and average thickness of the layer (thickness of the formation divided by the total count of the layers) were identified as the input variables that impacted the productivity of wells in Eagle Ford. In the context of Deep Recurrent Neural Networks, (Lee et al., 2019) used the Long short-term memory (LSTM) algorithm to develop a model for forecasting future shale-gas production. The gas production and shut-in period of the past were taken into account to deduce the input features. The training dataset was collected from 300 wells located in Alberta, Canada, at the Duverney formation. For 15 wells stationed in the same field, the model was tested. The trained model demonstrated the ability to predict production rates over a longer period (55 months). They found out that the method can be used even faster to forecast future production rates and analyze the impact of added attributes such as the shut-in period. It was highlighted that the approach would provide a more reliable and accurate forecast of the production of shale gas and that this method can be used in both traditional and unconventional scenarios. In terms of reliability and utilization, further tuning and improvement of the feature selection process will produce a system with improved predictive capabilities. Stimulation parameters attribute derived from geological knowledge, and refracturing were proposed to be included as possible features that have a critical impact on shale gas production and improve the methode the methodgeological knowledge, and hat the ahose circumstances, the high-intensity drilling associated with unconventional hydrocarbon resources and the underperformance of DCA make this technique more successful. (Zhan et al., 2019) checked the LSTM methoduded as possible features that have a critiduction of oil over two years or even further by using very little previous data acquired during the initial production phases. From over 300 wells stationed in unconventional onshore formations, the required dataset was obtained. Over the first few production years, it is possible to recover around 70% of the total EUR from shale wells, after which a rapid decline is observed. The steepness of the decline makes it hard to survey the trend that causes over-estimation. In such a dynamic situation, they highlighted this methodology's value for forecasting production and assessing the reservoir. They found that the average difference between the accumulated production estimated and observed stayed within 0.2%, while the variance did not exceed 5%. (Sagheer and Kotb, 2019) tested deep LSTM (DLSTM) network predictive efficacy in which more LSTM layers were stacked to address shallow structure limitations when operating with data from long interval time series. They figured that the proposed approach performed much better than other models used in the analysis, like those based on ARIMA, deep gated recurrent unit (GRU), and deep RNN. Based on their applicability, the models

were tested and validated in two real-field case studies, such as India's Cambay Basin oil field and China's Huabei oil field. An ensemble empirical mode decomposition (EEMD) based LSTM was suggested by (Liu et al., 2020) to increase the oil production forecasting speed and accuracy. Two real-field events, the JD and SJ oilfields based in China, were tested to determine and verify the efficacy of the model. The EEMD-LSTM model was contrasted with models EEMD-Suport Vector Machine (SVM) and EEMD-Neural netowrk. The EEMD-LSTM model has been found to work much better as compared to the other models by producing the forecast perfectly and with great quality. Although several machine learning and deep learning models have been proposed to learn better on how to handle multiple seasonal patterns in oil production data. However, to the best of our knowledge, no studies have yet applied such probabilistic model for production forecasting. The novelty of this work is to improve upon the existing techniques used by petroleum engineers to analyze and appraise oil wells. Evaluating oil well potential is a lengthy investigation process. This is because the production profiles can be complex, as they are driven by reservoir physics and made even more challenging by a variety of operational events. Petroleum engineers analyze and evaluate the production profiles of oil wells, understand their underlying behavior, forecast their expected production, and identify opportunities for performance improvements. The investigation process is, nevertheless, time-consuming. This introduces opportunities to optimize these processes. Thus, State-of-the-art level probabilistic machine learning methods are considered DeepAR (David et al., 2019) and Prophet time series analysis (Taylor and Letham, 2007), that are known to be effective in pattern recognition and outperforming the state-of-the-art forecasting methods on several problems. These two algorithms can be used to understand and predict the behavior of oil wells. Our objective is to determine the viability of these algorithms in predicting the distribution of future outcomes, specifically with time series data representing the oil production of petroleum without having substantial knowledge regarding the extraction process or physical relationship between the geological and dynamic parameters. In the remainder of this paper, we first review the DL and time series analysis modeling that will be used to accomplish the task. Thereafter, we explain the evaluation metrics used to assess the quality of the forecast; and finally, we present the experimental results and a discussion of our work.

Time series analysis and DCA

Time series analysis

A time series is a sequence of data obtained at many regular or irregular time intervals and stored in a successive time order; for example, a sequence of measured oil production rates over time. The objective of time series analysis is to extract useful statistical characteristics (e.g., trend, pattern, and variability) from a time series, to determine a model that describes the characteristics, to use the model for forecasting, and ultimately to leverage insights gained from the analysis for decision supporting and making. Traditionally, time series models can be classified into generative and discriminative models, depending on how the target outcomes are modeled (Ng and Jordan, 2002). The main difference between the two models is that generative models predict the conditional distribution of the future values of the time series given relevant covariates while the discriminative models use the past value. In this study, we will use discriminative models, as they are more flexible and require fewer parameters and structural assumptions than generative models. For more details about

generative and discriminative model, see (David et al., 2019; Gasthaus et al., 2019; Ng and Jordan, 2002; Ruofeng et al., 2018).

A critical aspect of discriminative models is the process of reconstructing a single sequence of data points to yield multiple response observations. To solve this, sequence-to-sequence (seq2seq) (Cho et al., 2014) and autoregressive recurrent networks (David et al., 2019) approaches were used to feed and generate output from time series prediction models. In seq2seq, the model is fed a sequence of time series as inputs, and it produces a time series sequence as output, unlike the autoregressive model, which reduces the sequence prediction to a one-step-ahead problem.

DCA

DCA is a type of time series analysis with data type of oil production data. DCA aims to predict the future production of a well or a field based on historical data. The prediction is useful for evaluating the economics of the future production and supporting decisions such as whether a well or a field should be abandoned. Pan's Combined Capacitance-Resistance Model (Pan CRM) is DCA method. It is designed to capture the major flow regimes–transient and semi-steady state flow regimes–relevant for an unconventional well. (Pan, 2016) proposed a model to capture the productivity index behavior over both linear transient and boundary-dominated flow. Its formula is given as:

$$J = \frac{\beta}{\sqrt{t}} + J_\infty \tag{1}$$

where J is the productivity, J_∞ is the constant productivity index that a well will eventually reach at boundary dominated flow, β is the parameter of the linear transient flow, β is related to the permeability in the analytical solution of linear flow into fractured wells presented by (Wattenbarger et al., 1998). Pan obtained the empirical solution of rate over time by combining the previous equation and a tank material balance equation.The standard form is given as:

$$q(t) = \Delta P(\frac{\beta}{\sqrt{t}} + J_\infty)e^{-(2\beta\sqrt{t}+J_\infty t/c_t V_p)} \tag{2}$$

where c_t the total compressibility, V_p the drainage pore volume, and ΔP is the difference between the initial reservoir pressure and the assumed constant flowing bottom hole pressure. For small t, the Pan CRM may offer an unrealistically high rate, as $q(t)$ approaches infinity when t approaches 0. The Pan CRM is analytically derived and has all the parameters associated with a reservoir system's physical quantities. In this study, for each single well, c_t, V_p, ΔP, β and J_∞ are determined through history matching with the goal to minimize a predefined loss (or objective) function by adjusting the model parameters.

Machine-learning models and techniques for time series analysis

Prophet forecasting model

The Prophet forecasting is a bayesian nonlinear univariate generative model for time series forecasting, which was developed by the Facebook Research team (Taylor and Letham,

2007) for the purpose of creating high-quality multistep-ahead forecasting. This model tries to address the following difficulties common to many types of time series forecasting and modeling:

- Seasonal effects caused by human behavior: weekly, monthly, and yearly cycles; dips and peaks on public holidays;
- Changes in trends due to new products and market events;
- Outliers.

The Prophet forecasting model utilizes the additive regression model, which comprises of the following components:

$$y(t) = g(t) + s(t) + h(t) + \varepsilon_t \tag{3}$$

where $y(t)$ is the variable of interest, $g(t)$ is the piecewise linear or logistic growth curve for modeling non-periodic changes in a time series, seasonality $s(t)$ represents periodic changes (e.g., weekly or yearly seasonality), $h(t)$ reflects the effects of irregular holidays, and ε_t represents the error term that accounts for any uncertain changes not accommodated by the model (usually, ε_t is modeled as normally distributed noise).

We invoke the growth trend $g(t)$ as a core component of the entire Prophet model. The trend illustrates how the entire time series expands and how it is projected to evolve in the future. For analysts, Prophet proposes two models: a piecewise-linear model and a saturating-growth model.

Nonlinear, saturating growth is modeled using the logistic growth model, which occurs as follows in its most basic form:

$$g(t) = \frac{C}{1 + exp^{-k(1-m)}} \tag{4}$$

where m is an offset parameter, k is the growth rate, and C is the carrying capacity. However, the value of C is not inherently a constant, which usually varies over time. It was then replaced by a time-varying capability $C(t)$. Moreover, the growth rate of k is not constant. Therefore, it is presumed that the change-point where growth rates change has been integrated and the growth rate between two change-points is constant.

The piecewise logistic-growth model is formed as follows:

$$g(t) = \frac{C}{1 + exp^{-(k+a(t)^T\delta)(t-(m+a(t)^T\gamma))}} \tag{5}$$

where γ is the vector of rate adjustments, δ is the vector of correct adjustments at change-points, and $k + a(t)^T\delta$ is the growth rate at time t. $a(t)$ is defined by the following:

$$a(t) = \left\{ \begin{array}{cc} 1 & t \geq s \\ 0 & otherwise \end{array} \right\} \tag{6}$$

where, s is the time point of change in the growth rate.

Linear growth is modeled using a constant growth rate piecewise, and its formula is given as:

$$g(t) = (k + a(t)^T\delta)t + (m + a(t)^T\gamma) \tag{7}$$

where $a(t)$, k, δ, and γ are the same as the nonlinear trend model.

In the time series, seasonality reflects periodic changes daily, weekly monthly and yearly seasonality. To provide a versatile model of periodic effects, the Prophet forecasting model depends on a Fourier series. Its smooth fitting formula is given as:

$$s(t) = \sum_{n=1}^{N}\left(a_n cos\left(\frac{2\pi nt}{P}\right) + b_n sin\left(\frac{2\pi nt}{P}\right)\right) \tag{8}$$

where P is a regular period that the time series may have (for example, $P = 7$ for weekly data or $P = 365$ for annual data) and N is the number of such cycles that we want to use in the model. The final seasonal model appears as follows when combining all seasonal time series models in $s(t)$ into a vector $X(t)$:

$$s(t) = X(t)\beta \tag{9}$$

where β $Normal(0, \sigma^2)$ is needed before the seasonality to enforce a smoothing.

Holidays and events: To completely understand the effect on holidays of a business time series or other major events such as workover, production shutdown for operations (for example, a workover), these constraints are explicitly set by the Prophet forecast model.

Recurrent neural network (RNN)

Compared with the traditional artificial neural network (ANN), the structure of RNN neuron is different from that of ANN by adding a cyclic connection, which form feedback loops in hidden layers, and hence the information of the last item in RNN can be transmitted to the current item. The structure of RNN neuron is shown in Figure 1. When the

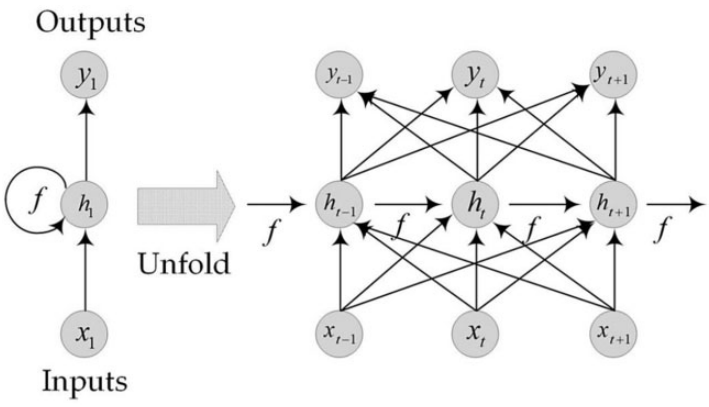

Figure 1. The structure of Recurrent Neural Network.

time series $X = (x_1, x_2, x_3, \ldots, x_n)$ is input, the sequence of hidden layer is $H = (h_1, h_2, h_3, \ldots, h_y)$ and the sequence of output layer is $Y = (y_1, y_2, y_3, \ldots, y_n)$.

The relationship of X, H and Y are listed in the following equations:

$$\left\{ \begin{array}{l} h_n = \sigma(W_{xh}x_n + W_{hh}h_{n-1} + b_h) \\ y_n = W_{hy}h_n + b_y \end{array} \right\} \tag{10}$$

where, σ is the non-linear activation function, W_{xh}, W_{hh} and W_{hy} are the weight matrix from input to hidden layer, hidden layer to hidden layer and hidden layer to output, respectively, b_h and b_y are biased terms.

Long short-term memory neural network (LSTM)

The LSTM neural network model (Greff et al., 2017; Hochreiter and Schmidhuber, 1997) is a type of RNN structure, which is widely used to solve sequence problems. An LSTM tends to learn long -term dependencies and solve the vanishing gradient problems[1] (Grosse, 2017), an issue observed in training ANN with gradient based learning techniques as well as backpropagation algorithms. An LSTM allows the storage of information extracted from data over an extended time period, and shares the same parameters (i.e., network, weights) across all timesteps.

The structure of the LSTM shown in Figure 2 consists of the long term state (c_t) and three multiplicative units N with g(i_t), output gate (o_t), and forget gate (f_t)— and equivalently write, read, and reset information within the model's cells. These three multiplicative gates enable the LSTM memory cells to store and access information over long time periods. The gates control the amount of information fed into the memory cell at a given timestep. Unlike traditional RNN methods that overwrite new content at each timestep, the LSTM state vector and weights are modified at each timestep to take into account any evolution of the input-output relation occurring over time and carry that information over a long

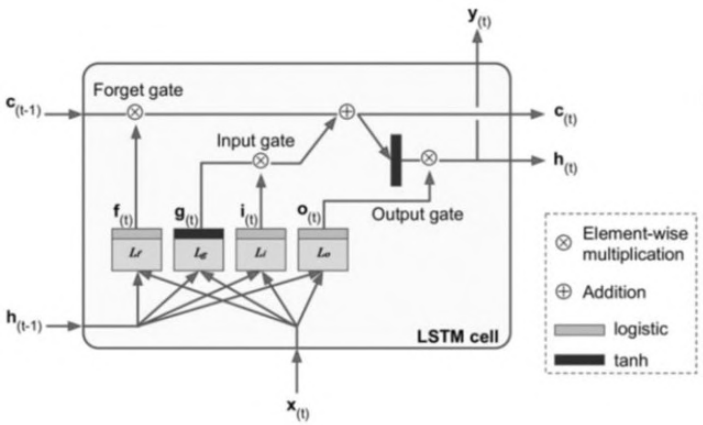

Figure 2. Architecture of an LSTM cell (Geron, 2017).

distance. The LSTM functions are listed as follows:

$$\left\{\begin{array}{l} i_t = \sigma(W_{hi}h_{t-1} + W_{ci}c_{t-1} + W_{xi}x_t + b_i) \\ f_t = \sigma(W_{hf}h_{t-1} + W_{cf}c_{t-1} + W_{xf}x_t + b_f) \\ \bar{c}_t = tanh(W_{hc}h_{t-1} + W_{xc}x_t + b_c) \\ c_t = f_t \odot c_{t-1} + i_t \odot \bar{c}_t \\ o_t = \sigma(W_{ho}h_{t-1} + W_{xo}x_t + b_o) \\ h_t = o_t \odot tanh(c_t) \end{array}\right\} \tag{11}$$

where the input gate (i_t), a forget gate (f_t) and previous cell state $(\bar{c}_t)$ control the current cell state (h_t), and the output gate (o_t) and current cell state (c_t) are used to control the hidden state (h_t) at time t. σ is the element-wise sigmoid function, $\odot$ denotes the elementwise dot product operator, (x_t) is the input vector at time t, and h_{t-1} is the hidden state vector that store all the useful information prior to time t. W_{xi}, W_{xf}, W_{xc}, and W_{xo} denote the weight matrices of different gates for input (x_t); W_{hi}, W_{hf}, W_{hc}, and W_{ho} are the weight matrices for hidden state h_t; W_{ci}, and W_{cf} denote the weight matrices of cell state c_{t-1}; and b_i, b_f, b_c, and b_o denote the bias vector.

Gated recurrent unit (GRU)

The GRU is similar to the LSTM, but with a simplified structure and parameters. It was first introduced by (Kyunghyun et al., 2014). GRUs have been used in a variety of tasks that require capturing long-term dependencies (Junyoung et al., 2014). Similar to the LSTM, the GRU contains gating units that modulate the flow of information inside the unit. However, unlike the LSTM, the GRU does not include separate memory cells, and contains only two gates—the update gate and the reset gate—as displayed Figure 3. The update gate z_t decides how often the unit updates its activation functions. This process takes a linear sum between the existing state and a newly computed state. The second gate within the GRU, the reset gate r_t, acts to forget the previously computed state. The updated functions are listed as follows:

$$\left\{\begin{array}{l} h_t = \left((1 - z_t)h_{t-1} + z_t\tilde{h}_t\right) \\ z_t = \sigma(W_z x_t + U_z h_{t-1}) \\ \tilde{h}_t = tanh(Wx_t + U(r_t \odot h_{t-1})) \\ r_t = \sigma(W_r x_t + U_r h_{t-1})) \end{array}\right\} \tag{12}$$

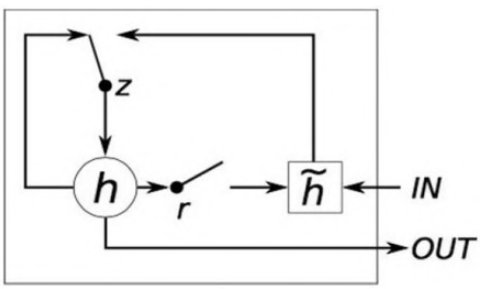

Figure 3. Gated Recurrent Unit: r) and z are the reset and update gates, and h_t and $\tilde{h}_t$ are the activation and the candidate activation (Kyunghyun et al., 2014).

where the activation h_t of the GRU at time t is a linear interpolation between the previous activation h_{t-1} and the candidate activation $\tilde{h}_t$, W denotes the weight matrices, x_t is the input vector at time t, and U denotes the weight matrices of the cell state.

DeepAR

DeepAR is a generative, auto-regressive model. It consists of a recurrent neural network (RNN) using Long Short-Term Memory (LSTM) or Gated Recurrent Unit (GRU) cells that takes the previous time points and covariates as input. In this study, We use the forecasting model from Salinas et al. (David et al., 2019). Unlike other methods of forecasting, DeepAR jointly learns from every time series. In (David et al., 2019) publication, DeepAR was outperforming the state-of-the-art forecasting methods on many problems.

Let $z_{i,t}$ be the value of time series i at time t, the objective is to model the conditional distribution $P(z_i, t_{0:T}|z_{i,1:t_0-1}, x_{i,1:T})$, of the future of each time series $[z_{i,t_0}, z_{i,t_{0+1}}, \ldots, z_{i,T}] := z_{i,t_{0:T}}$, given its past $[z_{i,1}, \ldots, z_{i,t_{0-2}}, z_{i,t_{0-1}}] := z_{i,1:t_{0-1}}$, where t_0 represents the time point from which $z_{i,t}$ is assumed to be unknown at prediction time, and $x_{i,1:T}$ are covariates that are presumed to be known for all time points. The time ranges $[1 : t_0 - 1]$ and $[t_0 : T]$ are the context range and the prediction range, respectively. The model is based on an auto-regressive recurrent network, summarised in Figure 4. The model distribution $Q_\Theta(z_{i,t_0}|z_{i,1:t_0}, x_{i,1:T})$, $x_{i,1:T}$ is considered to be a product of likelihood factors:

$$\begin{aligned} Q_\Theta(z_{i,t_0}|z_{i,1:t_0}, x_{i,1:T}) &= \prod_{t=0}^{T} Q_\Theta(z_{i,t}|z_{i,1:t-1}, x_{i,1:T}) \\ &= \prod_{t=0}^{T} l(z_{i,t}|\theta(h_{i,t}, \Theta)) \end{aligned} \tag{13}$$

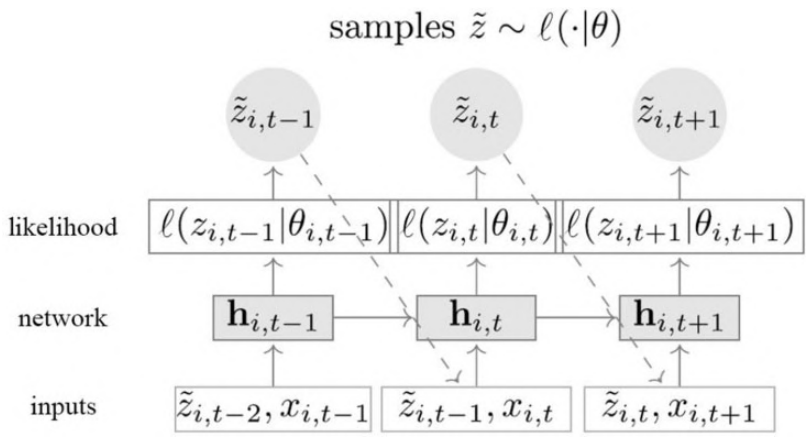

Figure 4. Model Summary: The network inputs are the covariates $x_{i,t}$ at each step t, the goal value at the previous step $z_{i,t-1}$, and the previous network output $h_{i,t-1}$ at each step t. The network output $h_{i,t} = h(h_{i,t-1}; z_{i,t-1}; x_{i,t}; \Theta)$ is then used to measure the parameters $\theta_{i,t} = \theta(h_{i,t}, \Theta)$ of the probability $l(z|\theta)$ that is used to train the parameters of the model. A sample $\hat{z}_{i,t} \sim l(\cdot|\theta_{i,t})$ is fed back to the next step instead of the true value when $z_{i,t}$ is unknown (David et al., 2019).

with $h_{i,t}$ the autoregressive recurrent network output $h_{i,t} = h(h_{i,t-1}; z_{i,t-1}; x_{i,t}; \Theta)$ which will be fed as the next timestep input for $h_{i,t+1}$- $h(\cdot)$ is a function that is implemented by a multi-layer recurrent neural network with LSTM or GRU cells parametrized by Θ, and the likelihood $l(z_{i,t}|\theta(h_{i,t}, \Theta)$ being a fixed distribution parametrized by a function $\theta(h_{i,t}, \Theta)$. The $h_{i;t_0-1}$, initial state contains $z_{i;t_0-1}$, context range information required to predict values in the prediction range.

Given the model parameters required to pred $\hat{z}_{i,t_0:T} \sim Q_\Theta(z_{i,t_0}|z_{i,1:t_0}, x_{i,1:T})$ can be obtained directly by ancestral sampling: First, h_{i,t_0-1} is obtained as as a recurrent network output, then we sample $\hat{z}_{i,t_0:T} \sim l(\cdot|\theta(\hat{h}_{i,t}, \Theta))$ for $t = 1, \ldots, t_0 - 1$, where $\hat{h}_{i,t} = h(h_{i,t-1}, \hat{z}_{i,t-1}, x_{i,t}, \Theta)$ is initialized with $\hat{h}_{i,t_0-1} = h_{i,t_0-1}$ and $\hat{z}_{i,t_0-1} = z_{i,t_0-1}$. The use of these samples makes it possible to calculate quantities, like the value distribution quantities, at a particular time in the prediction range.

Likelihood model. The probability of $l(z|\theta)$ should at best reflect the data statistical properties. It can be selected between any potential possibility, for example, Bernoulli, Gaussian, Binomial-negative, etc.

For instance, the mean and the standard deviation are the parameters $\theta = (\mu, \sigma)$ in the Gaussian likelihood case. These are provided to the network output respectively by the network output and softplus activation to ensure $\sigma > 0$:

$$\begin{aligned} l_G(z|\mu, \sigma) &= \frac{1}{\sqrt{2\pi\sigma^2}} exp(\frac{-(z-\mu)^2)}{2\sigma^2}), \\ \mu(h_{i,t}) &= w_\mu^T h_{i,t} + b_\mu, \\ \sigma(h_{i,t}) &= log(1 + exp(w_\sigma^T h_{i,t} + b_\sigma)) \end{aligned} \tag{14}$$

Loss function. The model parameter Θ which consists of the RNN $h(\cdot)$ parameters and the $\theta(\cdot)$ parameters, can be learned by maximizing the log-likelihood, as follows:

$$\imath = \sum_{i=1}^{N} \sum_{t=t_0}^{T} logl(z_{i,t}|\theta(h_{i,t}) \tag{15}$$

with the time series dataset $z_{i,1:T i:1,\ldots,N}$ and known related covariates $x_{i;1:T}$. No inference is needed to calculate the previous equation compared to state-space models with latent variables, as $h_{i,t}$ is a deterministic input function. It can therefore be explicitly optimized with respect to θ with stochastic gradient descent.

Measures for evaluating forecast

As previously mentioned, the purpose of this task is to predict several future timesteps in the target time series. Confidence intervals are also given and predicting the exact values (such as point forecasting). These are based on percentiles calculated from a probability

distribution based on a fixed number of samples (e.g. DeepAR model). To evaluate the forecast accuracy, we use the mean continuous ranked probability score (mean CRPS).

Mean (CRPS): used to quantify both the accuracy and precision of a probabilistic forecast (Hersbach, 2000). A higher value of mean CRPS indicates less accurate results. CRPS can be defined as:

$$CRPS = \int_{-\infty}^{\infty} [p(x) - H(x - x_{obs})]^2 dx \tag{16}$$

Here, $p(x) = \int_{-\infty}^{x} p(y) d_y$ is the cumulative distribution of a quantity of interest, and $H(x - x_{obs})$ is the step function, i.e.,

$$H(x) = \left\{ \begin{array}{ll} 0 & if < 0 \\ 1 & if \geqslant 0 \end{array} \right\} \tag{17}$$

For N samples, the CRPS can be evaluated as follows:

$$CRPS = \sum_{i=0}^{N} c_i c_i = \alpha_i p_i^2 + \beta_i (1 - p_i)^2 \tag{18}$$

where $p_i = P(x) = i/N$, for $x_i < x < x_{i+1}$ (piecewise constant function).

$$\alpha_i = \left\{ \begin{array}{lll} 0 & if & x_{obs} < x_i \\ x_{obs} - x_i & if & x_i < x_{obs} < x_{i+1} \\ x_{i+1} - x_i & if & x_{obs} > x_{i+1} \end{array} \right\} \tag{19}$$

$$\beta_i = \left\{ \begin{array}{lll} x_{i+1} - x_i & if & x_{obs} < x_i \\ x_{i+1} - x_{obs} & if & x_i < x_{obs} < x_{i+1} \\ 0 & if & x_{obs} > x_{i+1} \end{array} \right\} \tag{20}$$

Data collection and preparation procedure

In this work, we use oil production data from wells in the Midland field. We have selected 22 Midland wells, relatively smooth data, which indicates fewer significant operational changes. The selected Midland wells have been completed in a natural fractured reservoir and measured monthly. However, there are some missing measurements (i.e., no recorded values) for a few months for each selected well. We simply ignore these missing values. Some measurements have recorded zero values, and we suspect they indicate temporary shutdown for operations (e.g., a workover). The zero values may interfere with the training process, so we remove them from the data, then the datasets are rescaled with a standardization. The standardization is included in deep learning to improve neural networks convergence. Table 1 lists the lengths of production history of the selected wells. The lengths range from 105 to 362 months. No matter how long a well's production history is, we use the

Table 1. Production history length of selected midland field wells.

Well-ID	3	5	8	9	11	14	15	16	17	18	20
Length (months)	108	105	105	109	106	308	315	319	362	344	311
Well-ID	21	22	72	142	156	157	171	181	206	249	524
Length (months)	314	307	112	235	246	253	162	136	134	133	105

Table 2. DeepAR fixed training hyperparameters.

Hyperparameter	*Value*
Epochs	100
Batch size	32
Batches/epoch	100

Table 3. DeepAR hyperparameters to optimize for each well.

Hyperparameter	*Value*
Context length	24
Layers	1, 2, 4
Cell type	GRU, LSTM
Cell hidden state size	1,54,560
Gaussian number	1, 3, 8
Dropout rate	0.1, 0.4, 0.6
Learning rate	1e-4, 1e-3, 1e-2

data of the last 24 months (regarded as a short term) for the blind test. Taking Well-ID3 as an example: As shown in Figure 5, the data covers 108 months. The data from Month 1 to 84 are used for building training and forecasting model using DeepAR and Prophet model, and the data from Month 85 to 108 are used for blind testing to assess the performance of prediction results. The same procedure is applied to the 22 selected wells individually.

Models implementation

The two models considered, DeepAR and the Prophet time series, are evaluated based on Midland datasets. The experimental setup which is shared for each dataset evaluation is first described before the dataset experiments.

DeepAR. DeepAR is a model presented by (David et al., 2019) and then implemented in Gluon Time Series (GluonTS). GluonTS is a toolkit developed by Amazon scientists based on the Gluon framework (Alexander et al., 2019). It aims to regroup all the tools required to build deep learning models for time series forecasting and anomaly detection. DeepAR configurations are trained as it is not implemented without early stopping during its

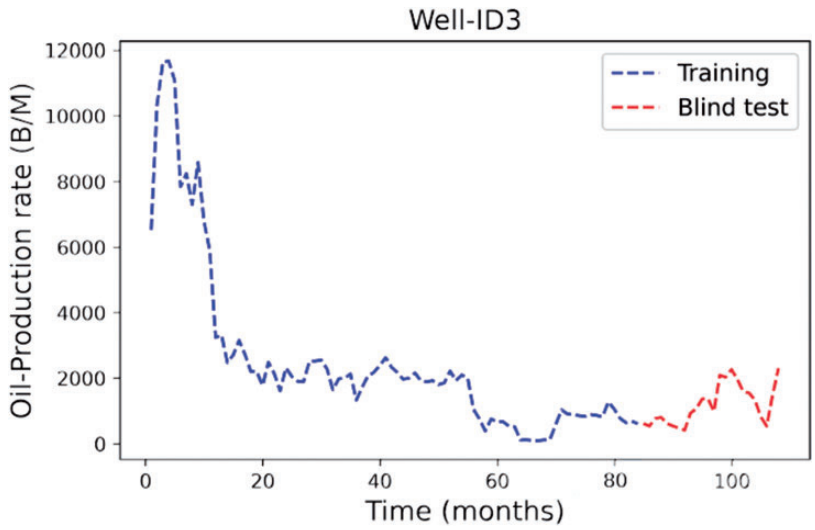

Figure 5. History of oil production rate, Well-ID3.

optimization (cf. Tables 2 and 3). If necessary, the final models are trained on the best parameters without early stopping or validation failure on a new training set. For each selected wells, the optimization is performed on the following parameters:

- The context length and the learning rate: The number of prior timesteps taken to make the most precise forecasts. The tested context lengths depend on the data provided.
- Stacking layer number: The number of layers in the recurrent neural network.
- The cell type: Cell type in the recurrent neural network (GRU or LSTM).
- The number of gaussians: The number of Gaussians considered to be the probability distribution of each timestep in Gaussians' mixture.
- The dropout rate: The output of each LSTM cell is feed to a Zoneout[2] cell which uses this dropout rate (David et al., 2017).

Prophet time series implementation. An open-source implementation of the Temporal Prophet time series model that was published with the paper (Taylor and Letham, 2007) can be found on this web documentation. For each well, the main hyperparameters which can be tuned are:

- Changepoint prior scale: This is likely the parameter that is most impactful. It determines the trend change points in particular. If it is, too, the trend will overfit, if it is too small, the trend will be underfitting, and variation that should have been modeled with trend changes will be treated with the noise term instead. The default value of 0.05 works for several time series, but this can be tuned; the range is [0.001, 0.5].
- Sasonality prior scale: This parameter regulates the flexibility of seasonality. Similarly, a large value helps the seasonality respond to large variations, a small value shrinks the magnitude of the seasonality. The default parameter is 10, with practically no regularisation being applied. This is because overfitting occurs here very rarely (there is inherent

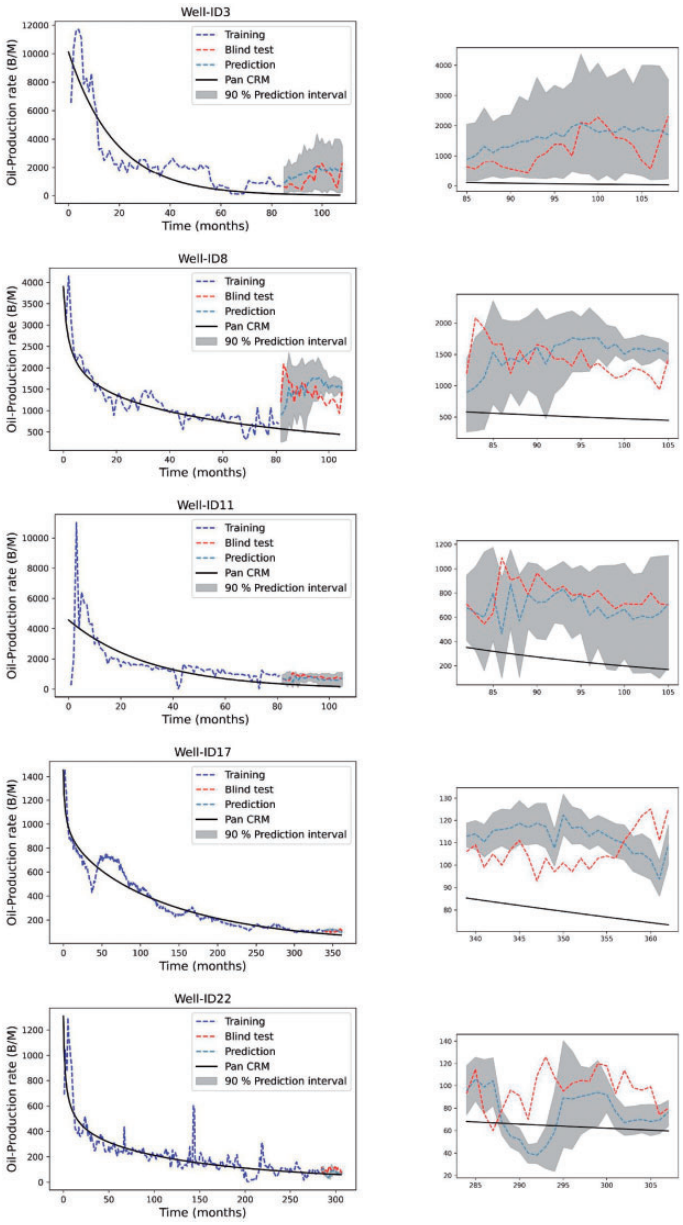

Figure 6. Oil production time series forecast - DeepAR. Left: Overview of forecast. Right: zoomed forecast.

Table 4. Mean CRPS of probabilistic forecast from DeepAR model.

Well-ID	3	5	8	9	11	14	15	16	17	18	20
Mean CRPS	69	29.15	74	93.5	80.9	15.25	7.89	19.17	9.91	12.01	15.18
Well-ID	21	22	72	142	156	157	171	181	206	249	524
Mean CRPS	23.18	22.14	8.35	27.39	3.47	10.50	21.67	21.37	19.69	27.80	29.91

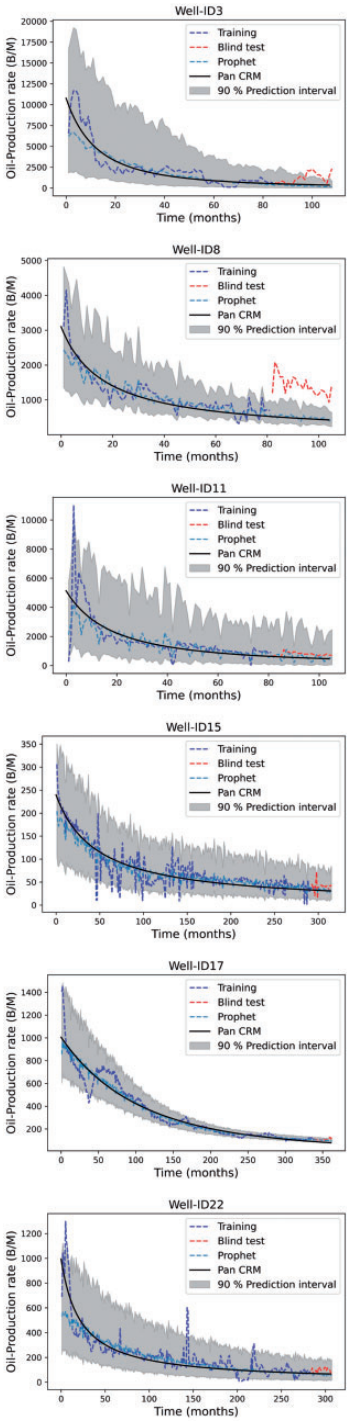

Figure 7. Oil production time series forecast - Prophet.

regularisation because it is modeled with a truncated Fourier sequence, so it is filtered practically low-pass). [0.01, 10] would possibly be a good range for tuning it.
- Growth: Options are 'linear' and 'logistic'.

Results

Figure 6 demonstrates the forecast results for some selected wells using the DeepAR, the means of forecasts (dashed steel blue curve) comparing to blind-test data (dashed red curve) and Pan CRM model (black line curve). In general, the production forecast seems to be reasonable, the DeepAR model can forecast both the upward and downward trends generally well and outperform the Pan CRM model, it is observed that the prediction intervals are, mostly, containing the correct values, except for the well-ID11, this could be explained by being incapable of predicting when changes in production are going to happen. We quantify the accuracy of the probabilistic forecast using the mean CRPS score as listed in Table 4. The results for prediction accuracy are quite satisfactory. In most cases, the mean CRPS decreases as the length of production history increases. This indicates that a longer production history (i.e., more data) will improve the DeepAR model forecast. A major drawback of DeepAR is that it has very little to no interpretability. We cannot interpret any physical meanings from the trained DeepAR model parameters.

Figure 7 shows forecasts from the trained Prophet models. The means of forecasts (the dashed Steel blue curve) follow the blind-test data (dashed red curve in Figure 7) generally well. The P5-P95 prediction intervals (grey band in Figure 7) covers most of the blind-test data. However, for Well-ID8, the forecast significantly deviates from blind-test data and fails to capture both trends and the peaks and troughs reasonably; more specifically, the forecast underestimates the oil production rates.

Compared to Prophet, the DeepAR models represent distinct trends in the mean CRPS score as listed in Table 5. This is possibly due to the DeepAR layer's capacity to "memorize" long-term patterns. In contrast, Prophet's predictions rely majorly on the pattern of the most previous historical data. Besides, DeepAR indicates that the lowest CRPS errors arise. Simultaneously, the difference in values is minimal, even though this statement is only valid for the 5-th and 95-th percentileses. This is demonstrated by the better coverage earned by the longer periods that compensate for the 50-th percentile's low accuracy.

Limitation: In the previous section, we presented DeepAR and Prophet trends in the mean CRPS score as liste months (2 years). We evaluate the performance of the two methods for a forecast horizon of 48 months, as displayed in both Figures 8 and 9, It can be obviously seen that the two methods exhibited quite similar performance almost equally well when the length of wells more than 300 months, for the most part, they well capture the trends of oil production rate in blind tests, and the predictions yielded by each of the models appear to be quite similar. The models were good at predicting trends and flat lines, but sometimes

Table 5. Mean CRPS of probabilistic forecast from Prophet model for each well.

Well-ID	3	5	8	9	11	14	15	16	17	18	20
Mean CRPS	63.4	29.15	174	153.5	180.9	22.83	14.45	32.06	9.41	16.45	25.73
Well-ID	21	22	72	142	156	157	171	181	206	249	524
Mean CRPS	38.21	33.06	14.55	34.27	13.42	14.20	24.65	27.24	18.39	28.63	36.21

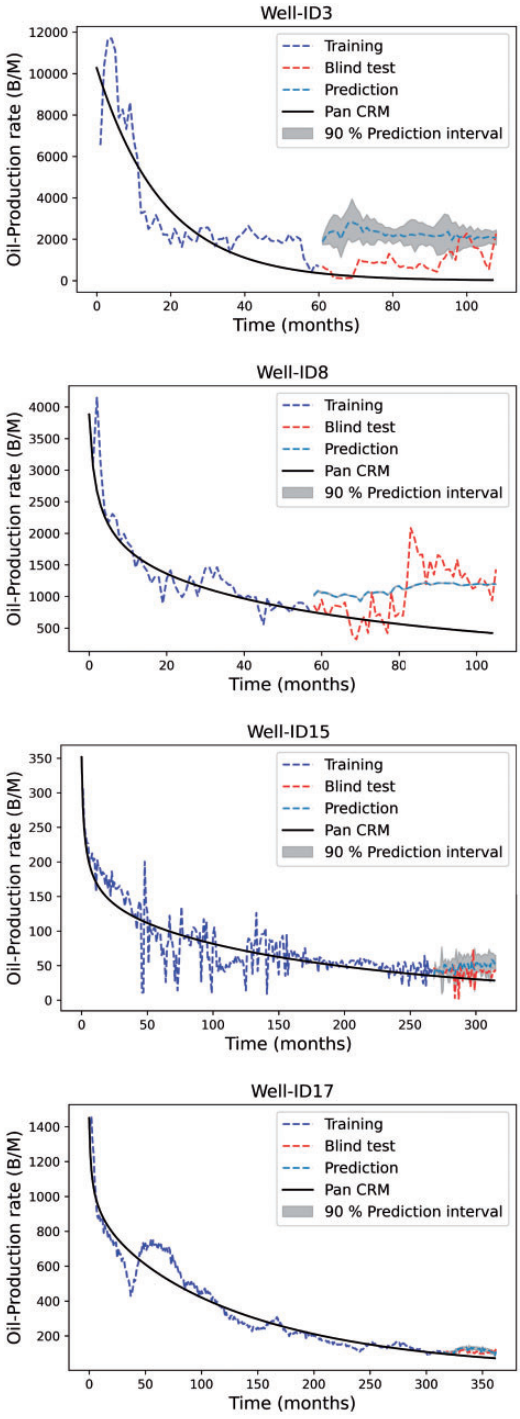

Figure 8. Oil production time series forecast - DeepAR - 48 months horizon forecast.

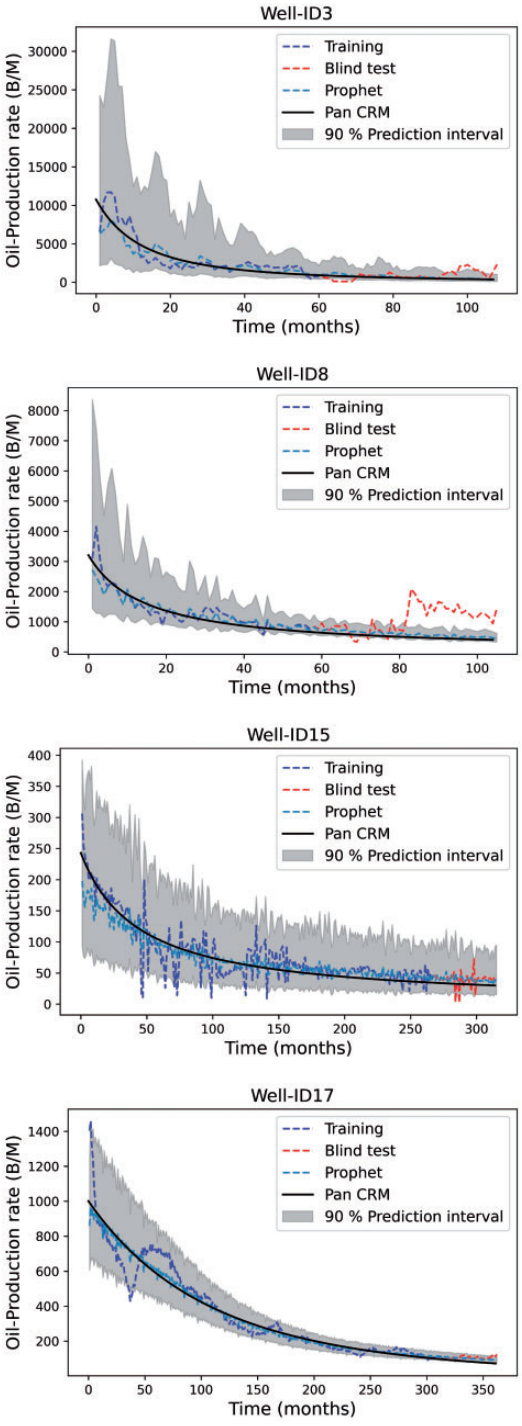

Figure 9. Oil production time series forecast- Prophet - 48 months horizon forecast.

undershot/overshot the peaks and troughs, i.e., Well-ID8. However, both the Prophet and DeepAR did not match production data including quantifying uncertainty, with a small historical data length. Based on the previous results, we can highlight that the two methods enrich the family of time series analysis models by extracting the weighted differencing/trend feature, and contribute to better performance in short-term oil production forecasts, and it can be an alternative way for oil production forecasting in practical application.

Discussion and conclusion

The purpose of this work is to demonstrate a method of machine learning that could replace or accelerate manual DCA for short-term oil and gas well forecasting. Probabilistic Prophet time series analysis and more accurate deep learning models, DeepAR, were considered to solve this problem. These two have been selected as they outperform the state-of-the-art methods of forecasting on many topics. For time series forecasting, Prophet is a Bayesian non-linear univariate generative model proposed by Facebook. The Prophet is also a structural time series analysis method that specifically models the impact of patterns, seasonality, and events. For the Prophet, the cyclical duration and event date parameters are set the same as our model. In contrast, DeepAR is an auto-regressive model based on cells with GRU or LSTM recurrent neural networks. It learns the parameters for each forecast horizon from a given probability allocation. Then, by sampling several times, one can sample from certain probability distributions to forecast each horizon or compute confidence intervals. The model validation was carried out on 22 separate midland reservoir field oil production datasets. Each has had their outliers removed and missing data replaced. They were also standardized as a pre- and post-processing to increase the model's accuracy. Their performances were evaluated based on mean CRPS metrics. The prediction length was initially fixed to 24 months and planned to be increased to 48 months. The models first went through a hyperparameter optimization to select to optimal parameters of each methods of each well. The results showed that the deep learning approach and Prophet analysis yield a satisfactory result in short term forecast, but they may fail to identify long-term trends in predictions unless the predictions are constantly adjusted. However, The both approaches relies on the volume and granularity of data to develop capability for predicting production over a long-time horizon.

This approach can be regarded as "model-free" because, unlike the traditional DCA, the selection of a specific decline curve model is not required. However, It is important to highlight some potential drawbacks of applying time series deep learning for oil production prediction. Deep learning models may suffer significant errors when used for long-term forecasts. This is in addition to their limited interpretability. That is because the predictions are computed sequentially and depend on past predictions that have been appended to the data. Thus, there is a gradual accumulation of error over time. Deep learning models have to be retrained periodically as more data are collected. Otherwise, their predictions become highly inaccurate after a long period. Furthermore, another difficulty that may arise when applying deep learning is that an intermediate-to-expert level of knowledge may be required during model creation and training, as opposed to other out-of-the-box machine learning methods that can be trained easily by adjusting their hyperparameters. Therefore, general NNs may require some adjustments to their cell architecture.

In conclusion, the precise prediction and learning performance presented in the paper suggests that both Prophet and DeepAR are eligible for use in the petroleum industry's

non-linear short-term forecasting problems. Many steps should be taken to further improve the performance of forecasting over long time horizons, such as the application to spatiotemporal tasks or the use of an encoder-decoder from sequence to sequence, where the contextual data (static and dynamic) would be integrated into the model architecture. Additionally, integrating physics constraints during the training of a deep neural network. An advantage of such approach is that physics can be introduced into ML approaches and could replace or speed up manual DCA to perform long term forecast of oil and gas well.

Acknowledgements

The authors acknowledge financial support from the Research Council of Norway through the Petromaks-2 project DIGIRES (RCN no. 280473) and the industrial partners AkerBP, Wintershall DEA, Vår Energi, Petrobras, Equinor, Lundin, and Neptune Energy.

Declaration of conflicting interests

The author(s) declared no potential conflicts of interest with respect to the research, authorship, and/or publication of this article.

Funding

The author(s) received no financial support for the research, authorship, and/or publication of this article.

Notes

1. The term vanishing gradient refers to the fact that in a feedforward network (FFN) the back-propagated error signal typically decreases (or increases) exponentially as a function of the distance from the final layer.
2. Zoneout is an application of dropout where the values are reset to their previous state ($h_t = h_{t-1}$) instead of being dropped out ($h_t = 0$).
3. https://facebook.github.io/prophet/

References

Adekoya F (2009) *Production decline analysis of horizontal well in gas shale reservoirs*. Master thesis, West Virginia University, Morgantown, WV, USA.

Aditya V, Akhil DG and Srikanta M (2017) Modeling early time rate decline in unconventional reservoirs using machine learning techniques. In: Abu Dhabi international petroleum exhibition & conference, Abu Dhabi, UAE, 13–16 November.

Alexander A, Konstantinos B, Michael BS, et al. (2019) Gluonts: Probabilistic time series models in python. Available at: https://arxiv.org abs/1906.05264

Arps JJ (1945) Analysis of decline curves. *Trans*.

Cho K, van Merrienboer B, Bahdanau D, et al. (2014) On the properties of neural machine translation: Encoder-decoder approaches. In: Eighth workshop on syntax, semantics and structure in statistical translation. Available at: https://nyuscholars.nyu.edu/en/publications/on-the-properties-of-neural-machine-translation-encoder-decoder-a

David K, Tegan M, János K, et al. (2017) Zoneout: Regularizing rnns by randomly preserving hidden activations.

David S, Valentin F and Jan G (2019) Deepar: Probabilistic forecasting with autoregressive recurrent networks.

Duong AN (2011) Rate-decline analysis for fracture-dominated shale reservoir. *SPE Reservoir Evaluation & Engineering* 14(3): 377–387.

Gasthaus J, Benidis K, Wang Y, et al. (2019) Probabilistic forecasting with spline quantile function rnns. In: Proceedings of machine learning research (eds K Chaudhuri and M Sugiyama), volume 89, pp.1901–1910.

George EPB, Gwilym MJ, Gregory CR, et al. (2015) *Time Series Analysis: Forecasting and Control*. Hoboken: John Wiley & Sons.

Geron A (2017) *Hands-On Machine Learning with Scikit-Learn and TensorFlow: Concepts, Tools, and Techniques to Build Intelligent Systems*. USA: OSA: Intelligent Sy

Gonzalez RA, Gong X and McVay DA (2012) Probabilistic decline curve analysis reliably quantifies uncertainty in shale gas reserves regardless of stage of depletion. In: *SPE eastern regional meeting*.

Greff K, Srivastava RK, Koutnik J, et al. (2017) Lstm: A search space odyssey. *IEEE Transactions on Neural Networks and Learning Systems* 28(10): 2222–2232.

Grosse R (2017) Lecture 15: Exploding and vanishing gradient. Available at: www.cs.toronto.edu/~rgrosse/courses/csc321_2017/readings/L15\%20Exploding\%20and\%20Vanishing\%20Gradients.pdf

Gupta S, Fuehrer F and Benin CJ (2014) Production forecasting in unconventional resources using data mining and time serie analysis. In: SPE/CSUR unconventional resources conference, Canada, 30 September–2 October 2014.

Han D, Jung J and Kwon S (2020) Comparative study on supervised learning models for productivity forecasting of shale reservoirs based on a data-driven approach. *Applied Sciences* 10(4): 1267.

Hersbach H (2000) Decomposition of the continuous ranked probability score for ensemble prediction systems. weather and forecasting. *Weather and Forecasting* 15(5): 559–570.

Hochreiter S and Schmidhuber J (1997) Long short term memory. *Neural Computation* 9(8): 1735–1780.

Hong A, Bratvold RB, Lake LW, et al. (2019) Integrating model uncertainty in probabilistic decline-curve analysis for unconventional-oil-production forecasting. *SPE Reservoir Evaluation & Engineering* 22(3): 861–876.

Joshi KJ (2012) *Comparison of various deterministic forecasting techniques in shale gas reservoirs with emphasis on the duong method*. PhD thesis, Texas A&M University, College Station, TX, USA.

Junyoung C, Caglar G, KyungHyun C, et al. (2014), Empirical evaluation of gated recurrent neural networks on sequence modeling.

Kyunghyun C, Bart van M, Caglar G, et al. (2014) Learning phrase representations using rnn encoder-decoder for statistical machine translation.

Lee K, Lim J, Yoon D, et al. (2019) Prediction of shale-gas production at duvernay formation using deep-learning algorithm. *SPE Journal* 24(6): 2423–2437.

Liu W, Liu DW and Gu J (2020) Forecasting oil production using ensemble empirical model decomposition based long short-term memory neural network. *Journal of Petroleum Science and Engineering* 189: 107013.

Luo G, Tian Y, Sharma A, et al. (2019) Eagle ford well insights using data-driven approaches. In: International petroleum technology conference, Beijing, China, March 2019.

Ma X and Liu Z (2018) Predicting the oil production using the novel multivariate nonlinear model based on arps decline model and kernel method. *Neural Computing and Applications* 29(2): 579–591.

Nelson PH (2009) Pore-throat sizes in sandstones, tight sandstones, and shales. *AAPG Bulletin* 93(3): 329–340.

Ng AY and Jordan MI (2002) On discriminative vs. generative classifiers: A comparison of logistic regression and naive bayes. *Advances in Neural Information Processing Systems* 14: 841–848.

Pan Z (2016) *Revised productivity index equation to improve transient history match for the capacitance resistance model*. Master thesis, University of Texas at Austin, Austin, USA.

Ruofeng W, Kari T, Balakrishnan N, et al. (2018), A multi-horizon quantile recurrent forecaster.

Sagheer A and Kotb M (2019) Time series forecasting of petroleum production using deep lstm recurrent networks. *Neurocomputing* 323: 203–213.

Taylor SJ and Letham B (2007) Forecasting at scale.

Valkó PP and Lee WJ (2010) A better way to forecast production from unconventional gas wells. In: *SPE annual technical conference and exhibition*.

Wattenbarger RA, El-Banbi AH, Villegas ME, et al. (1998), Production analysis of linear flow into fractured tight gas wells. In: SPE Rocky Mountain Regional/low-permeability reservoirs symposium, Denver, USA, 5–8 April.

Zhan C, Sankaran S, LeMoine V, et al. (2019) Application of machine learning for production forecasting for unconventional resources. In: Unconventional resources technology conference (URTEC).

Paper II

Bayesian Deep DCA: A New Approach for Well Oil Production Modeling and Forecasting.

Amine Tadjer, Reidar B. Bratvold and Aojie Hong.

Published in SPE Reservoir Evaluation & Engineering 2022.
https://doi.org/10.2118/209616-PA

Paper III

Managing Uncertainty in Geological CO2 Storage using Bayesian Evidential Learning.

Amine Tadjer and Reidar B. Bratvold.

energies

MDPI

Article

Managing Uncertainty in Geological CO_2 Storage Using Bayesian Evidential Learning

Amine Tadjer * and Reidar B. Bratvold

Department of Energy Resources, University of Stavanger, 4021 Stavanger, Norway; reidar.bratvold@uis.no
* Correspondence: amine.tadjer@uis.no; Tel.: +33-758-468-202

Abstract: Carbon capture and storage (CCS) has been increasingly looking like a promising strategy to reduce CO_2 emissions and meet the Paris agreement's climate target. To ensure that CCS is safe and successful, an efficient monitoring program that will prevent storage reservoir leakage and drinking water contamination in groundwater aquifers must be implemented. However, geologic CO_2 sequestration (GCS) sites are not completely certain about the geological properties, which makes it difficult to predict the behavior of the injected gases, CO_2 brine leakage rates through wellbores, and CO_2 plume migration. Significant effort is required to observe how CO_2 behaves in reservoirs. A key question is: Will the CO_2 injection and storage behave as expected, and can we anticipate leakages? History matching of reservoir models can mitigate uncertainty towards a predictive strategy. It could prove challenging to develop a set of history matching models that preserve geological realism. A new Bayesian evidential learning (BEL) protocol for uncertainty quantification was released through literature, as an alternative to the model-space inversion in the history-matching approach. Consequently, an ensemble of previous geological models was developed using a prior distribution's Monte Carlo simulation, followed by direct forecasting (DF) for joint uncertainty quantification. The goal of this work is to use prior models to identify a statistical relationship between data prediction, ensemble models, and data variables, without any explicit model inversion. The paper also introduces a new DF implementation using an ensemble smoother and shows that the new implementation can make the computation more robust than the standard method. The Utsira saline aquifer west of Norway is used to exemplify BEL's ability to predict the CO_2 mass and leakages and improve decision support regarding CO_2 storage projects.

Keywords: uncertainty quantification; carbon storage; Bayesian evidential learning; data assimilation

Citation: TADJER, A.; Bratvold, R.B. Managing Uncertainty in Geological CO_2 Storage Using Bayesian Evidential Learning. *Energies* **2021**, *14*, 1557. https://doi.org/10.3390/en14061557

Academic Editor: Muhammad Aziz and Adam Smoliński

Received: 8 February 2021
Accepted: 8 March 2021
Published: 11 March 2021

1. Introduction

Carbon capture and sequestration, also known as carbon capture and storage (CCS), represents a unique potential strategy to minimize carbon dioxide (CO_2) emissions into the atmosphere. It creates a pathway toward a neutral carbon balance, which cannot be achieved solely with a combination of energy efficiency and other forms of low carbon energy. However, it can be achieved if CCS is added as a routine technology to any process that uses fossil fuels. Thus far, geological reservoirs, such as depleted oil or gas fields, or deep saline aquifers, have been considered as appropriate geologic formations for storing CO_2 emissions at a depth of several thousand meters [1–3]. Saline aquifers provide large storage capacities, are broadly distributed geographically, and are more accessible to capture sites as they facilitate the entire CO_2 transport process [4]. Several projects from the pilot-to commercial-scale have been implemented worldwide [5,6]. Cumulative injection of CO_2 in some countries like the United States, Norway, and Canada, is as high as 220 million tons (Mt). The majority of this cumulative (about 75%) is associated with enhanced oil recovery operations [7], and estimates show that geological reservoirs can store between 8000 to 55,000 Gt of CO_2 [8], which is the capacity of over 200 years of current global CO_2 emissions.

However, uncertainties in geological models and rock properties affect the flow modeling and CO_2 storage capacities, mitigating the risk of CO_2 leakage and consequently the contamination of clean groundwater. Ensuring the CCS is safe and successful requires both the storage capacity and CO_2 plume migration estimation, because they are used to identifying the significant uncertainty present in geomodel parameters like porosity, permeability, and caprock elevation. Storage operations monitoring must ensure the CO_2 remains trapped within the reservoir after the injection has stopped.

The standard methods for quantifying uncertainty rely on the consideration of many plausible geological realizations (ensemble model) and quantification of the statistical measures of the ensemble parameters. Assessment of the static/volumetric capacity within a large ensemble model can be easily performed. However, creating highly resolved simulations for all members of a large model ensemble can quickly become computationally intractable, which can be solved either by reducing the number of members of the ensemble or accelerating the simulations required for acquiring each geomodel realization. The uncertainty of specific parameters has been discussed in several previous studies. For instance, Allen et al. [9] proposed a simplified method to investigate the causality and impact of uncertain parameters, including rock properties (permeability and porosity), fault transmissibility, top-surface elevation, and aquifer conditions in term of temperature and pressure in terms of both static trapping capacity and dynamic plume migration estimation.

Several studies have demonstrated the application of a data assimilation and optimization strategy for the minimization and mitigation of risks during CO_2 injections as well as the postinjection period at the storage sites. For instance, Dai et al. [10] introduced a method of analyzing data by employing the probabilistic collocation-based Kalman filter (PCKF) for the optimization of the surveillance operations within GCS projects. The method involves the development of surrogate models with the use of polynomial chaos expansions (PCE) that act as a replacement of the original flow model, followed by an assessment of the reduced variance of the field cumulative CO_2 leak by analyzing the data. Subsequently, a comparison of the data-worth values of each monitoring strategy is done in order to select an optimal monitoring operation scheme. Oladyshkin et al. [11] introduced a framework using polynomial chaos expansion (PCE) as well as bootstrap filters for the assimilation of the pressure data to reservoir models and quantifying the uncertainty reduction of the rate of CO_2 leak within the storage sites. Only three uncertainty parameters were considered: reservoir's permeability, reservoir's porosity, and wellbore's permeability. Sun and Nicot [12] and Sun et al. [13] utilized probability based collocations for the assessment of how detectable the CO_2 leaks were, with the use of the pressure data from the monitoring wells, for the heterogeneous aquifers that are not certain. Additionally, Chen et al. [14] introduced a method that focused on machine learning and filter-based data assimilations to create a CO_2 monitoring design, where one determines the optimal monitoring design by making a choice from the designs for the boosting of the model's ability to predict cumulative CO_2 leakage. Chen et al. [15] further introduced a framework that focuses on the ensemble smoother (ES) with multiple data assimilations (ES-MDA) and the geometric inflation factor (ES-MDA-GEO) to calibrate the reservoir model and monitor the data from storage sites to predict CO_2 migration or leakage detection. González-Nicolás et al. [16] made a comparison of the use of ES and the restarting of the ensemble Kalman filter (EnKF) algorithms to detect pathways of potential CO_2 leakage with the use of pressure data. In this vein, Cameron et al. [17] examined how pressure data works in a zone over the storage aquifer, identifying and quantifying potential leaks. It also performs CO_2 storage by using a particle swarm optimizing algorithm coupled with Karhunen–Loève representations porosities for model reductions, which detect the aquifer model that matches historical data. However, there are still conceptual and computational challenges associated with data assimilation and optimization procedure proposed in the previous listed methods, as generating a set of models properly conditioned to all historical data that preserve the geological realism is very challenging process. The limitations have been well-detailed in Olivier et al. [18], one issue is that of ensemble collapse, which may result in unrealistic un-

certainty and difficulty to coverage to the target distribution. Another practical limitation is to render these approaches relevant for a large variety of problems, such as different prior distributions, different forward models, etc. That also causes significant computational implementation challenges. This study attempts to introduce an alternative approach that can circumvent the different problems associated with model-based approaches.

Recently, several approaches have demonstrated that it is possible to provide the outcomes of subsurface models without the need for model updating and solving the inverse problem [19]. In relation to this context, Scheidt et al. [20] with Satija et al. [21] introduced a new protocol for making decisions under uncertainty called Bayesian evidential learning (BEL). Based on the description provided in [19,22]. BEL relies mainly on data, model, prediction, and decision under Bayesianism scientific methodologies. BEL is usually divided into six main stages : (1) Formulation and definition of the decision problem; (2) prior model definition and specification ; (3) Monte Carlo simulation and falsification of the prior uncertainty models; (4) Global sensitivity; (5) Uncertainty reduction using data; (6) Posterior falsification and decision making. In step 5, one may opt for classical inversion or direct forecasting (DF) [23]. DF utilizes a combination of statistical learning techniques and the Monte-Carlo sampling method to ensure direct relationships between the data and the prediction variables. It should be noted that this method requires no completed explicit model inversions. This results in it being less expensive by a computational amount when compared to the standard inversion methods. Despite the applications being still lower in number, DF was successful in applying case studies related to oil reservoir management, groundwater resources, and geothermal energy problems [21–25]. For instance, Satija et al. [23] used DF to forecast the future reservoir performance by mapping prior predictions into low-dimensional canonical space and estimating the joint distributions of historical and forecast data through linear Gaussian regression; they conclude by stating that this method displayed uncertainty estimates for production forecasts that reasonably agreed with rejection sampling. Yin et al. [22] proposed an extended approach based on direct forecasting, called direct forecasting of sequential model decompositions, in which both geological model parameters and borehole data are used simultaneously. The posterior results displayed large reductions of uncertainty both spatially, through a geological model and using gas volume predictions. In the context of CO_2 storage, Sun and Durlofsky [26] introduced a DF method named data-space inversion (DSI) that quantifies the uncertainties of CO_2 plume locations throughout GCS, where the generation of posterior forecasts of CO_2 saturation distributions were through the simulation results of prior model realizations along with observable data. Notably, the generation of posterior geological models were not in the DSI method, unlike the traditional methods of assimilating data, which involved ensemble-based data assimilations.

In this work, our intended contribution is to demonstrate how BEL protocol can be used in designing an uncertainty reduction strategy in predictions and minimizing the risk of CO_2 leakages, facing various sources in uncertainty in terms of permeability, porosity, temperature, pressure, and caprock depth. Here, we will use a case study problem based on the Utsira sand reservoir, which is a saline aquifer located in the Norwegian continental shelf (NCS). This paper also makes a key contribution in extending the DF procedure through implementing ES-MDA [26] and demonstrating that the DF with ES-MDA [27] is more robust than the standard procedure proposed in Satija et al. [21]. It also provides appropriate posterior uncertainty quantification with results that can be compared to those of the methods proposed in Yin et al. [22]. The paper is structured in multiple sections. In the following section, we present BEL framework and the associated statistical methods used to quantify uncertainty. Then, the proposed methodology can be tested by implementing it in Utsira CO_2 storage site involving many uncertainties. Finally, we provide some concluding remarks and recommend possible future research directions.

2. Methods: Uncertainty Quantification Framework

In this section, we will introduce the BEL procedure for the data assimilation. The BEL procedure is based on a Bayesian formulation in the data space, aiming to sample the conditional/posterior distribution of the interest quantities (in our case, the distribution of CO_2 mass and leakage in the top layer at a future time). BEL can usually be divided into six main stages [22]: (1) Formulation and definition of the decision problem; (2) prior model definition and specification; (3) Monte Carlo simulation and falsification of the prior uncertainty models; (4) Global sensitivity; (5) Uncertainty reduction using data; (6) Posterior falsification and decision making. Since this paper presents a hypothetical (but realistic) case study problem, we will focus on steps 2, 3, and 5.

2.1. Prior Model Definition

The prior sampling aims to identify the possible range of model parameterization and probability distribution for each geological parameter. Let m refer to the vector of uncertain parameters of a reservoir model using a historical data variable (CO_2 saturation near wellbore region, etc.) as vector d. The forecast (quantity of CO_2 mass and CO_2 leakage) is represented by h. The nonlinear function of m through both observed and forecast data forward model is defined as:

$$d = G_d(m) \quad and \quad h = G_h(m) \tag{1}$$

The functions, G_d and G_h, are generated through the use of a reservoir simulator and by forwarding them to prior geological model realizations, we obtain a set of N samples of both data and forecast variables.

$$d = (d^1, d^2, d^3, \ldots\ldots\ldots d^N), \quad and \quad h = (h^1, h^2, h^3, \ldots\ldots\ldots h^N) \tag{2}$$

Note that we refer d_{obs} as the vector of observation and acquired data.

2.2. Prior Model Falsification

Once the prior samples (both historical and forecast data) are extracted, it is important to check whether the observed (reference) prior data can predict posterior distribution that appertains to the prior range. Otherwise, there is a risk that the prediction may be erroneous. If the prior model is false, suggesting data inconsistency, we must revise the prior data distribution herein to assess the prior model's quality and ability to predict the posterior data [19]. A statistical procedure based on Mahalanobis distance *(MD)* [28] is used that handles high dimensional and different types of data measurements with the primary objective of detecting outliers and determining whether the prior model is false or not. The *MD* for each data variable realization d or d_{obs} can be computed as follows:

$$MD\ (d) = \sqrt{(d-\rho)\beta^{-1}((d-\rho)}, \quad for \ \ n = 1, 2, 3\ldots\ldots\ldots, N \tag{3}$$

Here ρ, and β are the mean and covariance of the data d. Assuming that the distribution of the data is multivariate Gaussian, the distribution of $[MD(dn)]^2$ would be chi-squared x_d^2. We set the 95th percentile of the x_d^2 as the tolerance threshold for the multivariate dimensional point d^n. If $MD\ (d_{obs})$ falls outside the tolerance threshold $(MD\ (d_{obs}) > MD\ (d^n)$, the d_{obs} would be regarded as outliers, and the prior model would be determined as false, as it would mean that it has a very small probability. It should also be noted that this method requires data distribution to be Gaussian; if it is not, other outlier detection techniques such as local outliers detection [29], isolation forest [30], and One-Class Support Vector Machines [31] are highly recommended.

Next, a machine learning dimension reduction method is applied (e.g., functional principal component analysis (FPCA) [32] and canonical functional component analysis (CFCA) [33]) are applied to generate reduced dimension vectors in canonical, d^c and h^c, where $dimension(d^c) << dimension(d)$; and $dimension(h^c,) << dimension(h)$.

2.3. Direct Forecasting

Direct forecasting (DF) is a prediction-focused analysis [21,23,25], the main objective is to build a statistical relationship between the observed data and prediction without resolving any geological model inversion problem. More precisely, the main idea behind DF is to make an estimation of the conditional distribution $f(h|d)$ from the prior Monte-Carlo sampling. This conditional distribution can be used to generate posterior samples h. In this paper, we introduce the method proposed in Satija and Caers (2017) [21], which has been successfully used in a variety of previous studies [19,24,25]. This learning strategy depends on mapping the problem into a lower-dimensional space through bijective transformations using machine learning reduction techniques- principal component analysis (PCA) and canonical correlation analysis (CCA) to maximize linearity between both data and prediction varaibles and then fitting the data through multivariate Gaussian distribution. In the multivariate Gaussian, all the conditional distributions can be identified analytically and described as follows:

The linear relationship between data variables and forecast implies that:

$$d^c = G_h^c \tag{4}$$

G is the linear coefficient that maps h^c to d^c. Then, the Gaussian likelihood model is formulated as:

$$L(h^c) = exp(-\frac{1}{2}(Gh^c - d_{obs}^c)^T C_{d^c}^{-1}(Gh^c - d_{obs}^c)) \tag{5}$$

Here, C_{d^c} is the data covariance matrix of the canonical space. Since the prior and likelihood data are multivariate Gaussian, the posterior is as well Gaussian, and the posterior mean and covariance are easily computed using the standard methods [34]. With the likelihood and prior data and a linear model being multivariate Gaussian, the posterior distribution $f(h^c|d_{obs})$ is also multivariate Gaussian with mean $\tilde{h}^c$ and covariance model $\tilde{C}^H$ that has an analytics solution:

$$\tilde{h}^c = \bar{h}_{prior}^c + C_h G^T (GC_h G^T + C_{d^c}) + C_T)^{-1}(d_{obs}^c + G\bar{h}_{prior}^c) \tag{6}$$

$$\tilde{C}_h = C_h - C_h G^T (GC_h G^T + C_{d^c} + C_T)^{-1} GC_h \tag{7}$$

where C_T is the error covariance that occurs as a result of the linear fitting. Thus, we can generate the posterior data by simply sampling from this multivariate Gaussian.

One key element of DF is the way a sufficient Monte-Carlo samples of size N are determined. Following the results of previous studies on hydrogeophysics [25], and on oil reservoirs [23], the range of the realizations size N is generally between 100 and 1000. DF can also be modified. Instead of using linear Gaussian, we can integrate the ensemble smoother with multiple data assimilation (ES-MDA).

2.4. Direct Forecasting-ES-MDA (DF-ES-MDA)

ES-MDA is an ensemble-based method introduced by Emerick and Reynolds in 2013 [27], as an alternative to the sequential data assimilation scheme of EnKF. ES-MDA has successfully improved the performance of history matching, and it is simple to implement. In its simplest form, the method employs the standard smoother analysis equation a predefined number of times along with the covariance matrix of the measured data error that is multiplied by a coefficient a. The coefficients must be selected in a way that the following equation is satisfied.

$$\sum_{k=1}^{N_a} \frac{1}{a_k} = 1 \tag{8}$$

Here, N_a is the number of times the analysis is repeated. The standard ES-MDA analysis that is applied to a vector of model parameters, m, can be written as:

$$m_i = m_i^b + C_{md}(C_{dd} + a_p C_D)^{-1}(d_{obs} - d_{sim,i}), \quad for\ i = 1 \ldots\ldots N \tag{9}$$

Here, the subscript i refers to the ith ensemble member, C_{md} is the cross-covariance matrix between the vector of model parameters m and predicted data d; C_{dd} is the auto covariance matrix of the predicted data d; a_p is the coefficient that inflates C_D, the covariance matrix of the observed data measurement error; d_{obs} is the observation data perturbed by the inflated observed data measurement error; d_{sim} the simulated data based on the previous simulation models; and N is the ensemble size (i.e., number of reservoir models in the ensemble). Conventionally, the ensemble-based history matching simultaneously updates N reservoir models. $C_{md}(C_{dd} + a_p C_D)^{-1}$ refers to Kalman gain K which is computed with regularization by SVD using 99.9% of the total energy in singular values. Refer to [27,35] for more information about the method.

In this work, we modified ES-MDA to generate samples of both historical and predicted data variables $d = [d^c, h^c]^T$, given that the vector of observations d^c_{obs} are considered after applying PCA and CCA. Thus, we can write the DF-ESMDA update equation as:

$$d_i^{k+1} = d_i^k + K^k(d^c_{obs} - d^{c,k}) \tag{10}$$

$$K^k = C_{h^c d^c}(C_{d^c d^c} + a_p C_e)^{-1} \tag{11}$$

$$C_{d^c d^c} = \frac{1}{N_e - 1}\sum_{i=1}^{N_e}(d_i^c - \bar{d^c})(d_i^c - \bar{d^c})^T \tag{12}$$

$$C_{dd^c} = \frac{1}{N_e - 1}\sum_{i=1}^{N_e}(d_i - \bar{d^c})(d - \bar{d^c})^T \tag{13}$$

Here, N_e is the number of components (selected dimension); K refers to the Kalman gain; C_{dd^c} is the cross-covariance matrix between the vector d and historical data; and $C_{d^c d^c}$ is the auto covariance matrix historical data.

2.5. Direct Forecasting on a Sequential Model Decomposition (DF-SMD)

DF can also be extended by replacing the prediction variable h with geological model variable m (porosity, permeability, etc.) to update the geological model variables and to obtain $f(m|_{dobs})$ without traditional iterative model inversions. We employ the same method of [22] which has been successfully applied to update geological uncertainty with borehole data. In case of a reservoir, the geological model m consists of structural model s, rock types r, petrophysical model p, and subsurface fluid distribution f, $m = (s, r, p, f)$.

The prior model uncertainty is defined as the sequential decomposition of specific model variables. In order to condition these model variables to wellbore data, we propose the following direct forecasting equation in a sequential scheme:

$$\begin{aligned} f(m|d_{obs}) = f(s, r, p, f|d_{obs}) = f(f|s_{posterior}, r_{posterior}, p_{posterior}, d_{obs}, f) \\ f(p|, s_{posterior}, r_{posterior}, d_{obs}, p) \\ f(p|s_{posterior}, d_{obs}, p) f(s|d_{obs}, p) \end{aligned}$$

From the equation above, the joint uncertainty quantification is equivalent to a sequential uncertainty quantification. Furthermore, the uncertainty quantification of a model component is conditioned to the near wellbore region data and posterior models of the previous components. Unlike the standard DF of a sequential model decomposition technique, the posterior realizations p and prior realizations f will aid in determining a conditional distribution $f(f|p_{posterior})$; subsequently, we assess this using near wellbore region observations d_{obs} of f.

Moreover, due to the high dimensionality of the model variables, distance-based generalized sensitivity analysis (DGSA) method [36,37] is performed to investigate the effect of model variables m on the data variables and select a subset with m parameters

that have the largest impact on the data variables. The main advantage of DGSA is that it does not require a functional form and it is easy to use and requires relatively low amount of simulations [19]. For more details, see [36–38].

2.6. Uncertainty Reduction Analysis

The uncertainty reduction analysis is considered as one of the important elements of decision assessment, and it is employed after the three methods of direct forecasting are completed. In this paper, we have conducted uncertainty reduction in two metric interests, including CO_2 mass and leakage.

Taking M_c as CO_2 mass and the prior probability density function (PDF) of M_c as $P(M_c)$. $P(M_c)$ is evaluated based on the prior reservoir models. We refer to the number of uncertainty distributions $U(P(M_c))$ in a CO_2 mass $P(M_c)$ as the following:

$$U(P(M_c)) = P_{90}P(M_c) - P_{10}P(M_c) \tag{14}$$

Here, $P_{90}P(M_c)$ and $P_{10}P(M_c)$ are the 90th and 10th percentiles, respectively. The posterior PDF of $P(Mc|d_obs)$ is computed using DF techniques. Therefore, the uncertainty reduction, U_R, is specified as the difference between prior uncertainty and posterior uncertainty in the model outcomes:

$$U_R = U(P(M_c)) - U(P(Mc|d_{obs})) \tag{15}$$

3. Materials

3.1. Model Description

We test the performance level of the proposed methodology in the Utsira sand, which is a saline reservoir located beneath the central and northern North Sea as displayed in Figure 1. In this location, there are over 20 reservoir formations (producing oil and gas fields, abandoned oil and gas fields and geological formations such as saline aquifers). We simply use the reservoir dataset provided by the Norwegian Petroleum Directorate (NPD), which only consists of top-surface and thickness maps and average rock properties. Utsira formation consists of weakly consolidated sandstone with interlayered shale beds that act as baffles for the upward migration of the injected CO_2, and it has an average top-surface depth of almost 800 m below the seabed (within the range of 300–1400 m). The storage capacity of the Utsira system is estimated to be 16 Gt, with a prospectivity of 0.5–1.5 Gt [39]. The boundaries of the aquifers are considered open. An open boundary means that there is communication between the aquifer and anything that lies adjacent to it, be it another aquifer or the sea bottom. The corresponding permeabilities in the Utsira geomodel range from 0.5 to 2.5 darcys. Another study Singh et al. [40] suggested that permeability could represent within the range of 1.1–5 darcys. Furthermore, In the NCS public datasets, there is no information about possible leakage through open boundaries or through the caprock. We acknowledge that these are important factors, but despite these limitations we have decided to use the Utsira available data to demonstrate BEL framework and discuss its advantages and potential benefits in future CCS operations. It is important to emphasize that in our study, some of the injected CO_2 can leave the computational domain during the simulation; these are considered as leaked volumes. Nonetheless, this cannot be the resulting CO_2 that has leaked back into the atmosphere; it will in most instances continue to migrate beyond the simulation model inside the rock volume.

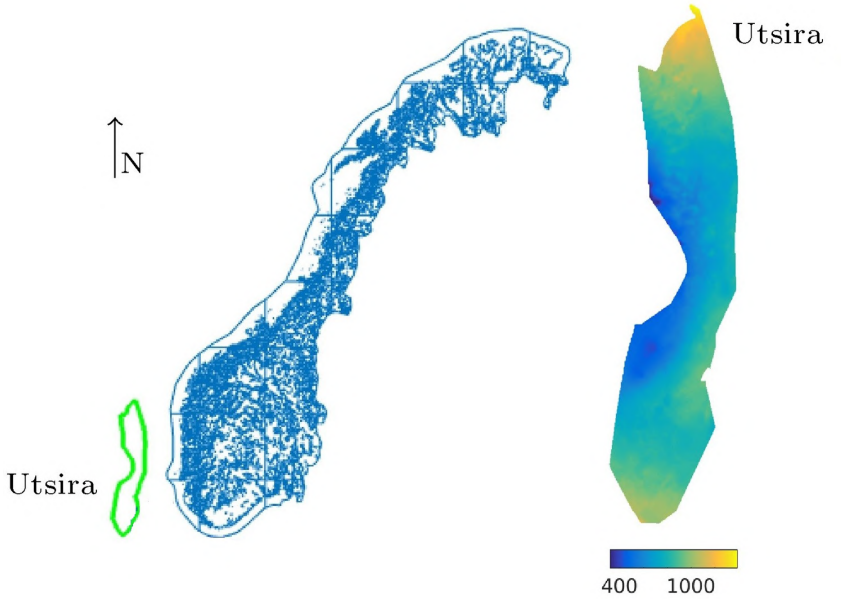

Figure 1. Utsira formation. Location of along the Norwegian Continental Shelf (**left**). Maps of geomodel depths in meters (below the seabed) (**right**) [9].

3.2. The General Setup

A total number of $N = 200$ prior geological realizations were generated using normal Gaussian distribution. There were uncertainties in terms of porosity, permeability, caprock elevation, temperature, and pressure. Following the case study by Nilsen et al. [3], which tested the sensitivity of CO_2 migration to many input parameters, it was found that porosity differences would influence the total volume of rock that the plume comes into contact with. Increasing the thickness of the pore decreases the overall volume of rock occupied by the plume, reducing the migration so that the plume does not move far. Permeability impacts the behavior of CO_2 plume flow by changing its speed and direction, creating a thinner plume that reaches further upslope. As shown in Figure 2, uncertain aquifer temperature and pressure may also affect the CO_2 density, which further impacts plume migration and storage ability estimates.

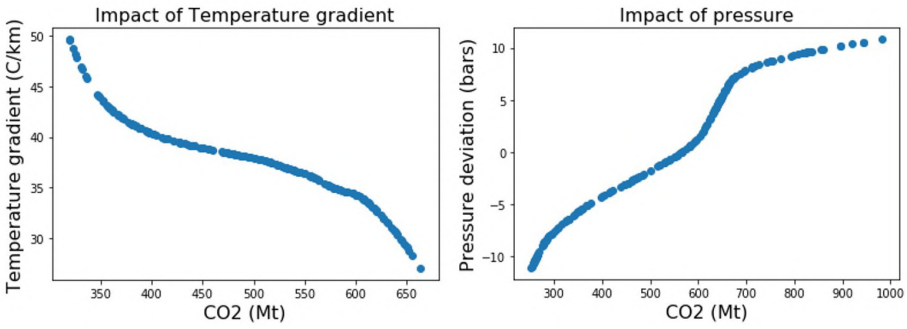

Figure 2. Impact of pressure and temperature gradient in CO_2 storage capacity.

Moreover, we assume that the Utsira reservoir has one injection well at 1012 m depth. Then, an injection rate of 10 Mt per year is considered for a period of 40 years, followed by a 3000-year migration (postinjection) period. Every flow simulation is performed by using the open-source software MRST-CO_2 lab developed by SINTEF [41], the Department of Applied Mathematics. CO_2 lab Computational tools in MRST was specifically designed for studying the long-term and large-scale storage of CO_2.

4. Results and Analysis

4.1. Scenario 1: Uncertainty Reduction Using Direct Forecasting

Prior Model. A set of N = 200 prior reservoir models is generated by using Monte-Carlo to the prior distributions. The selected number of models make certain that the prior distributions are adequately sampled. In all cases, a "reference" model, which is not incorporated in the set of N prior models, is considered. The prior models are forward modeled using a MRST-CO_2 lab over 3000 years. The CO_2 saturation data is collected at near wellbore region during the 40-year injection period. We intend to assess the quantity of CO_2 mass during the postinjection period and the corresponding CO_2 leakage at the end of time tracking period (3000 years). The prior distribution of modeled of the data variables for the injection well as well as the forecasts are shown in Figures 3 and 4. From both figures, we notice a large amount of uncertainties is involved.

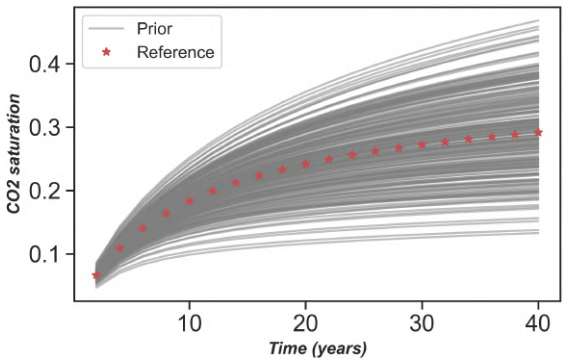

Figure 3. Prior measurement data variables.

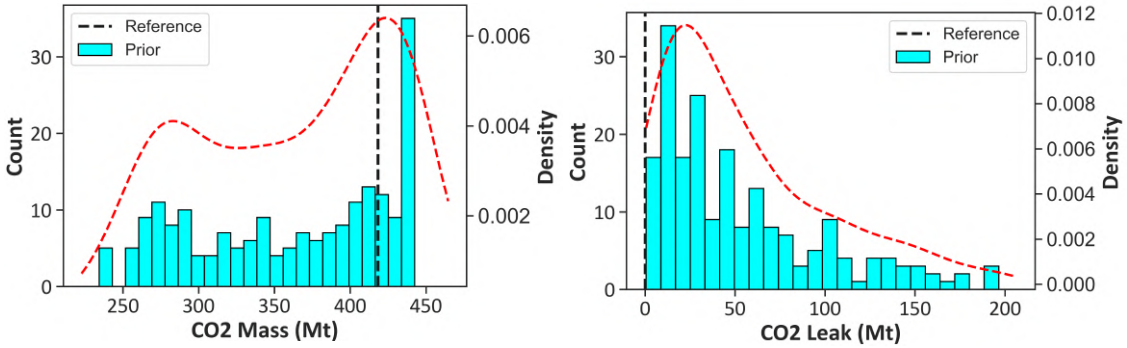

Figure 4. Prior distribution of prediction data variables—3000 years. The red dashed line is the prior probability density function.

Falsification. To assess the quality of the prior models, data variables (CO_2 saturation) of the injection well of 200 prior models are used with d_{obs} by employing the MD outlier detection. The MD of d_{obs} is found to be 2.261, which is below the 95-percentile threshold, which suggests that the prior model is correct. Figure 5 shows the comparison of MD with d_{obs} and MD with 200 prior models.

Dimension Reduction and Linearization. To establish a relationship between the data and forecast variables, it is first necessary to ensure low dimensionality in both variables. For this purpose, we perform FPCA on the data variables d and h by selecting the principal components (PCs) that preserve 90 % variance. Accordingly, three dimensions are retained for both the data and forecast variables (CO_2 mass and CO_2 leak). The choice of the three dimensions is based on a compromise—it is important to keep as much variance as possible while ensuring maximum reduction of the problem's dimensionality. Thereafter, CCA is conducted to the reduced data and prediction sets to maximize linearity between the reduced data and forecast. As shown in Figures 6 and 7, the relationship between the components in the functional domain is not linear; the application of CCA subsequently

increases the correlation between the components in the canonical space, except the third dimension as displayed in Figure 6—CCA fails to establish a unique linear relationship.

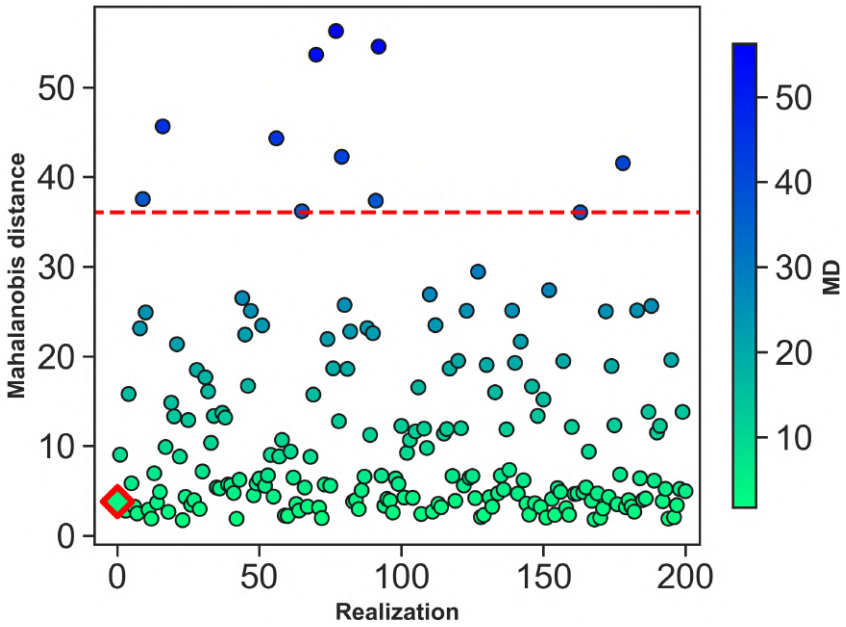

Figure 5. Prior falsification using Mahalanobis Distance (MD). The red square is the MD for d_{obs}. Circle dots Refer the MD Results of 200 data variable samples, and the red dashed line is the 95th percentile of the Chi-Squared distributed MD.

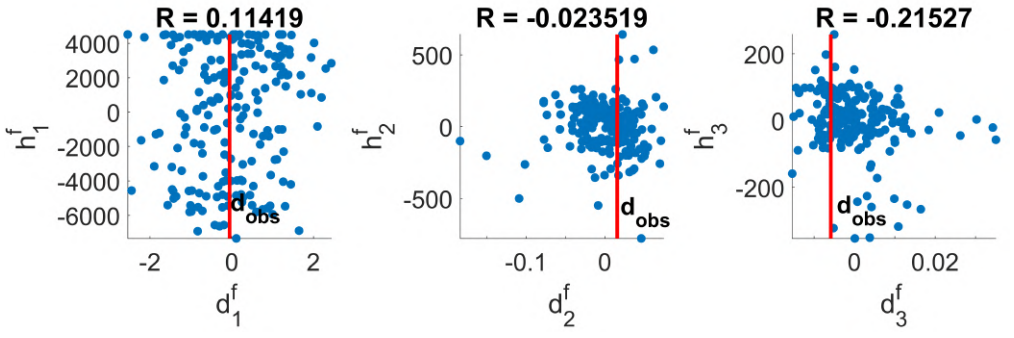

(**a**) PCA correlation analysis.

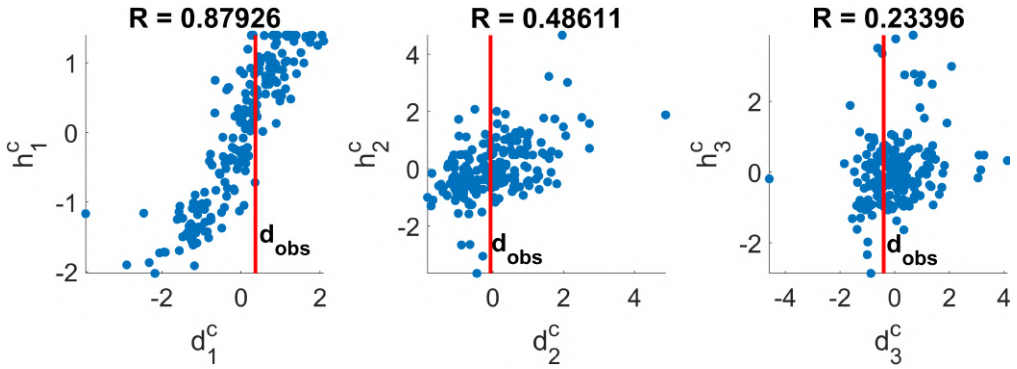

(**b**) PCA correlation analysis in canonical space.

Figure 6. Functional components correlation analysis. Red lines correspond to the observed (CO_2 mass).

Reconstruct Posterior Model. After a linear correlation in low dimensions has been established, we calculate the posterior distribution of the forecast components. First, we

use the linear Gaussian regression equation that has been explained in one of the previous sections, for which h^c must be first transformed using a normal score to get h^c_{gauss}. Thus, Gaussian regression generates a multivariate normal posterior $f(h^c_{gauss}|d_{obs})$ which can be easily used to sample forecast components that are conditioned to d^c_{obs}. Second, we apply modified ES-MDA explained in one of the previous sections to generate the posterior distribution of forecast variables h^c. Moreover, we used $Na = 4MDA$ iterations. It must be noted that we have added random Gaussian noise to d^c_{obs}, with a mean of zero and a standard deviation of 10%.

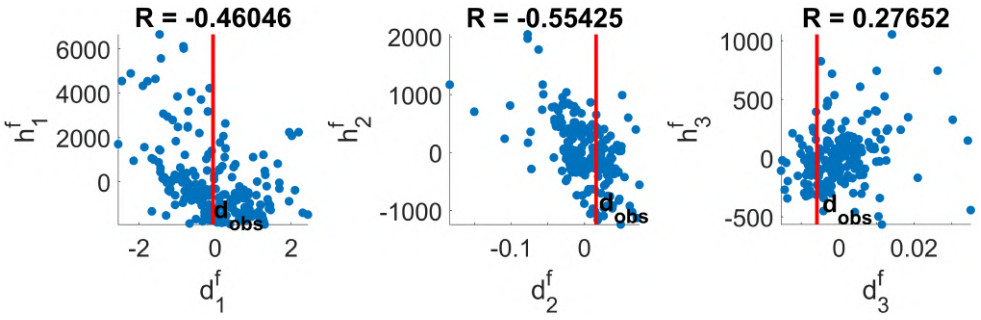

(**a**) PCA correlation analysis.

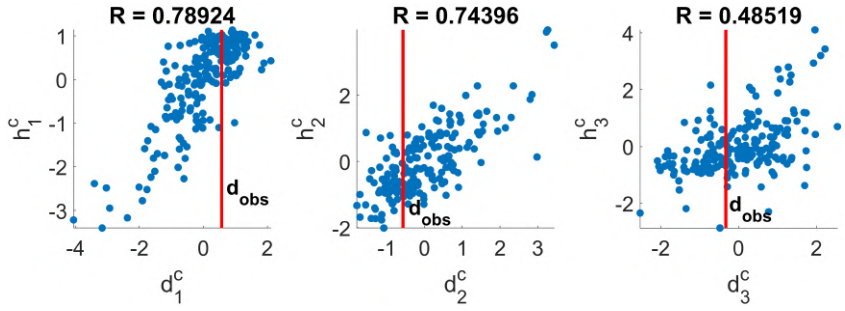

(**b**) PCA correlation analysis in canonical space.

Figure 7. Functional components correlation analysis. Red lines correspond to the observed (CO_2 Leak).

Once the posterior distribution of the prediction in the latent dimension space is established, it can be easily sampled and transformed back into the original initial space, where the posterior distribution of the prediction is shown in Figures 8 and 9; we notice that the DF with Gaussian regression techniques predicts a larger uncertainty range for both CO_2 mass and leakage after 3000 years compared to DF with ES-MDA, for which results are reasonable and data match is excellent, the uncertainty bands are reduced for both CO_2 mass and leakage at the end of 3000 years. The results stipulate that the proposed DF-ESMDA is more robust than the original DF. Both methods are fast in terms of computation, but they require running reservoir simulations of the prior ensemble, which definitely consumes a lot of the computational time.

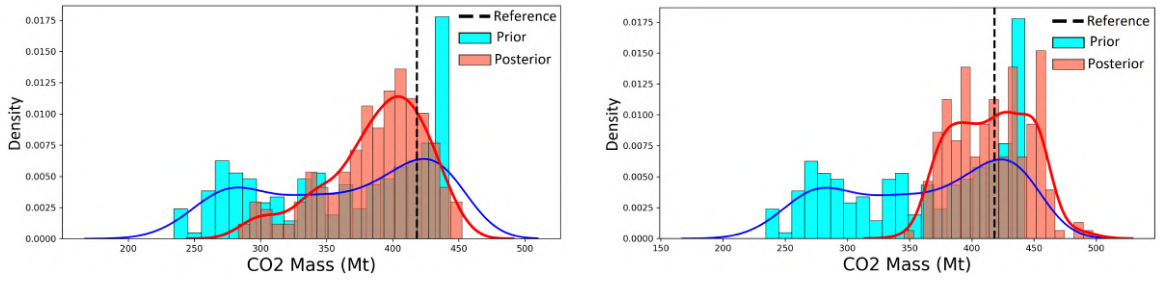

(**a**) DF. (**b**) DF-ES-MDA.

Figure 8. Reconstruct posterior CO_2 mass.

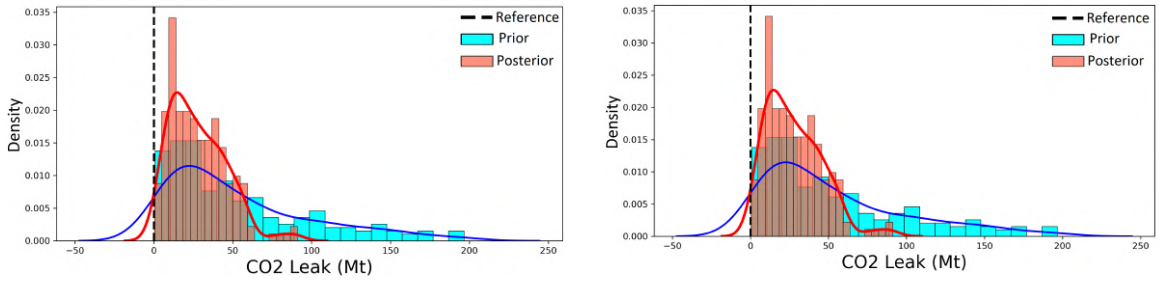

(**a**) DF. (**b**) DF-ES-MDA.

Figure 9. Reconstruct posterior CO_2 leak.

4.2. Scenario 2: Uncertainty Reduction Using Direct Forecasting on a Sequential Model Decomposition

We use the same generated prior model used in Scenario 1, but as discussed in the previous section, we replace the prediction variable h with geological model variable m to obtain $f(m|d_{obs})$.

Dimension Reduction. We perform PCA on the model variable m, which consists of permeability, porosity, temperature, and pressure; we select the PCs that preserve 90% variance. As displayed in Figure 10, 102 dimensions are retained for both permeability and porosity, and 165 dimensions are kept for temperature and pressure, respectively.

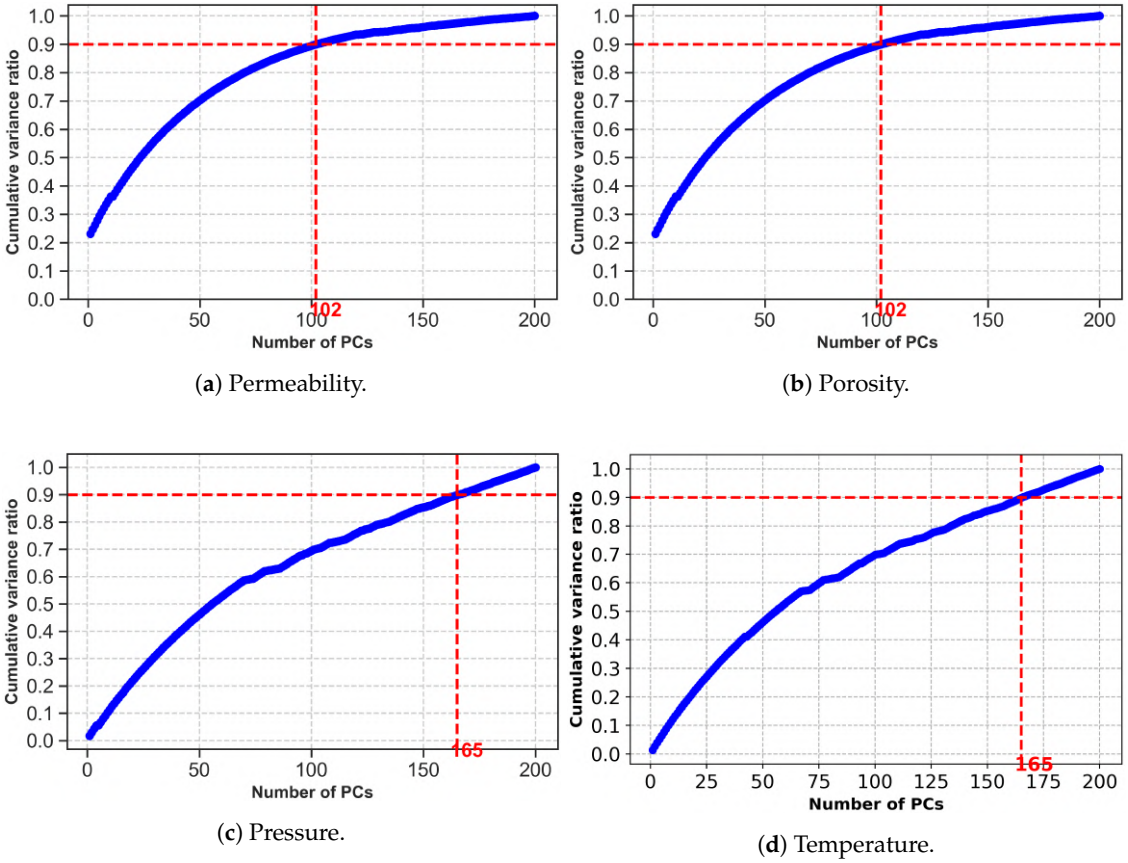

(**a**) Permeability. (**b**) Porosity.

(**c**) Pressure. (**d**) Temperature.

Figure 10. Cumulative sum of the PCA eigenvalues for the model m variables.

Global Sensitivity Analysis. In the next step, we would intend to find which PCA components impact the data prediction such that we can purpose a strategy for reducing the uncertainty of prediction variables. We apply DGSA based on a Euclidean distance to assess global sensitivity. Figure 11 outlines the main effects on a Pareto plot in which DGSA identifies the nonsensitive (measure of sensitivity < 1) and sensitive (measure of sensitivity > 1)

effects. In total, 18 sensitive principal components exist from the pressure spatial model, 22 for temperature, 11 for porosity, and 16 for permeability. These sensitive principal component and global variables scores are now assigned for uncertainty quantification.

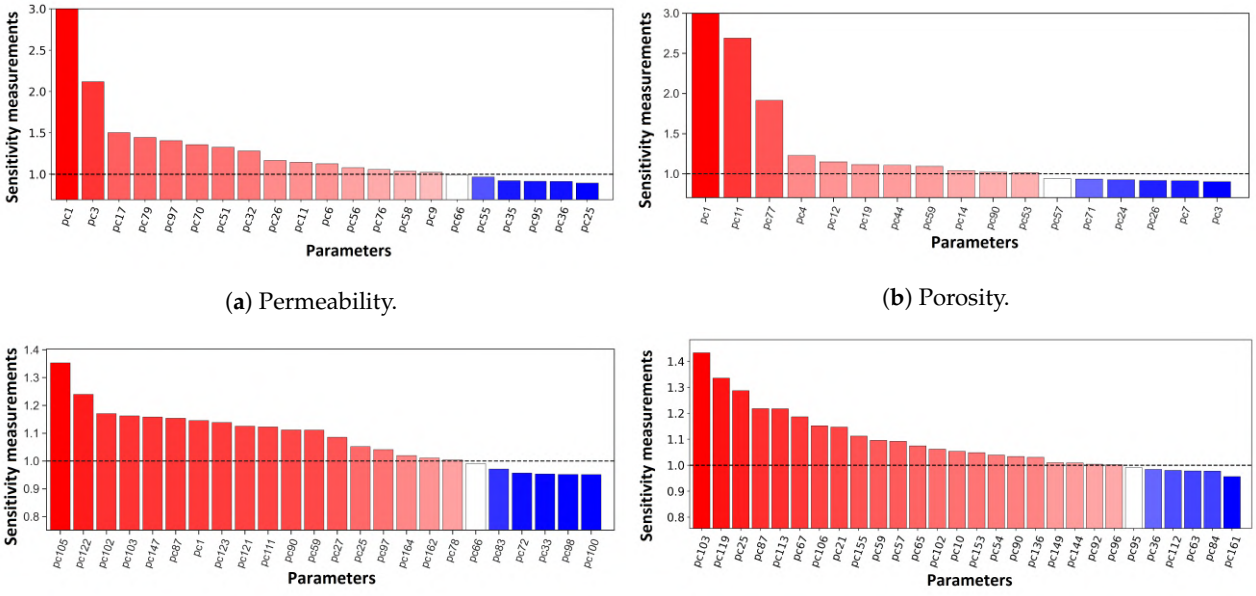

(**a**) Permeability.

(**b**) Porosity.

(**c**) Pressure.

(**d**) Temperature.

Figure 11. Global sensitivity of model parameters to measured data.

Linearization. After all sensitive model variables have been mapped into a lower-dimensional space, we require the application of CCA to establish a useful relationship between model variables and data variables. Figure 12 indicates that the primary canonical components d and m exhibit much stronger correlations.

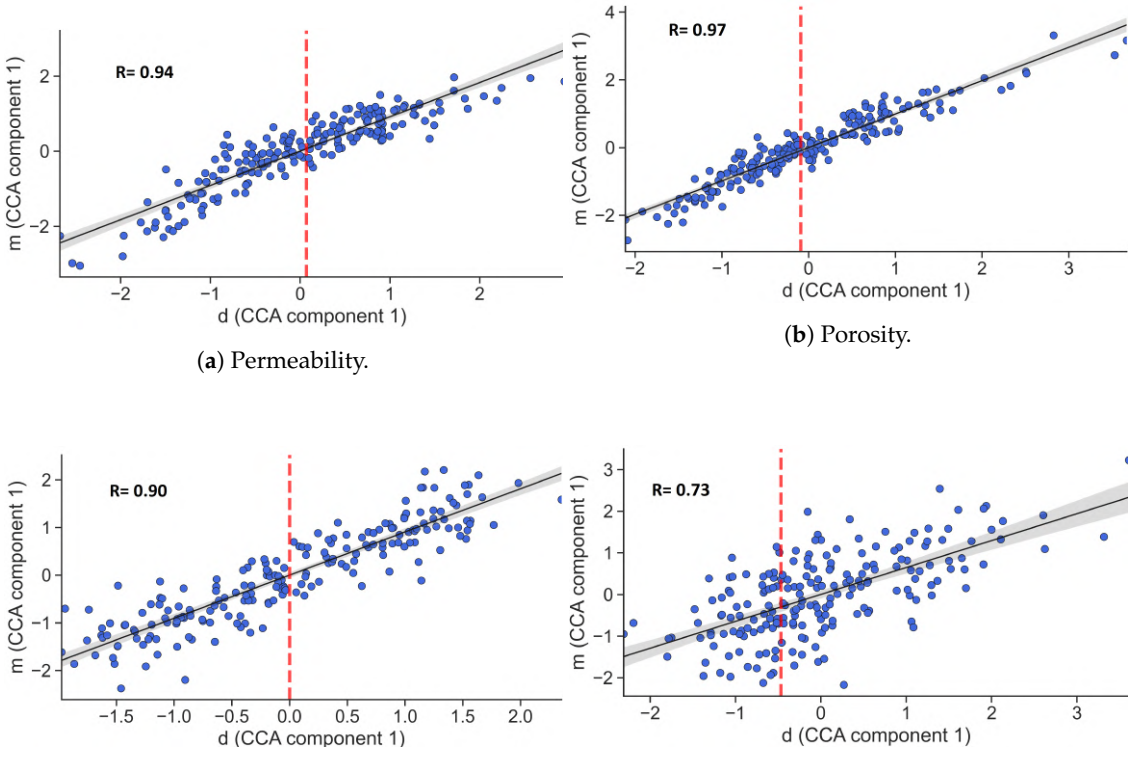

(**a**) Permeability.

(**b**) Porosity.

(**c**) Pressure.

(**d**) Temperature.

Figure 12. First canonical covariates of data and model variables. Red dashed lines correspond to the observed data.

Reconstruct Posterior Model. Once the linear correlation is maximized in low dimensions, it becomes easy to sample the posterior distribution and transform back lower-dimensional scores into original permeability, porosity, temperature, and pressure dimension scores. Figure 13 depicts the posterior distribution model realizations by comparing it to the following prior model, indicating that the model uncertainty range has reduced. We compare the score of both prior and posterior distribution along the two sensitive PCs with the highest score. From Figure 14, we notice that the prior samples' uncertainty has remarkably reduced. Note that the uncertainty quantification includes all the PCs sensitive score variables.

Figure 15 compares the Empirical CDF of the ensemble means of the sampled posterior log-perm, porosity, pressure, and temperature to their counterparts in the prior models. The results suggest a slight change on the distribution posterior model. Moreover, the uncertainty reduction is achieved, as the posterior samples are conditioned to the data variables of the well that are held in within the prediction domain. For verifying this results, we forward the posterior samples model m for simulation and extract the CO_2 mass and CO_2 leak posterior samples, and indeed, the posterior prediction distribution from evidential analysis accordingly reduces the uncertainty on the CO_2 mass and CO_2 leak as displayed in Figure 16; hence, this provides the input information required on the distribution of the data regarding CO_2 leakage at the end of migration tracking time (3000 years). From Table 1, it can be observed that integration of DF with ES-MDA would result in higher uncertainty reduction of CO_2 leakage (29.82–66.40 Mt) than the other techniques at both 40 years (after which we stop injection) and 3000 years.

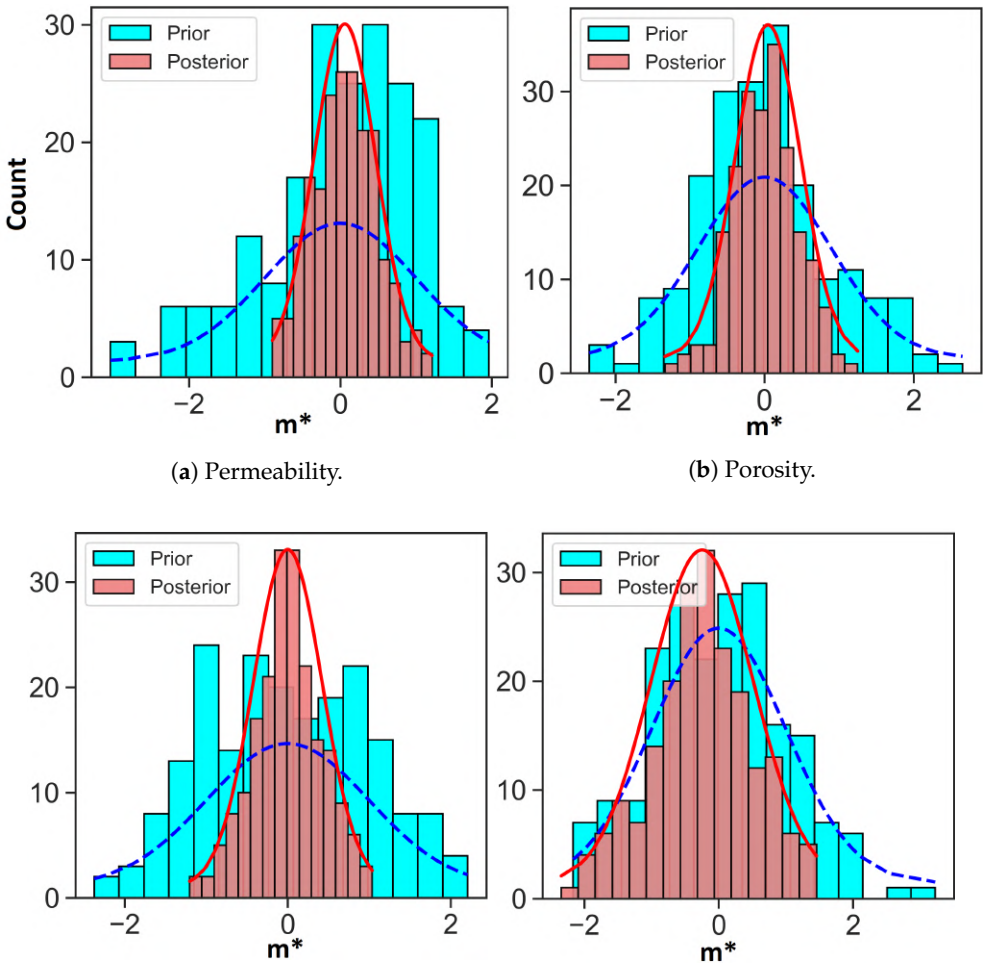

(**a**) Permeability. (**b**) Porosity.

(**c**) Pressure. (**d**) Temperature.

Figure 13. Posterior and prior distributions of model variables (first canonical components).

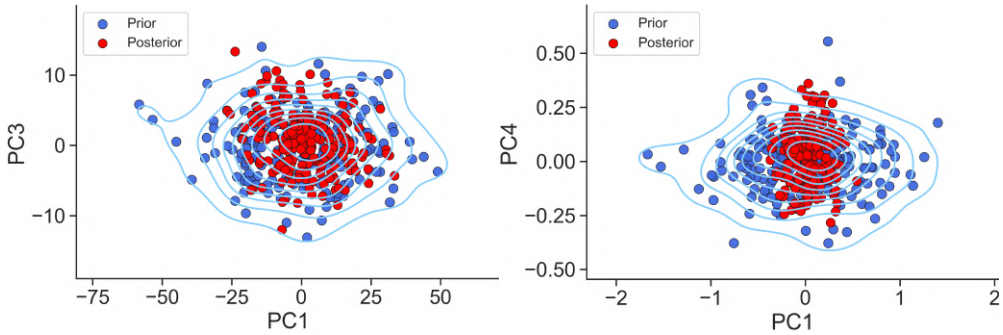

(**a**) Permeability. (**b**) Porosity.

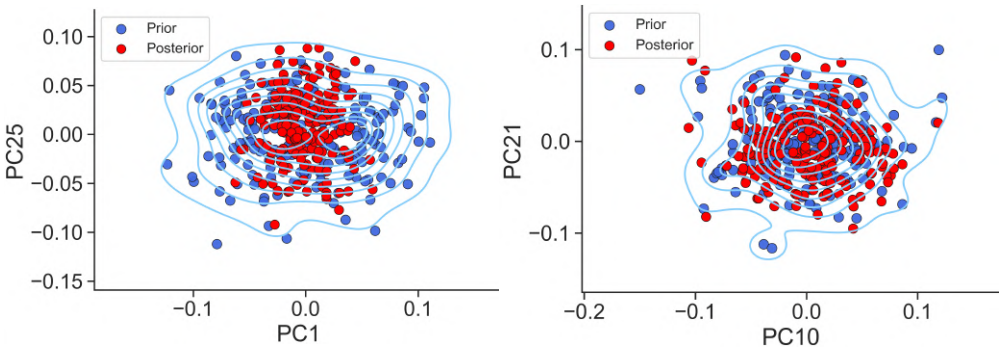

(**c**) Pressure. (**d**) Temperature.

Figure 14. Prior and posterior distribution of the scores of the two sensitive PCs with the highest variances.

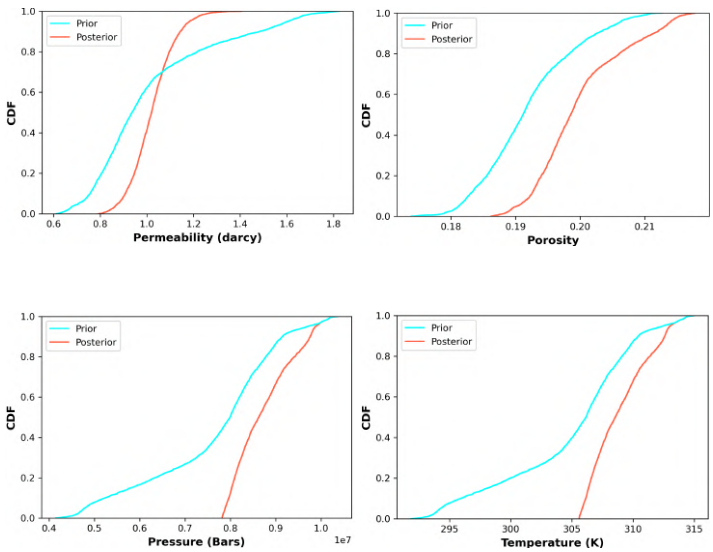

Figure 15. Empirical CDF computed from ensemble means of prior and posterior parameters.

Table 1. Uncertainty Reduction (UR) of CO_2 leak (Mt).

Methods	UR—40 Years	UR—3000 Years
DF	26.11	51.563
DF-ES-MDA	**29.82**	**66.40**
DF-SMD	28.35	56.83

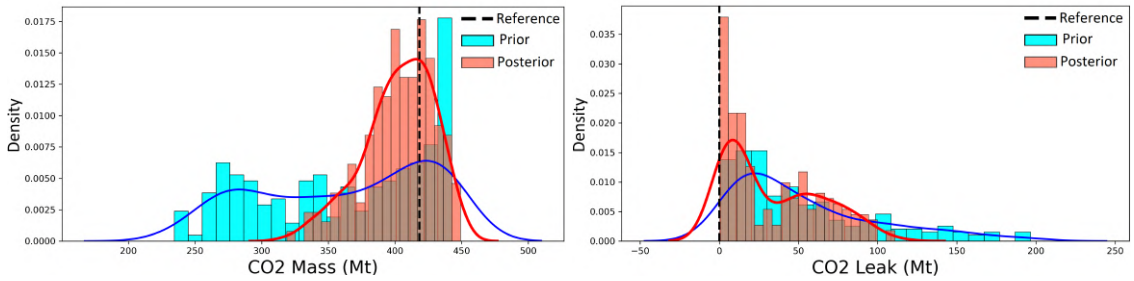

Figure 16. Posterior distribution of CO_2 mass and leakage at 3000 years using DF-SMD. Black dashed lines correspond to the observed data.

5. Discussion and Concluding Remarks

This paper makes a contribution by showing a novel approach to quantify uncertainty during the injection of CO_2 for its storage and migration in deep saline aquifers by applying a Bayesian evidential learning (BEL) framework that involves falsification, global sensitivity analysis, and direct forecasting (DF). We presented a new DF implementation coupled with ES-MDA. The proposed DF-ES-MDA was compared with the original DF proposed in [21,23] and DF with sequential model decomposition in [22]. Both of the original methods mitigate the uncertainty reduction to a linear problem by reducing the high dimensionality of the original data using PCA and CCA; then, we established a statistical relationship between the data and forecast for DF and among the model, data, and forecast for DF-SMD. This estimated relationship combined with Bayesian Gaussian regression is thus used to generate a statistical forecast of the interest quantities—in our study, CO_2 mass and leakage. The new implementation preserves the main advantage of the original DF—its ability to provide an ensemble of CO_2 mass and leakage forecasts without iterative data inversion or history matching problems that can be computationally expensive and difficult. The three methods are advantageous even though the time to execute the reservoir simulations for the prior models tends to be time consuming. We compared the DF-ES-MDA with the original DF and DF-SMD of a real field case. Moreover, we showed that the accuracy of the DF-ES-MDA was consistently enhanced and a higher degree of uncertainty reduction could be achieved.

However, some criteria must be addressed to ensure the high-quality formulation of the three methods, in that a key for successful BEL framework application is the definition of the prior model, which should retain geological realism, as an unrealistic large uncertainty range may impact the data-prediction relationship and minimize accuracy. As such, a multivariate outlier detection method is employed to examine the quality of the prior model distribution compared to the observed case. Furthermore, the dimension reduction method should be selected based on the nature of the variable itself. Accordingly, we observed that FPCA was practical in our study for smoothly diversified time-series dataset (CO_2 saturation around near wellbore region), while eigen-image analysis proved useful in reducing the dimension of the spatial maps, such as permeability, porosity, etc. Moreover, PCA was mainly chosen as it is simple and bijective. Notably, multiple dimension reduction techniques, such as auto-encoder [42] and Gaussian process latent variable models (GPLVM) [43,44], can be included in the BEL framework. Additionally, the choice of regression technique is guided by the type, dimension, and relationship of the measurements, data, and forecast variables (linear or nonlinear). Due to the high-dimensionality problems, parametric regression is usually chosen instead of nonparametric techniques, except that large number of prior samples are available [19]. This work could be improved and extended in several ways. It is important to note that for this study, we have only considered quantities such as CO_2 saturation through wellbores and their respective CO_2 mass and leakage. This approach can be applied to examine the effectiveness of monitoring and the monitoring duration to lower uncertainty in risk metrics, such as top-layer CO_2 saturation and plume mobility and seismic time-lapse data. Accordingly, it will also be useful to apply the DF procedures to more complex geological models, such as bimodal

channelized systems, which can be challenging for traditional (model-based) history matching methods, kernel density estimation [45], and extensions of CCA [46] can be included in the BEL framework to tackle more complex nonlinear inverse problems. Finally, using data space inversion (DSI), as described by Sun and Durlofsky [26], CO_2 leakage detection under uncertainty should also be considered.

Author Contributions: A.T. wrote the paper and contributed to tuning the model and analyzing the results. R.B.B. supervised the work and provided continuous feedback. Both authors have read and agreed to the published version of the manuscript.

Funding: This research is funded by Petromaks-2 project DIGIRES (RCN no. 280473), and the APC was funded by the library at University of Stavanger, Norway.

Acknowledgments: The author acknowledges financial support from the Research Council of Norway through the Petromaks-2 project DIGIRES (RCN no. 280473) and the industrial partners AkerBP, Wintershall DEA, ENI, Petrobras, Equinor, Lundin, and Neptune Energy. The author would also like to thank Stanford center for reservoir forecasting for providing Auto-BEL implementation code.

Data Availability Statement: Not Applicable.

Conflicts of Interest: The authors declare no conflict of interest.

References

1. Harp, D.R.; Stauffer, P.H.; O'Malley, D.; Jiao, Z.; Egenolf, E.P.; Miller, T.A.; Martinez, D.; Hunter, K.A.; Middleton, R.; Bielicki, J. Development of robust pressure management strategies for geologic CO_2 sequestration. *Int. J. Greenh. Gas Control* **2017**, *64*, 43–59. [CrossRef]
2. Jin, L.; Hawthorne, S.; Sorensen, J.; Pekot, L.; Kurz, B.; Smith, S.; Heebink, L.; Hergegen, V.; Bosshart, N.; Torres, J.; et al. Advancing CO_2 enhanced oil recovery and storage in unconventional oil play—Experimental studies on Bakken shales. *Appl. Energy* **2017**, *208*, 171–183. [CrossRef]
3. Nilsen, H.M.; Lie, K.A.; Andersen, O. Analysis of CO_2 trapping capacities and long-term migration for geological formations in the Norwegian North Sea using MRST-co2lab. *Comput. Geosci.* **2015**, *79*, 15–26. [CrossRef]
4. IPCC. *Climate Change 2014: Synthesis Report. Contribution of Working Groups I, II and III to the Fifth Assessment Report of the Intergovernmental Panel on Climate Change*; IPCC: Geneva, Switzerland, 2014; p. 151.
5. Hosa, A.; Esentia, M.; Stewart, J.; Haszeldine, H. Injection of CO_2 into saline formations: Benchmarking worldwide projects. *Chem. Eng. Res. Des.* **2011**, *89*, 1855–1864. [CrossRef]
6. Michael, K.; Golab, A.; Shulakova, V.; Ennis-King, J.; Allinson, G.; Sharma, S.; Aiken, T. Geological storage of CO_2 in saline aquifers—A review of the experience from existing storage operations. *Int. J. Greenh. Gas Control* **2017**, *4*, 659–667. [CrossRef]
7. Institute for Global Change. *Global Status of CCS: 2018*; Institute for Global Change: London, UK, 2018.
8. Jordan, K.; Gary, T.; Jeffrey, P.; Hans, T.; Haroon, K.; Yen-Heng, H.C.; Sergey, P.; Howard, H. Developing a Consistent Database for Regional Geologic CO_2 Storage Capacity Worldwide. *Energy Procedia* **2017**, *114*, 4697–4709.
9. Allen, R.; Nilsen, H.; Lie, K.A.; O, M.; Andersen, O. Using simplified methods to explore the impact of parameter uncertainty on CO_2 storage estimates with application to the Norwegian Continental Shelf. *Int. J. Greenh. Gas Control* **2018**, *75*, 198–213. [CrossRef]
10. Dai, C.; Li, H.; Zhang, D.; Xue, L. Efficient data-worth analysis for the selection of surveillance operation in a geologic CO_2 sequestration system. *Greenh. Gases Sci. Technol.* **2015**, *5*, 513–529. [CrossRef]
11. Oladyshkin, S.; Class, H.; Nowak, W. Bayesian updating via bootstrap filtering combined with data-driven polynomial chaos expansions: Methodology and application to history matching for carbon dioxide storage in geological formations. *Comput. Geosci.* **2013**, *17*, 671–687. [CrossRef]
12. Sun, A.Y.; Nicot, J. Inversion of pressure anomaly data for detecting leakage at geologic carbon sequestration sites. *Adv. Water Resour.* **2012**, *44*, 20–29. [CrossRef]
13. Sun, A.Y.; Zeidouni, M.; Nicot, J.; Lu, Z.; Zhang, D. Assessing leakage detectability at geologic CO_2 sequestration sites using the probabilistic collocation method. *Adv. Water Resour.* **2013**, *56*, 49–60. [CrossRef]
14. Chen, B.; Harp, D.R.; Lin, Y.; Keating, E.H.; Pawar, R.J. Geologic CO_2 sequestration monitoring design: A machine learning and uncertainty quantification based approach. *Appl. Energy* **2018**, *225*, 332–345. [CrossRef]
15. Chen, B.; Harp, D.R.; Lin, Y.; Lu, Z.; Pawar, R.J. Reducing uncertainty in geologic CO_2 sequestration risk assessment by assimilating monitoring data. *Int. J. Greenh. Gas Control* **2020**, *94*, 102926. [CrossRef]
16. González-Nicolás, A.; Baù, D.; Alzraiee, A. Detection of potential leakage pathways from geological carbon storage by fluid pressure data assimilation. *Adv. Water Resour.* **2015**, *86*, 366–384. [CrossRef]
17. Cameron, D.A.; Durlofsky, L.J.; Benson, S.M. Use of above-zone pressure data to locate and quantify leaks during carbon storage operations. *Int. J. Greenh. Gas Control* **2016**, *52*, 32–43. [CrossRef]

18. Oliver, D.S.; Chen, Y. Recent progress on reservoir history matching: A review. *Comput. Geosci.* **2011**, *15*, 185–221. [CrossRef]
19. Scheidt, C.; Li, L.; Caers, J. *Quantifying Uncertainty in Subsurface Systems*, 1st ed.; John Wiley & Sons: Hoboken, NJ, USA, 2018.
20. Scheidt, C.; Renard, P.; Caers, J. Prediction-focused subsurface modeling: Investigating the need for accuracy in flow-based inverse modeling. *Math. Geosci.* **2015**, *47*, 173–191. [CrossRef]
21. Satija, A.; Caers, J. Direct forecasting of subsurface flow response from non-linear dynamic data by linear least-squares in canonical functional principal component space. *Adv. Water Resour.* **2015**, *77*, 69–81. [CrossRef]
22. Yin, Z.; Strebelle, S.; Caers, J. Automated Monte Carlo-based Quantification and Updating of Geological Uncertainty with Borehole Data (AutoBEL v1.0). *Geosci. Model. Dev.* **2019**, *13*, 651–672. [CrossRef]
23. Satija, A.; Scheidt, C.; Li, L.; Caers, J. Direct forecasting of reservoir performance using production data without history matching. *Comput. Geosci.* **2017**, *21*, 315–333. [CrossRef]
24. Athens, N.D.; Caers, J. A Monte Carlo-based framework for assessing the value of information and development risk in geothermal exploration. *Appl. Energy* **2019**, *256*, 113932. [CrossRef]
25. Hermans, T.; Lesparre, N.; De Schepper, G.; Robert, T. Bayesian evidential learning: A field validation using push-pull tests. *Hydrogeol. J.* **2019**, *27*, 1661–1672. [CrossRef]
26. Sun, W.; Durlofsky, L.J. Data-space approaches for uncertainty quantification of CO_2 plume location in geological carbon storage. *Adv. Water Resour.* **2019**, *123*, 234–255. [CrossRef]
27. Emerick, A.A.; Reynolds, A.C. Ensemble smoother with multiple data assimilation. *Comput. Geosci.* **2016**, *55*, 3–15. [CrossRef]
28. De Maesschalck, R.; Jouan-Rimbaud, D.; Massart, D.L. The Mahalanobis distance. *Chemom. Intell. Lab. Syst.* **2000**, *50*, 1–18. [CrossRef]
29. Breunig, M.M.; Kriegel, H.P.; Ng, R.T.; Sander, J. LOF: Identifying Density-Based Local Outliers. *Assoc. Comput. Mach.* **2000**, *29*, 2.
30. Liu, F.T.; Ting, K.M.; Zhou, Z. Isolation Forest. In Proceedings of the 2008 Eighth IEEE International Conference on Data Mining, Pisa, Italy, 15–19 December 2008; pp. 413–422.
31. Schölkopf, B.; Williamson, R.; Smola, A.; Shawe-Taylor, J.; Platt, J. Support Vector Method for Novelty Detection. In Proceedings of the 12th International Conference on Neural Information Processing Systems, NIPS'99, Cambridge, MA, USA, 29 November–4 December 1999; pp. 582–588.
32. Springer. *Principal Component Analysis*, 2nd ed.; John Wiley & Sons: Hoboken, NJ, USA, 2002.
33. Hardoon, D.R.; Szedmak, S.; Shawe-Taylor, S. Canonical Correlation Analysis: An Overview with Application to Learning Methods. *Neural Comput.* **2004**, *16*, 2639–2664. [CrossRef] [PubMed]
34. Tarantola, A. *Inverse Problem Theory and Methods for Model Parameter Estimation*, 1st ed.; SIAM: New Orleans, LA, USA, 2005.
35. Emerick, A.A. Analysis of the performance of ensemble-based assimilation of production and seismic data. *J. Pet. Sci. Eng.* **2016**, *139*, 219–239. [CrossRef]
36. Fenwick, D.; Scheidt, C.; Caers, J. Quantifying Asymmetric Parameter Interactions in Sensitivity Analysis: Application to Reservoir Modeling. *Math. Geosci.* **2014**, *46*, 493–511. [CrossRef]
37. Park, J.; Yang, G.; Satija, A.; Scheidt, C.; Caers, J. DGSA: A Matlab toolbox for distance-based generalized sensitivity analysis of geoscientific computer experiments. *Comput. Geosci.* **2016**, *97*, 15–29. [CrossRef]
38. Spear, R.C.; Hornberger, G.M. Eutrophication in peel inlet-II. Identification of critical uncertainties via generalized sensitivity analysis. *Water Res.* **1980**, *14*, 43–49. [CrossRef]
39. Andersen, O.; Nilsen, H.M.; Lie, K.A. Reexamining CO_2 Storage Capacity and Utilization of the Utsira Formation. In Proceedings of the ECMOR XIV-14th European Conference on the Mathematics of Oil Recovery, Catania, Italy, 8–11 September 2014; pp. 1–18.
40. Singh, V.; Cavanagh, A.; Hansen, H.; Nazarian, B.; Iding, M.; Ringrose, P. Reservoir modeling of CO_2 plume behavior calibrated against monitoring data from Sleipner, Norway. In Proceedings of the SPE Annual Technical Conference and Exhibition, Florence, Italy, 19–22 September 2010.
41. Sintef. MRST-co2lab. Available online: https://www.sintef.no/projectweb/mrst/modules/co2lab/ (accessed on 6 February 2021).
42. Wang, W.; Huang, Y.; Wang, Y.; Wang, L. Generalized Autoencoder: A Neural Network Framework for Dimensionality Reduction. In Proceedings of the 2014 IEEE Conference on Computer Vision and Pattern Recognition Workshops, Columbus, OH, USA, 23–28 June 2014; pp. 496–503.
43. Lawrence, N.D. Learning for larger datasets with the Gaussian process latent variable model. In Proceedings of the Eleventh International Workshop on Artificial Intelligence and Statistics, San Juan, Puerto Rico, 21–24 March 2007.
44. Lawrence, N.D. Probabilistic non-linear principal component analysis with Gaussian process latent variable models. *J. Mach. Learn. Res.* **2005**, *6*, 1783–1816.
45. Lopez-Alvis, J.; Hermans, T.; Nguyen, F. A cross-validation framework to extract data features for reducing structural uncertainty in subsurface heterogeneity. *Adv. Water Resour.* **2019**, *133*, 103427. [CrossRef]
46. Lai, P.; Fyfe, C. A neural implementation of canonical correlation analysis, Neural Networks. *J. Mach. Learn. Res.* **1999**, *12*, 1391–1397.

Paper IV

Efficient Dimensionality Reduction Methods in Reservoir History Matching.

Amine Tadjer, Reidar B. Bratvold and Remus Hanea.

energies

MDPI

Article

Efficient Dimensionality Reduction Methods in Reservoir History Matching

Amine Tadjer [1,*], Reider B. Bratvold [1] and Remus G. Hanea [1,2]

[1] Department of Energy Resources, University of Stavanger, 4021 Stavanger, Norway; reidar.bratvold@uis.no (R.B.B.); remus.hanea@uis.no (R.G.H.)
[2] Equinor ASA, Forusbeen 50, 4035 Stavanger, Norway
* Correspondence: amine.tadjer@uis.no

Abstract: Production forecasting is the basis for decision making in the oil and gas industry, and can be quite challenging, especially in terms of complex geological modeling of the subsurface. To help solve this problem, assisted history matching built on ensemble-based analysis such as the ensemble smoother and ensemble Kalman filter is useful in estimating models that preserve geological realism and have predictive capabilities. These methods tend, however, to be computationally demanding, as they require a large ensemble size for stable convergence. In this paper, we propose a novel method of uncertainty quantification and reservoir model calibration with much-reduced computation time. This approach is based on a sequential combination of nonlinear dimensionality reduction techniques: t-distributed stochastic neighbor embedding or the Gaussian process latent variable model and clustering K-means, along with the data assimilation method ensemble smoother with multiple data assimilation. The cluster analysis with t-distributed stochastic neighbor embedding and Gaussian process latent variable model is used to reduce the number of initial geostatistical realizations and select a set of optimal reservoir models that have similar production performance to the reference model. We then apply ensemble smoother with multiple data assimilation for providing reliable assimilation results. Experimental results based on the Brugge field case data verify the efficiency of the proposed approach.

Keywords: uncertainty quantification; history matching; reservoir simulation; data assimilation; dimensionality reduction

Citation: Tadjer, A.; Bratvold, R.B.; Hanea, R.G. Efficient Dimensionality Reduction Methods in Reservoir History Matching. *Energies* **2021**, *14*, 3137. https://doi.org/10.3390/en14113137

Academic Editors: Vasily Demyanov; Leonardo Azevedo

Received: 25 February 2021
Accepted: 24 May 2021
Published: 27 May 2021

1. Introduction

Research scientists have worked for many years to develop viable methods to calibrate complex reservoir models. However, the uncertainty associated with reservoir models is highly significant, introducing considerable errors in the modeling process. There are several ways to quantify uncertainty in reservoirs. One is the conditioning of reservoir parameters to observed production data, a process referred to as inverse problem or history matching (HM). The first step of HM is parameterization, namely to independently define and vary the model variables in a numerical reservoir simulation model: porosity, permeability, the density and permeability of fractures, the initial depths of oil-water and gas-oil contacts, relative permeability curves, capillary pressure curves, fluid composition, aquifer strength, and the size and fault transmissibility [1]. It is not realistic to do so, however, because of the large area of possible adjustment caused by the large number of grid blocks and variables; the number of varying parameters should therefore be as small as possible. To do this, a reparameterization method based on the pilot point method, the spline function method, the wavelet function method, Karhunen–Loeve reparameterization, and discrete cosine transform was used [2]. The second step is to select the production data, which must be sensitive to the parameters needed to be history matched. The sensitivity becomes more complex, however, in cases using reservoirs with multiphase flow. In these cases, the cross-covariance of production data to model variables is used instead, its main

advantage being that it is generally smoother and can show a more global relationship between data and variables, since it is a product of sensitivities and covariances.

The algorithms for HM are diverse. Evolutionary algorithms are often considered the standard approach, since, by generating a new model combining two Gaussian reservoir models, the gradual deformation algorithm reduces the HM problem to a one-dimensional minimization problem [2]. Sambridge (1999) [3] introduced a neighborhood algorithm in which a resampling of the parameters is led by using information in an available ensemble. In addition, several other methods have been introduced to optimize reservoir models via particle swarm optimization [4], simulated annealing [5], and simultaneous perturbation stochastic approximation [6]. When solving the history matching problem, a key issue must be considered: uncertainty quantification. Uncertainty quantification requires strong knowledge of the reservoir characteristics, and uncertainty should be represented by a set of reservoir models (or realizations) instead of a single history-matched model. The Markov chain Monte Carlo method (McMC) [7], the randomized maximum likelihood method [8], the EnKF method [8–10], the ensemble smoother (ES) [11], and the ensemble smoother with multiple data assimilation (ES-MDA) [12,13] are useful methods to quantify uncertainty. For all of these techniques, accuracy and speed are two main factors due to the non-unique solutions and the ill-posed inverse problems.

Many parametrization methods used in DR have already been introduced. For instance, Vo and Durlofsky [14] used principal component analysis (PCA) to reparametrize high dimension data into low dimensional space, then regenerated new realizations based on principal parameters from PCA for data assimilation, while others have used singular value decomposition [15] and Kernel PCA (KPCA) [16]. Muzammil. H et al. [17] applied PCA to account for the model-error component during model calibration. Kang et al. (2017) and Kang et al. (2019) [18,19] also introduced PCA to select suitable models for EnKF. Tolstukhin et al. [20] demonstrated how data analytics can improve efficiency of ensemble history matching by analyzing the statistics that link the static model ensemble and the dynamic model ensemble update. Satija et al. [21] proposed a method known as direct forecasting (DF) based on projecting the prior predictions into a low-dimensional canonical space to maximize the projected oil data and estimate the joint distribution of historical and forecasted data through linear Gaussian regression; they concluded that this method provided uncertainty estimates regarding production forecast that reasonably agreed with rejection sampling. Park et al. [22] proposed an extended approach based on direct forecasting, where both of the geological model parameters and dynamic data are simultaneously used. Our approach in the current paper is different from the previous work in Kang et al. (2019) [19]. Dimensionality reduction techniques such as PCA and SVD, however, are linear approaches that may not accurately represent the relationship between high dimensional parameters and latent variables in reduced space, which likely lead to poor performance of model assimilation and prediction. In addition, the use of EnKF tends to be computationally prohibitive in certain circumstances and also generates spurious correlations leading to loss of geological realism and underestimation of uncertainties (ensemble collapse). In this work, we propose a novel scheme to reduce the number of ensemble members while preserving the prediction quality by combining ES-MDA with machine learning DR techniques and cluster analysis. In this paper, we demonstrate the efficiency of using the non-linear DR techniques t-distributed stochastic neighbor embedding (t-SNE) [11] and Gaussian process latent variable model (GPLVM) [23,24] along with clustering K-means to select effective reservoir models and save computational time without simulating and assimilating the entire initial ensemble. This study uses the Brugge field reservoir case to demonstrate that the new implementation can make computation faster and more robust than the standard procedure proposed in [12,13] and can provide appropriate posterior uncertainty quantification.

The paper is structured as follows. In the next section, we present the complete methodology, by which we tested the proposed workflow in the well-known Brugge field reservoir model. In addition, several cases, involving different reference models,

are considered. Finally, some concluding remarks and possible future work directions are provided.

2. Materials and Methods

The procedure applied in this study has four main stages:

1. The first stage includes generating ensemble reservoir models and analyzing whether the observed (reference) prior data can predict posterior distribution that appertains to the prior range.
2. The second stage involves reducing the ensemble dimension and constructing a 2D space by using t-SNE and GPLVM.
3. The third stage uses clustering K-means to extract a set of reservoir models with the least production error compared to the reference model.
4. After extracting the models and selecting the most informative ones, we began the HM process using ES-MDA, and finally we compared the performance of history matching analysis of the proposed workflow with the standard ES-MDA without using dimensionality reduction techniques.

The general steps of the approach are shown in Figure 1 and algorithm solutions employed are described in more detail later.

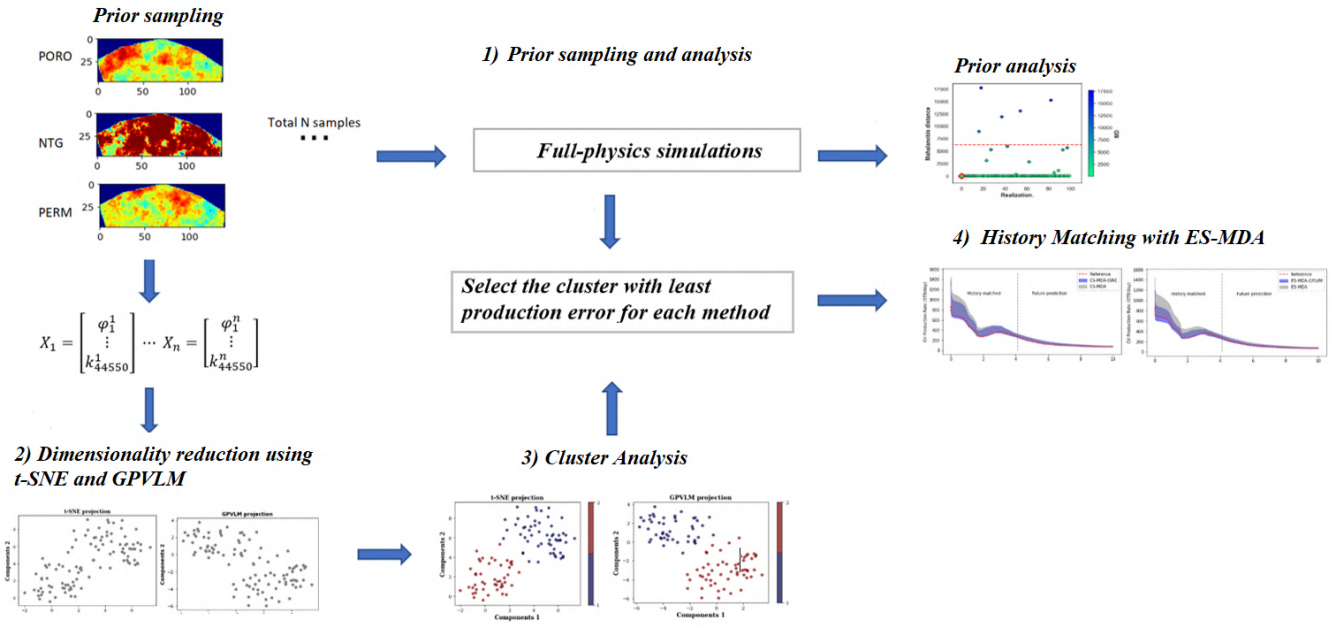

Figure 1. Flow chart for the history matching with dimensionality reduction framework.

2.1. Prior Sampling and Analysis

Due to the high dimensionality and nonlinearity of subsurface systems physics-based models, Monte Carlo simulations were used to sample and identify the possible prior range of model parameterization and probability distribution for each geological parameter (e.g., the structural model, rock types, the petrophysical model, and subsurface fluid distribution). Let $m \in \mathcal{R}^N$ denote the vector of uncertain static parameters of a reservoir model with a dynamic data variable (e.g., oil production and water cuts) as vector d. The nonlinear function data forward model is defined as

$$d = G_d(m) \tag{1}$$

The function $\mathcal{G}_d$ is generated through a reservoir simulator and by applying it to prior geological model realizations, $m = \{m^1, m^2, m^3, \ldots\ldots\ldots m^N\}$. We obtained a set of N samples of dynamic data variables, $d = \{d^1, d^2, d^3, \ldots\ldots\ldots d^N\}$. We refer to the vector of

observation data as d_{obs}. Once the prior samples are generated, it is important to check that the observed data can be predicted by the prior model, in order for the posterior distribution to appertain in the prior range. Otherwise, there is a risk that the prediction will be erroneous. If the prior model is falsified, which indicates inconsistency with the data, we must revise the prior data distribution herein to evaluate the quality of the prior model and its ability to predict the data. We proposed a statistical procedure based on Robust Mahalanobis distance (RMD) [25,26], which handles high dimensional and different types of measurements of the data, the main objective being to detect outliers and determine if the prior model is falsified or not. The RMD for each data variable realization d or d^{obs} was computed as follows:

$$RMD\ (d^{(n)}) = \sqrt{(d^{(n)} - \rho)\beta^{-1}(d^{(n)} - \rho)}, \quad for\ \ n = 1, 2, 3 \ldots\ldots\ldots, N \tag{2}$$

where ρ and β are the mean and covariance of the data d. Assuming the distribution of the data is multivariate Gaussian, the distribution of $[RMD(dn)]^2$ would be chi squared x_d^2. We set the 95th percentiles of x_d^2 as the tolerance threshold for multivariate dimensional point d^n. If $RMD\ (d_{obs})$ fell outside of the tolerance threshold $(RMD\ (d_{obs}) > RMD\ (d^n)$, the d_{obs} would be regarded as outliers, and the prior model would be falsified, as it has a very small probability. It should also be noted that this method requires data distribution to be Gaussian; if it is not, other outlier detection techniques such as isolation forest [27], local outliers detection [28], and one-class support vector machines [29] are highly recommended.

2.2. Dimensional Reduction

A single reservoir model is represented by numerous grid blocks, each with unique reservoir properties, such as permeability, porosity, and net-to-gross. Accordingly, we construct a vector X containing the reservoir properties of all grid blocks. We also use multiple ensembles of realizations to account for geological uncertainties $X \in R^{N,m}$. Furthermore, typical ensembles are formed by hundreds of realizations, in that we are faced with a high-dimensional problem. Geological realization with similar geological parameters trends will have similar production histories. As we aim to analyze the main geological distribution of the data, reducing the data dimensions is reasonable. Therefore, we utilize two different DR methods: t-SNE [11] and GPLVM [23,24], to characterize reservoir parameters efficiently by projecting the parameters into a 2D plane. However, t-SNE is a non-linear DR algorithm developed for exploring high-dimensional data. It maps multi-dimensional data to a two- or three-dimensional dataset that can be visualized in a scatter plot. Additionally, t-SNE learns joint probabilities defined by two points on a two-dimensional space to be as close as possible to conditional probabilities, defined by two points on high-dimensional space. For more details about t-SNE, one can refer to [11] and Appendix A. GPLVM differs from t-SNE, primarily because it is a Bayesian non-parametric DR method that uses Gaussian process to learn a low-dimensional representation of high-dimensional data. The main advantage of the GPLVM is that it allows the use of nonlinear covariance functions, i.e., that it can represent non-linear functions from the latent space to the data space. The probabilistic nature of the GPLVM also gives it advantages in dealing with missing data values. For more details about GPLVM, one can refer to [23,24] and Appendix A.

2.3. Clustering K-Means:

K-means clustering is an unsupervised learning method that is widely used because of its efficiency and simplicity. K-means is used to find the cluster configuration that minimizes the square error over all K clusters [30]:

$$J = \sum_{k=1}^{K} \sum_{x^{(l)} \in c_k}^{M} \left\| x^{(l)} - \mu^k \right\|^2, u^k = \frac{\sum^{x^{(l)} \in c_k} x^{(l)}}{|S_k|} \tag{3}$$

with u^k as the centroid of the cluster, and c_k refers to the mean of a point within the cluster, $|S_k|$ is the number of samples in the cluster c_k.

K-means clusters provide an optimal solution by minimizing of the distances between data and their centroids. The centroid is computed by the average of the data in each cluster. Several methods exist that allow the selection of the cluster sizes, including the gap statistics, elbow-method as well as the silhouette-method. In this study, we use the silhouette-method to determine the optimal number of clusters. The silhouette index varies between -1 and 1, where a value close to 1 means that the data is appropriate within its cluster. For all of the data-points, the silhouette value $s(i)$ can be determined with the following equation:

$$s(i) = \frac{b(i) - a(i)}{max\{a(i), b(i)\}} \tag{4}$$

where $a(i)$ represents average distances within a specific cluster and $b(i)$ is the minimum average distance from data in other separate clusters. Specifically, $a(i)$ shows how the i-th data is grouped within its cluster, and $b(i)$ indicates the closest distance of adjacent clusters. Therefore, if $a(i)$ is small, that means that the data are well grouped; however, if the silhouette value is close to 1, the $b(i)$ is large.

2.4. ES-MDA and the Localization Technique

Opposite to the production forecast where the "unknown" reservoir behavior is predicted by using the "known" reservoir model variables, history matching inverses the process and estimates the "unknown" reservoir model variables with the "known" observed reservoir behavior. The general objective function for history matching is

$$J(m) = \frac{1}{2}\|g(m) - d_{obs}\|^2 \tag{5}$$

where $g(m)$ is the simulated data with model variables m composed of reservoir variables (e.g., permeability, facies, porosity, and net to gross), and d_{obs} is the observed data. The goal of history matching is to minimize the objective function (m) by finding acceptable model variables m and $minJ(m)$. ES-MDA is an ensemble-based method introduced by Emerick and Reynolds [12]. In its simplest form, the method employs a standard smoother analysis equation a pre-defined number of times, with the covariance matrix of the measured data error multiplied by coefficient a. The coefficients must be selected such that the following condition is satisfied:

$$\sum_{k=1}^{N_a} \frac{1}{a_k} = 1 \tag{6}$$

where N_a is the number of times the analysis step is repeated. The ES-MDA analysis applied to a vector of model parameters, m, can be written as

$$m_i^a = m_i^b + K(d_{obs} - d_{sim,i}), \quad for\ i = 1 \ldots\ldots N \tag{7}$$

Here, i is defined as the ith ensemble members; m_i^a is defined as an updated uncertainty vector, m_i^b, the initial or previous uncertainty vector; K, the Kalman gain matrix, which is used to compute by regularizing with SVD using 99.9 % of all the energy; $d_{sim,i}$ refers to simulation data obtained from previous models. Ensemble-based HM updates N reservoir models simultaneously. In addition, the Kalman gain matrix can be determined as follows:

$$K = C_{md}\left(C_{dd} + a_p C_D\right)^{-1} \tag{8}$$

C_{md} is the cross-covariance matrix between the vector of model parameters m and predicted data d; C_{dd} is the auto covariance matrix of predicted data d; a_p is the coefficient to inflate C_D, which refers the covariance matrix of the observed data measurement error.

However, there are still conceptual and computational challenges associated with ES-MDA, one issue is that of ensemble collapse, which may result in unrealistic uncertainty

and difficulty to cover the target distribution. To avoid this, a localization technique is implemented in the equation by introducing a correlation matrix R via an element-by-element multiplication, also known as Schur product ($\circ$). There are different ways of computing R. One of the most common approaches is the distance-dependent localization [31], in which all data points (oil rate, water rate) and model variables (permeability, porosity) are presumed to have certain physical locations connection. The ES-MDA equation is updated to:

$$m_i^a = m_i^b + R \circ K(d_{obs} - d_{sim,i}), \quad for\ i = 1 \ldots\ldots N \tag{9}$$

The parameter R is assumed to be from 0 to 1 depending on the distances for well locations [32]:

$$R(h,L) = \left\{ \begin{array}{cc} -\frac{1}{4}(\frac{h}{L})^5 + \frac{1}{2}(\frac{h}{L})^4 + \frac{5}{8}(\frac{h}{L})^3 + \frac{5}{8}(\frac{h}{L})^2 + 1 & ,0 \leqslant h < L \\ \frac{1}{12}(\frac{h}{L})^5 - \frac{1}{2}(\frac{h}{L})^4 + \frac{5}{8}(\frac{h}{L})^3 + -\frac{5}{3}(\frac{h}{L})^2 - 5(\frac{h}{L}) + 4 - \frac{2}{3}(\frac{h}{L})^{-1} + 1 & ,L < h \leqslant 2L \\ 0 & ,h > 2L \end{array} \right\} \tag{10}$$

where h is the Euclidean distance between a specific grid cell and well location, and L refers to the critical length, corresponding to influential regions for every well data. Therefore, a high value of R means that grid blocks are close to the wells.

2.5. General Setup

We tested the performance of the proposed methodology in the Brugge field case study. The Brugge field is a complex oilfield constructed by TNO [33]. The model consists of nine layers, and each layer has 139 × 48 gridblocks. The total number of gridblocks is 60,048, with 44,550 active cells. There are 20 producers and 10 injectors in the reservoir models.The reservoir is being depleted by voidage replacement. The producers and injectors are "smart wells", i.e., with vertical flow control, with three perforation intervals per well. For each producer well, the fluid rate is set to max value of 3000 bbl/day, and flowing bottom hole pressure superior to 50 Bar. For each injector well, the fluid rate is set to a max value of 4000 bbl/day, and the corresponding flowing bottom hole pressure less than 180 Bar. We used 104 initial geostatistical realizations provided by TNO and assumed one of 104 as a reference model. In the HM analysis, oil production rates (OPR), water cuts (WCT), and the bottom hole pressure (BHP) were considered, and the model variables to be updated included permeability (PERMX, PERMY, and PERMZ), porosity, and NTG in all active cells. Figure 2 shows the log permeability in the first layer for six random realizations. For more information about the Brugge benchmark, see [33].

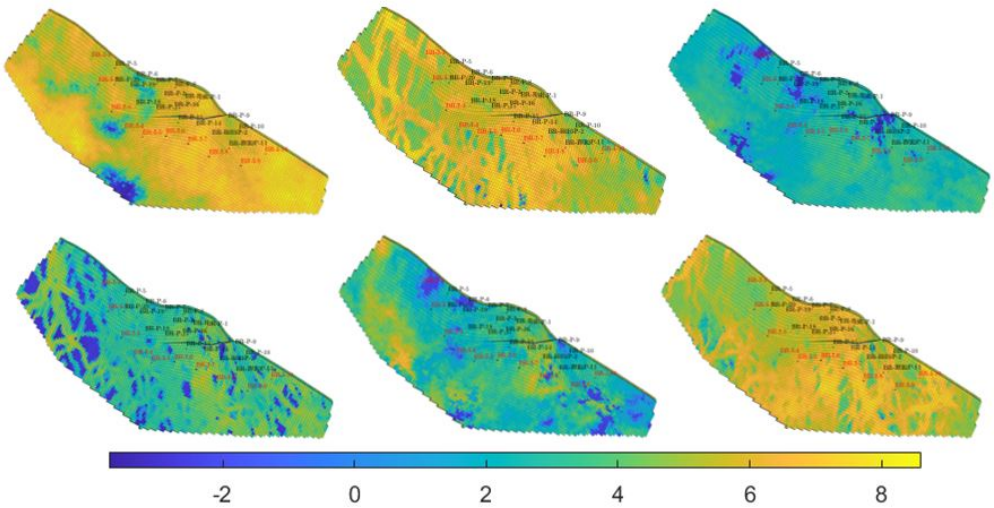

Figure 2. Example log of permeability (K) distribution for six of 103 different geological realizations of the Brugge field.

3. Results

3.1. ES-MDA with DR

The data assimilations were conducted using ES-MDA with localization, with Na = 5. Besides the ES-MDA-t-SNE and ES-MDA-GPLVM, we performed the HM on assimilation observation data for the first 4 years and the rest (6 years) for forecasting.

To assess the quality of prior models, a field oil production rate of 103 prior models was used with d_{obs} by applying the RMD outlier detection. The RMD of d_{obs} was found to be 8.802, which is below the 95th percentile threshold. This means that the prior is not incorrect. Figure 3 shows a comparison between RMD with d_{obs} and RMD with 103 prior models.

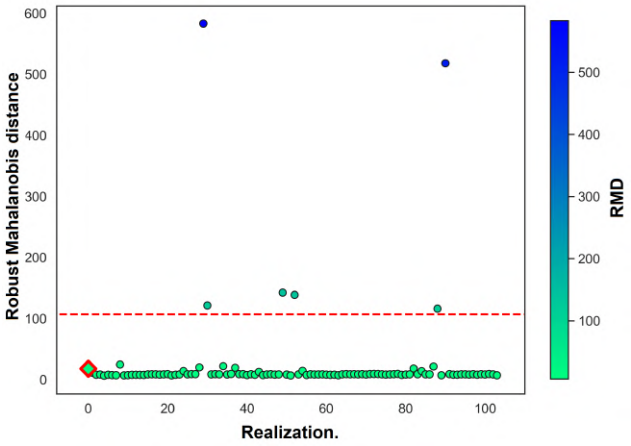

Figure 3. Prior falsification using RMD. The red diamond is the RMD for d_{obs}. Circle dots refer to the RMD results of 103 data variable samples, and the red dashed line is the 95th percentile of the chi-squared distributed RMD.

We applied t-SNE and GPLVM to reservoir models and reduced the dimension into 2D space. Additionally, the silhouette method is used to find optimal cluster numbers (ranges of 2 to 7 clusters) for both GPLVM and t-SNE 2D space. As displayed in Figure 4, the dashed line is used to denote the average silhouette, the silhouette plot with 2 clusters showed the highest value. Therefore, each model was divided into 2 clusters.

Figures 5 and 6 show a scatter plot of the 103 models on a 2D plane, with each dot indicating individual models. When selecting the cluster with the least production error and comparing the forecast accuracy of different forecasting methods among several data sets, there are many performance measures from which to select. In this study, we chose to evaluate, for our forecasting results, a probabilistic metric called the mean continuous ranked probability score (CRPS). The mean CRPS quantifies both accuracy and precision [34], and higher values of the CRPS indicate less accurate results. The mathematical formulations of the mean CRPS are listed in Appendix A. We compared the field oil production rate (FOPR) errors between each cluster and reference model and selected the cluster with the least production error for the data assimilation process, as displayed in Table 1. Only 46 models were selected using t-SNE and 44 models using GPLVM. In Figure 7, we compare the average permeability values between initial 103 models and the selected 46 and 44 models using t-SNE and GPLVM, respectively. Both selected models with t-SNE and GPLVM have a quite similar distribution and quite similar selected reservoir models, and differences were found only in two models.

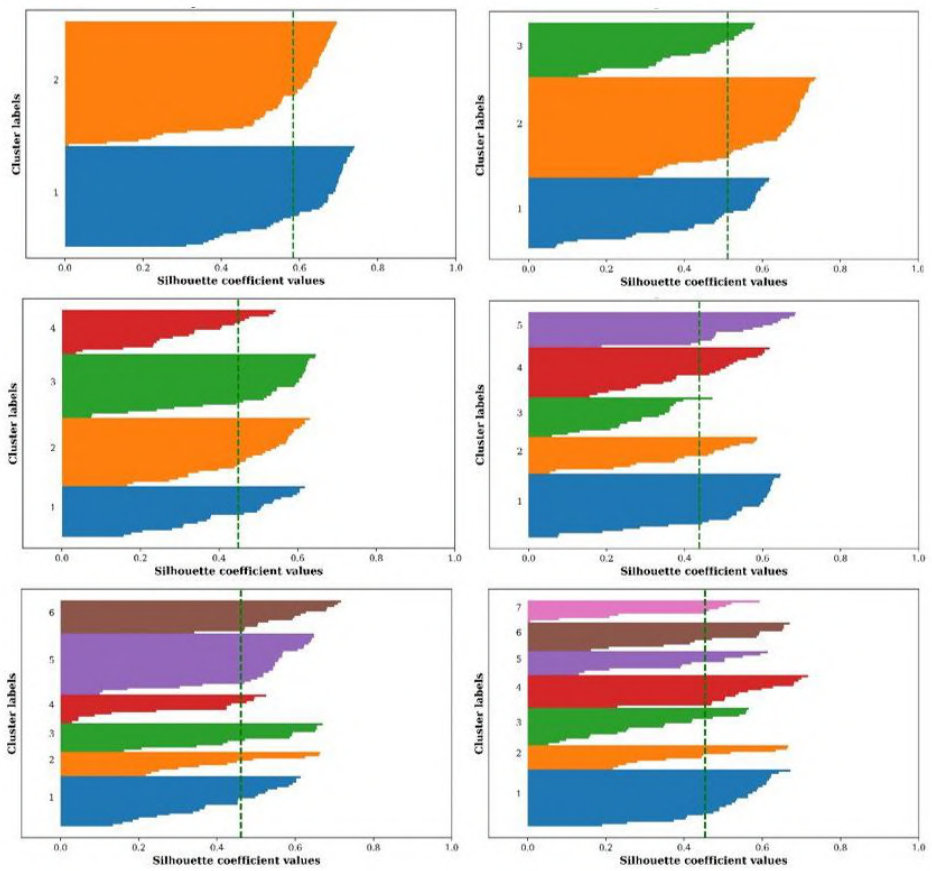

Figure 4. Silhouette plots with different cluster numbers—t-SNE 2D space.

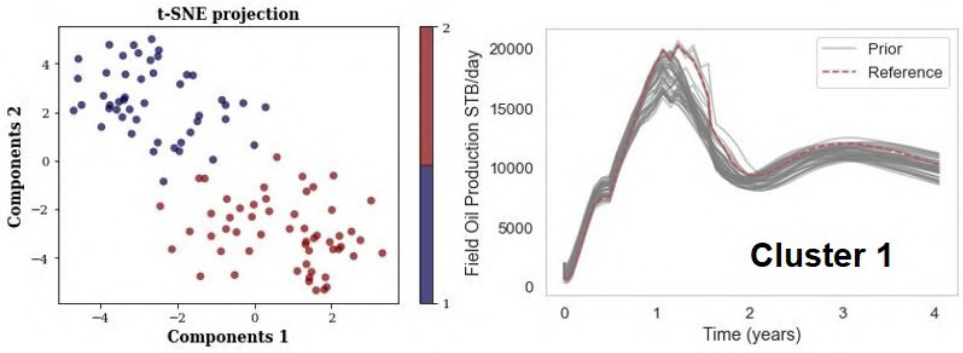

Figure 5. Model selection using t-SNE.

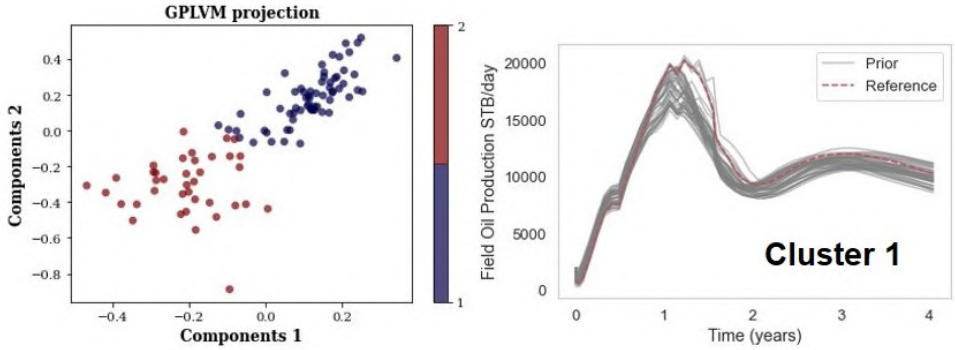

Figure 6. Model selection using GPLVM.

Table 1. Measurement error between the reference model and each cluster.

Methods	t-SNE		GPLVM	
	CRPS	Realization	CRPS	Realization
Cluster 1	89.78	46	96.77	44
Cluster 2	130.67	57	128.66	59

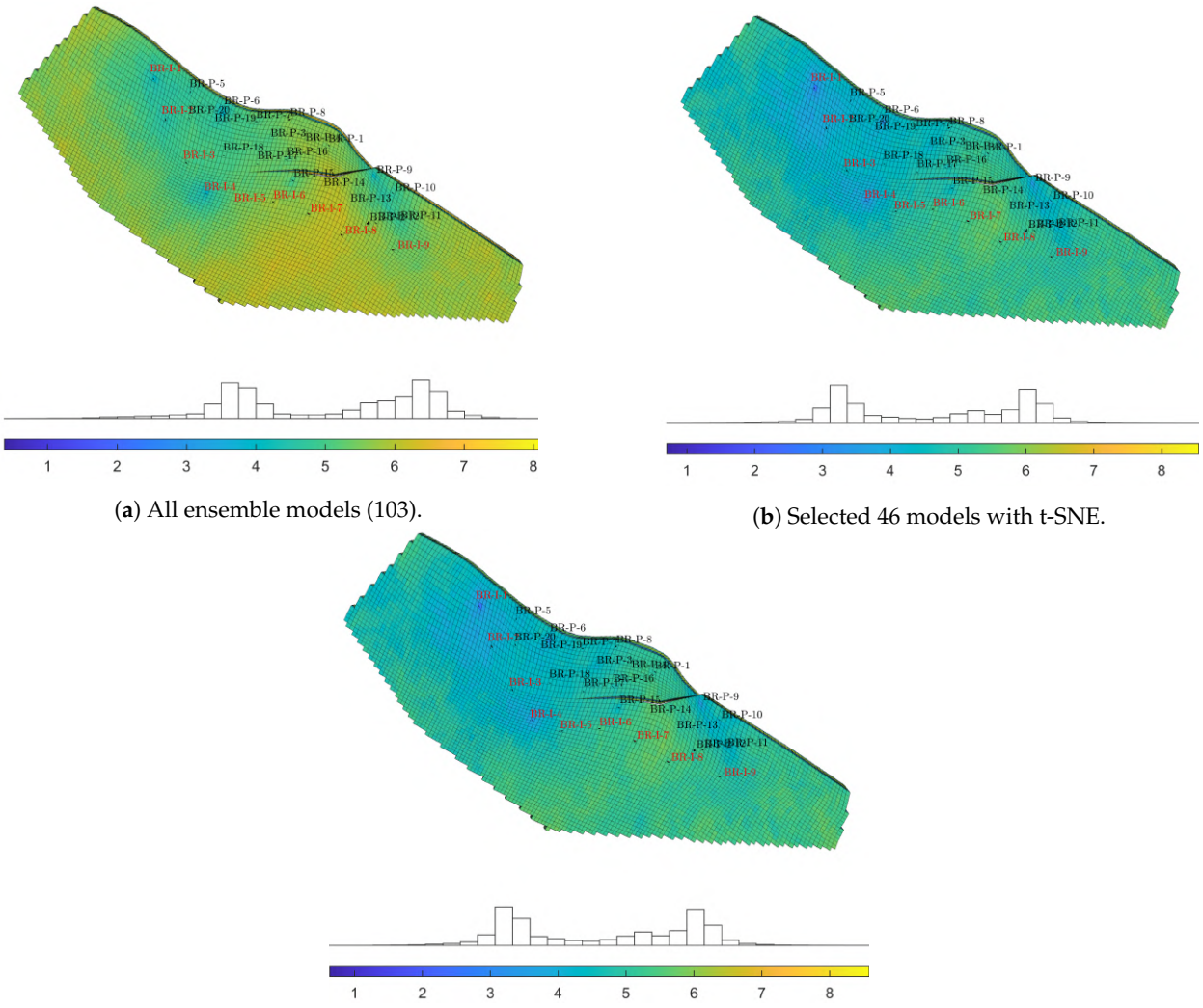

(**a**) All ensemble models (103).

(**b**) Selected 46 models with t-SNE.

(**c**) Selected 44 model with GPLVM.

Figure 7. Mean of permeability Darcy values in logarithmic scale.

The total simulation for each method is listed in Table 2. We can see that ES-MDA uses around 220 min for the entire process, while ES-MDA-t-SNE and ES-MDA-GPLVM use around 120 and 101.5, respectively. By employing reduction techniques, more than 45% of the total simulation time was saved.

Table 2. CPU time for the whole process.

Methods	CPU Time (Minutes)	Time Reduction
ES-MDA	220	0
ES-MDA-t-SNE	120	45.5%
ES-MDA-GPLVM	101.5	53.86%

Figures 8 and 9 compare the ensemble means distribution of the reconstructed updated posterior log-perm and porosity on Layer 1 using the standard ES-MDA, ES-MDA-t-SNE, and ES-MDA-GPLVM to their counterparts in the prior models. The results suggest a slight change on the posterior model in areas where the wells are located. Moreover, the uncertainty reduction is achieved, as the posterior samples are conditioned to the dynamic data variables of the well that are contained within the prediction domain. The results show quite similar posterior permeability and porosity distribution for both ES-MDA-t-SNE and ES-MDA-GPLVM, which is expected, as they differ only in two models.

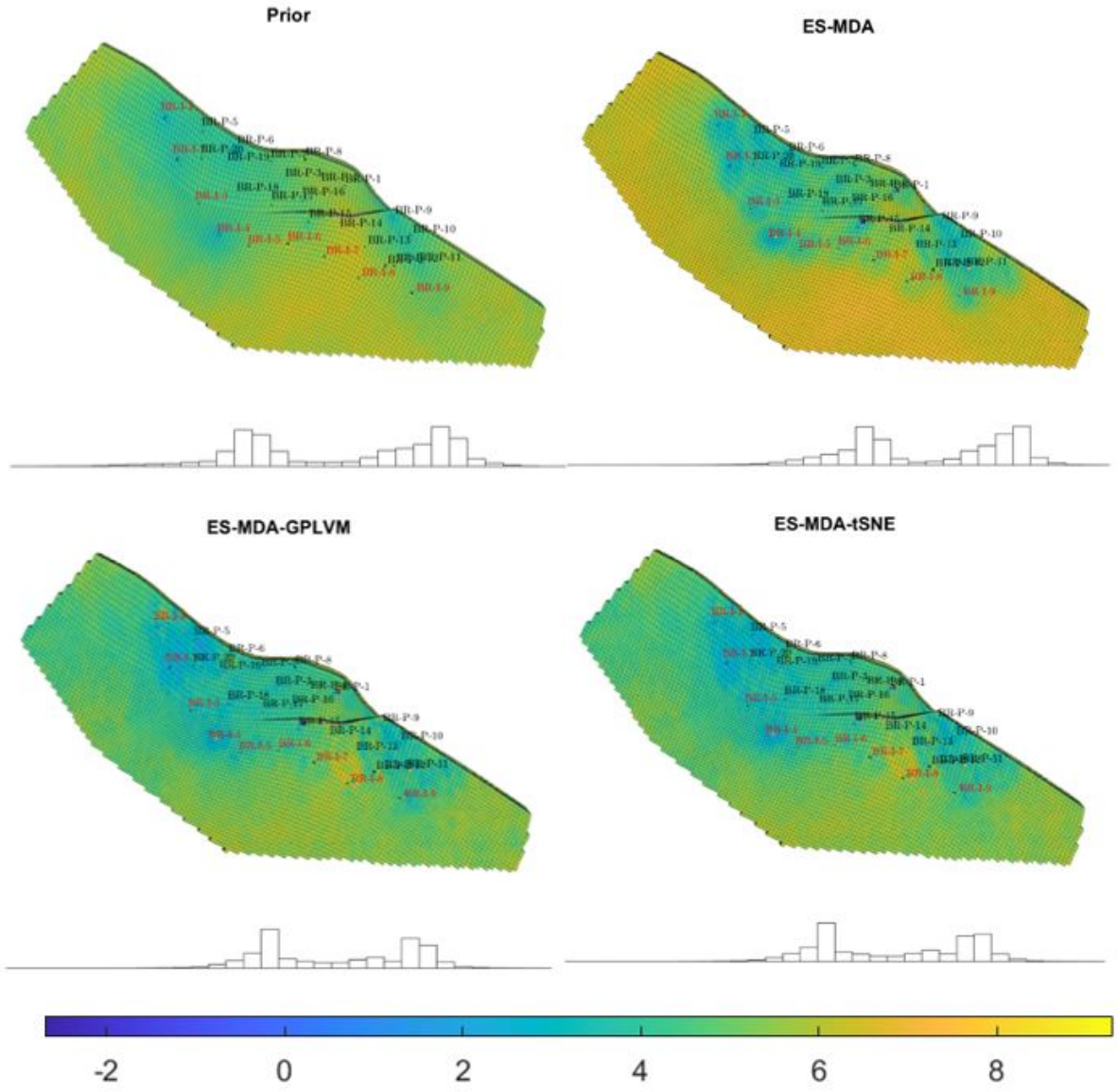

Figure 8. Average log–permeability distribution on Layer 1 from an initial ensemble, the corresponding updated model by ES-MDA, ES-MDA-t-SNE, and ES-MDA-GPLVM.

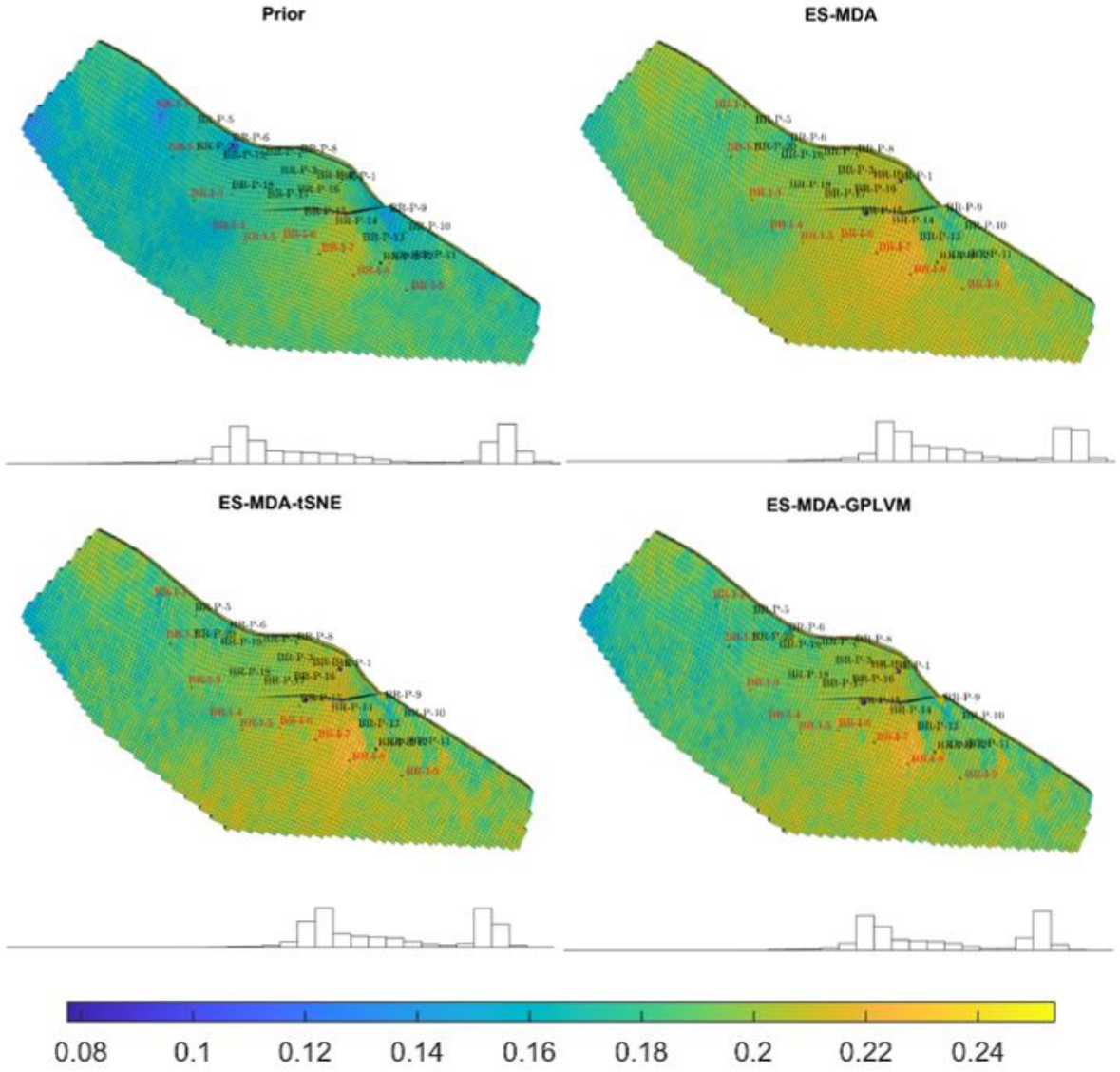

Figure 9. Average porosity distribution on Layer 1 from an initial ensemble, the corresponding updated model by ES-MDA, ES-MDA-t-SNE, and ES-MDA-GPLVM.

Figures 10 and 11 depict the HM profiles for both oil and water cuts of two methods (ES-MDA-t-SNE and ES-MDA-GPLVM) at producers BR-P5, BR-P6, and BR-P19, with respect to the standard ES-MDA and reference model. The vertical dashed line represents the last time of the HM process. The production forecast seems to be reasonable and reliable in the two methods compared to the standard ES-MDA, although only 45.54% and 53.86% of the simulation time is required for ES-MDA-t-SNE and ES-MDA-GPLVM, respectively. The ES-MDA-t-SNE, however, predicts the WOPR data at BR-P6 better than the ES-MDA-GPLVM does, which is likely related to the fact that the WWCT data of BR-P6 are better when using ES-MDA-t-SNE. The matching and forecast ranges with ES-MDA-GPLVM, however, deviate from the reference, especially in BR-P5 and BR-P6.

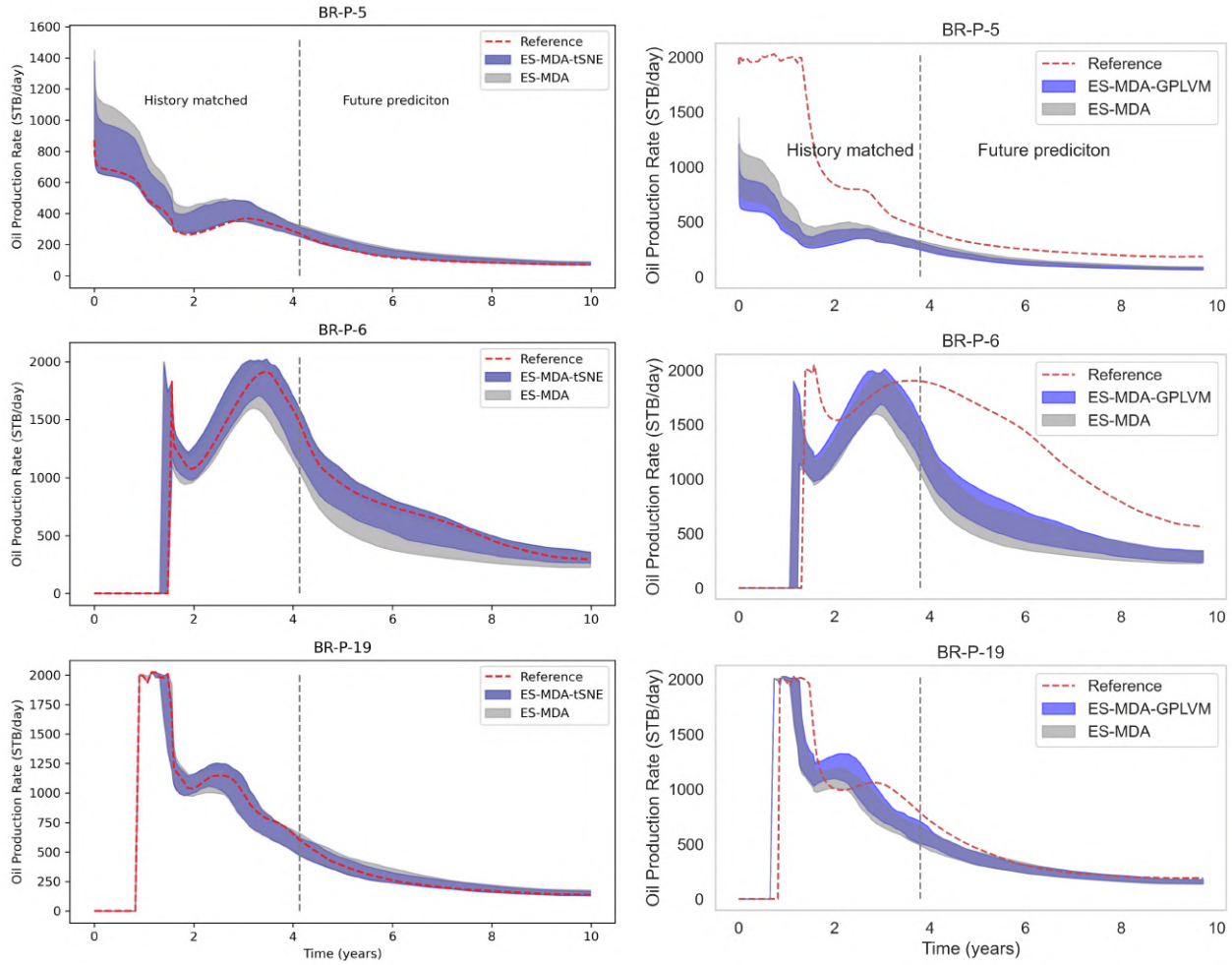

Figure 10. Oil production rate STB/day for three wells with ESMDA, ES-MDA-tSNE and ES-MDA-GPLVM. The blue dashed line is utilized as an indication of the end of historical data and the start of the prediction period. The red dashed line represents the observed data points. The grey region refers to the forecast within P10 and P90 obtained with the ES-MDA. The light blue region represents P10-P90 obtained from ES-MDA-tSNE or ES-MDA-GPLVM.

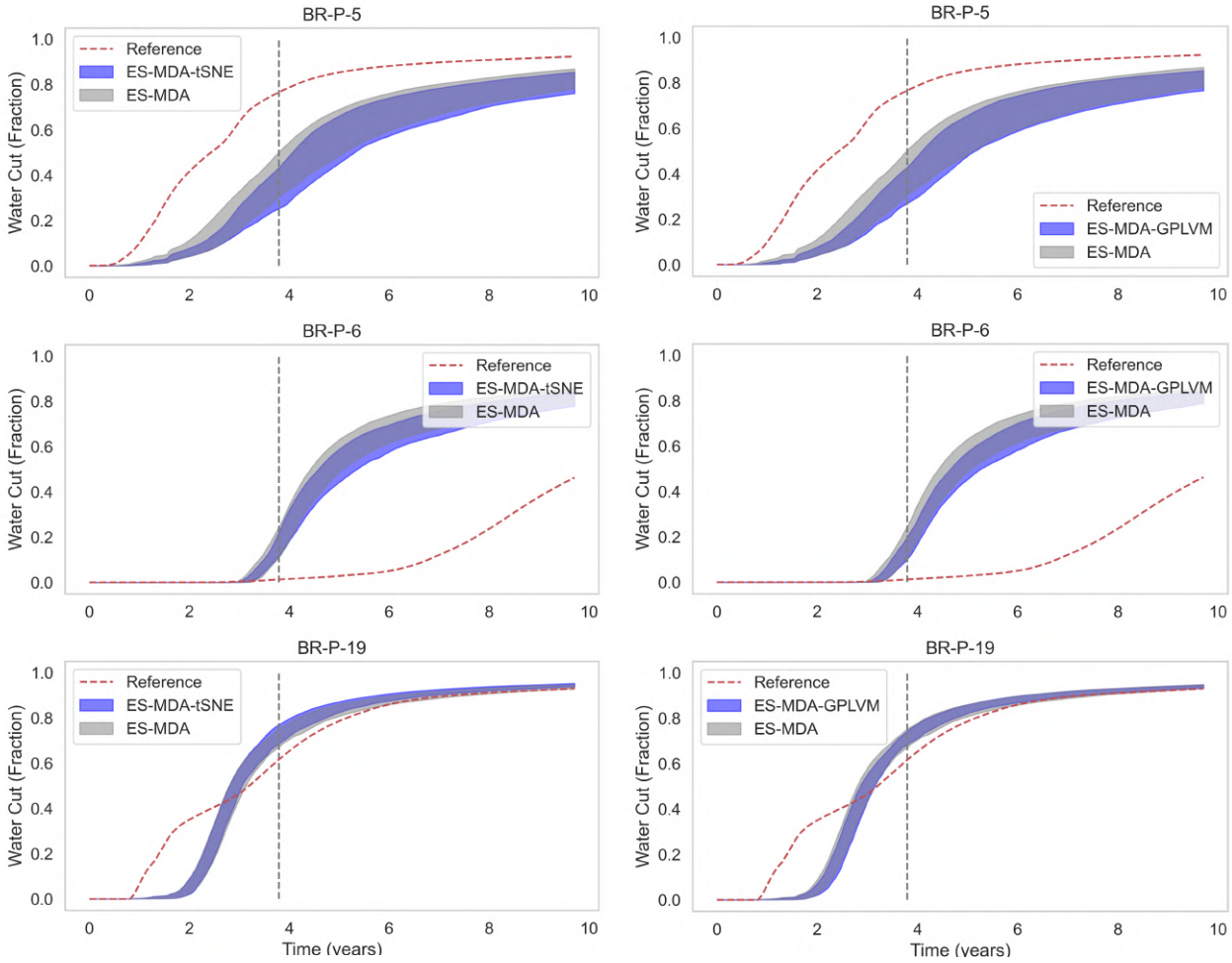

Figure 11. Water cuts for three wells with ESMDA, ES-MDA-tSNE and ES-MDA-GPLVM. The blue dashed line is utilized as an indication of the end of historical data and the start of the prediction period. The red dashed line represents the observed data points. The grey region refers to the forecast within P10 and P90 obtained with the ES-MDA. The light blue region represents P10-P90 obtained from ES-MDA-tSNE or ES-MDA-GPLVM.

For a quantitative comparison, we applied the mean CRPS metric to further evaluate the methods used at all simulated well data from the history-matched ensembles over the historical and prediction period, as displayed in Figure 12. The ES-MDA-t-SNE and ES-MDA-GPLVM provide interesting results, with the lowest CRPS average compared to the prior model, and although we used few ensembles models and saved around 45–53% of the simulation time, the results seem to be comparable to the standard ES-MDA.

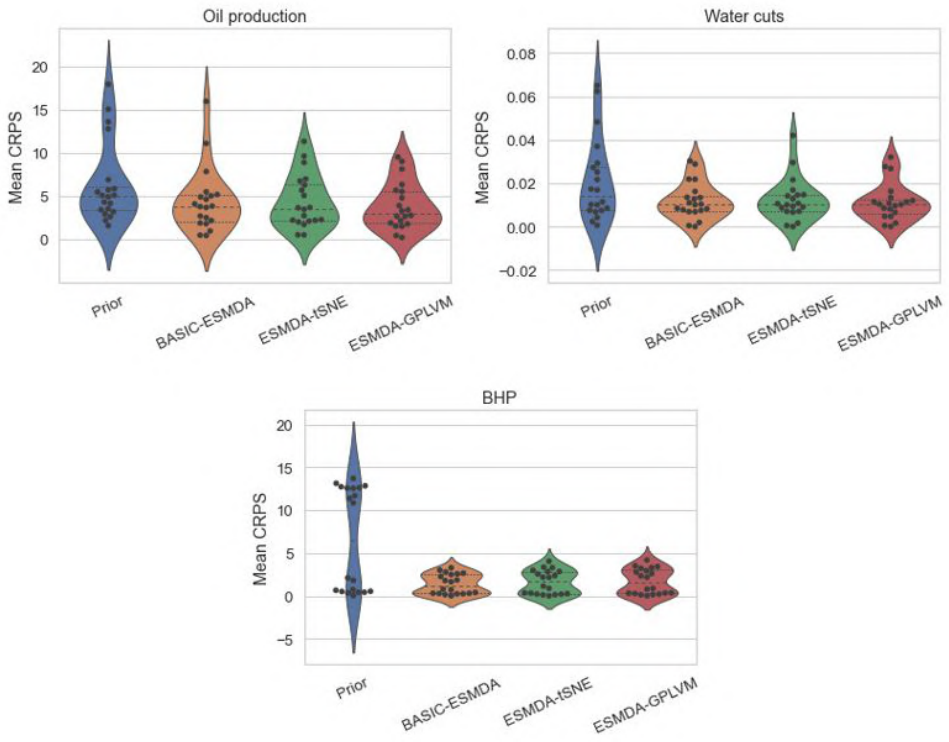

Figure 12. Violin plot of the mean CRPS of the historical and prediction data (OPR, water cuts, and BHP).

Since the uncertainty ranges are quantified in all wells at the three cases, we conducted another comparison by boxplots of the normalized field cumulative oil and water production predicted by each method, as displayed in Figure 13. It should be noted that the values are normalized to the cumulative production from the reference case, which is also added for comparison. Both ES-MDA-t-SNE and ES-MDA-GPLVM cover the true values for both oil and water production in the box ranges.

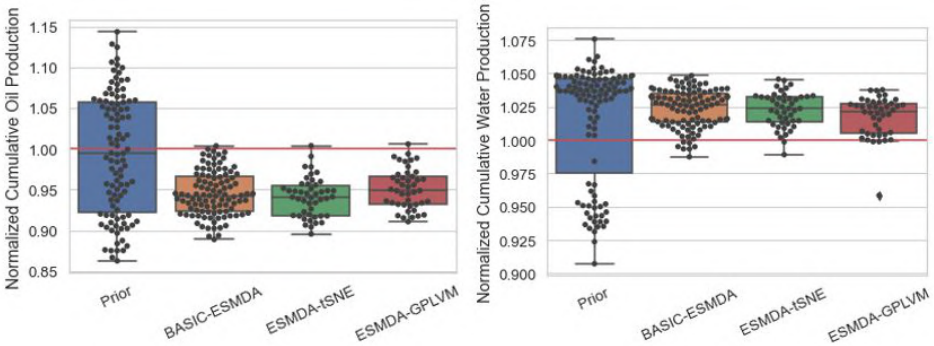

Figure 13. Boxplot of the normalized cumulative production after 10 years.

3.2. Effect of Different "Reference" Models

The previous section evaluated the ES-MDA-DR procedure on a single 'reference' model. We now evaluate the methodology on five additional 'referred' models: Test Case 1, Test Case 2, Test Case 3, Test Case 4, and Test Case 5 (we reiterate that neither reference model was included in the set of N = 103 prior models). Similarly, the data assimilations were conducted using ES-MDA with localization. Apart from the ES-MDA-t-SNE and ES-MDA-GPLVM, we performed the HM on assimilation observation data for the first 4 years and the rest (6 years) for forecasting. Note that the reference value varies considerably between the test cases, as shown in Figure 14. The cumulative distribution

function (CDF) for each test case is quite different, except the test case-1 and case-3, which show some similarities.

Table 3 demonstrates the posterior normalized field cumulative oil and water production predicted by each method in terms of P10 and P90 statistics at 10 years. For four cases, the ES-MDA, ES-MDA-t-SNE, and ES-MDA-GPLVM, predictions surround the reference data within the the P10 to P90 range and showed a narrower range of uncertain prediction results. However, in Test Case 2, the cumulative oil production is biased in comparison with the reference production, which is likely explained by whether the problems with the prior ensemble or the selected reference model. The ensemble means distribution of the reconstructed updated permeability posterior for the top-layer for all five cases, as shown in Figure 15. The results suggest a slight change in the posterior model where the wells are located. Additionally, one can expect uncertainty reductions due to the conditioning of the posterior samples to dynamic data variables of wells that are contained within the forecast domain. The results exhibit quite similar posterior permeability distribution for both ES-MDA-t-SNE and ES-MDA-GPLVM. In sum, the results for the five different test cases imply that the DR procedure can indeed provide updated geological models and predictions with different reference models at a significantly reduced computation time.

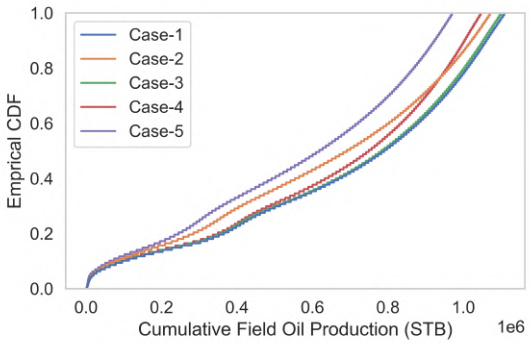

Figure 14. Empirical CDF computer from field oil production total for different test cases.

Table 3. Posterior prediction for different test cases. The P10 and P90 statistics are computed using the forecast results for field cumulative oil at 10 years.

		Reference	P10	P90
	Prior	-	9.099×10^5	1.114×10^6
Test Case 1	ES-MDA	1.108×10^6	1.045×10^6	1.112×10^6
	ES-MDA-t-SNE		1.049×10^6	1.114×10^6
	ES-MDA-GPLVM		1.053×10^6	1.124×10^6
Test Case 2	ES-MDA	1.071×10^6	9.752×10^5	1.042×10^6
	ES-MDA-t-SNE		9.764×10^5	1.013×10^6
	ES-MDA-GPLVM		9.609×10^5	1.016×10^6
Test Case 3	ES-MDA	1.099×10^6	1.037×10^6	1.116×10^6
	ES-MDA-t-SNE		1.052×10^6	1.121×10^6
	ES-MDA-GPLVM		1.050×10^6	1.111×10^6
Test Case 4	ES-MDA	1.046×10^6	1.008×10^6	1.088×10^6
	ES-MDA-t-SNE		1.012×10^6	1.081×10^6
	ES-MDA-GPLVM		1.018×10^6	1.078×10^6
Test Case 5	ES-MDA	9.698×10^5	9.361×10^5	9.993×10^5
	ES-MDA-t-SNE		9.428×10^5	9.986×10^5
	ES-MDA-GPLVM		9.340×10^5	9.867×10^5

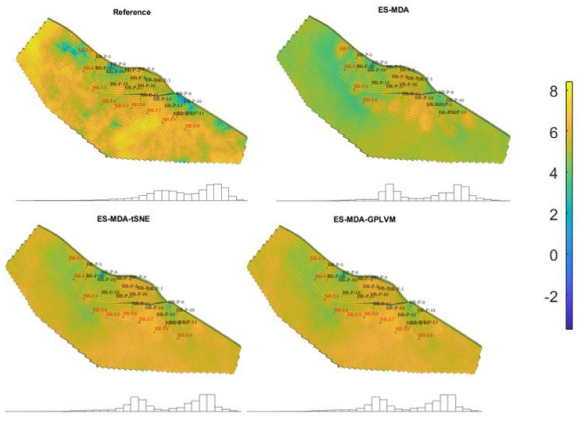

(**a**) Test cases 01

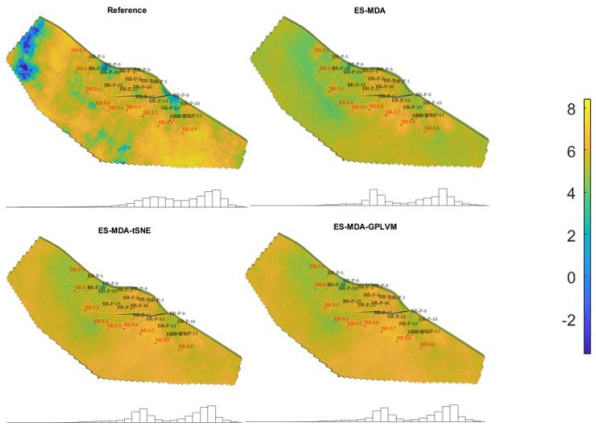

(**b**) Test cases 02

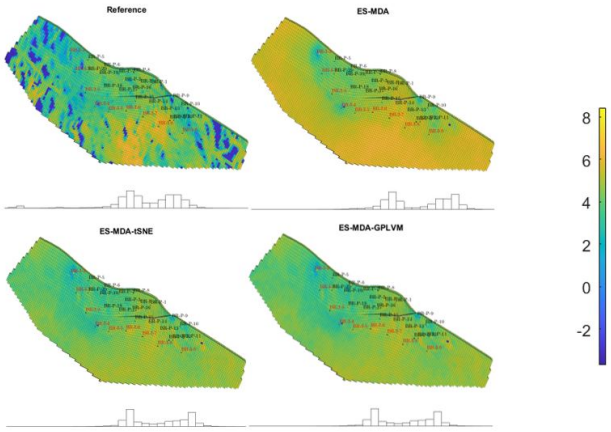

(**c**) Test cases 03

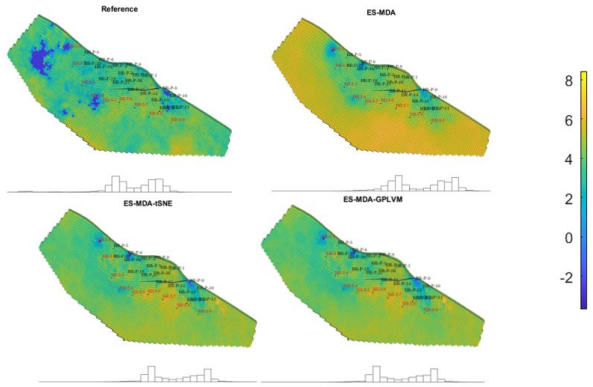

(**d**) Test cases 04

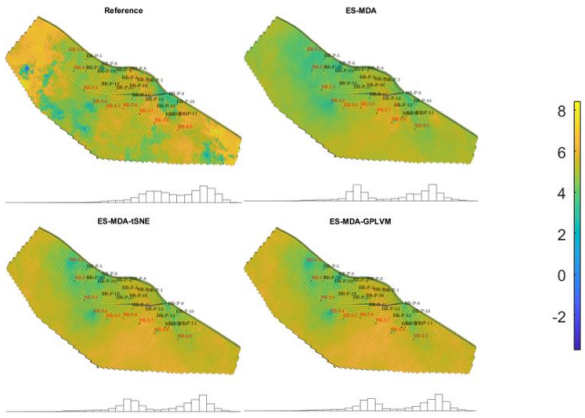

(**e**) Test cases 05

Figure 15. Average log permeability distribution on Layer 1 using different reference models.

3.3. Effect of Reference Model Parameters Outside Prior Distribution

In the previous section, we presented the results of ES-MDA, ES-MDA-t-SNE, and ES-MDA-GPLVM for tests where every 'reference' model was within the prior distributions. This indicates that there is consistency between the prior realizations used in the three methods with the underlying 'reference model. Here, we aim to evaluate the performance of the three methods for cases that involve a reference model, which is not consistent with the prior realizations. More precisely, the reference model is characterized by parameters that fall outside the prior ranges. Figure 16 displays the permeability cumulative distribution function (CDF) between the generated reference model along with P10 and P90 prior ensemble. We observe that the 'reference' model permeability parameters for this example lie outside the range of the prior distributions. RMD outlier detection was used as displayed in Figure 17 to verify the prior uncertainty variables (field oil production) on the reference variable. The results show that the RMD of d_{obs} falls above the 95th percentile threshold, in that the prior model is falsified.

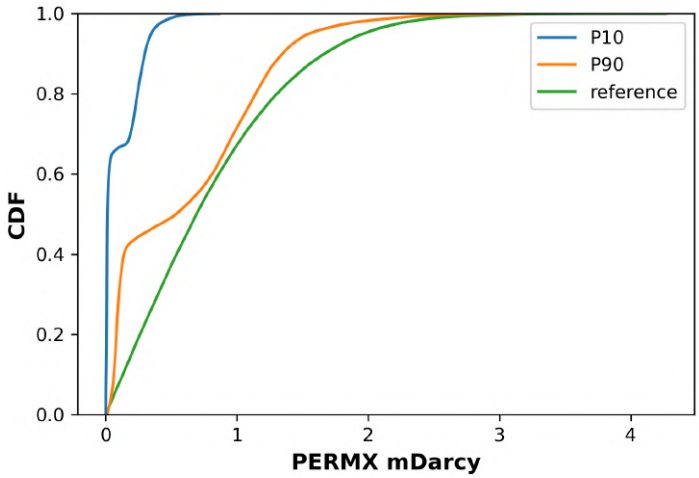

Figure 16. Empirical CDF computed from prior permeability (P10 and P90) and the reference model.

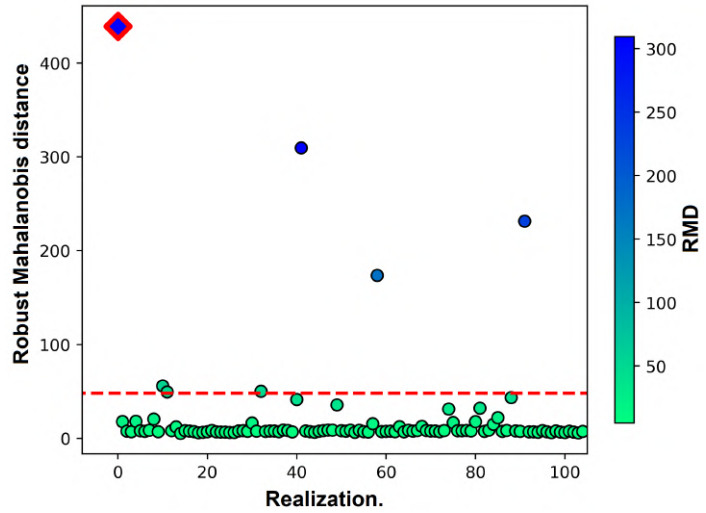

Figure 17. Prior falsification using Robust Mahalanobis distance (RMD). The red diamond is the RMD for d_{obs}. Circle dots refer to the RMD results of 104 data variable samples, and the red dashed line is the 95th percentile of the chi-squared distributed RMD.

Figures 18 and 19 depict the HM profiles for both oil and water cuts of three methods at producers BR-P5, BR-P6, and BR-P19, with respect to the prior ensemble and reference model. The results indicate that the standard ES-MDA and ES-MDA with DR failed to

match the reference data, and the predictions from the referenced models do not lie within the predicted P10 to P90 percentile. Figure 20 displays a boxplot of field cumulative water and oil production obtained by each method and the prior ensemble. Overall, the results do not cover the reference values, which is clearly explained by the lack of representativeness of the prior realizations. The previous results evidently demonstrate the success of our procedure based on a degree of the quality in terms of the prior parameter ranges. We emphasize that it is crucial that the prior simulation results contain the observations. Otherwise, we would not expect ES-MDA with DR to provide reasonable posterior predictions, and in practice, we should adapt the prior ensemble before using it for model conditioning.

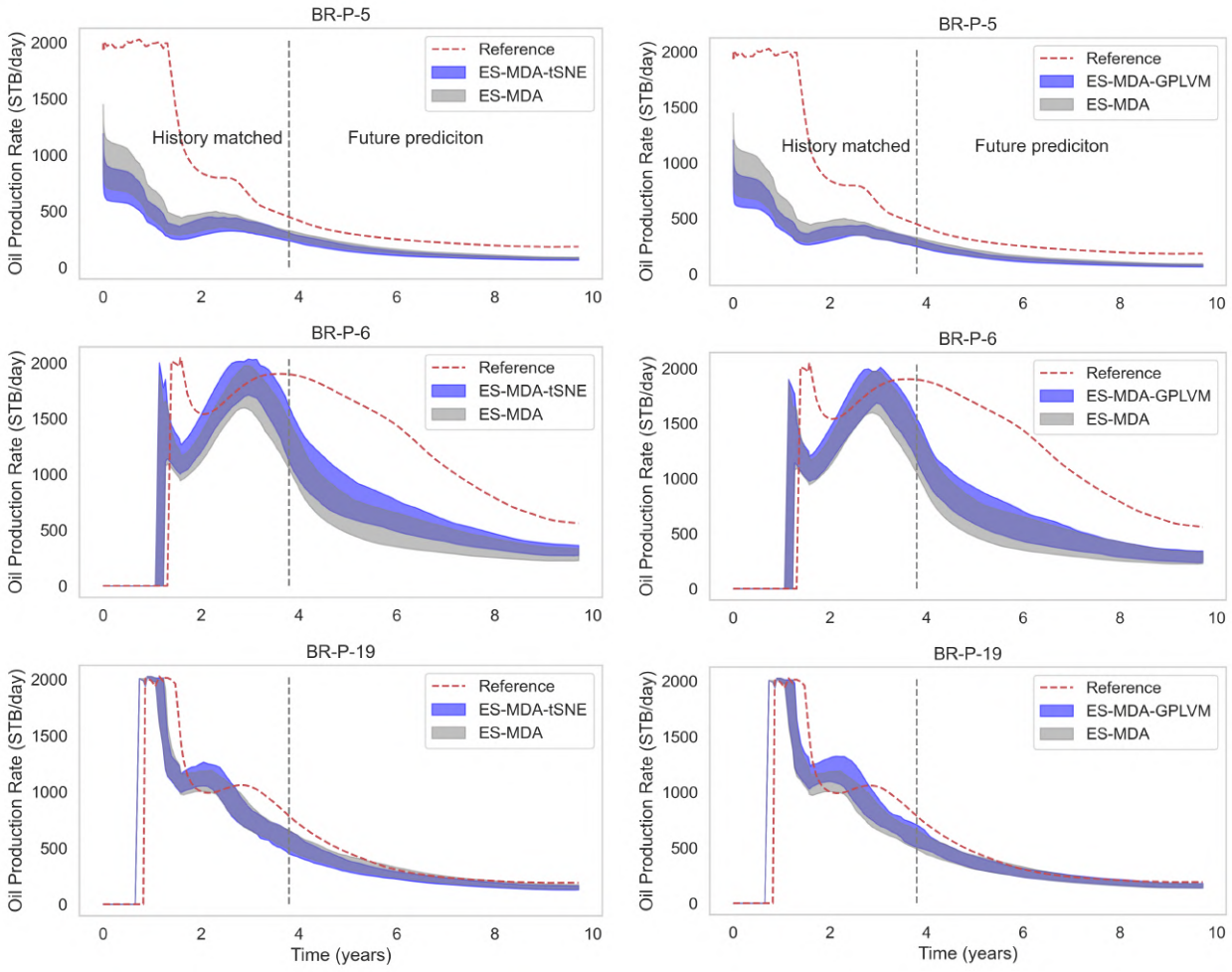

Figure 18. Oil production rate STB/day for three wells with ESMDA, ES-MDA-tSNE and ES-MDA-GPLVM. The blue dashed line is utilized as an indication of the end of historical data and start of prediction period. The red dashed line represents the observed data points. The grey region refers to the forecast within P10 and P90 obtained with the ES-MDA. The light blue section represents P10-P90 obtained from ES-MDA-tSNE or ES-MDA-GPLVM.

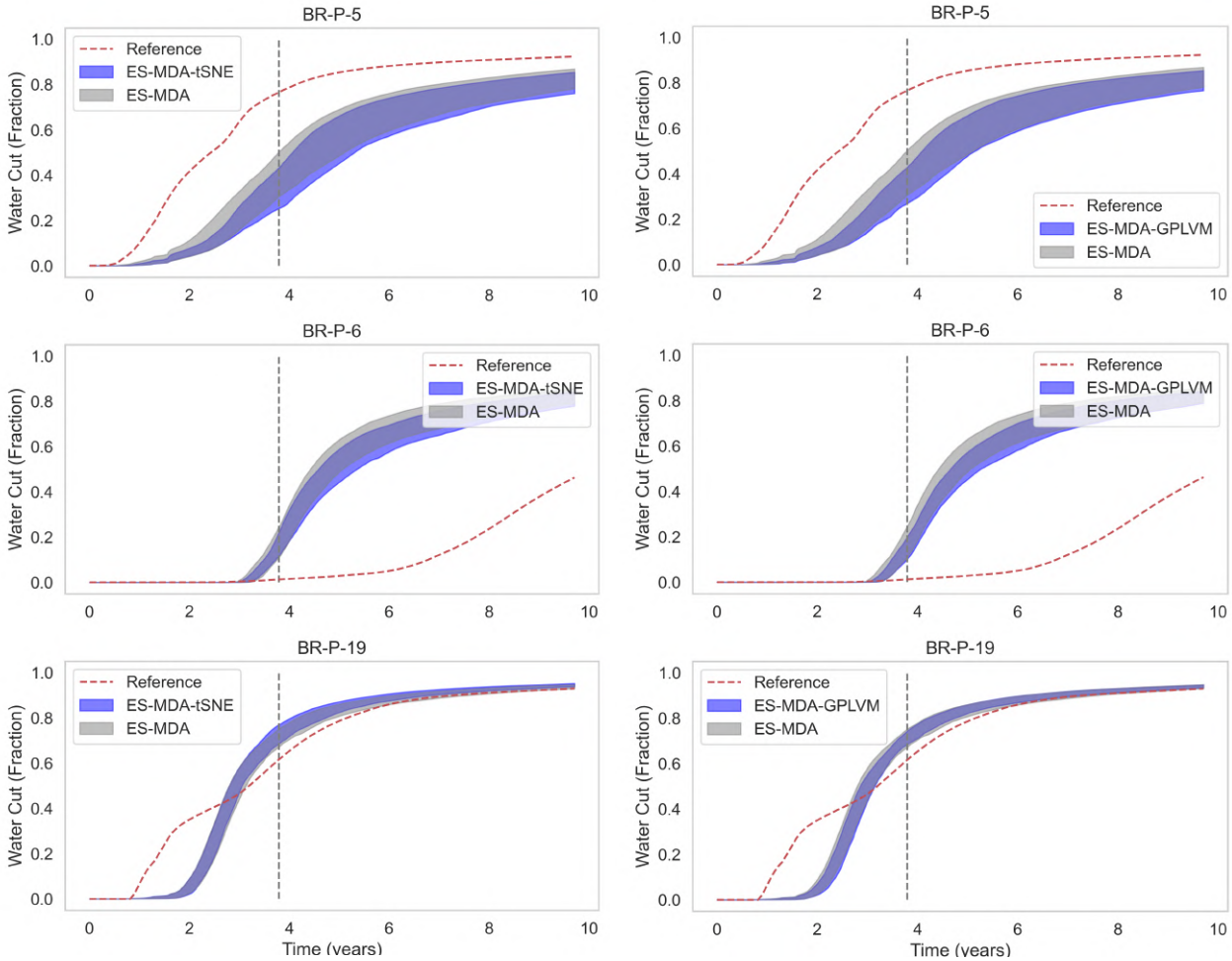

Figure 19. Water cuts for three wells with ESMDA, ES-MDA-tSNE and ES-MDA-GPLVM. The blue dashed line is utilized as an indication of the end of historical data and the start of the prediction period. The red dashed line represents the observed data points. The grey region refers to the forecast within P10 and P90 obtained with the ES-MDA. The light blue section represents P10-P90 obtained from ES-MDA-tSNE or ES-MDA-GPLVM.

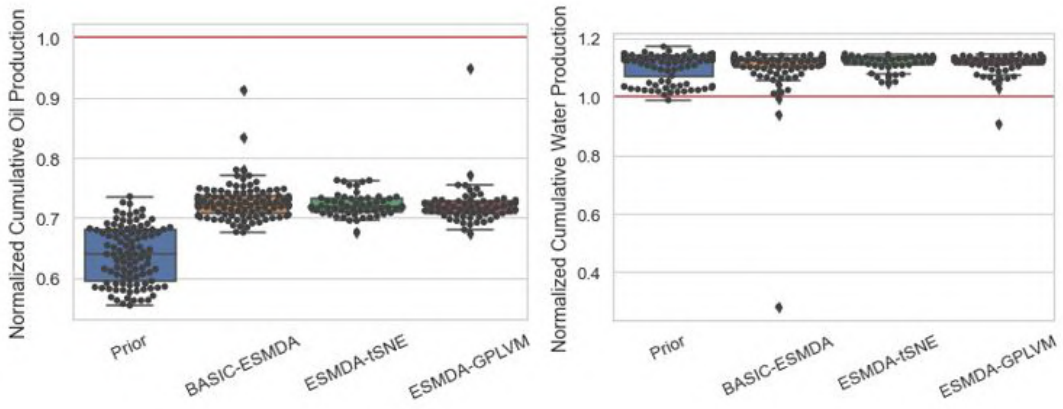

Figure 20. Boxplot of the normalized cumulative production after 10 years. The red line indicates the cumulative production of the reference case.

4. Concluding Remarks

In this study, we presented a novel history matching framework with DR while preserving realistic geology and matching the production data, which was achieved by

explicitly integrating t-SNE, GPLVM, and clustering K-means with ESMDA to reduce the simulation time and quantify the uncertainty on reservoir models. The proposed procedure yielded reliable results by selecting a set of good prior ensemble reservoir models, with similar production performance to the reference model, before applying the data assimilation process. Accordingly, we compared the new implementation with the standard ES-MDA in a field reservoir problem with a large number of wells and a long production history. Based on the obtained results, the proposed ES-MDA with DR is concluded to be computationally faster than the original one, and it is very simple to implement and integrate with different types of data and models. We also evaluated our procedure with five different 'reference' models, where we observed that the ES-MDA with DR posterior predictions displayed considerably less uncertainty, and was indeed able to provide improved geological models and predictions at a significantly reduced computation time. Moreover, we also considered a test case where the reference model lay outside the prior distributions, but the results were clearly inconsistent and biased. In conclusion, the accuracy of both methods is highly relied on the ability and quality of the prior realizations to provide appropriate estimates of the prior uncertainty.

We recommend that further studies apply our procedures to more complex geological models such as bimodal channelized systems. This approach can be applied to examine and overcome the challenges in 4D seismic history matching as capturing the value of 4D seismic data can lead to better reservoir management decisions. It will also be interesting to introduce into the framework more non-linear DR techniques, such as a deep autoencoder, a stacked autoencoder, and a generative adversarial network. Additionally, combining the data-space inversion (DSI) method with ES-MDA may more accurately predict oil production with computationally faster simulation.

Author Contributions: A.T. wrote the paper and contributed to tuning the model and analyzing the results R.B.B. and R.G.H. supervised the work and providing continuous feedback. All authors have read and agreed to the published version of the manuscript.

Funding: This research is funded by Petromaks-2 project DIGIRES (RCN no. 280473).

Acknowledgments: The authors acknowledge financial support from the Research Council of Norway through the Petromaks-2 project DIGIRES (RCN no. 280473) and the industrial partners AkerBP, Wintershall DEA, ENI, Petrobras, Equinor, Lundin, and Neptune Energy. The authors would like also to thank TNO for providing the Brugge reservoir model dataset.

Conflicts of Interest: The authors declare no conflict of interest.

Appendix A

Appendix A.1. t-Distributed Stochastic Neighbor Embedding (t-SNE)

t-SNE is a non-linear dimensionality reduction algorithm developed for exploring high-dimensional data [14]. It maps multi-dimensional data to a two- or three-dimensional dataset $Y = \{y_1, y_2, ..., y_n\}$ that can be visualized in a scatter plot. The t-SNE algorithm begins by computing a joint probability distribution pij over pairs of points x_i,x_j($i \neq j$):

$$p_{j|i} = \frac{exp(-\left\|x_i - x_j\right\|^2/2\tau_i^2)}{\sum_{l,s\in[n],l\neq s}(1+\|y_l - y_s\|^2)^{-1}} \quad , p_{ij} = \frac{p_{i|j}+p_{j|i}}{2n} \tag{A1}$$

where τ_i is a tunable parameter that controls the bandwidth of the Gaussian kernel around point x_i. In two-dimensional map $Y = \{y_1, y_2, ..., y_n\} \subset R^2$, the affinity q_{ij} between points y_i and y_j ($i \neq j$) is defined as:

$$q_{ij} = \frac{(1 + \left\|y_i - y_j\right\|^2)^{-1}}{\sum_{l,s\in[n],l\neq s}(1 + \|y_l - y_s\|^2)^{-1}} \tag{A2}$$

t-SNE then attempts to find points y_i in R^2 that minimize the KL-divergence between p and q:

$$f(y_1, y_2, ..., y_n) := KL(p \parallel q) = \sum_{i,j \in [n], i \neq j} p_{ij} log \frac{p_{ij}}{q_{ij}} \quad \text{(A3)}$$

The objective function f is minimized using the following gradient descent:

$$\frac{\partial f}{\partial y_i} = 4 \sum_{j \in [n] \setminus \{i\}} (p_{ij} - q_{ij}) q_{ij} Z(y_i - y_j) \quad , i \in [n] \quad \text{(A4)}$$

Appendix A.2. Gaussian Process Latent Variable Model (GPLVM)

GPLVM, introduced by Lawrence (2005) [23], is a Bayesian non-parametric dimensionality reduction method that uses a Gaussian process to learn a low-dimensional Q representation of high-dimensional data D. In Gaussian process regression (GP) settings, where we are given inputs X and outputs Y, we choose a kernel and learn hyperparameters that best describe the mapping from X to Y. The GP likelihood function is written as:

$$p(Y \mid X) = \prod_{d=1}^{D} p(y_d \mid X) \quad \text{(A5)}$$

Here, y_d represents the d^{th} columns of Y and:

$$p(Y \mid X) = \mathcal{N}(y_d \mid 0, K_{NN} + \beta^{-1} I_N) \quad \text{(A6)}$$

$\mathcal{N}$ is the number of the observation, and K_{NN} is the covariance matrix defined by the covariance or kernel function $K(x, \acute{x})$. The kernel function was modified to a squared exponential form to fit the automatic model selection of the dimensionality of latent space:

$$K(x, \acute{x}) = \sigma_f^2 exp\left(\frac{1}{2} \sum_{q=1}^{Q} \alpha_q (x_q - \acute{x}_q)^2\right) \quad \text{(A7)}$$

In the GPLVM, we do not have X; we are only given Y. We need to learn X along with the kernel hyperparameters. We do not perform maximum likelihood inference on X. Instead, we set a Gaussian prior for X and learn the mean and variance of the approximate (Gaussian) posterior $p(Y \mid X)$.

$$p(X) = \prod_{n=1}^{N} \mathcal{N}(x_n \mid 0, I_Q) \quad \text{(A8)}$$

With each x_n the n^{th} row of X. The joint probability model for the GPLVM model is:

$$p(Y, X) = p(Y \mid X) p(X) \quad \text{(A9)}$$

The hyper parameters of the model are the kernel parameters $\theta == (\sigma_f^2, \alpha_1, \alpha_2, ..., \alpha_Q)$ and the inverse variance parameter β.

Appendix A.3. Mean Continuous Ranked Probability Score (CRPS)

Mean CRPS is used to quantify both the accuracy and precision of a probabilistic forecast [34]. A higher value of mean CRPS indicates less accurate results. CRPS can be defined as:

$$CRPS = \int_{-\infty}^{\infty} [p(x) - H(x - x_{obs})]^2 dx \quad \text{(A10)}$$

Here, $p(x) = \int_{-\infty}^{x} p(y) d_y$ is the cumulative distribution of a quantity of interest, and $H(x - x_{obs})$ is the step function,

$$H(x) = \begin{Bmatrix} 0 & if < 0 \\ 1 & if \geqslant 0 \end{Bmatrix} \tag{A11}$$

For N samples, the CRPS can be evaluated as follows:

$$CRPS = \sum_{i=0}^{N} c_i c_i = \alpha_i p_i^2 + \beta_i (1 - p_i)^2 \tag{A12}$$

where $p_i = P(x) = i/N, for\ x_i < x < x_{i+1}$ (piecewise constant function)

$$\alpha_i = \begin{Bmatrix} 0 & if & x_{obs} < x_i \\ x_{obs} - x_i & if & x_i < x_{obs} < x_{i+1} \\ x_{i+1} - x_i & if & x_{obs} > x_{i+1} \end{Bmatrix} \tag{A13}$$

$$\beta_i = \begin{Bmatrix} x_{i+1} - x_i & if & x_{obs} < x_i \\ x_{i+1} - x_{obs} & if & x_i < x_{obs} < x_{i+1} \\ 0 & if & x_{obs} > x_{i+1} \end{Bmatrix} \tag{A14}$$

References

1. Oliver, D.S.; Chen, Y. Recent progress on reservoir history matching: A review. *Comput. Geosci.* **2011**, *15*, 185–221. [CrossRef]
2. Jafarpour, B.; McLaughlin, D.B. History matching with an ensemble Kalman filter and discrete cosine parameterization. *Comput. Geosci.* **2008**, *12*, 227–244. [CrossRef]
3. Sambridge, M. Geophysical inversion with a neighborhood algorithm—II. Appraising the ensemble. *Geophys. J. Int.* **1999**, *138*, 727–746. [CrossRef]
4. Jin, L.; Alpak, F.O.; van den Hoek, P.; Pirmez, C.; Fehintola, T.; Tendo, F.; Olaniyan, E. A comparison of stochastic data-integration algorithms for the joint history matching of production and time-lapse-seismic data. *SPE Reserv. Eval. Eng.* **2012**, *15*, 498–512. [CrossRef]
5. Jeong, J.; Park, E. Theoretical development of the history matching method for subsurface characterizations based on simulated annealing algorithm. Journal of Petroleum science and engineering. *J. Pet. Sci. Eng.* **2019**, *180*, 545–558. [CrossRef]
6. Gao, G.; Li, G.; Reynolds, A. A Stochastic optimization algorithm for automatic history matching. *SPE J.* **2007**, *12*, 196–208. [CrossRef]
7. Barker, W.J.; Cuypers, M.; Holden, L. Quantifying uncertainty in production forecasts: Another look at the PUNQ-S3 problem. *SPE J.* **2000**, *6*, 433–441. [CrossRef]
8. Gao, G.; Zafari, M.; Reynolds, A.C. Quantifying uncertainty for the PUNQ-S3 problem in a Bayesian setting with RML and EnKF. *SPE J.* **2006**, *11*, 506–515. [CrossRef]
9. Gu, Y.; Oliver, D.S. The ensemble Kalman filter for continuous updating of reservoir simulation models. *J. Energy Resour. Technol.* **2006**, *128*, 79–87. [CrossRef]
10. Evensen, G. Sampling strategies and square root analysis schemes or the EnKF. *Ocean. Dyn.* **2004**, *54*, 539–60. [CrossRef]
11. Van der Maaten, L.; Hinton, G. Visualizing Data Using t-SNE. *J. Mach. Learn. Res.* **2008**, *9*, 2579–2605.
12. Emerick, A.; Reynolds, A. Ensemble smoother with multiple data assimilation. *Comput. Geosci.* **2013**, *55*, 3–15. [CrossRef]
13. Emerick, A. Analysis of the performance of ensemble-based assimilation of production and seismic data. *J. Pet. Sci. Eng.* **2016**, *139*, 219–239. [CrossRef]
14. Vo, H.; Durlofsky, L. A new differentiable parameterization based on principal component analysis for the low-dimensional representation of complex geological models. *Math. Geosci.* **2014**, *46*, 775–308. [CrossRef]
15. Rezaie, J.; Saetrom, J.; Smorgrav, E. Reducing the Dimensionality of Geophysical Data in Conjunction with Seismic History Matching. In *74th EAGE Conference and Exhibition incorporating EUROPEC*; European Association of Geoscientists & Engineers: Houten, The Netherlands, 2012.
16. Sarma, P.; Durlofsky, L.J.; Aziz, K. Kernel principal component analysis for efficient, differentiable parameterization of multi point geostatistics. *Math. Geosci.* **2008**, *40*, 3–32. [CrossRef]
17. Muzammil, R.; Ahmed, H.E.; Yan, C. Identifiability of Model Discrepancy Parameters in History Matching. In Proceedings of the SPE Reservoir Simulation Conference, Galveston, TX, USA, 10–11 April 2019.
18. Kang, B.; Choe, J. Regeneration of initial ensembles with facies analysis for efficient history matching. *J. Energy Resour. Technol.* **2017**, *139*, 042903. [CrossRef]
19. Kang, B.; Kim, S.; Jung, H.; Choe, J.; Lee, K. Characterization of three-dimensional channel reservoirs using ensemble Kalman filter assisted by principal component analysis. *Petroleum Sci.* **2019**, *17*, 182–195. [CrossRef]
20. Tolstukhin, E.; Barrela, E.; Khrulenko, A.; Halotel, J.; Demyanov, V. Ensemble History Matching Enhanced with Data Analytics-A Brown Field Study. *Eur. Assoc. Geosci. Eng.* **2019**, *2019*, 1–5.

21. Satija, A.; Scheidt, C.; Li, L.; Caers,J. Direct Forecasting of Reservoir Performance Using Production Data without History Matching. *Comput. Geosci.* **2017**, *21*, 315–333. [CrossRef]
22. Park, J.; Caers, J. Direct forecasting of global and spatial model parameters from dynamic data. *J. Comput. Geosci.* **2020**, *143*, 104567. [CrossRef]
23. Lawrence, N.D. Learning for larger datasets with the Gaussian process latent variable model. In Proceedings of the Eleventh International Workshop on Artificial Intelligence and Statistics, San Juan, Puerto Rico, 21–24 March 2007.
24. Lawrence, N.D. Probabilistic non-linear principal component analysis with Gaussian process latent variable models. *J. Mach. Learn. Res.* **2005**, *6*, 1783–1816.
25. De Maesschalck, R.; Jouan-Rimbaud, D.; Massart, D. The Mahalanobis distance. *Cemometrics Intell. Lab. Syst.* **2000**, *50*, 1–18. [CrossRef]
26. Yin, Z.; Strebelle, S; Caers, J. Automated Monte Carlo-based Quantification and Updating of Geological Uncertainty with Borehole Data (AutoBEL v1.0). *Geosci. Model. Dev.* **2019**, *13*, 651–672. [CrossRef]
27. Liu, F.T.; Ting, K.M.; Hua, Z. Isolation forest. In Proceedings of the 2008 Eighth IEEE International Conference on Data Mining, Pisa, Italy, 15–19 December 2008.
28. Breunig, M.M.; Kriegel, H.P.; Ng, R.T.; Sander, J. LOF: Identifying density-based local outliers. In Proceedings of the 2000 ACM SIGMOD International Conference on Management of Data, Dallas, TX, USA, 16–18 May 2000.
29. Schölkopf, B.; Williamson, R.C.; Smola, A.J.; Shawe-Taylor, J.; Platt, J.C. Support vector method for novelty detection. In Proceedings of the Advances in Neural Information Processing Systems, Denver, CO, USA, 29 November–4 December 1999.
30. Jain, A.K. Data clustering: 50 years beyond K-means. *Pattern Recognit. Lett.* **2010**, *31*, 651–666. [CrossRef]
31. Watanabe, S.; Datta-Gupta, A. Use of phase streamlines of covariance localization in Ensemble Kalman Filter for three-phase history matching. In Proceedings of the SPE Western North American Region Meeting, Anchorage, AK, USA, 7–11 May 2011.
32. Gaspari, G.; Cohn, S. Construction of correlation functions in two and three dimensions. *Q. J. R. Meteorol. Soc.* **1999**, 723–757. [CrossRef]
33. Peters, E.; Arsts, R.; Brouwer, G.; Geel, C.R.; Cullick, S.; Lorentzen, R.J.; Chen, Y.; Dunlop, N.B.; Vossepoel, C.; Xu, R.; et al. Brugge Brenchmard study for flooding Optimiztion and History Matching. *SPE Reserv. Eval. Eng.* **2010**, *13*, 391–405. [CrossRef]
34. Hersbach, H. Decomposition of the Continuous Ranked Probability Score for Ensemble Prediction Systems. *Weather. Foracsting* **2000**, *15*, 559–570. [CrossRef]

Paper V

Application of Machine Learning to Assess the Value of Information in Polymer Flooding.

Amine Tadjer, Aojie Hong, Reidar B. Bratvold and Remus Hanea.

Petroleum Research xxx (xxxx) xxx

Contents lists available at ScienceDirect

Petroleum Research

journal homepage: http://www.keaipublishing.com/en/journals/petroleum-research/

Application of machine learning to assess the value of information in polymer flooding

Amine Tadjer [a, *], Reidar B. Bratvold [a], Aojie Hong [a], Remus Hanea [b]

[a] University of Stavanger, Norway
[b] Equinor, Norway

ARTICLE INFO

Article history:
Received 19 February 2021
Received in revised form
21 May 2021
Accepted 23 May 2021
Available online xxx

Keywords:
Value of information
Reservoir development plan
Approximate dynamic programming
Machine learning

ABSTRACT

In this work, we provide a more consistent alternative for performing value of information (VOI) analyses to address sequential decision problems in reservoir management and generate insights on the process of reservoir decision-making. These sequential decision problems are often solved and modeled as stochastic dynamic programs, but once the state space becomes large and complex, traditional techniques, such as policy iteration and backward induction, quickly become computationally demanding and intractable. To resolve these issues and utilize fewer computational resources, we instead make use of a viable alternative called approximate dynamic programming (ADP), which is a powerful solution technique that can handle complex, large-scale problems and discover a near-optimal solution for intractable sequential decision making. We compare and test the performance of several machine learning techniques that lie within the domain of ADP to determine the optimal time for beginning a polymer flooding process within a reservoir development plan. The approximate dynamic approach utilized here takes into account both the effect of the information obtained before a decision is made and the effect of the information that might be obtained to support future decisions while significantly improving both the timing and the value of the decision, thereby leading to a significant increase in economic performance.

1. Introduction

Reservoir management is defined as the utilization of available technology, financial assets, and human resources to maximize the economic recovery of a reservoir. This type of management involves a series of operations and decisions, from the initial stage of the discovery of a reservoir to the final stage of field abandonment (Wiggins and Startzman, 1990). A significant number of decision-making problems related to reservoir management are regarded as sequential problems, as most petroleum engineers and geoscientists are used to considering the information gathered, supporting their future decision making, and maximizing the value created by the reservoirs. However, the models for reservoir management decisions may be computationally prohibitive and intractable if several sequential decisions and uncertainties are involved. To solve this issue and successfully execute good reservoir management, decision analysis (DA) is recommended due to its several advantages (Evans, 2000). (Howard, 1988) stated that "DA is a systematic procedure for transforming opaque decision problems into transparent decision problems through a series of transparent procedures." In the context of reservoir management, DA is used as a consistent means of evaluating different approaches and alternatives to determine the optimal scenario to maximize the net present value (NPV) of any project (Evans, 2000). Enhanced oil recovery (EOR) is an important phase in the field development planning process and is mainly applied whenever the primary and secondary recovery mechanism are not sufficient to displace the hydrocarbon from the remaining reserve. EOR methods include gas-flooding, polymer flooding, surfactant flooding, CO_2 flooding, and thermal flooding. However, EOR may not be applied to the process if it is not cost-effective. Therefore, a key decision in the development the planning process pertaining to the implementation of EOR methods is determining the best time to initiate an EOR process. With this method, oil companies can estimate the period for which the field will be economically profitable. However, since the initiation of EOR demands a high cost, it is important to assess

* Corresponding author.
E-mail address: amine.tadjer@uis.no (A. Tadjer).

https://doi.org/10.1016/j.ptlrs.2021.05.006

its impact on the decision-making process. The value of information is a type of decision analytics that is suited to quantifying the value of prior information (Schlaifer, 1959). was the first to introduce and define the concept of VOI in the context of business decision-making. Since then, the VOI approach has appeared in several textbooks and references, e.g., (Raiffa and Schlaifer, 1961; Howard, 1966; Clement, 1991; Bratvold and Begg, 2010; Howard and Abbas, 2016). The first application of this concept in the oil and gas (O&G) industry was done by (Grayson, 1960). (Bratvold et al., 2009) presented an overview of the use of VOI analysis in the O&G industry. Recently (Eidsvik et al., 2016), and (Dutta et al., 2019) demonstrated a comprehensive application of this method in the domain of earth sciences and subsurface energy. In the O&G industry, two different approaches are used to include the impact of information: closed-loop reservoir management (CLRM) and sequential reservoir decision making (SRDM). These approaches serve as a priori analyses, and each technique is implemented before the collection of additional information. Thus, whenever additional data are gathered, both CLRM and SRDM can be readily applied to make use of those data. However, for a complicated decision-making problem with many uncertain outcomes, alternatives, and decision points, these approaches suffer from the "curse of dimensionality." For a more detailed description of SRDM and CLRM, see (Howard and Abbas, 2016; Bratvold et al., 2009; Barros et al., 2015; Hong et al., 2018).

In previous studies (Hong et al., 2018), illustrated a method for ADP, specifically the Least-Squares Monte Carlo (LSM) algorithm, which was proposed by (Longstaff and Schwartz, 2001). This algorithm can be implemented with a production model based on exponential declines to determine the optimal time to switch from one recovery phase to another. Theoretically, LSM implementation is independent of production models but still suffers from the curse of dimensionality in the action space, where the computational effort of LSM will increase exponentially with the number of both alternatives and decision points, according to (Powell, 2016) and (Hong et al., 2018). Apart from this (Alkhatib and Babaei, 2013), showed that LSM can be used in a homogenous reservoir model in the context of surfactant flooding.

Our approach in the current study is different from that of (Alkhatib and Babaei, 2013) and (Hong et al., 2018). Here, the objective is to do a VOI analysis of in the context initiating polymer flooding in reservoir development plan, where a decision problem is constructed where to determine the optimal time to switch from water flooding to polymer injection based on the information from production profiles and oil prices, and the switch happens only once. The analysis is done on a constructed case study involving both homogenous and heterogeneous reservoir model, Further, we use various machine learning regression approach that lies within the domain of ADP to directly estimate the conditional expected value given the data outcomes without approximating the posterior probabilities of reservoir properties. The ADP approach utilized here accounts for both the effect of the information of both production profiles and oil prices obtained before a decision is made and the effect of the information that might be obtained to support future decisions.

The paper is divided into multiple sections. In the following section, we provide a consistent basic concept and equation for VOI computation. Second, we propose a workflow of assessing VOI using machine learning methods and, following this, we test the proposed methodology by implementing it in an ensemble homogenous and heterogeneous reservoir model, where we perform fast analysis of the optimal EOR switch time using the proposed workflow. Fourth, we include oil price as uncertain economic parameter, and finally, some concluding remarks are added.

2. Value of information and decision making

The VOI in any information gathering activity depends on two fundamental uncertainties; (1) the uncertainties we hope to learn but cannot directly observe; which we call events of interests, and (2) the test results referred as the observable distinctions (Bratvold et al., 2009). In Reservoir management data gathered until time t which a decision will be made is the observable distinction, and future prediction production after time t is the events of interest. We denote the observable distinction as x, since x is very high dimension; it is difficult to represent the distribution of x in analytical form, we usually approximate the distribution of x by Monte Carlo sampling. Assuming a risk neutral decision maker, VOI is defined as:

$$VOI = \begin{bmatrix} Expected\ value\ with \\ additional\ information \end{bmatrix} - \begin{bmatrix} Expected\ value\ without \\ additional\ information \end{bmatrix}$$

In mathematical form, this is:

$$VOI = \{0, \Delta\} \tag{1}$$

$$\Delta = EVWII - EVWOI \tag{2}$$

The lower limit of VOI is always 0, since if Δ is negative when $EVWOI > EVWII$, the decision-maker can always choose not to gather information.

In a decision-making context, the decision without information (DWOI) is the alternative that optimizes the expected value (EV) over the prior value, and *EVWOI* is the optimal EV over the prior.

$$EVWOI = max_{a\in A}\left[\int v(x,a)p(x)dx\right] \approx max_{a\in A}\left[\frac{1}{b}\sum_{b=1}^{B} v\left(x^b, a\right)\right] \tag{3}$$

where a is the decision alternative from the a set of A, x is the distinctions of interests, $v(x, b)$ is the value function that assigns a value to each alternative outcome pair for a given x and realization b, and $p(x)$ is the prior probability distribution of x.

Similarly, if we have perfect information regarding the value of x that the distinction of interests would take, we would choose the optimal action for that value of x. The decision with imperfect information (DWII) is the alternative that optimizes the expected value over the posterior value:

$$EVWII = \int max_{a\in A}\left[E(v(x,a)|y) \times]p(y)dy \approx \frac{1}{B}\sum_{b=1}^{B} max_{a\in A}E\left[v(x,a)|y^b\right]\right] \tag{4}$$

Where $p(y)$ is the marginal probability distribution over y.

Additionally, the decision with perfect information (DWPI) can also be determined in this decision-making context. For instance, in reservoir engineering, perfect information is the information that reveals the true reservoir properties and the impacts of the recovery mechanism. Taking the EOR initiation problem as an example, the EV With Perfect Information (EVWPI) is the maximum NPV for every path based on prior realizations or distributions. Then, averaging these NPVs over the paths would result in the *EVWPI*. In this way, every path would have an optimal decision with perfect information. The difference between *EVWPI* and *EVWOI* is the value of the perfect information (VOPI).

3. Value computation by ADP

We use an ADP method called the simulation-regression (or least-squares Monte Carlo) method to calculate the expected value with imperfect information. The simulation regression method involves Monte Carlo simulation and regression for (approximately) calculating the conditional expected value given data.

Monte Carlo simulation:

1. Many possible realizations of state variables (x^b) such as porosity and permeability are generated using Monte Carlo simulation model.
2. Forward modelling is performed to generate modeled (future) production data (y^b) from t_0 to t_{end}, with the addition of random noises generated from the statistics measurements errors to the modeled production data.
3. For each decision alternative a, the $NPV(x^b, a)$ is calculated.
4. The EVWOI is then calculated using the following equation:

$$EVWOI = \left[\frac{1}{b}\sum_{b=1}^{B} NPV\left(x^b, a^*_{DWOI}\right)\right] \; a^*_{DWOI} = argmax_{a\in A}\left[\frac{1}{b}\sum_{b=1}^{B} NPV\left(x^b, a\right)\right]$$

where a^*_{DWOI} is the optimal decision without information and it is identical to each realization.

Backward induction.

1. Starting recursively from the last decision point in time, in order to estimate the expected NPV (ENPV) with alternative a conditional on the modeled production data, $ENPV(x, a)|y$, we regress $[NPV_{1j}, NPV_{2j}, \ldots, NPV_B(x, a)]$ on the modeled production profiles. This procedure is repeated for each of the alternatives.
2. The optimal decision is then determined by choosing the alternative that achieves the highest value of conditional ENPV given the known information.
3. The EVWII is then as follows: $EVWII = \frac{1}{b}\sum_{b=1}^{B} NPV\left(x^b, a^*_{DWII}\left(y^b\right)\right)\; a^*_{DWII}\left(y^b\right) = arg\,\frac{1}{b}\sum_{b=1}{}^{B} max_{a\in A} E\left[NPV\left(x^b, a\right)\middle| y^b\right]$, $where\ a^*_{DWII}\left(y^b\right)$ is the optimal decision with given information y^b
4. Finally, the VOI is given by $max\{0, EVWII - EVWOI\}$

The process of ADP is further detailed in Hong et al. (2018); Longstaff and Schwartz (2001).

Various methods (linear or non-linear) can be used for regression to calculate the conditional ENPV given data. In the next section, we will review the regression methods used in this study.

3.1. Machine learning algorithms (regression methods)

- **Least Squares Monte Carlo Methods (LSM)**, is a state-of-the-art dynamic programming approach used in financial engineering with real options initially proposed by (Longstaff and Schwartz, 2001). (Jafarizadeh and Bratvold, 2009) recommended the use of the LSM technique as a potential real option valuation technique for the oil industry (Willigers and Bratvold, 2009). explained how LSM simulation can handle more realistic valuation situations with multiple uncertain variables. One of the limitations of the LSM method is its high-dimensional space, through which the computational time can increase exponentially (Hong et al., 2018).

The mathematical depiction of the ordinary least square is the following:

$$y_n = \sum_{i=0}^{k} \beta_i x_{ni} + \epsilon \tag{5}$$

where x_i is the explanatory variable i.e. production profiles, and y is a dependent variable i.e. NPVs. The coefficient β minimizes the error prediction.

- **Partial Least square (PLS)**, is a regression technique that is frequently used for high-dimensional methods (Rosipal and Krämer, 2006 34–51). It takes into account the structures of both the explanatory variable and the dependent variable. This model is linear, as shown in Eq (5). However, β coefficients are found in a different way than with the ordinary least squares method. The principal of PLS regression involves data x and y, which are decomposed into their latent structures in an iterative process such that the covariance of the latent structure is maximized.
- **Principal Component Regression (PCR)**, reduces a large number of explanatory variables x_i in a regression model to a small number of principal components. PCR mainly differs from PLS in that the dependent variables in the former are regressed on the principal components of the data using linear regression Abdi (2010).
- **Neural Network (NN)**, often simply called multilayer perceptron MLP), is a nonlinear method for either classification or regression (Liu et al., 2019). The NN model consists of several layers, each containing a large number of neurons. Each neuron receives an input and provides a corresponding output through functional operations such as weight, bias, and transfer function (see Fig. 1). In mathematical form, the MLP parameters is given as follows:

$$\theta = (W_1, b_1, W_2, b_2, \ldots, W_L, b_L) \tag{6}$$

where W_i is a weight matrix and b_i is the corresponding bias vector of the $L - th$ neural layer. A function can then be given as follows:

$$y(x) = F(x|\theta) \tag{7}$$

For neurons, the standard form is given as:

$$z_i^l = \phi^l\left(\sum_j w_{ij}^l z_j^{l-1} + b^l\right) \tag{8}$$

Where z_i^l denote the value of the $i - th$ neuron in the $l - th$ layer; z_j^{l-1} is the $i - th$ neuron in the $(l - 1)$ layer; and $w_{ij}^l \in w_l, b_{ij}^l \in b_l$. When $l = 0$, $z^o = x$ the input explanatory variables i.e. production profiles, when $l = L, z^L = y$ is the network dependent output variable i.e. NPVs. z^l represents an intermediate variable. The function $\phi(.)$ represents the hidden node output, and is given as an activation function e.g. $Relu, \phi(x) = max(x, 0); Sigmoid, \phi(x) = \frac{1}{1+e^{-x}}$

- **Gaussian process regression (GPR)**, is a non-parametric Bayesian machine learning technique, used to model an unknown value function with the help of a Gaussian process (Rasmussen, 2004). A Gaussian process $V \sim GP(m, k)$, is completely specified by its mean function $m(x) = E[V(x)]$ and covariance function $\sim k(x, \acute{x}) = \frac{1\sqrt{2\pi\sigma^2}}{e}^{\frac{\|x-\acute{x}\|}{2}} 2\sigma^2$. GPR is a kernel-based which does not attempt to identify "best-fit" models of the data. Instead, GPR computes the posterior Gaussian process

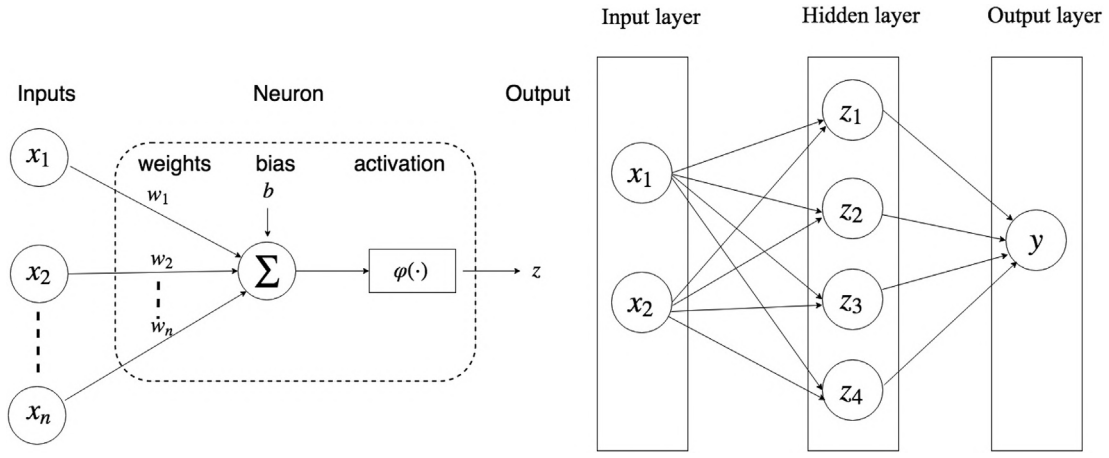

Fig. 1. Illustration of a neuron and multi-layer perceptron configuration (Liu et al., 2019).

by conditioning on the observed the values. In this study, we choose k to be the Gaussian radial basis function, $k(x,x') = \frac{1}{\sqrt{2\pi\sigma^2}} e^{\frac{\|x\|}{22\sigma^2}}$ and assume that we observe $y = V(x) + \varepsilon$, where $\varepsilon \sim \mathcal{N}(0, \sigma_\varepsilon^2), \varepsilon$ is the gaussian noise …

- **Automated Machine Learning (Auto ML)**, in general, machine learning typically requires substantial human resources to determine a relevant pipeline (including various types of pre-processing and the choice of the regression method and hyperparameters). In response to this, various Auto ML techniques have been developed to build systems that can automate the process of designing and optimizing machine learning pipelines. In our study, we use an Auto ML technique called the Tree-Based Pipeline Optimization Tool (TPOT). TPOT was first proposed by (Olson and Moore, 2019). In short, TPOT optimizes machine learning pipelines using a stochastic search algorithm such as genetic programming.

4. VOI in polymer flooding recovery

In this section, we use two more realistic examples to illustrate how the methodology discussed in sections 2 and 3 can be applied to reservoir simulations and modeled to solve the EOR initiation time problem.

4.1. 2D reservoir model

Consider a simple 2D reservoir model with homogenous permeability and porosity fields. This model simulates the displacement of oil to the producer by two water-well injections. We used an ensemble of N = 500 realizations for the permeability. The top view of this reservoir model and the well position are shown in Fig. 2, and other important reservoir parameters and PVT properties are shown in Table 1.

Problem setting: For the problem setting of this example, a total period of 6 years of production time is supposed. We consider two recovery phases: water flooding and polymer. We will analyze the optimal time to switch from water flooding to polymer injection. This analysis will provide useful insights into the reservoir development plan, and the decision will affect the learning over time. After each year of production, the decision of whether or not to inject a polymer has to be made, but the switch happens only once. This indicates that there will be 5 different switch times and decisions to be made (see Table 2 and Fig. 3).

The oil and water production of 500 ensembles are modeled

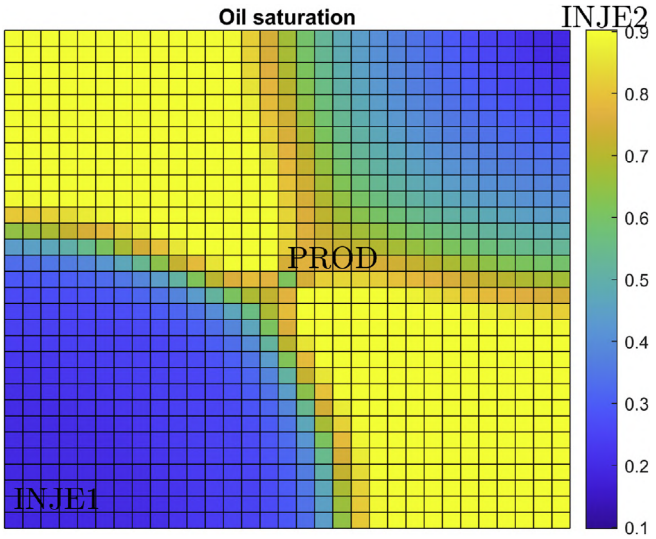

Fig. 2. The front view of the 2D reservoir model.

Table 1
Values of important reservoir parameters and PVT properties – the 2D reservoir model.

Water density, kg/m3	1080
Oil density, kg/m3	962
Water viscosity, pa.s	0.48×10^{-3}
Oil viscosity, pa.s	5×10^{-3}
Water compressibility, 1/bar	4.28×10^{-5}
Oil compressibility, 1/bar	6.65×10^{-5}
Initial reservoir pressure, bar	234
Porosity	0.3
Polymer Concentration INJECT 1, kg	4
Polymer Concentration INJECT 2, kg	1

using the reservoir simulation model and inform the decision-making. Thus, to obtain the measured rates, the measurement errors should be normally distributed with a mean of zero and a standard deviation of 10% of the modeled rates and then added to the modeled rates. Fig. 4 shows the oil and water production for all realization of some decision alternatives.

The value function is defined as the NPV for each decision alternative corresponding to each realization. NPV is a function of revenue from the oil production and costs for water production,

Table 2
Decision problem setting.

Injection period	6 years
Alternative	Continue or switch the injection at times {1, 2,3,4,5}
Uncertainty	permeability and porosity.
Value derived from the decision situation	Net present value
Information data	Oil and water production profiles

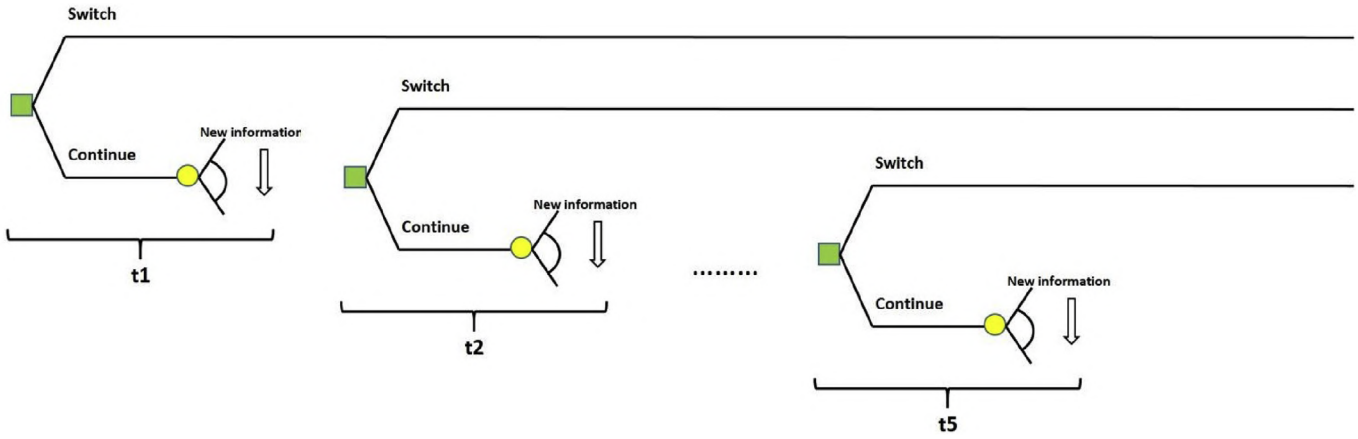

Fig. 3. Decision flow chart for Polymer flooding injection.

water injection, and polymer injection. The NPV is calculated using the following equation:

$$v\left(x^b,a\right)=\sum_{k=1}^{n_T}\frac{\left[q_0^k\left(x^b,a\right)P_0-q_{wp}^k\left(x^b,a\right)P_{wp}-q_{wi}^k\left(x^b,a\right)P_{wi}-q_{ci}^k\left(x^b,a\right)P_{ci}\right]t}{(1+r)^{t_k/\tau}} \tag{9}$$

Where k is the index of time step, n_T is total number of time steps,b realization of reservoir, q_0^k is the field oil production rate at time k, q_{wp}^k is the field water production rate at k, q_{wi}^k is the field water injection at time k, q_{ci}^k is the total polymer injection rate at time t_k; P_0, P_{wp}, P_{wi} and P_{ci}. The values of economic parameters used is also listed in Table 3.

Results: To compute the VOI of the polymer injection, we need to regress the NPVs on the simulated oil and water production profiles for each decision alternative. The various machine learning techniques discussed in section 3 are employed to perform the regression in this case. To prevent and reduce "the overfitting" in the machine learning training process, we use a 10-fold cross-validation (Crowley and Ghojogh, 2019Crowley and Ghojogh, 2019). Fig. 5 shows the box plots of squared logarithmic error regression loss (RMSLE),[1] for each decision alternative under each ML method and LS. GP, LS, PLS, and Auto-ML perform significantly better than PCR and NN. We measured the CPU running time for each ML method. The results show that GP, LR, PLR, and PCR required more-or-less the same time and were notably faster than NN, which required 8 min and approximately 3 h for Auto-ML.

[1] https://www.rdocumentation.org/packages/corer/versions/0.2.0/topics/meansquaredlogerror

The DWOI is to have the polymer injection finished by the end of first year, and the EVWOI is found to be $ 55.59 million. Moreover, the EVWPI is estimated to be $57.18 million. This makes the VOPI $1.59 million. The highest EVWII corresponding to the machine learning was obtained through the Auto-ML (see Table 4), which is $56.64 million. The respective VOI is $0.842 million. This result indicates that it is not economical to proceed with any information-gathering activity if the cost of the activity is more than $0.842 million. This result also illustrates that including the effect of future information and decisions could improve the EV by 1.73%, which is the percentage of the fraction of VOI to EVWOI.

The cumulative distribution functions (CDFs) of the NPVs associated with DWOI, DWII, and DWPI are plotted in Fig. 6. In this figure, the DWII moves the CDF of the NPV corresponding to the DWOI to the right. In this way, integrating the effects of future information and decisions into the decision-making process would increase the ENPV. Here, some realizations result in a smaller NPV with DWII than the NPV with DWOI since the recovery efficiency increment is very small or ML approach fails to find a near-optimal solution. Furthermore, the DWPI moves the curve of CDF even further to the right, as shown in Fig. 6. This occurs because the NPVs corresponding to the DWPI are always higher, which would lead to a higher ENPV than the values of DWII and DWOI.

The normalized frequency distribution (NFDs) of Waterflooding injection lifetime is illustrated in Fig. 7. Based on these results, it is more worthwhile to switch from water flooding to polymer at the end of year 1 (i.e., there is an 72.8% chance that the polymer recovery mechanism should be used starting at the end of the first

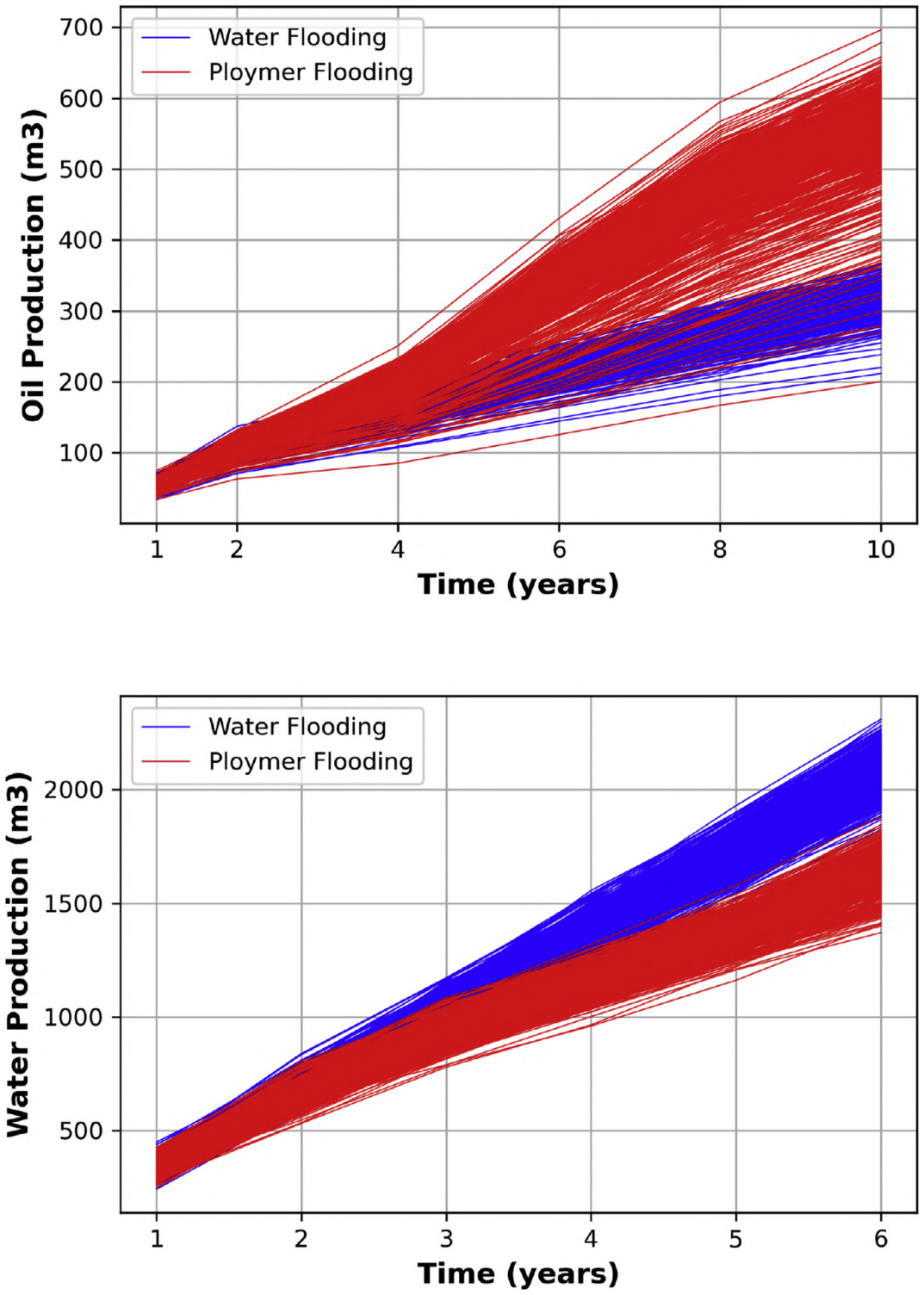

Fig. 4. Ensemble oil production and water production profile for the alternative "inject polymer flooding at the end of the first year" and for the alternative "inject water flooding".

year). There is only a 23% chance that it is optimal to switch after 5 years and 4.6% after 4 years of water-flooding recovery. The specific switch time depends mainly on the simulated production and the uncertainty geological realization.

4.2. 3D reservoir model

Here, we consider a modified version of the standard Egg reservoir model, which is a 3D channel model (Jansen et al., 2014)

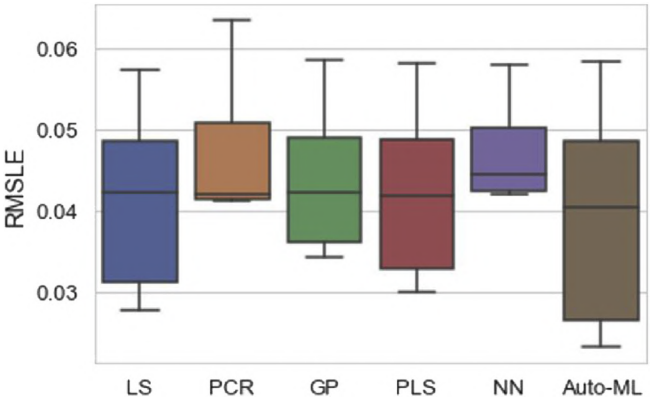

Fig. 5. Boxplot of RMSLE for the entire decision alternative.

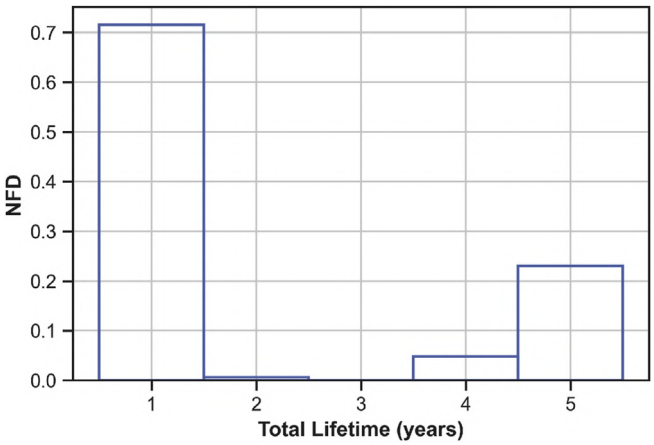

Fig. 7. NFDs of the polymer injection corresponding to decision with ML.

Table 3
Values of economic parameters.

Parameter	Value	Unit
P_0	220	$\$/m^3$
P_{wp}	47.5	$\$/m^3$
P_{wi}	12.5	$\$/m^3$
P_{ci}	12	$\$/kg$
r	8%	–
τ	365	*days*
Δt	30	*days*

Table 4
VOI obtained by machine learning algorithms.

	VOI $ million	**VOI/EVWII**
LR	0.523	0.94%
PLR	0.602	1.08%
Auto-ML	0.842	1.73%
GP	0.536	0.96%
PCR	0.559	1.01%
NN	0.369	0.66%

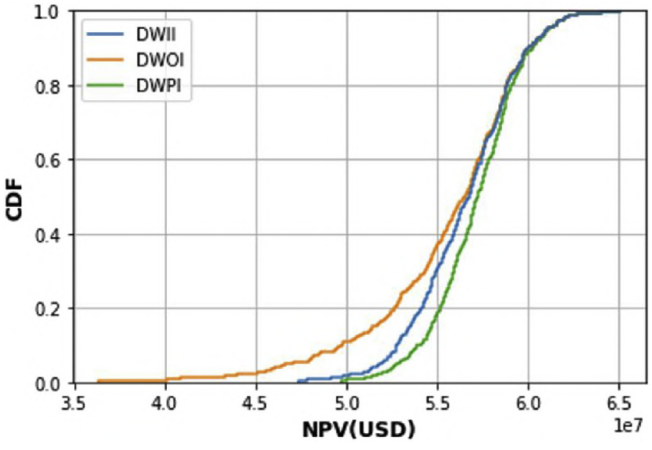

Fig. 6. CDFs of NPVs corresponding to DWOI, DWPI, and DWOII.

that contains 8 injection wells and 4 production wells. The model consists of 100 realizations of channelized reservoirs with $60 \times 60 \times 7$ grid cells of which only 18,553 cells are active, thus producing the shape of an egg, as illustrated in Fig. 8.

The average reservoir pressure is set at 400 bar, and the initial water saturation is considered uniform over the reservoir at a value of 0.1. The remaining geological and fluid properties used in this study are presented in Table 5. We modified the oil viscosity in the standard Egg model to make the reservoir a candidate to undergo polymer flooding.

Problem setting: The problem setting in this example is largely the same as that of the 2D reservoir model. Here, we consider a maximum life cycle of 10 years in total. We will analyze the optimal time to switch from water flooding to polymer injection after each year of production, but the switch happens only once. This indicates that there would be 9 different switch times and decisions to be made.

The oil and water production levels of 100 ensembles are modeled using the reservoir simulation model and inform the decision. Fig. 9 shows the oil and water production for all realizations (i.e., to inject polymer during the ninth year or to maintain the water-flooding recovery process for the whole life of the production cycle).

Results: For the Egg reservoir model, the DWOI involves injecting the polymer by the end of 9 years. The corresponding EVWOI is $133.91 million, and the EVWPI is estimated to be $136.7 million. Thus, the VOPI is $2.79 million. The highest EVWII corresponding to machine learning was obtained by Auto-ML and provides an EVWII of $135.92 million for information from oil and water production profiles. The related VOI is $2.01 million. Therefore, the operator should not proceed with any information-gathering activity if the cost of the activity is more than $2.01 million; further, the effects of future information and decisions would improve the EV by 1.5% (2.01/133.91).

Fig. 10 compares the CDFs corresponding to the different methods. Here, the NPV resulting from the ML approach (DWII) is higher than that of the DWOI, as ML allows learning over time. The DWPI moved the CDF curve further to the right, leading to higher ENPV than that of ML and DWOI.

Fig. 11 shows that for the optimal switch time to inject polymer flooding corresponding to the decision-making with ML, there is a 51% chance of initiating the EOR phase at the end of the year after 9 years, with 33% optimal chances of switching after 8 years, and 16% after 7 years of water-flooding recovery. The mean oil production rate (shown in Fig. 12) decreases significantly with a close similarity measurement, but after 7 years, the rate corresponding to DWII increases slightly, as the decision to switch is applied for some realizations.

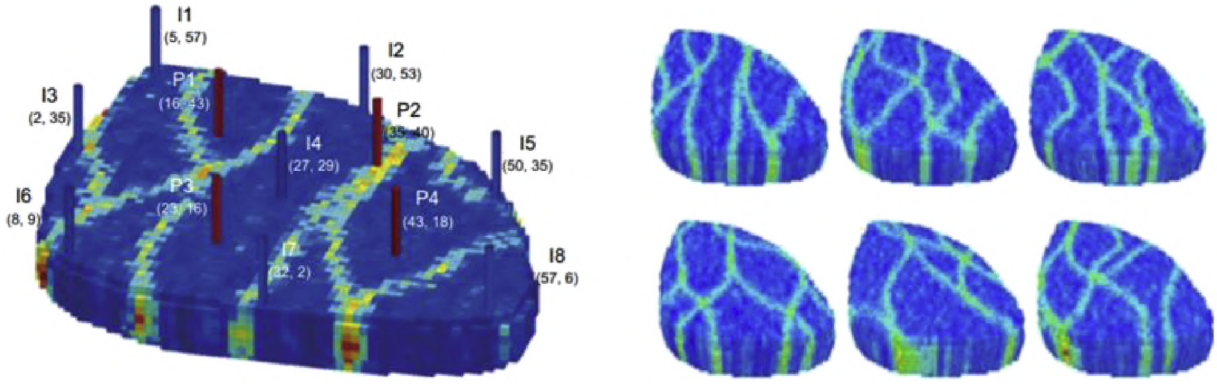

Fig. 8. (Left) Reservoir model displaying the position of the injectors (blue) and producers (red). (Right) Six randomly chosen realizations. (From (Jansen et al., 2014)).

Table 5
Reservoir parameters of Egg model.

Water density, kg/m3	1000
Oil density, kg/m3	900
Water viscosity, pa.s	10−3
Oil viscosity, pa.s	20 × 10-3
Water compressibility, 1/bar	10−5
Oil compressibility, 1/bar	10−5
Initial reservoir pressure, bar	400
Porosity	0.2
Polymer Concentration	2

4.3. Uncertainty in oil price

In both previous studies, we did not include uncertainties into the economic parameters even though they have a significant impact on the decision. Therefore, in this work, oil price is treated as an uncertain parameter and considered in the regression analysis for determining the optimal stopping time given a switch time in the EGG reservoir model. Uncertain economic variables must be modeled as Markovian processes and variants over time. Hence, we follow a stochastic process. There are two commonly used stochastic models for describing uncertainties in economic variables: the Geometric Brownian Motion (GBM; also known as the random-walk model) and the Ornstein–Uhlenbeck (OU) Stochastic Process (also known as the mean-reverting model; refer to Uhlenbeck and Ornstein (1930)for more details).

A process "S" can be stochastically modeled using the Ornstein-Uhlenbeck process as shown below:

$$dSt = \theta\,(\mu - S_t)dt + \sigma dW_t \tag{10}$$

where θ is the speed of mean reversion, μ is the long-term mean which the process reverts, σ is the measure of process volatility, and W_t stands for a Brownian motion, where $dW_t \sim N(0, \sqrt{d_t})$. To implement this stochastic equation in a simulation, it must be discretized. (Gillespie, 1996) noted that only when the discretized time, Δ_t, is sufficiently small, the simulation of the process work well. Thus, the discretized equation is shown below:

$$S_t = \left(S_{t-1} \times e^{-\theta\Delta t}\right) + \mu\left(1 - e^{-\theta\Delta t}\right) + \left[\sigma \times \sqrt{\frac{1 - e^{-2\theta\Delta t}}{2\theta}} \times dW_t\right] \tag{11}$$

However, if any commodity price, including oil prices or any other cost, is modeled using the above discrete time expression, negative values might be generated. This is not realistic, as negative commodity prices never exist. To avoid this problem, the lognormal distribution of the commodity price is used. Thus, in this context, the logarithm of the modeled parameter, namely $\pi_t = ln[St]$, is assumed to follow the mean-reverting process. This process can then be mathematically described as follows:

$$d\pi_t = \kappa[\bar{\pi} - \pi_t]d_t + \sigma\pi dz_t \tag{12}$$

where κ is the speed of mean reversion, $\bar{\pi}$ is the long-term mean to which the logarithm of the variable reverts, $\sigma\pi$ stands for the volatility of process, and dz_t describes the increments of standard Brownian motion. Subsequently, to numerically solve for π_t, the stochastic equation is discretized as shown below (by assuming $dz_t \sim (0, \sqrt{d_t})$, where $d_t = 1$ year).

$$\pi_t = \left(\pi_{t-1} \times e^{-\kappa\Delta t}\right) + \bar{\pi}\left(1 - e^{-\kappa\Delta t}\right)\Big] + \left(\sigma_\pi \times \sqrt{\frac{1 - e^{-2\kappa\Delta t}}{2\theta}} \times N(0,1)\right) \tag{13}$$

After calculating π_t, the value of S_t cannot directly be obtained using the equation of $S_t = e^{\pi t}$. This is because the mean of the lognormal distribution is added with half of the variance, namely $0.5 \times var(\pi_t)$, for the exponential of a normal distribution. Therefore, half of the variance is deducted using the equation below:

$$Var(\pi_t) = \left[1 - e^{-\kappa\Delta t}\right] \times \frac{{\sigma_\pi}^2}{2\kappa} \tag{14}$$

To use this model, a decision must be made to determine its parameters. This process is known as calibration, and since the logarithm of the variables is assumed to follow the mean-reverting process, least squares regression, which was suggested by (Smith, 2010), is conducted on the datasets of $\pi_t = ln[S_t]$. To calibrate the OU parameters for modeling the oil price, a set of oil price data is required. For illustration, we used the annual oil price data from the NYMEX future prices of 1985–2020 (considering only historical data) (EIA and U.E.I.A, 2019), as shown in Fig. 13. These data are available on the U.S. Energy Information Administration website.

To begin the procedure of calibration, the following equations are used:

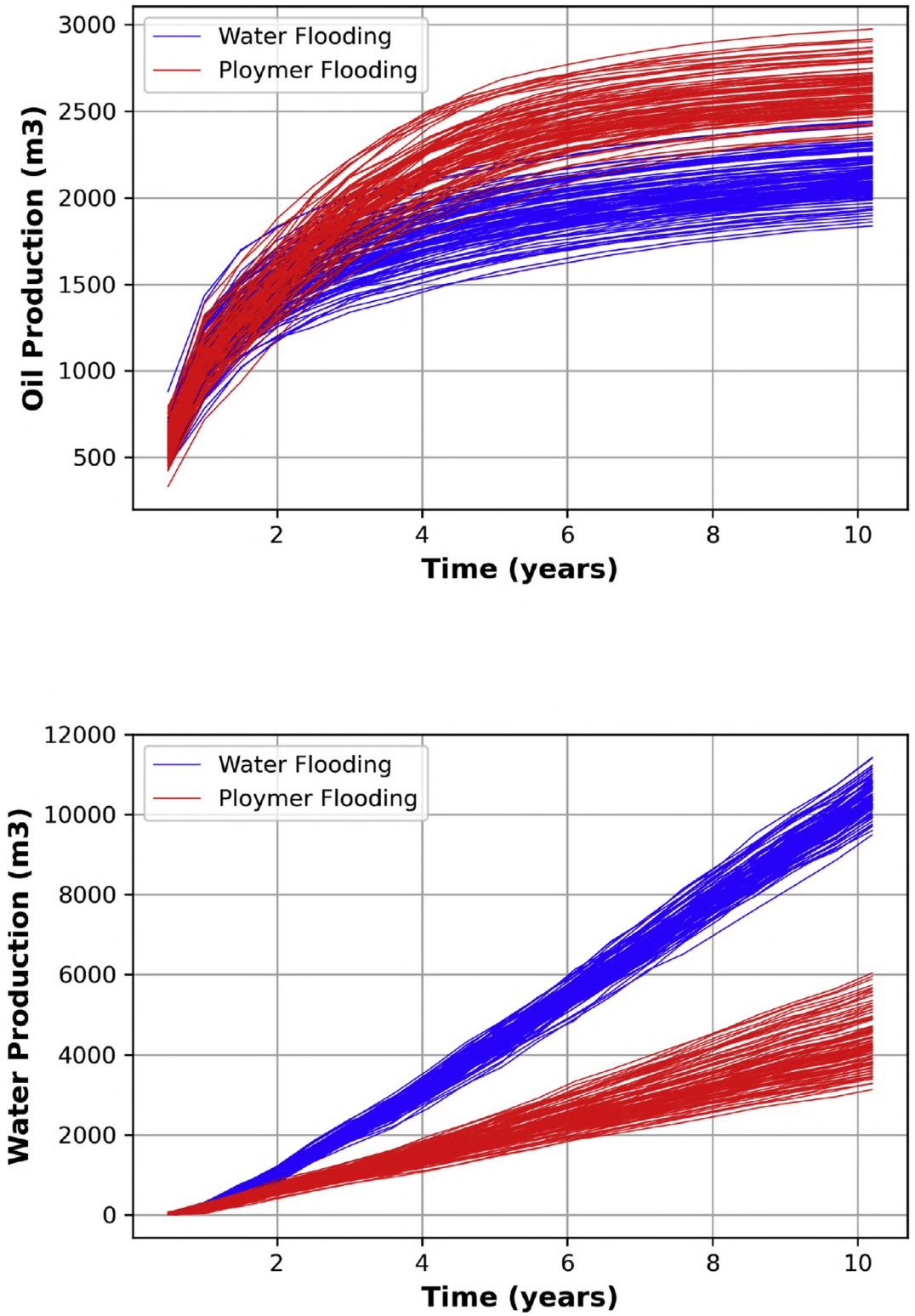

Fig. 9. The oil production and the water production profile for the realization of the alternative "inject polymer flooding at the end of the first year" and for the alternative "inject water flooding".

$$x_t = \pi_t - \Delta_t = ln[Pt - \Delta_t] \quad (15)$$

$$y_t = \pi_t = ln[Pt] \quad (16)$$

$$y_t = ax_t + b + \delta] \quad (17)$$

The OU parameters are estimated using the values of a and b:

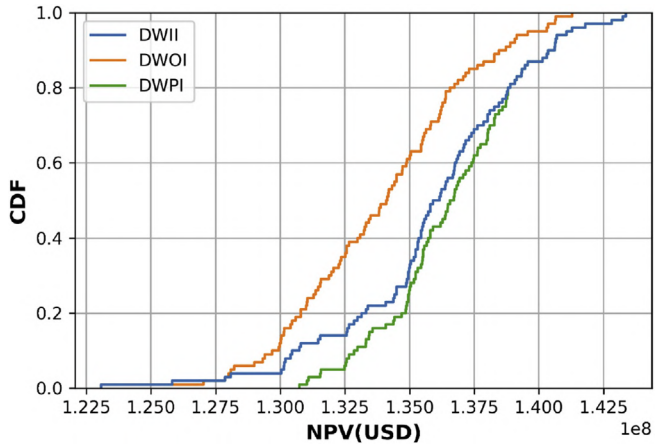

Fig. 10. CDFs of NPVs corresponding to DWOI, DWPI, and DWII.

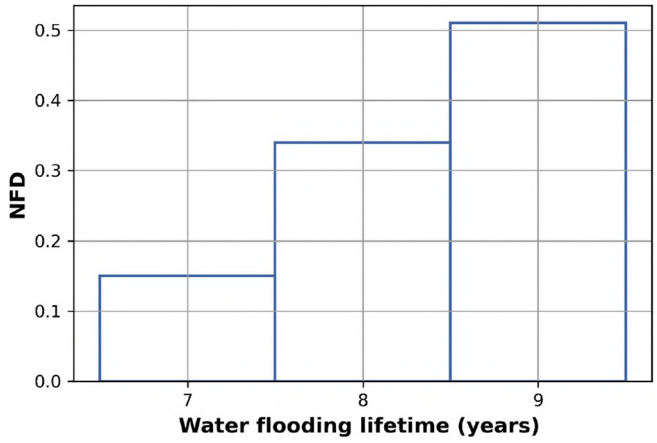

Fig. 11. NFDs of the polymer injection corresponding to the decision-making with ML.

$$\bar{\pi} = \frac{b}{1-a},\ \kappa = \frac{-ln\ a}{\Delta t},\ \sigma_\pi = \sigma_\delta \sqrt{\frac{-2ln\ a}{\Delta t(1-a^2)}} \tag{18}$$

where δ is the approximation error introduced in the least-squares regression, σ_δ stands for the standard deviation of the approximation errors, and Δt is the difference in two time-steps. Refer to (Smith, 2010) for more details regarding the derivation of the equations.

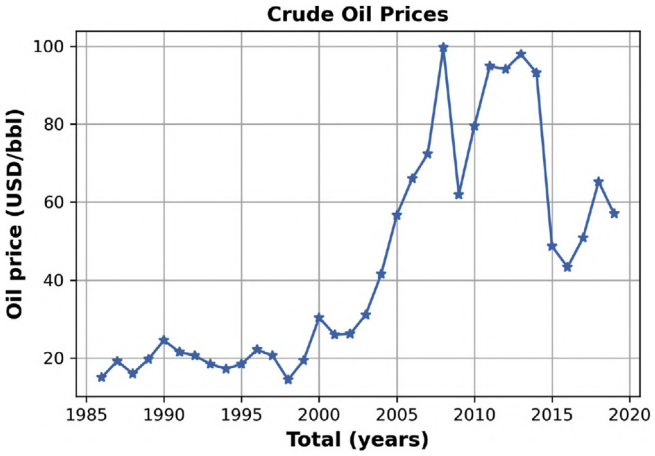

Fig. 13. Historical of annual oil prices from 1985 to 2020.

Table 6
Values of parameters used in the mean-reverting model.

Parameter	Oil price
Initial value	26.25
Equilibrium Value	26.25
Volatility σ_δ	0.2719
Mean reversion speed, κ	0.1165
$\boldsymbol{d_t}$, year	1

Using the parameters in Table 6, the oil price corresponding to the respective costs is modeled forward in time. Fig. 14 presents the probabilistic model of the oil price.

Results: By adding the uncertain oil price to the previous results obtained in the egg reservoir model, the DWOI provides 9 years of water-flooding recovery and then one-year polymer recovery. This results in a total lifetime of 10 years. Thus, the EVWOI is found to be $134.53 million. Moreover, the EVWPI is estimated to be $137.98 million, which makes the VOPI $3.46 million. The EVWII corresponding to the ML approach was obtained with through Auto-ML,

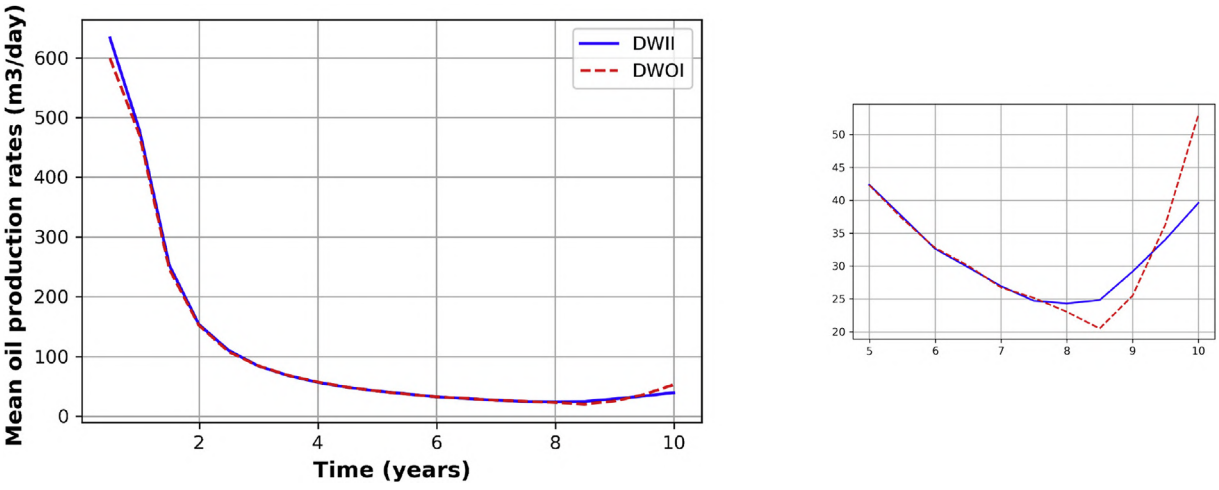

Fig. 12. Mean oil production rate corresponding to the DWOI and DWII. Left: Overview of the rate. Right: zoomed rate (last 5 years).

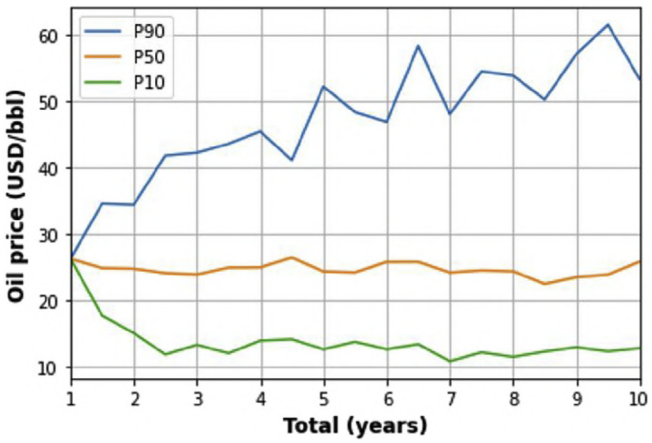

Fig. 14. Oil prices modeled using the mean-reverting process.

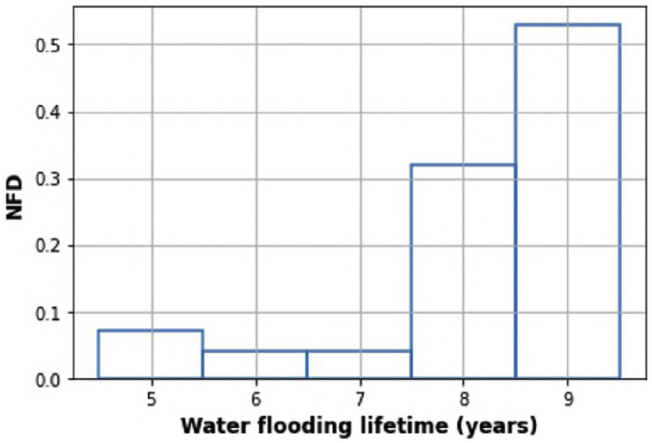

Fig. 15. NFDs of the polymer injection corresponding to the decision with ML.

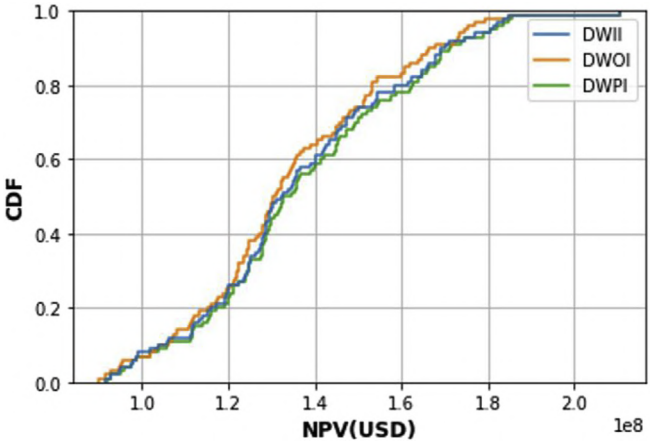

Fig. 16. Graph of CDFs against NPVs with respect to DWOI, DWII, and DWPI.

with an estimate of $136.04 million. This yields a special VOI of $ 1.52 million, which indicates that it is not economical to proceed with any information-gathering activity if the cost of the activity is more than $1.52 million. Moreover, this result also illustrates that including the effect of future information and decisions would improve the EV by 1.13%, which is the percentage of the fraction of VOI to EVWOI.

The NFDs of the total lifetime corresponding to the decisions with machine learning are displayed in Fig. 15. This result recommends switching from water flooding to polymer injection at the end of years 8 and 9 (i.e., there is a 53% chance that the polymer recovery mechanism should be started after year 9). There is only a 32% chance that will be optimal to switch after 8 years and 5% after both 6 and 7 years of water-flooding recovery. The specific switch time depends mainly on the measured production uncertainty of geological realization and oil prices.

Fig. 16 compares the CDFs of the NPVs associated with DWOI, DWII, and DWPI. Here, DWII approaches move the CDFs of the NPVs corresponding to the DWOI to the right (i.e., the ENPV increases), which allows for learning over time. Some realizations ultimately yield a smaller NPV with DWII than the NPV with the DWOI. This is possibly due to a suboptimal decision, as the machine learning algorithm is an approximate method that, for some of the path decisions, makes suboptimal choices. The DWPI further moves the CDF curve to the right, leading to a higher ENPV. This is obvious because when perfect information is available, all realizations will have a higher NPV.

5. Concluding remarks

In this paper, we demonstrated and described the usefulness of utilizing the concepts of decision analysis and value information to support the recovery phase in the field of oil development with limited computational resources. We applied some linear and nonlinear machine learning regressions to compute the VOI, which yielded comparable results and globally optimal solutions. The methodology could be adapted and applied to other fields such as energy storage and well-placement optimization.

However, the value of machine learning may be small and not very significant, as there is always an approximation error when applying the machine learning regression function. Moreover, how closely a regression function can estimate the actual expected values and the accuracy of this method also largely depend on a prior sample of Monte Carlo simulations, alternatives, and information; furthermore, in some cases, the model choice may not be material.

Therefore, we conclude that for solving the optimal EOR initiation time for both 2D and 3D channel reservoir models, the machine learning regression method can be used to approximate the value functions that appear in dynamic programming and can be considered a robust approach, as it includes and quantifies uncertainties in dynamic and state variables, including uncertainty in economic parameters, which are important to make good and insightful decisions. However, this method's computational effort is still subject to a finite and limited number of alternatives and decision points. Therefore, we believe that a new theory and methodology based on clustering techniques, in combination with proxy models, must be developed to reduce computational costs and reliably solve real-world sequential decision-making problems.

Author contributions

Amine wrote the paper and contributed to tuning the model and analyzing the results. Pr. Bratvold, Dr. Hong and Dr. Hanea supervised the work and providing continuous feedback.

Acknowledgments

The authors acknowledge financial support from the Research Council of Norway through the Petromaks-2 project DIGIRES (RCN no. 280473) and the industrial partners AkerBP, Wintershall DEA, ENI, Petrobras, Equinor, Lundin, and Neptune Energy.

Nomenclature

2D/3D	Two Dimensional/Three Dimensional
ADP	Approximate Dynamic Programming
AutoML	Automated Machine Learning
CDF	Cumulative Density Function
CLRM	Closed Loop Reservoir Management
DWI	Decision with Additional Information
DWOI	Decision without Additional Information
DWPI	Decision with Perfect Information
ENPV	Expected NPV
EOR	Enhanced Oil Recovery
EV	Expected Value
EVWI	EV with Additional Information
EVWOI	EV without Additional
GPR	Gaussian process regression
LS	Least Squares
LSM	Least-Squares Monte Carlo
MCMC	Markov-Chain Monte Carlo
MCS	Monte Carlo Simulation
NFD	Normalized Frequency Distribution
NN	Neural Network
NPV	Net Present Value
PCR	Principal Component Regression
PLS	Partial Least square
RMSLE	Root Mean Squared Logarithmic Error
VOI	Value-of-Information
VOPI	Value-of-Perfect-Information

References

Abdi, H., 2010. Partial least squares regression and projection on latent structure regression (pls regression). WIREs Computational Statistics 2, 97–106. https://doi.org/10.1002/wics.51.

Alkhatib, A., Babaei, M., King, P.R., 2013. Decision making under uncertainty: applying the least-squares Monte Carlo method in surfactant-flooding implementation. SPE J. 18, 721–735. https://doi.org/10.2118/154467 PA.

Barros, E., Leeuwenburgh, O., Van den Hof, P., et al., 2015. Value of multiple production measurements and water front tracking in closed-loop reservoir management. In: SPE Reservoir Characterisation and Simulation Conference and Exhibition, Abu Dhabi. https://doi.org/10.2118/175608-MS.

Bratvold, R., Bickel, J., Lohne, H., 2009. Value of information in the oil and gas industry : past, present, and future. SPE Reservoir Eval. Eng. 2 (4), 630–638. https://doi.org/10.2118/110378-PA.

Bratvold, R.B., Begg, S., 2010. Making Good Decisions. Society of Petroleum Engineers, Texas.

Clement, R., 1991. Making Hard Decision : an Introduction to Decision Analysis. Pws Pub Co, Boston, USA.

Crowley, M., Ghojogh, B., 2019. The Theory behind Overfitting, Cross Validation, Regularization, Bagging, and Boosting: Tutorial. https://arxiv.org/abs/1905.12787.

Dutta, G., Mukerji, T., Eidsvik, J., 2019. Value of information analysis for subsurface energy resources applications. Appl. Energy 252. https://doi.org/10.1016/j.apenergy.2019.113436.

(EIA), U.E.I.A, 2019. Nymex futures price data. https://www.eia.gov/dnav/pet/pet1.htm.

Eidsvik, J., Mukerji, T., Bhattacharjya, D., 2016. Value of Information in the Earth Sciences. Cambridge Univeristy Press, Cambridge.

Evans, R., 2000. Decision analysis for integrated reservoir management. In: SPE European Petroleum Conference Paris. https://doi.org/10.2118/65148-MS.

Gillespie, D.T., 1996. Exact numerical simulation of the ornstein-uhlenbeck process and its integral. Geosci. Data J 54, 2084–2091. https://doi.org/10.1103/PhysRevE.54.2084.

Grayson, C., 1960. Decision under Uncertainty : Drilling Decision by Oil and Gas Operators. Harvard University Press, Boston, USA.

Hong, A., Bratvold, R., Lake, L.W., 2018. Fast analysis of optimal ior switch time using a two-factor production model and least- squares Monte Carlo algorithm. SPE Reservoir Eval. Eng. https://doi.org/10.2118/191327-PA.

Howard, R., 1966. Information value theory. IEEE Trans. Syst. Sci. Cybern. 2 (1), 22–26. https://doi.org/10.1109/TSSC.1966.300074.

Howard, R., 1988. Decision analysis: practice and promise. Manag. Sci. 34, 679–695. https://doi.org/10.1287/mnsc/34.6.679.

Howard, R., Abbas, A., 2016. Foundation of Decision Analaysis. Pearson Education Limited, England.

Jafarizadeh, B., Bratvold, R., 2009. Taking real options into real world: asset valuation through option simulation. In: SPE Annual Technical Conference and Exhibition. https://doi.org/10.2118/124488-MS. New Orleans, Louisiana.

Jansen, J., Fonseca, R., Kahrobaei, S., Siraj, M., Van Essen, G., Van den Hof, P., 2014. The egg model – a geological ensemble for reservoir simulation. Geosci. Data J 1, 192–195. https://doi.org/10.1002/gdj3.21.

Liu, S., Oosterlee, C., Bohte, S., 2019. Pricing options and computing implied volatilities using neural networks. Risks 7. https://doi.org/10.3390/risks7010016.

Longstaff, F., Schwartz, E., 2001. Valuing american options by simulation: a simple least-squares approach. Rev. Financ. Stud. 14 (1), 113–147. https://doi.org/10.1093/rfs/14.1.113.

Olson, R., Moore, J., 2019. A tree-based pipeline optimization Tool for automating machine learning. In: Hutter, F., Kotthoff, L., Vanschoren, J. (Eds.), Automated Machine Learning. The Springer Series on Challenges in Machine Learning. Springer.

Powell, W., 2016. Approximate Dynamic Programming: Solving the Curses of Dimensionality. John Wiley and Sons, Princeton, New Jersey.

Raiffa, H., Schlaifer, R., 1961. Applied Statistical Decision Theorys. Harvard University, Wiley, Boston, Massachusetts.

Rasmussen, C., 2004. Gaussian processes in machine learning. In: Bousquet, O., von Luxburg, U., Rätsch, G. (Eds.), Advanced Lectures on Machine Learning. ML 2003. Lecture Notes in Computer Science. Springer, Berlin, Heidelberg.

Rosipal, R., Krämer, N., 2006. Overview and recent advances in partial least squares subspace. Latent Struct Feature Select 34–51. https://doi.org/10.1007/11752790_2.

Schlaifer, R., 1959. Probability and Satastics for Business Decisions. McGraw-Hill, New York, USA.

Smith, W., 2010. On the simulation and estimation of the mean-reverting ornstein-uhlenbeck process. In: https://commoditymodels.files.wordpress.com/2010/02/estimating-the-parameters-of-a-mean-reverting-ornsteinuhlenbeck-process1.pdf.

Uhlenbeck, G., Ornstein, L., 1930. On the theory of the brownian motion. Phys. Rev. 36, 823–841. https://doi.org/10.1103/PhysRev.36.823.

Wiggins, M.L., Startzman, R.A., 1990. An approach to reservoir management. SPE annual technical conference and exhibition. https://doi.org/10.2118/20747-MS.

Willigers, B., Bratvold, R., 2009. Valuing oil and gas options by least-squares Monte Carlo simulation. SPE Proj. Facil. Constr. 4, 146–155. https://doi.org/10.2118/116026-PA.

Paper VI

A Sequential Decision and Data Analytics Framework for Maximizing Value and Reliability of CO2 Storage Monitoring.

Amine Tadjer, Aojie Hong and Reidar B. Bratvold.

Journal of Natural Gas Science and Engineering 96 (2021) 104298

Contents lists available at ScienceDirect

Journal of Natural Gas Science and Engineering

journal homepage: www.elsevier.com/locate/jngse

A sequential decision and data analytics framework for maximizing value and reliability of CO_2 storage monitoring

Amine Tadjer *, Aojie Hong, Reidar B. Bratvold

Univerisity of Stavanger, Norway

ARTICLE INFO

Keywords:
Value of information
CO_2 storage monitoring
Approximate dynamic programming
Machine learning
Time-lapse seismic monitoring

ABSTRACT

Carbon capture and sequestration (carbon capture and storage or CCS) represents a unique potential strategy that can minimize CO_2 emissions in the atmosphere, and it creates a pathway toward a neutral carbon balance, which cannot be solely achieved by combining energy efficiency and other forms of low carbon energy. To contribute to the decision-making process and ensure that CCS is successful and safe, an adequate monitoring program must be implemented to prevent storage reservoir leakage and contamination of drinking water in groundwater aquifers. In this paper, we propose an approach to perform value of information (VOI) analyses to address sequential decision problems in reservoir management in the context of monitoring the geological storage of CO_2 operations. These sequential decision problems are often solved and modeled by approximate dynamic programming (ADP), which is a powerful technique for handling complex large-scale problems and finding a near-optimal solution for intractable sequential decision-making. In this study, we tested machine learning techniques that fall within ADP to estimate the VOI and determine the optimal time to stop CO_2 injections into the reservoir based on information from seismic surveys. This ADP approach accounts for both the effect of the information obtained before a decision and the effect of the information that might be obtained to support future decisions while significantly improving the timing, value of the decision, and uncertainty of the CO_2 plume behavior, thereby significantly increasing economic performance. The Utsira saline aquifer west of Norway was used to exemplify ADP's ability to improve decision support regarding CO_2 storage projects.

1. Introduction

Carbon capture and storage (CCS) is increasingly considered a promising strategy for reducing CO_2 emissions. Geological reservoirs, such as depleted oil or gas fields or deep saline aquifers, are being considered as appropriate geological formations that can store CO_2 emissions at a depth of several thousand meters (Harp et al., 2017; Jin et al., 2017; Nilsen et al., 2015a). However, uncertainties in geological models and rock properties affect flow modeling and CO_2 storage capacities, mitigating the risk of CO_2 leakage and contaminating clean groundwater. To contribute to the decision-making process and ensure that CCS is successful and safe, a monitoring program must be implemented in addition to regulations based on conformance (understanding of CO_2 behavior), containment (ensuring control of CO_2 migration), and contingency (detecting and addressing significant anomalies and leakages) (Dupuy et al., 2017). Several studies have demonstrated the utility of applying time-lapse seismic and electromagnetic surveys to adequately monitor CO_2 storage in geological formations. For instance, seismic surveys of the Sleipner storage site have been conducted regularly. From these surveys, a large quantum of data has become accessible for research, resulting in several published studies (for instance, (Arts et al., 2004; Dupuy et al., 2017; Furre et al., 2017)). Furre et al. (2017) summarized 20 years of monitoring CO_2 injection at Sleipner. The authors concluded that the monitoring program at Sleipner, which is strongly reliant on seismic surveys, has been successful, with CO_2 contained safely in the storage unit. However, since time-lapse seismic data are costly, it is important to assess their impact on the necessary decisions and design monitoring programs effectively to optimize the relationship between value and cost. One possible method of estimating the value of a monitoring scheme is the decision-analytic metric of the value of information (VOI) (Howard, 1966). VOI is an estimate of the additional value that information brings to a decision situation (Howard, 1966). If the prospect values linked to the different decision alternatives are specified in monetary units, the VOI provides a monetary calculation of the additional value of data collection before deciding. From a decision-analytical viewpoint, information is useful not only if it eliminates uncertainty but also if it promotes better decisions and maximizes value results by reducing uncertainty. In the context of underground reservoir management, the

* Corresponding author.
E-mail address: amine.tadjer@uis.no (A. Tadjer).

https://doi.org/10.1016/j.jngse.2021.104298
Received 29 April 2021; Received in revised form 27 September 2021; Accepted 20 October 2021
Available online 6 November 2021

concept of VOI has been applied to decision analysis in petroleum exploration and production (Newendorp, 1975; Riis, 1999). The importance of seismic information has been studied regularly. Decision tree models have been used to measure the economic effect of seismic imaging on reservoir management (Bickel et al., 2008). Although seismic information is considered imperfect, a significant value can be extracted from this information. Furthermore, Bickel et al. (2008) introduced a general VOI model that can drive multiple objectives, budgetary limitations, and quantitative models relating seismic parameters to reservoir properties. The decision model also provides objective estimates of seismic measurement reliability. In addition, (Bratvold et al., 2009) extensively reviewed the application of VOI in petroleum exploration and formed a rather interesting argument. In Eidsvik et al. (2015) work, VOI analysis was integrated with geostatistical modeling to provide applications for the petroleum industry as well as mining and groundwater management.

In general, applications of VOI analyses in the context of CCS operation monitoring are limited. For instance, Sato (2011) provided two demonstrations of VOI applied to the CO_2 sequestration problem. The first example considered a storage reservoir with a fault (potential leak-pathway), followed by a cross-well interference test conducted to determine whether the fault is tight or permeable. A discrete probability was assigned to the reliability of the test. The second example considered a continuous uncertainty: the net present value (NPV) of the project was linked to the radial extent of the saline aquifer, which was assumed to be lognormally distributed. The accuracy of the information gathering was not based on empirical data, but rather assumed to be described by a triangular probability density function. Puerta-Ortega et al. (2013) later extended Sato's work; they quantified VOI by prior scenarios based on the reservoir's current knowledge, contractual conditions, and regulatory constraints.

In real-world applications, the analytical calculation of the VOI is generally challenging. Therefore, a computationally efficient approach to estimate the VOI in such cases is the approximate dynamic programming (ADP), which is presented and used in the field of financial engineering with real options (Longstaff and Schwartz, 2001; Jafarizadeh and Bratvold, 2009). Hong et al. (2018a) illustrated a specific method for ADP, the least-squares Monte Carlo (LSM) algorithm. This approach uses Monte Carlo sampling and statistical regression techniques to estimate the VOI. This algorithm can be implemented with a production model based on exponential declines to determine the optimal time to switch from one recovery phase to another. Theoretically, the implementation of LSM is independent of production models; however, LSM still suffers from dimensionality in the action space, where the computational effort of LSM increases exponentially with the number of both alternatives and decision points. Eidsvik et al. (2017), Dutta et al. (2019) used a simulation-regression approach to approximate the VOI; an ensemble was used as part of this approach to compute the predicted values directly. Anyosa et al. (2021) developed a statistical learning method to assess the probability of an early CO_2 leakage detection through a key fault at the Smeaheia site and then conducted a VOI analysis of monitoring strategies, considering an underlying decision situation connected to continued injection of CO_2, or termination of this process. In this setting, geophysical monitoring is valuable if it leads to improved decisions for the injection program.

Our approach in the current study is different from that of Anyosa et al. (2021). Specifically, a decision problem is constructed where CO_2 is injected into a reservoir and the decision-maker conducts seismic surveys to decide between continuing or stopping the injection based on information from the survey results. The actual VOI calculation in our case was computed using the ADP methodology. The ADP methodology used here illustrates both the impact of the seismic survey data obtained before a decision is made and the effect of the data information that can be obtained to support future decisions. The analysis was performed on a constructed case study involving the Utsira storage site. Further, we use a machine learning regression approach that lies within the domain of ADP to estimate the VOI and determine the optimal time to stop the CO_2 injections into the reservoir.

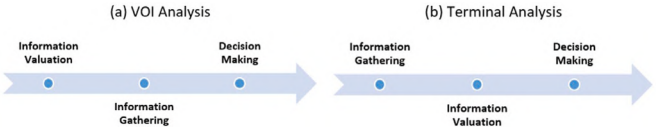

Fig. 1. Steps of a – VOI analysis, and b – Terminal analysis.

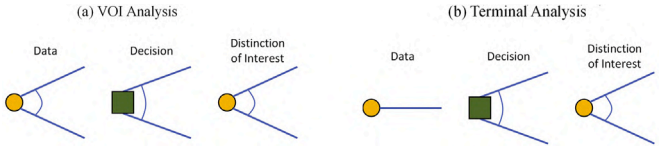

Fig. 2. Decision tree elements of VOI versus terminal analysis Hong et al. (2018b).

This paper is divided into multiple sections. In the following section, we distinguish between the VOI and terminal analysis, define VOI, and present the general steps in terms of its assessment. Next, we present the Utsira Formation along with the methods used to generate seismic data. Subsequently, we present a complete methodology for assessing the VOI using machine learning methods and then test the proposed methodology by implementing it in the Utsira reservoir fields. Finally, we offer concluding remarks and recommendations for future research directions.

2. Background

In this section, we provide a brief background of the VOI analysis. We also introduce the Utsira saline aquifer along with the standard approach employed to estimate model 4D seismic data.

2.1. Decision analysis and VOI in the energy industry

Decision analysis has been extensively used in the energy industry since the 1960s. Bratvold et al. (2009) identified several papers in the O&G literature that present cases where the information value is calculated after the information has been gathered. This can take the form of historical lookbacks to document the impact of information (Aylor Jr., 1999; Waggoner, 2000). Raiffa and Schlaifer (1961) referred to this as "terminal analysis". Terminal analysis involves the evaluation of selection between alternatives after a test (actual or hypothetical) has been conducted and the data have been gathered, whereas VOI analysis, often called "preposterior analysis" (Raiffa and Schlaifer, 1961), regards the decision problem as it appears before a test has been conducted. Fig. 1 illustrates the stages of VOI and terminal analyses. Fig. 2 depicts the decision-tree elements of VOI versus terminal analysis, where the circles and squares represent the uncertainty and decision nodes, respectively. The data of concern in a VOI analysis (Fig. 2a) are future data, which are unknown and treated as uncertain. In contrast, the data of concern in terminal analysis (Fig. 2b) are historical data, which are already known and treated as certain.

Although a terminal analysis might offer valuable insights, it is not a replacement for VOI analysis. Furthermore, it introduces bias for two reasons. First, from a communication and publishing perspective, there is a strong incentive to not publish or communicate unsuccessful (those unable to demonstrate any value creation) information-gathering activities. Second, it ignores cases in which information was not gathered but should have been.

VOI in any information-gathering activity depends on two fundamental uncertainties: (1) the uncertainties we hope to learn about but cannot directly observe; these are called "events of interest", and (2)

the test results referred to as observable distinctions (Bratvold et al., 2009). In reservoir management, the data gathered until time t when a decision is made is the observable distinction, and prediction after the time t runs out constitutes the event of interest. We denote the observable distinction as x. Since x has very high dimensions, it is difficult to represent the distribution of x in an analytical form because we usually approximate it with the help of Monte Carlo sampling. In terms of a risk-neutral decision maker, VOI is defined as follows:

$$VOI = \begin{bmatrix} Expected\ value\ with \\ additional\ information \end{bmatrix} - \begin{bmatrix} Expected\ value\ without \\ additional\ information \end{bmatrix}$$

In mathematical form,

$$VOI = \{0, \Delta\} \tag{1}$$

$$\Delta = EVWII - EVWOI \tag{2}$$

The lower limit of VOI is always 0 because if Δ is negative when $EVWOI > EVWII$, the decision-maker can always choose not to gather information.

In a decision-making context, the decision without information (DWOI) is the alternative that optimizes the expected value (EV) over the prior, and $EVWOI$ is the optimal EV over the prior.

$$EVWOI = max_{a\in A}\left[\int v(x,a)p(x)dx\right] \approx max_{a\in A}\left[\frac{1}{b}\sum_{b=1}^{B} v(x^b,a)\right] \tag{3}$$

where a is the decision alternative from the a set of A, x is the distinctions of interests, $v(x,b)$ is the value function that assigns a value to each alternative outcome pair for a given x and realization b, and $p(x)$ is the prior probability distribution of x.

Similarly, if we have perfect information regarding what value x the distinction of interests will assume, we can choose the optimal action for that value of x. The decision with information (DWI) is an alternative that optimizes the expected value over the posterior.

$$EVWII = \int max_{a\in A}[E(v(x,a)|y)]p(y)dy \approx \frac{1}{B}\sum_{b=1}^{B} max_{a\in A}E[v(x,a)|y^b] \tag{4}$$

Where $p(y)$ is the marginal probability distribution over y.

Furthermore, the decision with perfect information (DWPI) can also be determined in this decision-making context. For instance, in reservoir engineering, perfect information is the information that reveals the true reservoir properties and impacts of the recovery mechanism. Considering the CO_2 injection operation problem as an example, the EV with perfect information (EVWPI) is the maximum NPV for every path based on prior realizations or distributions. Averaging these NPVs over the paths would result in $EVWPI$. In this respect, every path has its optimal decision with perfect information. The difference between $EVWPI$ and $EVWOI$ is the value of perfect information (VOPI).

2.2. Utsira CO_2 storage

Utsira is a saline reservoir located beneath the central and northern North Sea as shown in Fig. 3. In this location, there are over 20 reservoir formations (producing or abandoned oil and gas fields and geological formations such as saline aquifers). We used the reservoir dataset provided by the Norwegian Petroleum Directorate, which consists of only top-surface and thickness maps and average rock properties. The Utsira Formation consists of weakly consolidated sandstone with interlayered shale beds that act as baffle for the upward migration of the injected CO_2, and it has an average top-surface depth of approximately 800 m below the seabed (within the range of 300–1400 m). The storage capacity of the Utsira system is estimated to be 16 Gt, with a prospectivity of 0.5–1.5 Gt (Andersen et al., 2014). The boundaries of the aquifers were considered open. An open boundary means that

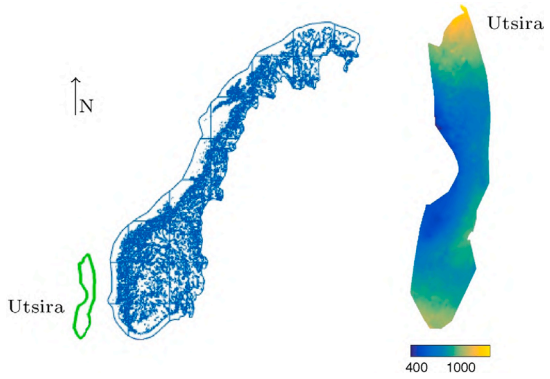

Fig. 3. Location of Utsira formation along the Norwegian Continental Shelf (left). Maps of geomodel depths in meters (below the seabed) (right) (Allen et al., 2018).

there is communication between the aquifer and anything that lies adjacent to it, be it another aquifer or the sea bottom. The corresponding permeabilities in the Utsira geomodel range from 0.5–2.5 darcys. Another study (Singh et al., 2010) suggested that permeability could be within the range of 1.1–5 darcys. Furthermore, the NCS public datasets contain no information about possible leakage through open boundaries or the caprock. We acknowledge that these are important factors, but despite these limitations, we decided to use the Utsira available data to demonstrate the ADP framework and discuss its advantages and potential benefits in future CCS operations. In our study, some of the injected CO_2 can leave the computational domain during the simulation; these are considered as leaked volumes. Nonetheless, this cannot result in CO_2 leaking into the atmosphere; in most instances, it will continue to migrate beyond the simulation model inside the rock volume.

2.3. Rock physics model and 4D seismic data

The most favorable reservoir conditions for seismic monitoring can be calculated by forward modeling of the seismic response to long-term CO_2 storage. This study includes a mathematical model that can indicate the impact of fluid and mineral substitution and the effect of porosity changes on the seismic properties of the reservoir, resulting in subsequent variations in the seismic wave velocities of the rock. To describe the changes in seismic velocity, we used the Gassmann model (Gassmann, 1951), which is more effective than other models, such as Krif's, Duff Mindlin's, and Wyllies' time-average models because of its simplicity and clarity (Nguyen and Nam, 2011). The Gassmann model can be used to calculate seismic velocities using the bulk module, which is ultra sensitive to fluid saturation variation (Han and Batzle, 2004).

The p-wave velocity of a saturated rock can be measured on the bulk modulus, shear modulus μ_{sat} and the density ρ_{sat} of the rock, and the s-wave velocity depends on ρ and μ_{sat}. The interaction was given by Avseth et al. (2005).

$$v_p = \sqrt{\frac{K_{sat} + \frac{4}{3}\mu_{sat}}{\rho_{sat}}} \tag{5}$$

$$v_s = \sqrt{\frac{\mu_{sat}}{\rho_{sat}}} \tag{6}$$

Considering the porosity value ϕ, the Gassmann equation is used to calculate the bulk modulus K_{sat} as follows:

$$K_{sat} = K_d + \frac{(1 - K_d/k_m)^2}{\frac{\phi}{k_f} + \frac{1-\phi}{k_m} + \frac{k_d}{k_m^2}} \tag{7}$$

K_d, K_m, and K_f are bulk moduli of dry rock, solid matrix, and pore fluid, respectively. The shear modulus μ_{sat} is dependent only on the

shear modulus of dry rock μ_d at generally low frequencies (since the shear modulus of a fluid is zero), considering the following:

$$\mu_{sat} = \mu_d \tag{8}$$

The density of a saturated rock can be calculated as follows:

$$\rho = \phi\rho_f + (1 - \phi_{mi}) \tag{9}$$

where ρ_f is the fluid density and ϕ_m is the mineral density.

Since porosity, density, and moduli including K_d, K_m and μ_d of the core are known or measured before the core flooding experiment, we can obtain V_p after calculating the values of K_f and ρ_f of the core.

As there are two different pore fluids (water and CO_2) in CO_2-injected reservoirs, one should further consider measuring the bulk modulus K_f and fluid density ρ_f, yet part of the injected CO_2 is dissolved in the pore water. We considered only the pore fluid as a mixture of pure water and pure CO_2 for convenience, meaning that $S_{CO_2} + S_w = 1$.

For the computation of K_f, we use Wood's equation (Wood, 1941):

$$\frac{1}{K_f} = \frac{S_w}{K_w} + \frac{(1 - S_w)}{K_{CO_2}} \tag{10}$$

where K_w and K_{CO_2} are the bulk moduli of water and CO_2, respectively. The bulk density of the fluids rho_f can be obtained as a weighted average with respect to water saturation S_w:

$$\rho_f = S_w\rho_w + (1 - S_w)\rho_{CO_2} \tag{11}$$

where ρ_w and ρ_{CO_2} are the densities of water and CO_2, respectively.

As CO_2 is injected into a reservoir, S_w decreases to change the values of K_f and ρ_f, and thus, also V_p. Therefore, we can estimate S_w and S_{CO_2} by monitoring V_p.

In the current study, we aimed to use seismic data to map the CO_2 plume within a reservoir. We assumed the elastic properties to be homogeneous in the individual layers. Each layer has elastic properties such as p-wave velocity V_p, s-wave velocity V_s, and bulk density ρ. Furthermore, we assumed that the elastic properties when the rock is saturated only by brine are known, and they are denoted as V_P^1, V_S^1, and ρ^1. The new values of the elastic properties, after CO_2 has partially replaced the brine, are denoted as V_P^2, V_S^2, and ρ^2.

For conventional Amplitude versus offset (AVO) analysis, the AVO responses are approximated by linear trigonometric functions of the offset or angle. An approximate way to describe the relationship between R and G is given by Avseth et al. (2005):

$$R(\theta) \approx R_0 + Gsin^2\theta \tag{12}$$

where R_0 (intercept) and G (curvature) are AVO attributes that depend on elastic properties at a given point in the subsurface. Let $\Delta V_p = V_{p2} - V_{p1}$ and $V_pm = (V_{p2} + V_{p1})/2$ (arithmetic mean). We define similar quantities of V_s and ρ. Approximate relationships between the AVO attributes and elastic properties were given by Avseth et al. (2005):

$$R_0 = \frac{1}{2}\left(\frac{\Delta V_p}{\Delta V_{pm}} + \frac{\Delta\rho}{\Delta\rho_m}\right) \tag{13}$$

$$G = \frac{1}{2}\frac{\Delta V_p}{\Delta V_{pm}} - 2\left(\frac{V_s}{V_p}\right)^2\left(2\frac{\Delta V_s}{\Delta V_{sm}} + \frac{\Delta\rho}{\Delta\rho_m}\right) \tag{14}$$

The AVO attributes for a given point can be estimated by recording the seismic amplitudes at different reflection angles.

3. Value computation by ADP

We used an ADP method called the simulation-regression (or LSM) method to calculate the expected value with imperfect information. The simulation regression method involves Monte Carlo simulation and regression for approximately calculating the conditional expected value of given data.

Monte Carlo simulation:

1. Numerous possible realizations of state variables (x^b) such as porosity permeability, temperature, pressure and caprock elevation are generated using Monte Carlo simulation model.
2. Forward modeling is performed to generate modeled AVO attributes data, with the addition of random noises generated from the statistics measurements errors to the modeled AVO data.
3. For each decision alternative a, the $NPV(x^b, a)$ is calculated.
4. The EVWOI is then calculated using the following equation:

$$EVWOI = \left[\frac{1}{b}\sum_{b=1}^{B} NPV(x^b, a^*_{DWOI})\right]$$

$$a^*_{DWOI} = argmax_{a\in A}\left[\frac{1}{b}\sum_{b=1}^{B} NPV(x^b, a)\right]$$

Where a^*_{DWOI} is the optimal decision without information and it is identical to each realization.

Backward induction

1. Starting recursively from the last decision point in time, to estimate the expected NPV (ENPV) with alternative a conditional on the modeled AVO data, $ENPV(x, a)|y$, we regress $[NPV_{1j}, NPV_{2j}, \ldots, NPV_B(x, a)]$ on the AVO data. This procedure is repeated for each of the alternatives.
2. The optimal scenario was then determined by selecting the option that achieves the highest NPV value, given the known information. The EVWII is then as follows:

$$EVWII = \frac{1}{b}\sum_{b=1}^{B} NPV(x^b, a^*_{DWII}(y^b))$$

$$a^*_{DWII}(y^b) = arg\frac{1}{b}\sum_{b=1}^{B} max_{a\in A} E[NPV(x^b, a)|y^b]$$

$a^*_{DWII}(y^b)$ is the optimal decision with given information y^b

3. Finally, the VOI is given by $max\{0, EVWII - EVWOI\}$.

The process of ADP is further detailed in Hong et al. (2018a,b), Longstaff and Schwartz (2001).

Since the dimensions of the time-lapse data are much larger than the number of realizations, simple regression techniques, such as linear regression, do not work in this case. Instead, we used nonlinear regression.

4. VOI for time-lapse seismic data in the utsira field CO_2 storage

4.1. Decision problem definition

With regard to the problem setting of this example, we assumed that the Utsira reservoir has one injection well at a depth of 1012 m; then, an injection rate of 10 Mt per year is considered for a period of 40 years, followed by a 3000-year migration (post-injection) period. Every flow simulation was performed using the open-source software MRST-CO_2 lab developed by Sintef (Lie, 2019). We considered two options: continuing or stopping the injection. We then analyzed the optimal time to stop the injection based on seismic surveys, which have the highest value when detecting a potential leakage of CO_2. This analysis provides useful insights into the reservoir development plan, and the decision affects learning occurring over time. A total of N=100 prior geological realizations were generated using a normal Gaussian distribution. Here, there is uncertainty in permeability, porosity, temperature, pressure, and caprock elevation. Following the case study by Nilsen et al. (2015a), which tested the sensitivity of CO_2 migration to many input parameters, it was found that porosity differences would influence the total volume of rock with which the plume comes into contact. Increasing the thickness of the pore decreases the overall volume of the rock occupied by the plume, reducing the migration so that the plume does not move far. Permeability impacts the behavior of the CO_2 plume flow by changing its speed and direction, creating a thinner plume that reaches further upslope. As shown in Fig. 4, uncertain aquifer temperature and pressure may also affect the density of CO_2, which further impacts the plume migration and storage ability estimates.

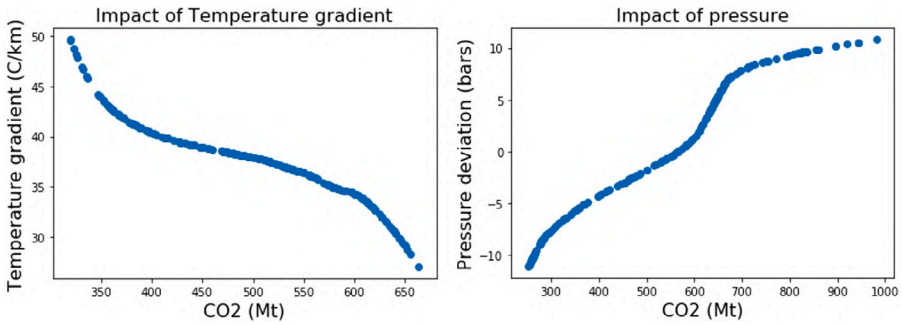

Fig. 4. Impact of pressure and temperature gradient in CO_2 storage capacity.

Table 1
Decision problem setting.

Injection period	60 years
Alternative	Continue or stop the injection at times {14,26,32,40,50,55}
Uncertainty/States	Permeability, porosity, temperature, pressure, and caprock elevation (100 realizations)
Value derived from the decision situation	Net present value
Information data	AVO attributes

In addition, we let $t \in (14, 26, 32, 40, 50, 55)$, and denoted the time in years when the decision of whether to entirely stop the CO_2 injection operation has to be made. We assumed that the injection cannot be resumed once it has stopped. This indicates that the number of decision points in this case is 1200 ($alternatives \times time\ point \times realizations$) (see Table 1).

4.2. Modeling the data and the value outcomes

For each simulation and decision alternative, we extracted CO_2 saturations for each cell in a particular area of the reservoir at different times. This area is marked in blue in Fig. 5 and contains the injection well. We were interested in the saturation at the top of the reservoir to generate the AVO data simulation for each cell. Fig. 6 shows the average saturation for the two scenarios at different times. On average, CO_2 plumes behave differently depending on the injection stop time. However, the injection stopping times are not the only factors that differ between the simulations; they also have different porosities, permeabilities, caprock elevation, temperature, and pressure, which affect the behavior of the plume.

Fig. 7 demonstrates the comparison between CO2 saturation at injection well in two different alternatives (1 : stop injection at 14 years, 7 : stop injection at 60 years) for 100 realizations, one can point out that significant uncertainties are involved.

To estimate the elastic properties and simulate the AVO data, we followed what was presented in the previous section; to estimate the elastic properties of the caprock and initial p- and s-wave velocities at the top of the reservoir, we used well-log data from Dupuy et al. (2017). The initial velocities of the top of the reservoir were estimated by selecting the average value of the velocities over a thickness of 60 m into the reservoir. The estimated values correspond to the values presented by Dupuy et al. (2017). We calculated the initial bulk density of the reservoir for different cells with varying porosities using Eq. 12. The initial velocities of the reservoir may also depend on porosity. Following Dupuy et al. (2017) the authors found that the p-wave velocity decreased rapidly when a small percentage of CO_2 replaced the brine and remained relatively constant for CO_2 saturations greater than 50%. In addition, VS increases with SCO_2, and a linear behavior is shown by the S-wave velocities and bulk density. Variations in the S-wave velocity are limited because VS fluid dependence is found only in the density term (shear modulus is independent of fluid properties). The properties of fluids and minerals are also derived from Dupuy et al. (2017) as shown in Table 2.

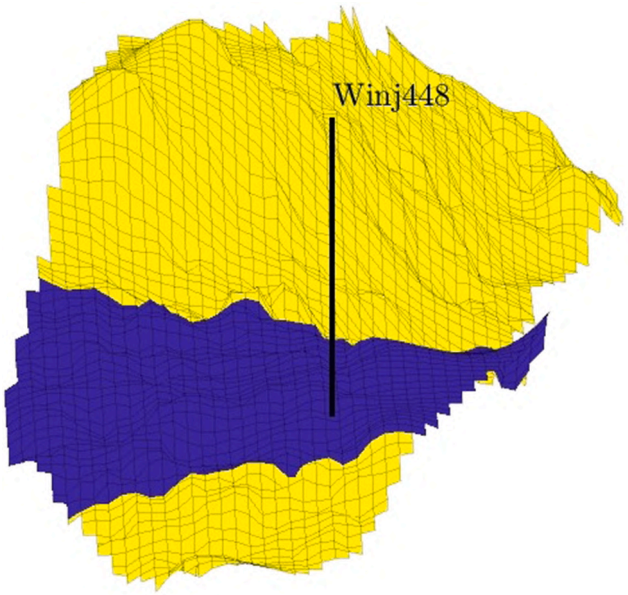

Fig. 5. Reservoir grid, with the area of the seismic survey marked in Blue.

Table 2
Brine, CO_2 properties and rock frame in Utsira sands. The values are derived from (Furre et al., 2017) and (Dupuy et al., 2017).

Properties	Parameter	Value
Utsira sands	K_s (GPa)	39.3
	G_s (GPa)	44.8
	ρ_s (kg/m^3)	2664
Brine	K_w (GPa)	2.31
	ρ_w (kg/m^3)	1030
	η (Pa.s)	0.00069
CO_2	K_{CO_2} (GPa)	0.08
	ρ_{CO_2} (kg/m^3)	700
	η_{CO_2} (Pa.s)	0.000006
Rock frame	m	1
	ϕ	0.37
	k_o (m^2)	2 10–12
	k_D (GPa)	2.56
	G_D (GP)	8.5

Fig. 8 shows the average R_0 attributes for the two different scenarios at different times. Comparing this with Fig. 6, we see that the average

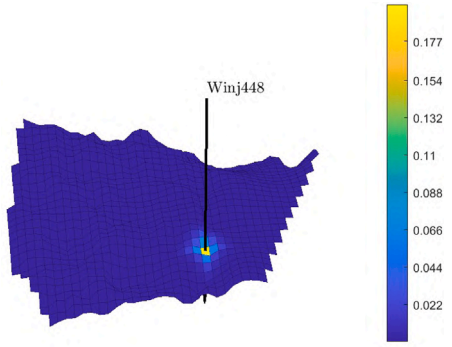

(a) time 14 years.

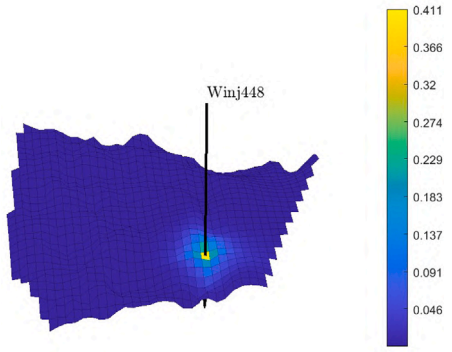

(b) time 50 years.

Fig. 6. Average saturations at times 14 and 50 Years.

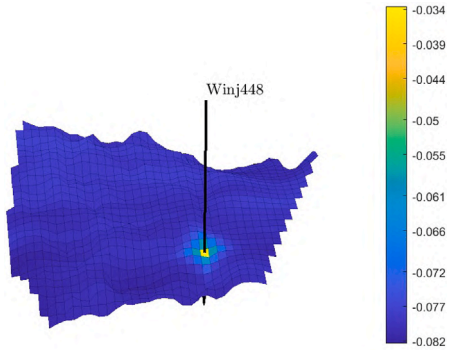

(a) time 14 years.

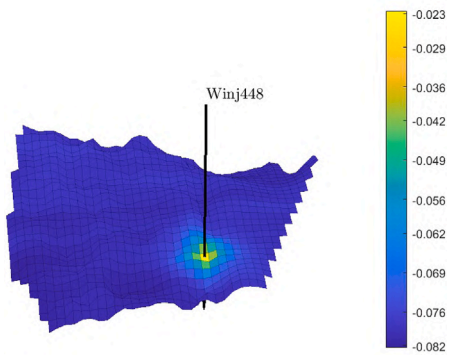

(b) time 50 years.

Fig. 8. Average R_0 attributes at time 14 and 50 years.

of R_0 attributes offers a clear picture of the average saturation. Fig. 9 illustrates the average G attributes for the two different scenarios at different times. Comparing this with Fig. 6, we notice that the average G attributes provide an excellent picture of the average saturation.

To compute the VOI using ADP, the NPV for each decision alternative corresponding to each realization must be evaluated. As our objective is to minimize excess leakage and preserve caprock integrity, the simplest objective function would be measuring the amount of CO_2 injected M_{inj} and penalizing the amount of CO_2 M_{leak} that has left the aquifer through the open boundaries or by leakage through the caprock, which can be associated with project costs and penalty fine if leakage occurs. The NPV function will then conceptually be of the form of the amount of money saved by storing CO_2 minus both the project costs and the penalty fine. For illustration purposes, \$34/t CO_2 would be deployed as the market price in the form of carbon credits to avoid CO2 emissions. Also, \$1.2/t CO_2 would be utilized as a leakage-related fine. The cost of the CO_2 captured is in the range of \$11/t CO_2–\$32/t CO_2 (Puerta-Ortega et al., 2013), this value was fixed at approximately \$25/t CO_2 for our study (Sintef, 2019). Furthermore, \$3.5/t CO_2 was set to cover the costs of construction, operation, and maintenance (Bock et al., 2003). The cost estimate for storage in the onshore USA saline formation is \$2.8/t CO_2 (IPCC, 2005), and the monitoring cost is in the range of \$0.2/t CO_2. The net cost would be then \$25/t CO_2 + \$3.5/t CO_2 + \$2.8/t CO_2 + \$0.2/t CO_2 = \$31.5/t CO_2; hence, the NPV can be expressed as the following:

$$NPV = Revenue - Cost - Penalty$$

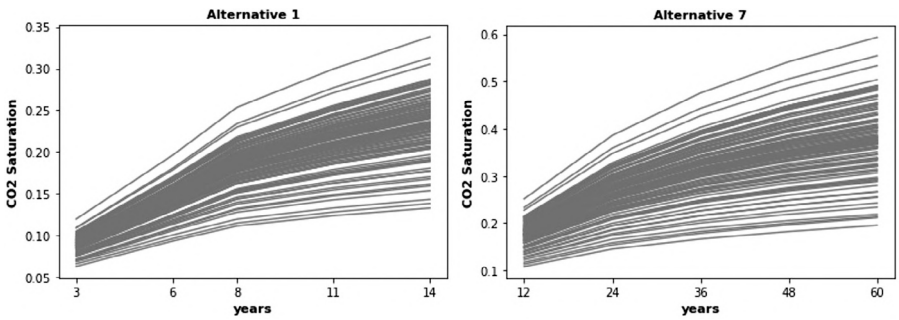

Fig. 7. CO_2 saturation profiles for all realizations: Alternatives 1 and 7.

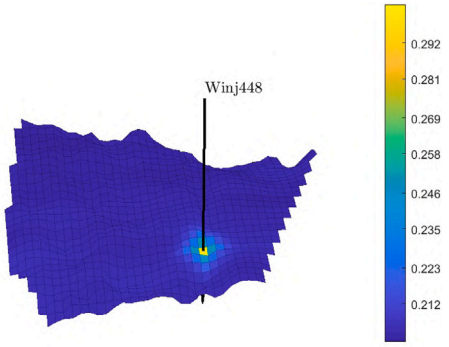

(a) time 14 years.

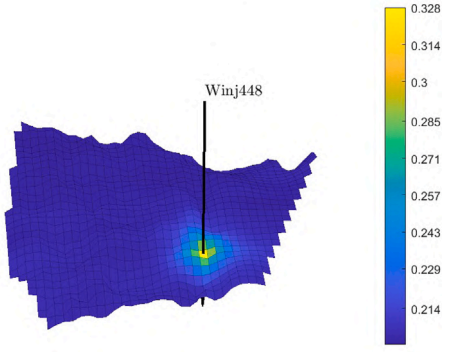

(b) time 50 years.

Fig. 9. Average G attributes at time 14 and 50 years.

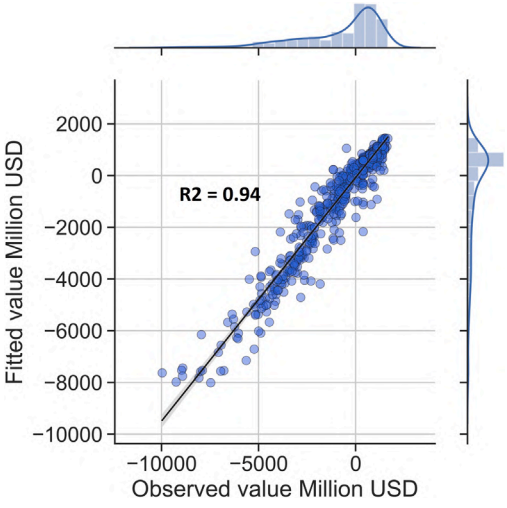

Fig. 10. Plot of fitted values versus observed value using the $R_0 - G$ data.

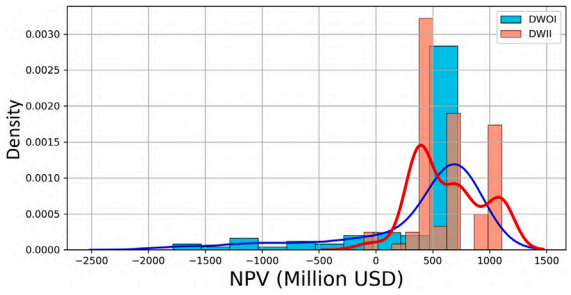

Fig. 11. Graph of PDFs against NPVs with respect to DWOI and DWII.

where,

$$Revenue = \$34/tCO_2 \times (M_{inj} - M_{leak})$$
$$Cost = \$31.5/tCO_2 \times M_{inj}$$
$$Penalty = \$1.2/tCO_2 \times M_{leak}$$

4.3. Value regression using machine learning

To compute the VOI of time-lapse seismic data, we needed to regress the NPVs on the measured AVO attributes for each decision alternative and boundary conditions. We used an automated machine learning (Auto ML) technique called the tree-based pipeline optimization tool (TPOT). The TPOT was first proposed by Olson and Moore (2019). In short, the TPOT optimizes various machine learning pipeline techniques using stochastic search algorithms such as genetic programming. To prevent and reduce overfitting in the machine learning training process, we used 5-fold cross-validation. Cross-validation was run separately for each strategy. Fig. 10 shows a plot of the fitted values using machine learning versus the observed values for the entire sample. A high correlation was observed between the fitted and observed values, with a correlation coefficient of approximately 0.94.

The DWOI is to finish the CO_2 injection by the end of 26 years, and the EVWOI is found to be \$385.63 million. Moreover, the EVWPI is estimated to be \$891.48 million. This pegs the VOPI at \$505.85 million. The highest EVWII corresponding to machine learning was obtained through the Auto ML and provided an EVWII of \$628.46 million, with a related VOI of \$242.85 million. This result indicates that it is uneconomical to proceed with any information-gathering activity if it costs more than \$242.85 million. This result also illustrates that including the effect of future information and decisions could improve the EV by 62.97%, which is the percentage of the fraction of VOI to EVWOI.

The probability density function (PDF) of NPVs associated with DWOI and DWII are plotted in Fig. 11. From this figure, we notice that the NPV resulting from the ML approach (DWII) is higher than that of the DWOI. In this aspect, integrating the effects of future information and decisions in decision-making would increase the ENPV. Some realizations end up with a smaller NPV with DWII than the NPV with DWOI, which may be due to a suboptimal decision, as the machine learning algorithm is the approximate method, which, for some of the path decisions, makes suboptimal choices.

The normalized frequency distribution (NFD) of the CO_2 injection is illustrated in Fig. 12. Based on these results, it is more worthwhile to cease CO_2 injection between 14 and 40 years (i.e., there is a 38% and 32% chance that the CO_2 injection mechanism should be stopped at the end of 14 and 26 years, respectively). There is only a 22% less chance that it is optimal to stop the same after 40 years. The specific stop time depends mainly on the measured seismic data and geological realization, including the uncertainty in permeability, porosity, caprock elevation, pressure, and temperature.

4.4. Sensitivity analysis in AVO attributes

The next step is to assume the AVO attributes R_0 and G to be noisy and normally distributed:

$$(R_0, G)^T \approx \mathcal{N}(m, T)$$

where the mean m is calculated using Eqs. 11 and 12. Following Eidsvik et al. (2015), the covariance matrix corresponding to the one set for the

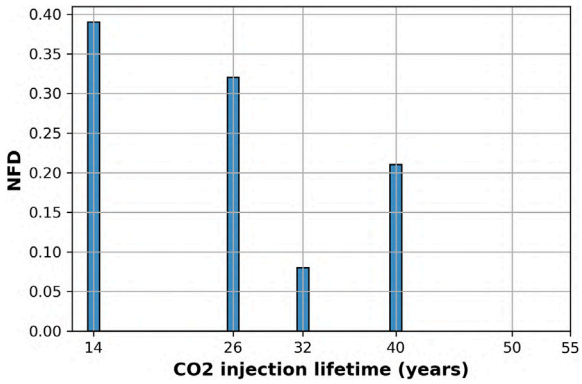

Fig. 12. NFDs of the CO_2 optimal stop injection time corresponding to the decision-making with ML.

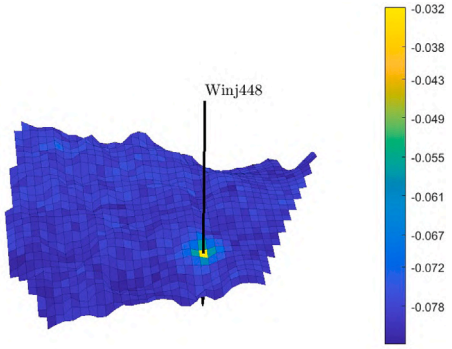

(a) time 14 years.

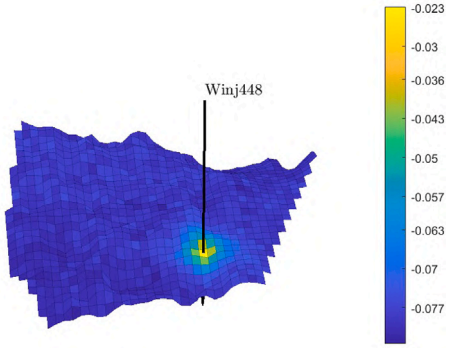

(b) time 50 years.

Fig. 13. Average R_0 attributes at times 14 and 50 years.

likelihood model for AVO data was set to the following:

$$T = c \begin{pmatrix} 0.06^2 & -0.7 \times 0.06 \times 0.17 \\ -0.7 \times 0.06 \times 0.17 & 0.17^2 \end{pmatrix}$$

Where c > 0.

Figs. 13 and 14 demonstrate R_0 and G attributes, respectively, for the two different scenarios. Comparing these with Fig. 6, which contains the same simulations, we observe that the R_0 attributes present an effective picture of the saturation; however, there is significant noise for the R_0 attributes. This is expected as the variance is higher for G than for R_0.

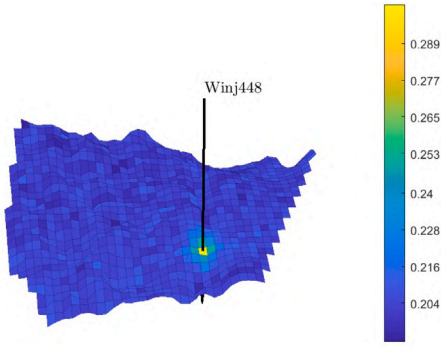

(a) time 14 years.

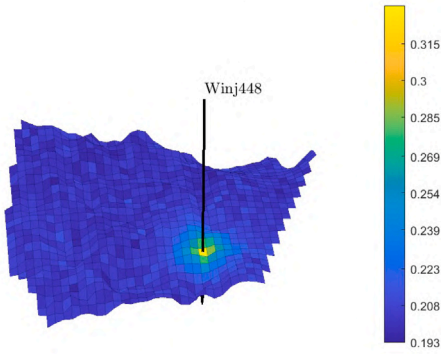

(b) time 50 years.

Fig. 14. Average G attributes at times 14 and 50 years.

By adding uncertainty in AVO attributes, the EVWII is estimated to be $617.11 million. This makes the VOI $231.48 million. This result indicates that it is uneconomical to proceed with any information-gathering activity if it costs more than $231.48 million. This result also illustrates that including the effect of future information and decisions could improve the EV by 60.03%, which is the percentage of the fraction of VOI to EVWOI.

The NFDs of the total lifetime corresponding to the decisions with machine learning are displayed in Fig. 16. This result recommends stopping CO_2 injection at the end of years 14 and 26 (i.e., there is more than a 60% chance that the CO_2 injection mechanism should be stopped after year 26). There is only less than 5% chance that it will be optimal to stop the injection after 32 and 40 years. The specific stop time depends mainly on the perturbed measured seismic data and uncertainty of geological realization.

Fig. 15 shows a comparison of the PDFs corresponding to the different methods. The NPV resulting from the ML approach (DWII) is higher than that of the DWOI, as ML allows learning over time. Moreover, some realizations resulted in a smaller NPV with ML than with the DWOI. This may be due to suboptimal decisions.

4.4.1. Sensitivity analysis in carbon price

In both previous studies, we did not include uncertainties in the carbon price, even though it significantly impacted the decision. Therefore, in this work, the carbon price was treated as an uncertain parameter and considered in the regression analysis to determine the optimal stopping time in CO_2 injection monitoring.

The carbon price is modeled as Markovian processes and variants over time. Hence, it is assumed to follow a stochastic process. There are two commonly used stochastic models to describe uncertainties in

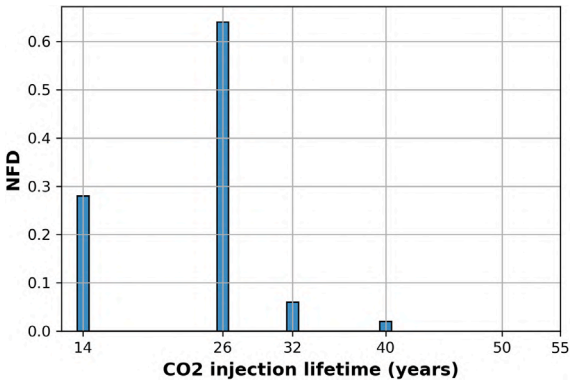

Fig. 15. NFDs of the CO_2 optimal stop injection time corresponding to the decision-making with ML.

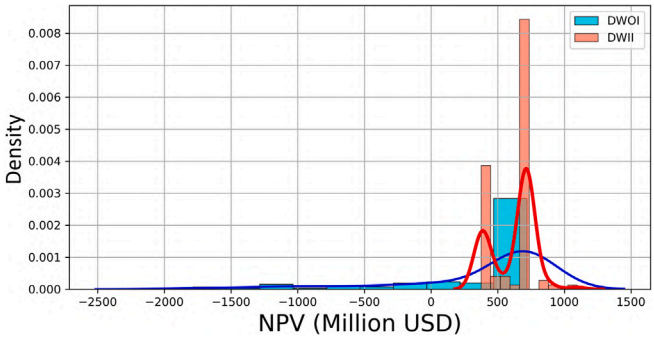

Fig. 16. Graph of PDFs against NPVs with respect to DWOI and DWII.

economic variables: the geometric Brownian motion (also known as the random-walk model) and the Ornstein–Uhlenbeck (OU) stochastic process (also known as the mean-reverting model; refer to Uhlenbeck and Ornstein (1930) for more details).

A process "S" can be stochastically modeled using the Ornstein–Uhlenbeck process as shown below:

$$dS_t = \theta\,(\mu - S_t)dt + \sigma dW_t \tag{15}$$

where θ is the speed of mean reversion, μ is the long-term mean which the process reverts, σ is the measure of process volatility, and W_t stands for a Brownian motion, where $dW_t \sim N(0, \sqrt{d_t})$. This stochastic equation must be discretized to be implemented in the simulation. Gillespie (1996) opined that the simulation of the process would work well only when the discretized time Δ_t is sufficiently small. Thus, the discretized equation is as follows:

$$S_t = (S_{t-1} \times e^{-\theta\Delta t}) + \mu(1 - e^{-\theta\Delta t}) + \left[\sigma \times \sqrt{\frac{1 - e^{-2\theta\Delta t}}{2\theta}} \times dW_t\right] \tag{16}$$

However, if any commodity price, including carbon prices per unit, or any other cost is modeled using the above discrete-time expression, negative values might be generated. This is not realistic, because negative commodity prices never exist. To avoid this problem, we used the lognormal distribution of commodity prices. Thus, in this context, the logarithm of the modeled parameter, namely $\pi_t = ln[St]$, is assumed to follow the mean-reverting process. This process can be mathematically described as follows:

$$d\pi_t = \kappa[\bar{\pi} - \pi_t]d_t + \sigma\pi dz_t \tag{17}$$

where κ is the speed of mean reversion, $\bar{\pi}$ is the long-term mean that the logarithm of the variable reverts, $\sigma\pi$ stands for the volatility of process, and dz_t describes the increments of standard Brownian motion. Subsequently, to numerically solve for π_t, the stochastic equation is

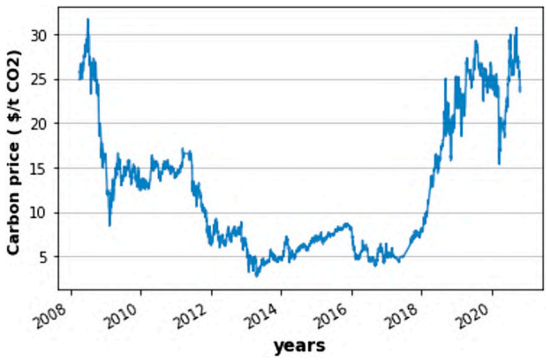

Fig. 17. Historical of carbon prices from 1985 to 2021.

discretized as shown below (by assuming $dz_t \sim (0, \sqrt{d_t})$, where d_t = 1 year).

$$\pi_t = (\pi_{t-1} \times e^{-\kappa\Delta t}) + \bar{\pi}(1 - e^{-\kappa\Delta t}) + \left(\sigma_\pi \times \sqrt{\frac{1 - e^{-2\kappa\Delta t}}{2\theta}} \times N(0,1)\right) \tag{18}$$

After calculating π_t, the value of S_t cannot directly be obtained using the equation of $S_t = e^{\pi t}$. This is due to the fact that half of the variance is added to the mean of the lognormal distribution, namely $0.5 \times var(\pi_t)$, for the exponential of a normal distribution. Therefore, half of the variance is deducted using the following equation:

$$Var(\pi_t) = [1 - e^{-\kappa\Delta t}] \times \frac{{\sigma_\pi}^2}{2\kappa} \tag{19}$$

To use this model, a decision must be made to determine its parameters. This process is known as calibration, and since the logarithm of the variables is assumed to follow the mean-reverting process, the least-squares regression, which was suggested by Smith (2010), was conducted on the datasets of $\pi_t = ln[S_t]$. To calibrate the OU parameters for the modeling of the carbon credit price, a set of carbon credit price data is required. For illustration, the annual carbon credit price data, namely prices from 2008 to 2020 (considering only historical data), which is available on the European Union Emissions Trading System carbon market price European Union Emissions Trading System carbon market price (2021), were used as displayed in Fig. 17.

To start the procedure of calibration, we used the following equations:

$$x_t = \pi_t - \Delta_t = ln[Pt - \Delta_t] \tag{20}$$

$$y_t = \pi_t = ln[Pt] \tag{21}$$

$$y_t = ax_t + b + \delta \tag{22}$$

The OU parameters are estimated using the values of a and b:

$$\bar{\pi} = \frac{b}{1-a},\ \kappa = \frac{-ln\ a}{\Delta t},\ \sigma_\pi = \sigma_\delta \sqrt{\frac{-2ln\ a}{\Delta t(1-a^2)}} \tag{23}$$

where δ is the approximation error introduced in the least-squares regression, σ_δ is the standard deviation of the approximation errors, and Δt is the difference in two time-steps. Refer to Smith (2010) for more details regarding the derivation of the equations.

Using the parameters in Table 3, the carbon price corresponding to the respective costs is modeled forward in time. Fig. 18 presents the probabilistic model of the oil price.

By adding uncertainty in the carbon price, the DWOI provides 14 years CO_2 injection time, and the EVWOI is found to be $432.50 million. Moreover, the highest EVWII corresponding to machine learning was $870.23 million, which also illustrates that including the effect of future information and decisions improves the net present value. The

Table 3
Values of parameters used in the mean-reverting model.

Parameter	Carbon price
Initial value	34
Equilibrium value	34
Volatility σ_δ	0.4811
Mean reversion speed, κ	0.2647
d_t, year	1

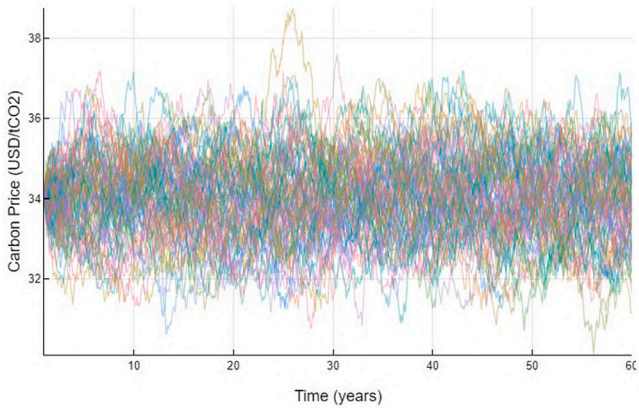

Fig. 18. Carbon prices modeled using the mean-reverting process.

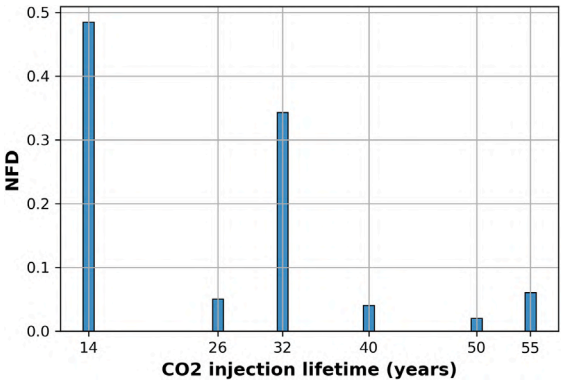

Fig. 19. NFDs of the CO_2 optimal stop injection time corresponding to the decision-making with ML.

NFDs of the total lifetime corresponding to the decision with machine learning are shown in Fig. 20. This result recommends stopping CO_2 injection mostly at the end of years 14 or 32 (i.e., there is a more than 32% chance that the CO_2 injection mechanism should be stopped after years 14 and 32). There is only a less than 10% chance that it is optimal to stop the injection after 26, 40, 50, and 55 years. The specific switch time depends mainly on the uncertainty of geological realization and perturbed modeled AVO attributes, including uncertainty in carbon prices.

Fig. 19 shows a comparison of the PDFs of NPVs associated with DWOI and DWOII. The NPV resulting from the ML approach (DWII) is higher than that of the DWOI, as ML allows learning over time. Furthermore, some realizations resulted in a smaller NPV with ML than with the DWOI. This may be due to suboptimal decisions.

5. Discussion and concluding remarks

We presented a VOI framework that can be used to compute the VOI in a reservoir development plan. Specifically, we applied the framework to evaluate the VOI of time-lapse seismic data in the context

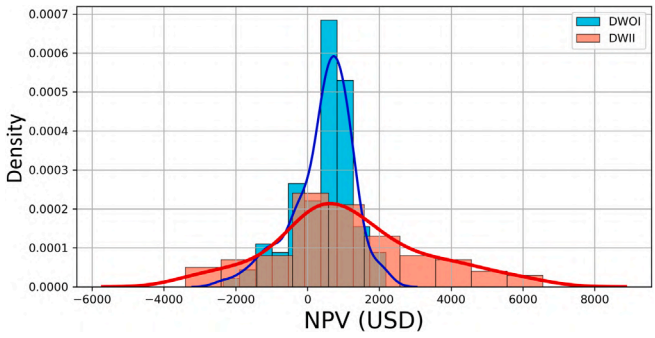

Fig. 20. Graph of PDFs against NPVs with respect to DWOI and DWII.

of CO_2 storage and the detection of potential CO_2 leakage. A case has been developed where, based on information from seismic surveys and carbon credit prices, a decision-maker must decide on the best time to continue or stop the CO_2 injection. The reliability of a seismic survey and carbon prices are likely to increase with time and the amount of CO_2 injected into the reservoir. In this context, the decision of when to perform the survey becomes a trade-off between test reliability and the amount of CO_2 at risk of leakage. For this study, we used the Utsira field CO_2 storage atlas, which is located in the North Sea, and considered a storage location for the full-scale Norwegian CCS project. We used an approximate dynamic approach to estimate the VOI for seismic surveys. Nevertheless, when a seismic survey is most important, the VOI estimates do not provide an accurate response. Notwithstanding, we may tentatively claim that in the injection phase, a seismic survey should not be performed too early or too late. In addition, the value of learning induced by machine learning may be small and insignificant, as there is always an approximation error when applying the machine learning regression function. In addition, the closeness of a regression function to estimate the actual expected values and the accuracy of this method mainly depend on the prior sample of Monte Carlo, alternatives, and information, and, in some cases, the model choice may not be material.

In conclusion, the VOI framework can generally be applied to any type of spatial data and in the context of decisions other than reservoir development. The framework can be evaluated as an interplay between three key factors: the decision-making situation consisting of alternatives and prospect values, the uncertain variables of interest that affect the prospect values, and the data that informs about these variables of interest. Moreover, the approximate dynamic methodology can be applied to estimate the conditional expectation of prospect values given the data outcomes, and thereby to evaluate the VOI. This computational efficiency of ADP allows VOI computation in complex decision situations where the rigorous Monte Carlo methodology is intractable. However, the VOI is still quite uncertain, and to consistently estimate the VOI in complex sequential decision cases, it might be beneficial to increase the number of realizations or reduce the number of alternatives in innovative ways. Therefore, a new procedure and methodology based on clustering techniques, in combination with proxy models, must be developed to reduce computational costs and efficiently solve real-world sequential decision-making problems.

CRediT authorship contribution statement

Amine Tadjer: Wrote the paper, Contributed to tuning the model, Analyzing the results. **Aojie Hong:** Supervised the work, Providing continuous feedback. **Reidar B. Bratvold:** Supervised the work, Providing continuous feedback.

Declaration of competing interest

The authors declare that they have no known competing financial interests or personal relationships that could have appeared to influence the work reported in this paper.

Acknowledgments

The author acknowledges financial support from the Research Council of Norway through the Petromaks-2 project DIGIRES (RCN no. 280473) and the industrial partners AkerBP, Wintershall DEA, ENI, Petrobras, Equinor, Lundin, and Neptune Energy. All authors have read and agreed to the published version of the manuscript.

References

Allen, R., Nilsen, H., Lie, K., O., M., Andersen, O., 2018. Using simplified methods to explore the impact of parameter uncertainty on CO_2 storage estimates with application to the Norwegian Continental Shelf. Int. J. Greenhouse Gas Control 75, 198–213.

Andersen, O., Nilsen, H., Lie, K.A., 2014. Reexamining CO_2 storage capacity and utilization of the utsira formation. 2014, 1–18.

Anyosa, S., Bunting, S., Eidsvik, J., Romdhane, A., Bergmo, P., 2021. Assessing the value of seismic monitoring of CO_2 storage using simulations and statistical analysis. Int. J. Greenhouse Gas Control 105, 103219. http://dx.doi.org/10.1016/j.ijggc.2020.103219, URL: https://www.sciencedirect.com/science/article/pii/S1750583620306447.

Arts, R., Eiken, O., Chadwick, A., Zweigel, P., Van der Meer, L., Zinszner, B., 2004. Monitoring of CO_2 injected at sleipner using time-lapse seismic data. Energy 29, 1383–1392. http://dx.doi.org/10.2118/65148-MS.

Avseth, P., Mukerji, T., Mavko, G., 2005. Quantitative Seismic Interpretation: Applying Rock Physics Tools To Reduce Interpretation Risk. Cambridge University Press, http://dx.doi.org/10.1017/CBO9780511600074.

Aylor Jr., W., 1999. Measuring the impact of 3D seismic on business performance. J. Petrol. Techno 51 (6), 52–56. http://dx.doi.org/10.2118/56851-JPT.

Bickel, J.E., Gibson, R.L., McVay, D.A., Pickering, S., R, J., 2008. Quantifying the reliability and value of 3D land seismic. SPE Res. Eval. Eng. 11, 832–841. http://dx.doi.org/10.2118/102340-PA.

Bock, B., Rhudy, R., Herzog, H., Klett, M., Davison, J., Ugarte, D.G.D.L.T., Simbeck, D., 2003. Economic evaluation of CO_2 storage and sink enhancement options. http://dx.doi.org/10.2172/826435, URL: https://www.osti.gov/biblio/826435.

Bratvold, R., Bickel, J., Lohne, H., 2009. Value of information in the oil and gas industry : Past, Present, and Future. SPE Reserv. Eval. Eng. 2 (4), 630–638. http://dx.doi.org/10.2118/110378-PA.

Dupuy, B., Ghaderi, A., Querendez, E., Mezyk, M., 2017. Constrained AVO for CO_2 storage monitoring at sleipner. Energy Procedia 114, 3927–3936. http://dx.doi.org/10.1016/j.egypro.2017.03.1524.

Dutta, G., Mukerji, T., Eidsvik, J., 2019. Value of information analysis for subsurface energy resources applications. Appl. Energy 252, 113436. http://dx.doi.org/10.1016/j.apenergy.2019.113436.

Eidsvik, J., Dutta, G., Mukerji, T., Bhattacharjya, D., 2017. Simulation–regression approximations for value of information analysis of geophysical data. Math. Geosci. 49 (4), 467–491. http://dx.doi.org/10.1007/s11004-017-9679-9.

Eidsvik, J., Mukerji, T., Bhattacharjya, D., 2015. Value of Information in the Earth Sciences. Cambridge Univeristy Press, Cambridge.

European Union Emissions Trading System carbon market price, 2021. Daily EU ETS carbon market price (Euros). URL: https://ember-climate.org/data/carbon-price-viewer/.

Furre, A.-K., Eiken, O., Alnes, H., Vevatne, J.N., Kiær, A.F., 2017. 20 years of monitoring CO_2-injection at sleipner. Energy Procedia 114, 3916–3926. http://dx.doi.org/10.1016/j.egypro.2017.03.1523.

Gassmann, F., 1951. Über die elastizität poröser medien: Vierteljahrsschrift der Naturforschenden Gesellschaft in Zurich. 96, pp. 1–23.

Gillespie, D., 1996. Exact numerical simulation of the Ornstein-Uhlenbeck process and its integral. Geosci. Data J. 54, 2084–2091. http://dx.doi.org/10.1103/PhysRevE.54.2084.

Han, D.-H., Batzle, M., 2004. Gassmann's equation and fluid-saturation effects on seismic velocities. GEOPHYSICS 69 (2), 398–405. http://dx.doi.org/10.1190/1.1707059, arXiv:https://doi.org/10.1190/1.1707059.

Harp, D.R., Stauffer, P.H., O'Malley, D., Jiao, Z., Egenolf, E.P., Miller, T.A., Martinez, D., Hunter, K.A., Middleton, R., Bielicki, J., 2017. Development of robust pressure management strategies for geologic CO_2 sequestration. Int. J. Greenhouse Gas Control 64, 43–59.

Hong, A., Bratvold, R., Lake, L., 2018a. Fast analysis of optimal IOR switch time using a two-factor production model and least- squares Monte Carlo algorithm. SPE Reserv. Eval. Eng. http://dx.doi.org/10.2118/191327-PA.

Hong, A., Bratvold, R., Thomas, P., Hanea, R., 2018b. Value-of-information for model parameter updating through history matching. J. Pet. Sci. Eng. 165, 253–268. http://dx.doi.org/10.1016/j.petrol.2018.02.004, URL: https://www.sciencedirect.com/science/article/pii/S0920410518300998.

Howard, R., 1966. Information value theory. IEEE Trans. Syst. Sci. Cybern. 2 (1), 22–26. http://dx.doi.org/10.1109/TSSC.1966.300074.

Jafarizadeh, B., Bratvold, R., 2009. Taking real options into real world: Asset valuation through option simulation. In: SPE Annual Technical Conference and Exhibition. New Orleans, Louisiana, http://dx.doi.org/10.2118/124488-MS.

Jin, L., Hawthorne, S., Sorensen, J., Pekot, L., Kurz, B., Smith, S., Heebink, L., Hergegen, V., Bosshart, N., Torres, J., Dalkhaa, C., Peterson, K., Gorecki, C., Steadman, E., Harju, J., 2017. Advancing CO_2 enhanced oil recovery and storage in unconventional oil play—Experimental studies on bakken shales. Appl. Energy 208, 171–183.

Lie, K.-A., 2019. An Introduction To Reservoir Simulation using MATLAB/GNU Octave: User Guide for the MATLAB Reservoir Simulation Toolbox (MRST). Cambridge University Press, http://dx.doi.org/10.1017/9781108591416.

Longstaff, F., Schwartz, E., 2001. Valuing American options by simulation: a simple least-squares approach. Rev. Financ. Stud. 14 (1), 113–147. http://dx.doi.org/10.1093/rfs/14.1.113.

Newendorp, P., 1975. Decision analysis for petroleum exploration. URL: https://www.osti.gov/biblio/7318461.

Nguyen, P., Nam, M., 2011. Review on methods for constructing rock physics model of saturated reservoir rock for time-lapse seismic. Geosyst. Eng. 14 (2), 95–107. http://dx.doi.org/10.1080/12269328.2011.10541336.

Nilsen, H., Lie, K.A., Andersen, O., 2015a. Analysis of CO_2 trapping capacities and long-term migration for geological formations in the Norwegian North Sea using MRST-co2lab. Comput. Geosci. 79, 15–26.

Olson, R., Moore, J., 2019. A tree-based pipeline optimization tool for automating machine learning. In: Hutter F., V.J. (Ed.), Automated Machine Learning. In: The Springer Series on Challenges in Machine Learning, Springer.

Puerta-Ortega, C., Bickel, J.E., Hovorka, S., 2013. Assessing the value of permeability data in a carbon capture and storage project. Int. J. Greenhouse Gas Control 17, 523–533. http://dx.doi.org/10.1016/j.ijggc.2013.06.003, URL: https://www.sciencedirect.com/science/article/pii/S175058361300251X.

Raiffa, H., Schlaifer, R., 1961. Applied Statistical Decision Theorys. Harvard University, Wiley.

Riis, T., 1999. Quantifying the value of information. Pet. Eng. Int. 72 (6), URL: https://www.osti.gov/biblio/354456.

Sato, K., 2011. Value of information analysis for adequate monitoring of carbon dioxide storage in geological reservoirs under uncertainty. Int. J. Greenhouse 5 (5), 1294–1302. http://dx.doi.org/10.1016/j.ijggc.2011.07.010.

Singh, V., Cavanagh, A., Hansen, H., Nazarian, B., Iding, M., Ringrose, P., 2010. Reservoir modeling of CO_2 plume behavior calibrated against monitoring data from sleipner, Norway. In: SPE Annual Technical Conference and Exhibition. Florence, Italy, Society of Petroleum Engineers.

Smith, W., 2010. On the simulation and estimation of the mean-reverting Ornstein-Uhlenbeck process. URL: https://commoditymodels.files.wordpress.com/2010/02/estimating-the-parameters-of-a-mean-reverting-ornsteinuhlenbeck-process1.pdf.

Uhlenbeck, G., Ornstein, L., 1930. On the theory of the Brownian motion. Phys Rev 36, 823–841. http://dx.doi.org/10.1103/PhysRev.36.823.

Waggoner, J., 2000. Lessons learned from 4D projects. SPE Reserv. Eval. Eng. 3 (4), 310–318.

Wood, A., 1941. A Textbook of Sound. G. Bell and Sons LTD, London.